



UNIVERSITY OF NAPLES FEDERICO II
PH.D. PROGRAMME IN
SEISMIC RISK
XXVII CYCLE

Maria Teresa De Risi

SEISMIC PERFORMANCE ASSESSMENT OF RC
BUILDINGS ACCOUNTING FOR STRUCTURAL
AND NON-STRUCTURAL ELEMENTS



UNIVERSITY OF NAPLES FEDERICO II

*Department of Structures
for Engineering and Architecture*

PH.D. PROGRAMME IN
SEISMIC RISK
COORDINATOR PROF. ALDO ZOLLO
XXVII CYCLE



MARIA TERESA DE RISI

PH.D. THESIS

**SEISMIC PERFORMANCE ASSESSMENT OF RC
BUILDINGS ACCOUNTING FOR STRUCTURAL
AND NON-STRUCTURAL ELEMENTS**

TUTOR PROF. ING. GERARDO M. VERDERAME
CO-TUTOR DR. ING. PAOLO RICCI

2015

*To my Mother and my Father
To my great and wonderful Family, my force, my serenity, my wealth*

Acknowledgements

I would like to express deep gratitude and sincere thanks to my tutor Professor Gerardo Mario Verderame, that was my scientific guide during these years. He taught me how working hard can make the difference in the world of research. His advice, encouragement, and guidance made the completion of this research possible.

I express my thanks to Professor Gaetano Manfredi for the opportunity he gave me to be part of the Department of Structures for Engineering and Architecture of the University of Naples Federico II and of his research group.

I would like to express sincere gratitude to my co-tutor Paolo Ricci for his significant contribution to this work and his competence shared with me in our debates. He taught me that only paying attention to details can lead towards a research of quality.

Special thanks also to all the research team members; in these years, they often provided, in different ways, a great support to my research activities.

I am thankful to my mother, my father and my brothers for their unconditional love, encouragement, and support, without which I would not reached this objective today. No words can explain how grateful I am and how fortunate I feel.

Finally, I would express a special thanks for the love of who is closest to me and has given me times full of happiness and beautiful surprises.

Naples, March 2015

Abstract

Among the natural hazards, earthquakes are paramount due to their impact on civil structures worldwide. The considerable direct economic losses (property losses) due to earthquakes in conjunction with social impact and indirect economic losses have prompted a great interest in performance assessment of the civil structures to future seismic events. Therefore, performance evaluations beyond the traditional goal of life safety, are required to rightly estimate expected losses. A key ingredient of this evaluation process is the fragility, that describes the probability of failure to meet a performance objective depending on demand on the system, providing the link between seismic hazard and building losses estimation.

A correct fragility evaluation necessitates the development of reliable nonlinear analysis models that are able to simulate the behavior of structures from the onset of damage through collapse. Therefore, proper prediction of the nonlinear behavior and formulation of analytical models are essential prerequisites for a reliable evaluation of structural fragility and, then, of seismic performance and risk assessment of Reinforced Concrete (RC) structures. Moreover, within the *performance-based* approach, it is also essential to understand which mechanisms/elements have the higher influence on seismic performance depending on the analyzed performance level.

A lot of work should still be done towards this direction, especially for existing *under-designed* or *non-ductile* structures. With *under-designed* or *non-ductile* terms it will be referred to structures designed for gravity loads only or according to obsolete seismic and technical codes.

A contribution towards this direction is carried out in this work.

Starting from the analysis of typical deficiencies of non-ductile RC frames and the definition of performance levels of interest, this work aimed to contribute to PBEE framework with (i) a critical overview on analysis methodologies and modeling approaches of the salient components of RC frames, namely flexural or shear-dominated beams and columns, and more in

detail, beam-column joints and masonry infills, the core of this work, and (ii) with new proposals in terms of nonlinear modeling and analysis procedures to provide a more reliable evaluation of seismic performance and risk assessment of infilled RC structures, accounting for structural and non-structural (in particular masonry infills) elements at different performance levels.

For these purposes, existing analytical modeling techniques for RC frames' critical components were first reviewed and discussed. Then, a deep investigation on the influence of infills on seismic performance at different limit states, also for new constructions, has been carried out, in order to highlight the critical points that can interest also this kind of structures regarding infill presence.

The effect of infills on the global seismic behavior of RC frames was investigated, by analyzing their influence on global stiffness and strength, on the kind of collapse mechanism, on the displacement capacity and, consequently, on seismic capacity and seismic fragility at different performance levels, depending on the main characteristics of the RC frame, such as the design typology and the number of stories.

Recognized the importance of infills especially at lower seismic intensity and the widespread of linear analysis methodology among practitioner, new procedures are proposed as tools to better taking into account damage to infills also in linear analyses with or without the explicit modeling of infills in the numerical model. The attention has been focused both on the design of new constructions and the assessment of existing structures, providing a contribution towards desirable more comprehensive future code prescriptions at lower seismic intensity - that depend on mechanical properties of infills and proper displacement capacity thresholds - within the context of linear analyses.

From the point of view of the bare structure (without infills in the structural model) and in particular referring to higher intensity levels, proceeding from Damage Limitation (DL) LS towards Near Collapse (NC) LS, the analysis of RC frames different for design typology has highlighted the vulnerability points of such frames, already pointed out by experimental tests and past seismic events. In particular the influence of beam-column unreinforced joints is deeper investigated.

In literature there is not yet a commonly accepted approach for the determination of the shear strength and for nonlinear modeling of RC beam-column joints in moment resisting RC frames. In many studies, beam-column connections are modeled as rigid. However, many nonlinear joint models are

available, but most of them may be unsuitable for modeling all sources of nonlinearity for the assessment of older concrete buildings. Some of them were developed and calibrated for confined beam-column joints or they are too complicated to implement.

On the basis of an extensive and critical review of previous experimental tests and existing joint modeling approaches, a new cyclic shear constitutive relationship is proposed for exterior unreinforced joints, different for failure typology, in order to describe nonlinear behavior of joint panels, to be used in conjunction with an explicit bond-slip spring, thus taking into account all sources of nonlinearity and different possible kinds of deficiencies.

Then, the influence of joint behavior on seismic performance at different performance levels, both in terms of strength and deformability contribution, also taking into account the record-to-record variability, was investigated in nonlinear dynamic analyses of under-designed frames.

Finally, after the investigation about the sensitivity of joint response to the main mechanical and geometrical properties of beam-column sub-assemblages, the results of two experimental tests are presented and discussed. The specimens have deformed bars and show different failure typology. These tests conducted under cyclic loading aim to improve the understanding of exterior joints seismic performance without transverse reinforcement in existing RC buildings. Experimental results are analyzed herein and compared with numerical results carried out through the adoption of the proposed numerical model.

Keywords: Seismic assessment, RC buildings, performance levels, masonry infills, beam-column joints, fragility analysis, static pushover, incremental nonlinear analysis, experimental tests.

Tables of contents

ABSTRACT	7
TABLES OF CONTENTS	10
LIST OF FIGURES	14
LIST OF TABLES	22
CHAPTER 1	26
INTRODUCTION	26
1.1 MOTIVATION	26
1.2 RESEARCH OBJECTIVES.....	29
1.3 DISSERTATION OUTLINE	32
REFERENCES	33
CHAPTER 2	35
BACKGROUND AND CRITICAL ISSUES IN MODELING OF NON-DUCTILE RC BUILDINGS	35
2.1 MODELING OF CRITICAL COMPONENTS.....	36
2.1.1. <i>Beam/column elements</i>	36
2.1.1.1 <i>Classification issue</i>	36
2.1.1.2 <i>Flexural behavior</i>	38
2.1.1.3 <i>Shear behavior</i>	40
2.1.2. <i>Beam – column joints</i>	44
2.1.2.1 <i>Beam – column joints shear strength</i>	45
2.1.2.2 <i>Modeling of joint shear behavior</i>	49
2.1.2.3 <i>Shear constitutive relationship of the joint panel</i>	54
2.1.3. <i>Infills</i>	57
2.2 STRUCTURAL PERFORMANCE LEVELS.....	61
REFERENCES	65
CHAPTER 3	71
INFLUENCE OF INFILL DISTRIBUTION AND DESIGN TYPOLOGY ON SEISMIC PERFORMANCE OF LOW- AND MID-RISE RC BUILDINGS	71
3.1 INTRODUCTION.....	72
3.2 CASE STUDY STRUCTURES.....	74
3.2.1. <i>Analysis methodology</i>	79

Table of contents

3.3	SENSITIVITY ANALYSIS.....	82
3.3.1.	<i>Selected random variables</i>	82
3.3.2.	<i>Analysis of results</i>	86
3.3.2.1	<i>IN2 curves</i>	90
3.4	COMPARISONS AND REMARKS: INFILL DISTRIBUTION, DESIGN TYPOLOGY AND NUMBER OF STORIES.....	99
3.4.1.	<i>Influence of the infill configuration</i>	99
3.4.2.	<i>Influence of the design typology</i>	102
3.4.3.	<i>Influence of the number of stories</i>	105
3.4.4.	<i>A generalization attempt</i>	105
3.5	FRAGILITY ANALYSIS	107
3.5.1.	<i>Methodology</i>	107
3.5.2.	<i>Analysis of results</i>	109
3.5.2.1	<i>A comparison between fragility analysis and observed damage</i>	116
3.5.3.	<i>Evaluation of failure probability</i>	118
3.6	SUMMARY	122
REFERENCES.....		124
CHAPTER 4		129
LIMITATION OF DAMAGE TO INFILL PANELS IN SEISMIC DESIGN AND ASSESSMENT OF RC FRAMES VIA LINEAR METHODS.....		129
4.1	INTRODUCTION.....	130
4.2	CODE PROVISIONS AND LITERATURE REVIEW	133
4.2.1.	<i>Code provisions on infill modeling and acceptance criteria</i>	133
4.2.2.	<i>Literature review on drift capacity of unreinforced masonry infill panels</i>	137
4.3	METHODOLOGY	139
4.3.1.	<i>Bare model: equivalent IDR capacity</i>	141
4.3.2.	<i>Infilled model: effective stiffness of infill panels</i>	143
4.4	APPLICATION EXAMPLES	146
4.4.1.	<i>Case study frames</i>	146
4.4.2.	<i>Modeling and analysis</i>	147
4.4.3.	<i>Ground motion records selection</i>	150
4.4.4.	<i>Results</i>	151
4.4.4.1	<i>Analysis of results: equivalent IDR</i>	152
4.4.4.2	<i>Analysis of results: effective stiffness for infill panels</i>	157
4.4.4.3	<i>Analysis of ASCE/SEI 41 approach</i>	163
4.5	SUMMARY	169
REFERENCES.....		171
CHAPTER 5		176
A NONLINEAR MACRO MODEL OF EXTERIOR RC JOINTS WITHOUT TRANSVERSE REINFORCEMENT UNDER SEISMIC LOAD		176
5.1	INTRODUCTION.....	178
5.2	EXPERIMENTAL DATABASE.....	181

5.2.1.	<i>Experimental investigations from literature</i>	181
5.2.2.	<i>Analysis of the collected database</i>	185
5.2.3.	<i>Experimental versus predicted joint shear strength</i>	186
5.2.4.	<i>Anchorage failure</i>	192
5.3	PROPOSED JOINT MODELING	195
5.3.1.	<i>Calibration of shear stress-strain relationship of the joint panel</i>	196
5.3.2.	<i>Bond slip spring</i>	205
5.4	VALIDATION BY EXPERIMENTAL TESTS	209
5.5	SUMMARY	225
APPENDIX 5: M_J-τ_J RELATIONSHIP		227
REFERENCES		229
CHAPTER 6		234
INFLUENCE OF JOINT RESPONSE ON SEISMIC ASSESSMENT OF NON-CONFORMING RC FRAMES		234
6.1	INTRODUCTION.....	236
6.2	STRUCTURAL MODELING	237
6.2.1.	<i>Beams and columns modeling</i>	239
6.2.2.	<i>Joints modeling</i>	241
6.2.2.1	<i>Exterior joints</i>	243
6.2.2.2	<i>Interior joints</i>	246
6.2.3.	<i>Post-processed failure modes</i>	248
6.2.3.1	<i>Shear failure in columns</i>	248
6.2.3.2	<i>Axial failure in beam-column joints</i>	251
6.2.4.	<i>Modeling limitations</i>	251
6.3	CASE STUDY FRAMES	252
6.4	SELECTED GROUND MOTION RECORDS AND PERFORMANCE LEVELS	262
6.5	PRELIMINARY NONLINEAR STATIC ANALYSES	265
6.5.1.	<i>OLD SLD frame</i>	265
6.5.1.1	<i>Rigid joints</i>	265
6.5.1.2	<i>With joints</i>	267
6.5.1.3	<i>Comparison</i>	268
6.5.2.	<i>GLD frame</i>	269
6.5.2.1	<i>Rigid joints</i>	269
6.5.2.2	<i>With joints</i>	271
6.5.2.3	<i>Comparison</i>	272
6.6	NONLINEAR DYNAMIC ANALYSES	274
6.6.1.	<i>OLD SLD frame</i>	275
6.6.1.1	<i>Rigid joints</i>	275
6.6.1.2	<i>With joints</i>	278
6.6.1.3	<i>Comparison</i>	281
6.6.2.	<i>GLD frame</i>	285
6.6.2.1	<i>Rigid joints</i>	285
6.6.2.2	<i>With joints</i>	287
6.6.2.3	<i>Comparison</i>	291
6.7	SUMMARY	295

APPENDIX 6: SELECTED GROUND MOTION RECORDS.....	298
REFERENCE	300
CHAPTER 7	302
EXPERIMENTAL INVESTIGATION ON EXTERIOR NON-CONFORMING BEAM-COLUMN JOINTS.....	302
7.1 INTRODUCTION.....	303
7.2 EXPERIMENTAL PROGRAM.....	304
7.2.1. <i>Specimens: design and construction</i>	304
7.2.2. <i>Materials</i>	309
7.2.3. <i>Test setup</i>	310
7.2.4. <i>Load Pattern</i>	313
7.3 ANALYSIS OF RESULTS	315
7.3.1. <i>Global response and observed damage</i>	316
7.3.1.1 <i>Beam lateral load versus drift</i>	316
7.3.1.2 <i>Observed damage</i>	319
7.3.1.3 <i>Dissipated energy</i>	332
7.3.2. <i>Local behavior</i>	335
7.3.2.1 <i>Joint panel response</i>	335
7.3.2.2 <i>Fixed-end-rotation</i>	338
7.3.2.3 <i>Beam bars strains</i>	343
7.3.2.4 <i>Bar buckling – Test #2</i>	346
7.4 COMMENTS AND COMPARISONS	348
7.4.1. <i>Strength models from literature</i>	348
7.4.2. <i>Comparison between experimental results and the proposed model</i>	350
7.5 SUMMARY.....	356
APPENDIX 7A: STRESS-STRAIN BEHAVIOR OF STEEL SAMPLES	357
APPENDIX 7B: EXPERIMENTAL DATA	358
APPENDIX 7C: DATA FROM STRAIN GAUGES ON BEAM LONGITUDINAL BARS	362
REFERENCES.....	366
CHAPTER 8	368
CONCLUSIONS AND FUTURE DEVELOPMENTS	368

List of figures

Figure 1.1. Critical components of under-designed RC frames.....	28
Figure 2.1. Classification: shear (a), flexure-shear (b), and flexural behavior (De Luca and Verderame 2015).....	37
Figure 2.2. Flexural modeling - adapted from Dierlein (2010)	39
Figure 2.3. Examples of modeling of columns shear behavior – Pincheira et al.(1999) (a), Lee and Elnashai (2000) (b), Jeon et al. (2015) (c), Elwood (2004) (d)	43
Figure 2.4. Models by Alath and Kunnath (1995)(a),Biddah and Ghobarah (1999) (b), Youssef and Ghobarah (2001)(c), Lowes and Altoontash (2003) (d),Altoontash (2004) (e), Sharma et al. (2011) (f)	53
Figure 2.5. Constitutive relationship proposed in literature: Priestley (1997) and Pampanin (2003) (a), Sharma et al. (2011) if anchorage failure occurs (b), Park and Mosalam (2013) (c)	56
Figure 2.6. Examples of FEM modeling (b), multi-struts (b, c), and equivalent strut (d) models for infills	60
Figure 2.7. Idealized pushover curve (Dierlein et al. 2003)	62
Figure 3.1. Uniformly infilled (a), Pilotis (b) and Bare (c) frames – four-storeys seismic loads design case-study structure.....	77
Figure 3.2. Panagiotakos and Fardis (1996): single-strut infill model.....	77
Figure 3.3. Load-displacement relationships of the infill trusses for median values of F_{infill} and D_{infill} (red), for the variation of F_{infill} respect to median values (blue) and for the variation of D_{infill} respect to median values (green).....	84
Figure 3.4. SPO (black), multi-linearized SPO (red) and IN2 in terms of $S_{ac}(T_{eff})$ (blue) curves, deformed shape and element damage at NC for Models#1 (4-storey SLD)	87
Figure 3.5. SPO (black), multi-linearized SPO (red) and IN2 in terms of $S_{ae}(T_{eff})$ (blue) curves, deformed shape and element damage at NC for Models#1 (4-storey GLD).....	88
Figure 3.6. Change in PGA capacity (%) respect to Model#1 due to variations of the assumed RVs – GLD case study structures: Uniformly Infilled – Upper values (blue) and Lower values (red) of RVs	91

List of figures

Figure 3.7. Change in PGA capacity (%) respect to Model#1 due to variations of the assumed RVs – GLD case study structures: Pilotis – Upper values (blue) and Lower values (red) of RVs	92
Figure 3.8. Change in PGA capacity (%) respect to Model#1 due to variations of the assumed RVs – GLD case study structures: Bare – Upper values (blue) and Lower values (red) of RVs.....	93
Figure 3.9. Change in PGA capacity (%) respect to Model#1 due to variations of the assumed RVs – SLD case study structures: Uniformly Infilled – Upper values (blue) and Lower values (red) of RVs	94
Figure 3.10. Change in PGA capacity (%) respect to Model#1 due to variations of the assumed RVs – SLD case study structures: Pilotis – Upper values (blue) and Lower values (red) of RVs	95
Figure 3.11. Change in PGA capacity (%) respect to Model#1 due to variations of the assumed RVs – SLD case study structures: Bare – Upper values (blue) and Lower values (red) of RVs.....	96
Figure 3.12. IN2 curves in terms of PGA – four-story SLD and GLD case study structures – Uniformly Infilled (red), Pilotis (black) and Bare (blue) configurations	100
Figure 3.13. IN2 curves in terms of PGA – eight-story SLD and GLD case study structures – Uniformly Infilled (red), Pilotis (black) and Bare (blue) configurations	101
Figure 3.14. IN2 curves in terms of PGA – four-story case study structures – GLD (cyan) and SLD (blue).....	103
Figure 3.15. IN2 curves in terms of PGA – eight-story case study structures – GLD (cyan) and SLD (blue).....	104
Figure 3.16. Percentage variation of PGA_{UI} with respect to PGA_B for GLD and SLD case study structures, at NC and DL LSs.....	106
Figure 3.17. (a) Fragility curves – GLD case study structures	111
Figure 3.18. (b) Fragility curves – SLD case study structures	114
Figure 3.19. Fragility curve at DL LS structure independent on direction – 4 storey GLD (a); AeDES results –4 storey RC structures with regularity in plan and infill distribution (b).....	117
Figure 3.20. Failure probabilities P_f in 50 years for SLD and GLD case study structures	119
Figure 4.1. Example of experimental response of the unreinforced infilled RC frame (by Calvi and Bolognini, 2001) (a); IDR values corresponding to DL LS from literature (b)	139

Figure 4.2. Schematic example of the procedure: research of the equivalent IDR capacity ($IDR_{DL,equiv}$)	142
Figure 4.3. Steps of the procedure: research of the effective stiffness for infill panels .	145
Figure 4.4. Schematic example of the result of the procedure: research of the effective stiffness for infill panels	145
Figure 4.5. Four story case-study infilled RC GLD (SLD) frame.....	147
Figure 4.6. Hysteretic behavior of RC members (a) and “simple hysteresis rule” (Fajfar et al. 2001) of infill panels (b).....	149
Figure 4.7. Force-drift envelope for infills in the case-study frames and drift ranges from literature (see Section 4.2).....	149
Figure 4.8. Equivalent IDR capacity (for $\alpha_{RC}=1$): 4-story GLD (a) and SLD (b) frames 8-story GLD (a) and SLD (b) frames	153
Figure 4.9. Equivalent IDR depending on the parameter α_{RC}	154
Figure 4.10. Equivalent IDR when IDR_{DL} is assumed equal to 1‰ (a) or 3‰ (b)	156
Figure 4.11 - IDR_{DL} to be assumed to obtain 5‰ equivalent IDR	157
Figure 4.12. Nonlinear IDAs and Linear IDA for α_w : 4-story GLD (a) and SLD (b) frames; 8-story GLD (c) and SLD (d) frames.....	159
Figure 4.13. IDR demand at each story - 4-story GLD (a) and SLD (b) frames, 8-story GLD (c) and SLD (d) frames	160
Figure 4.14. Variation of α_w depending on α_{RC} for GLD (a) and SLD (b) frames	161
Figure 4.15. Variation of width-to-diagonal length ratio depending on α_{RC} for GLD (a) and SLD (b) frames	163
Figure 4.16. Schematic example of the analysis of conservativeness of ASCE/SEI 41 approach.....	165
Figure 4.17. Analysis of the conservativeness of ASCE/SEI 41 approach (with $\alpha_{RC}=1$): 4-story GLD (a) and SLD (b) frames; 8-story GLD (a) and SLD (b) frames	167
Figure 5.1. Schematic representation of joint shear failure typologies prior to (J) or after than (BJ) beam yielding	179
Figure 5.2. Comparison between experimental and predicted joint shear strength for tests from database	189
Figure 5.3. Bond stress-slip model by Model Code 2010: local bond stress-slip relationship in case of pull-out failure (“other bond conditions”) (a); influence of steel strains (b) and transverse pressure (expressed as axial load ratio) (c).....	193
Figure 5.4. Longitudinal beam bar anchored into the joint core	195
Figure 5.5. Proposed joint modeling	196
Figure 5.6. Schematic proposed stress-strain relationship for joint panel	198

List of figures

Figure 5.7. Shear stress-strain envelopes for joints tested by Clyde et al. (2000) – BJ-failure (a) and Pantelides et al. (2002) – J-failure (b)	198
Figure 5.8. Proposed stress-strain relationship for joint panel (for J- and BJ-mode of failure) (a); comparison between proposed model and models by Celik and Ellingwood 2008 (b), Priestley 1997 (c), and Sharma et al. 2011 (d).	202
Figure 5.9. Rotation θ_s due to slip of end-hooked (a) and straight (b) longitudinal bars	207
Figure 5.10. Quadri-linear springs without (a) and with (b) anchorage failure	209
Figure 5.11. Numerical model for beam-column joint sub-assemblages simulations..	210
Figure 5.12. Comparisons between experimental and numerical results	213
Figure 5.13. Schematic sketch of the errors in terms of drift at 60% of the peak Force ($e[D_{60}]$), peak drift ($e[D_{peak}]$), and residual Force ($e[F_{res}]$).	215
Figure 5.14. Relative error in terms of peak drift ($e[D_{peak}]$), drift at 60% of the peak Force ($e[D_{60}]$), and residual Force ($e[F_{res}]$).	220
Figure 5.15. Comparisons between experimental and numerical results for tests which exhibited anchorage failure: El-Amoury-Ghobarah 2002 (a), Genesis JT1-3 2012 (b), Shafaei et al. 2014 (c), Murty et al. 2011 (d); gray dotted line identifies yielding of the beam.....	223
Figure 6.1. Adopted structural modeling	238
Figure 6.2. Monotonic backbone (a) and hysteretic degradation (b) in model by Haselton et al (2007).....	240
Figure 6.3. Pinching4 uniaxial material (Lowe et al. 2003)	243
Figure 6.4. Cyclic behavior calibration for tests by Pantelides (a, c, e, g); Clyde et al. (2000) (b, d, f, h). Experimental backbone and cyclic response are reported in red and grey, respectively; numerical cyclic response is reported in black.....	245
Figure 6.5. Case-study frames: frontal (a) and in plane (b) view	253
Figure 6.6. OLD SLD frame	256
Figure 6.7. GLD frame	257
Figure 6.8. Joint moment-rotation backbones for OLD SLD (a) and GLD (b) frames ..	262
Figure 6.9. Pseudo-acceleration spectra of the selected ground motion records	263
Figure 6.10. Characteristic points of columns (a) and joints (b) response	264
Figure 6.11. SPO curve and collapse mechanism – OLD SLD - rigid joints.....	266
Figure 6.12. IDR distributions and deformed configuration at peak load (a) and at last step (b) – OLD SLD - rigid joints.....	266
Figure 6.13. SPO curve and collapse mechanism – OLD SLD - with joints	267

Figure 6.14. IDR distributions and deformed configuration at peak load (a) and at last step (b) – OLD SLD - with joints	268
Figure 6.15. Comparison in terms of SPO curves – OLD SLD	269
Figure 6.16. SPO curve and collapse mechanism – GLD – rigid joints.....	270
Figure 6.17. IDR distributions and deformed configuration at peak load (a) and at last step (b) – GLD – rigid joints.....	270
Figure 6.18. SPO curve and collapse mechanism – GLD - with joints	271
Figure 6.19. IDR distributions and deformed configuration at peak load (a) and at last step (b) – GLD – with joints	272
Figure 6.20. Comparison in terms of SPO curves –GLD	273
Figure 6.21. IDA curves and median IDA – OLD SLD – rigid joints	275
Figure 6.22. Fragility curves at IO, SD, and CP LSs – OLD SLD – rigid joints	276
Figure 6.23. Fragility curves at FY, FC, FPC LSs - OLD SLD – rigid joints	277
Figure 6.24. IDA curves and median IDA – OLD SLD – with joints	278
Figure 6.25. Fragility curves at IO, SD, and CP LSs – OLD SLD – with joints.....	279
Figure 6.26. Fragility curves at FY, FC, FPC LSs - OLD SLD – with joints	279
Figure 6.27. Fragility curves at FcrJ, FpPJ, FPJ, and FRJ LSs - OLD SLD – with joints	280
Figure 6.28. Fragility curve at FAXJ – OLD SLD – with joints	281
Figure 6.29. Comparison between median IDA curves – OLD SLD.....	282
Figure 6.30. Comparison between fragility curves at IO, SD, and CP LSs – OLD SLD	282
Figure 6.31. Fragility curves at FSF with rigid joints (noJ) and with joints (wJ) in force-based approach (FSF_V) – OLD SLD	283
Figure 6.32. Fragility curves at FSF with rigid joints (noJ) and with joints (wJ) in displacement-based approach (FSF_IDR) – OLD SLD	284
Figure 6.33. IDA curves and median IDA – GLD – rigid joints.....	285
Figure 6.34. Fragility curves at IO, SD, and CP LSs – GLD – rigid joints.....	286
Figure 6.35. Fragility curves at FY, FC, FPC LSs - GLD – rigid joints.....	287
Figure 6.36. IDA curves and median IDA – GLD – with joints	288
Figure 6.37. Fragility curves at IO, SD, and CP LSs – GLD – with joints	289
Figure 6.38. Fragility curves at FY, FC, FPC LSs - GLD – with joints	289
Figure 6.39. Fragility curves at FcrJ, FpPJ, FPJ, and FRJ LSs - GLD – with joints	290
Figure 6.40. Fragility curve at FAXJ – GLD – with joints	291
Figure 6.41. Comparison between median IDA curves – GLD	292

List of figures

Figure 6.42. Comparison between fragility curves at IO, SD, and CP LSs - GLD	293
Figure 6.43. Fragility curves at FSF with rigid joints (noJ) and with joints (wJ) in displacement-based approach (FSF_IDR) - GLD	294
Figure 7.1. Geometry and reinforcement details - Test #1	306
Figure 7.2 . Geometry and reinforcement details - Test #2	307
Figure 7.3. Specimens construction	308
Figure 7.4. Test setup	311
Figure 7.5. Instrumentation layout	312
Figure 7.6. Linear potentiometers (LPs) on joint panel (a) and strain gauges location (b)	312
Figure 7.7. Test setup (a) and joint panel instrumentation (b)	313
Figure 7.8. Imposed displacement (a) and drift (b) history	314
Figure 7.9. Convention on sign of beam load, beam drift, joint shear strain and fixed-end-rotation	315
Figure 7.10. Beam lateral load-drift response - Test #1	317
Figure 7.11. Beam lateral load-drift response - Test #2	318
Figure 7.12. Evolution of damage - Test #1	322
Figure 7.13. Final damage state: joint panel and beam-joint interface - Test #1	323
Figure 7.14. Global response and corresponding damage states of the joint panel - Test#1	324
Figure 7.15. LPs displacements along the diagonals of the joint panel - Test #1	324
Figure 7.16. Joint cracking strength - Test #1	325
Figure 7.17. Evolution of damage - Test #2	329
Figure 7.18. Final damage state: joint panel and beam-joint interface - Test#2	329
Figure 7.19. Global response and corresponding damage states of the joint panel - Test#2	330
Figure 7.20. LPs displacements along the diagonals of the joint panel - Test #2	331
Figure 7.21 - Joint cracking strength - Test #2	332
Figure 7.22. Dissipated energy - Test #1	333
Figure 7.23. Dissipated energy - Test #2	333
Figure 7.24. Dissipated energy - comparison	334
Figure 7.25. Normalized dissipated energy - comparison	334

Figure 7.26. Joint shear strain calculation	336
Figure 7.27. Joint shear stress – strain experimental response – Test #1	337
Figure 7.28. Joint shear stress – strain experimental response – Test #2.....	338
Figure 7.29. Fixed-end-rotation measures for beam (a) and top and bottom columns (b)	339
Figure 7.30. Fixed-end-rotation related to the beam – Test #1	340
Figure 7.31. Fixed-end-rotation related to the top column	340
Figure 7.32. Fixed-end-rotation related to the bottom column – Test #1	341
Figure 7.33. Fixed-end-rotation related to the beam evaluated through LPs 50-5 and 50- 6 (a) or evaluated through LVDTs 037 and G (b) – Test #2.....	342
Figure 7.34. Fixed-end-rotation related to the top column – Test #2.....	342
Figure 7.35. Fixed-end-rotation related to the bottom column – Test #2.....	342
Figure 7.36. Sum of joint shear panel and beam fixed-end-rotation ($\theta_{s,tot}$) – Test #1....	343
Figure 7.37. Sum of joint shear panel and beam fixed-end-rotation ($\theta_{s,tot}$)– Test #2....	343
Figure 7.38. Beam bars strain – Test #1.....	344
Figure 7.39. Beam bars strain – Test #2.....	345
Figure 7.40. Bar buckling – Test #2.....	346
Figure 7.41. Hydraulic jack M2 acting on column.....	347
Figure 7.42. LVDT-F displacement versus beam lateral load V_b (a); LVDT-F displacement versus step (b)	347
Figure 7.43. Joint shear stress-strain: envelope and comparison between experimental response and strength models from literature - Test #1	348
Figure 7.44. Joint shear stress-strain: envelope and comparison between experimental response and strength models from literature - Test #2.....	350
Figure 7.45. Comparison between experimental and predicted joint response – Test #1	351
Figure 7.46. Comparison between experimental and predicted joint response – Test #2	352
Figure 7.47. Numerical simulation through proposed joint model in terms of joint panel cyclic response (experimental envelope) - Test #1	353
Figure 7.48. Numerical simulation through proposed joint model in terms of joint panel cyclic response (experimental envelope) - Test #2	353
Figure 7.49. Numerical simulation through proposed joint model in terms of load-drift envelope - Test #1	354

List of figures

Figure 7.50. Numerical simulation through proposed joint model in terms of load-drift envelope - Test #2355

List of tables

Table 2.1. Joint shear coefficients according to ASCE-SEI 41 (2007)	45
Table 3.1. Joint shear coefficient according to ASCE-SEI 41 (2007).....	83
Table 3.2. Stories involved in the collapse mechanism for the Models#1 of each analyzed structure	89
Table 3.3. Stories involved in the achievement of DL LS for the Models#1 of each analyzed structure	89
Table 3.4 Effects and remarks about sensitivity analysis -	97
Table 3.5. Effects and remarks about sensitivity analysis -	98
Table 3.6. Random Variables assumed to evaluated fragility curves	108
Table 3.7 Estimated parameters of the cumulative lognormal distributions fitting the fragility curve	115
Table 3.8. Failure probabilities P_f in 50 years for SLD and GLD case study structures	121
Table 4.1. Mechanical properties of RC and Infill	150
Table 4.2. Selected ground motion records	151
Table 4.3. Elastic periods of infilled frames; PGA and $S_a(T_1)$ capacity at DL LS.....	151
Table 4.4. Equivalent IDR if $IDR_{DL}=2.2 \text{ ‰}$	154
Table 4.5. Equivalent IDR if $IDR_{DL}=1 \text{ ‰}$ or $IDR_{DL}=3 \text{ ‰}$	155
Table 4.6. IDR_{DL} to be assumed to obtain 5‰ equivalent IDR.....	157
Table 4.7. Obtained values of α_w (with $\alpha_{RC}=1$) and corresponding elastic periods.....	158
Table 4.8. Variation of α_w depending on α_{RC}	160
Table 4.9. Analysis of the conservativeness of ASCE/SEI 41 approach depending on the parameter α_{RC}	168
Table 5.1. Experimental database of planar unreinforced RC beam-column joints - no-anchorage failure.....	190
Table 5.2. Experimental database of planar unreinforced RC beam-column joints - anchorage failure.....	191
Table 5.3. Stress-strain relationships for joint panel for BJ- and J-mode of failure	199

List of tables

Table 5.4. Summary of the proposed backbone for the joint panel.....	201
Table 5.5. Comparison between the proposed model and other models from literature in terms of γ_j	204
Table 5.6. Experimental values and percentage errors (e) of peak drift (D_{peak}), for the proposed model (Prop.), models by Celik and Ellingwood (C&E), Park and Mosalam (P&M), Priestley (Priest.) and ASCE	217
Table 5.7. Experimental values and percentage errors (e) of drift at 60% of the peak Force (D_{60}) for the proposed model (Prop.), models by Celik and Ellingwood (C&E), Park and Mosalam (P&M), Priestley (Priest.) and ASCE	218
Table 5.8. Experimental values and percentage errors (e) of residual Force (F_{res}) for the proposed model (Prop.), models by Celik and Ellingwood (C&E), Park and Mosalam (P&M), Priestley (Priest.) and ASCE	219
Table 5.9. Experimental values and percentage errors (e) of peak force (F_{peak}) and peak drift (Δ_{peak}) for the proposed model (Prop.) - anchorage failure.....	224
Table 6.1. Parameters adopted to reproduce the hysteretic behavior of exterior unreinforced joints in Pinching4 material	246
Table 6.2. Geometric dimensions of the case-study frames	253
Table 6.3. Dead and live loads applied for design and assessment	253
Table 6.4. Material properties.....	255
Table 6.5. Flexural and shear characterization of exterior columns - OLD SLD.....	258
Table 6.6. Flexural and shear characterization of interior columns - OLD SLD.....	258
Table 6.7. Main properties related to beams - OLD SLD	259
Table 6.8. Beam/column hierarchy and joints classification - OLD SLD	259
Table 6.9. Flexural and shear characterization of exterior columns - GLD	260
Table 6.10. Flexural and shear characterization of interior columns - GLD.....	260
Table 6.11. Main properties related to beams - GLD.....	261
Table 6.12. Beam/column hierarchy and joints classification - GLD	261
Table 6.13. IDR thresholds for the selected performance levels	263
Table 6.14. Additional LSs acronyms	264
Table 6.15. Elastic periods - OLD SLD frame	265
Table 6.16. Comparison in terms of peak base shear and peak displacement in SPO - with joint (wJ) and rigid joints (noJ) - OLD SLD.....	268
Table 6.17. Elastic periods - GLD frame	269

Table 6.18. Comparison in terms of peak base shear and peak displacement in SPO – with joint (wJ) and rigid joints (noJ) - GLD	272
Table 6.19. Fragility parameters at IO, SD, and CP LSs - OLD SLD – rigid joints	276
Table 6.20. Fragility parameters at FY, FC, FPC LSs - OLD SLD – rigid joints.....	277
Table 6.21. Fragility parameters at IO, SD, and CP LSs - OLD SLD – with joints.....	279
Table 6.22. Fragility parameters at FY, FC, FPC, FcrJ, FpPJ, FPJ, and FRJ LSs – OLD SLD – with joints	280
Table 6.23. Fragility parameters at FAXJ LSs – OLD SLD – with joints	281
Table 6.24. Comparison between median Sa(T ₁) capacity with rigid joints (noJ) and with joints (wJ) – OLD SLD	283
Table 6.25. Fragility parameters at FSF LS – OLD SLD	284
Table 6.26. Fragility parameters at IO, SD, and CP LSs - GLD – rigid joints	286
Table 6.27. Fragility parameters at FY, FC, FPC LSs - GLD – rigid joints	287
Table 6.28. Fragility parameters at IO, SD, and CP LSs - GLD – with joints	289
Table 6.29. Fragility parameters at FY, FC, FPC, FcrJ, FpPJ, FPJ, and FRJ LSs – GLD – with joints.....	290
Table 6.30. Fragility parameters at FAXJ LSs – GLD – with joints.....	291
Table 6.31. Comparison between median Sa(T ₁) capacity with rigid joints (noJ) and with joints (wJ) – GLD	293
Table 6.32. Fragility parameters at FSF LS – GLD	294
Table 7.1. Properties of concrete	309
Table 7.2. Properties of steel	309
Table 7.3. Pattern load program.....	314
Table 7.4. “Peak points” and yielding beam load	318
Table 7.5. Description of the evolution of damage during Test #1	323
Table 7.6. Beam lateral load, displacement, drift and secant stiffness corresponding to joint cracking – Test #1.....	325
Table 7.7. Description of the evolution of damage during Test #2.....	330
Table 7.8. Beam lateral load, displacement, drift and secant stiffness corresponding to joint cracking – Test #2.....	332
Table 7.9. Experimental strength and models from literature – Test #1	349
Table 7.10. Experimental strength and models from literature - Test #2.....	350
Table 7.11. Characteristic points of joint stress-strain “predicted” response – Test #1	351

Table 7.12. Characteristic points of joint stress-strain “predicted” response – Test #2
.....352

Chapter 1

INTRODUCTION

1.1 Motivation

Among the natural hazards, earthquakes are paramount due to their impact on civil structures worldwide. The considerable direct economic losses (property losses) due to earthquakes in conjunction with social impact and indirect economic losses have prompted a great interest in performance assessment of the civil structures to future seismic events. Therefore, performance evaluations beyond the traditional goal of life safety, are required to rightly estimate expected losses.

Realistic losses evaluations require more accurate seismic risk assessment tools, in order to help decision- and policy-makers both in pre-earthquake planning to mitigate probable losses and in post-earthquake planning to develop emergency response and recovery strategies.

Performance-Based Earthquake Engineering (PBEE) seeks to improve seismic risk decision-making through assessment and design methods that are transparent, scientific, and informative to stakeholders (Dierlein et al. 2003), defining performance metrics that are relevant to decision making for seismic risk mitigation and loss estimation. Generally speaking, these metrics reflect direct dollar losses (repair and restoration costs), loss in functionality (or downtime), and risk of casualties. According to a performance-based approach, modern seismic codes worldwide define performance levels aimed at avoiding collapse under major earthquakes and ensuring control and limitation of damage under more frequent but less severe earthquakes, in order to minimize economic and functionality losses.

In this framework, seismic vulnerability and risk assessment of buildings and other structures are essential, starting from the characterization of earthquake hazard, and going on with determination of structural response

(structural demand), identification of performance limits (structural capacity), and degrees of structural damage and losses associated with specific damage states. A key ingredient of this evaluation process is the fragility, that describes the probability of failure to meet a performance objective depending on demand on the system, providing the link between seismic hazard and building loss estimation.

In particular, a correct fragility evaluation necessitates the development of reliable nonlinear analysis models that are able to simulate the behavior of structures from the onset of damage through collapse. These models have to provide engineering demand parameters that are then related with damage measures and describe the damage of a building and its components. To accurately simulate dynamic response of structures up to collapse, it is important to model as well as possible all critical components, by calibrating or validating models on the basis of large sets of experimental data.

Therefore, proper prediction of the nonlinear behavior and formulation of analytical models are essential prerequisites for a reliable evaluation of structural fragility and, then, of seismic performance and risk assessment of RC structures. Moreover, within the performance-based approach, it is also essential to understand which mechanisms/elements have the higher influence on seismic performance depending on the analyzed performance level.

A lot of work should still be done towards this direction, especially for existing structures, designed for gravity loads only or according to obsolete seismic and technical codes, that are referred to as under-designed hereinafter.

In fact, previous experimental and analytical studies about seismic performance of under-designed RC buildings, as well as related previous research in the areas of seismic vulnerability and risk assessment, highlighted a very high vulnerability of existing structures, revealing a salient influence of masonry infills, shear-dominated columns, and beam-column joints (Figure 1.1).

Past seismic events and experimental or numerical tests proved these deficiencies, as briefly discussed below.



Figure 1.1. Critical components of under-designed RC frames

During L'Aquila earthquake (6th April 2009), for example, most of the damage involved infill panels and documented building collapses were essentially caused by irregularities in plan or elevation caused also by infills distribution (Ricci et al., 2010). Moreover, during Lorca earthquake (2011), most of the losses were caused by non-structural damage (Cabañas et al., 2011; Goula et al., 2011) and masonry infills have provided an important additional strength to RC buildings - especially because no proper seismic principle was present in the design of most of Lorca RC buildings - avoiding in many cases the collapse of the structure (Gómez-Martínez et al., 2012). Nevertheless they are generally considered as non-structural elements and not included in numerical models, masonry infills are critical components both in under-designed and also new-codes-conforming structures, because of

- (i) the onset of possible local interaction effects between infill panel and the surrounding frame (Shing et al. 2002, Verderame et al. 2011),
- (ii) possible out-of-plane failures, causing high economic loss and a danger for life-safety (Morandi et al. 2013),

(iii) the localization of displacement demand, favoring local or partial collapse mechanisms, thus reducing structural displacement capacity (Dolsek et al. 2001).

Damage observed after the most recent earthquakes (e.g. L'Aquila earthquake 2009) and experimental investigations highlighted also the vulnerability of the beam-column joint region (Ricci et al, 2010, Bayhan et al 2013), especially if no transverse reinforcement are present, and columns that can experience brittle failures (Elwood 2004, Ricci et al 2010). From this point of view, under-designed structures are usually characterized by

(i) little amount or no transverse shear reinforcement within the beam-column joints leading to high damage level in joint panel zone and shear failure of the joint that can evolve up to axial failure (Pessiki et al. 1990, Beres et al. 1992, 1996, Hassan 2011),

(ii) a short embedment length of bottom reinforcement in the beams within the beam-column joints leading to premature anchorage failure (Hassan 2011),

(iii) columns that have bending moment capacities that are close to or less than those of the joining beams, promoting column-sidesway or soft-story mechanisms (Aycardi et al. 1992, 1994),

(iv) low longitudinal reinforcement ratio in columns (Celik 2007),

(v) minimal transverse reinforcement amount in columns to provide an adequate shear resistance and confinement, leading to likely shear failures (Elwood, 2004).

1.2 Research Objectives

Starting from the analysis of typical deficiencies of non-ductile RC frames and the definition of performance levels of interest, this work aims to contribute to PBEE framework with (i) a critical overview on analysis methodologies and analytical modeling of the salient components of RC frames, namely flexural or shear-dominated beams and columns, and more in detail, beam-column joints and masonry infills, the core of this work, and (ii) with new proposals in terms of nonlinear modeling and analyses procedures to provide a more reliable evaluation of seismic performance and risk assessment

of infilled RC structures, accounting for structural and non-structural elements, at different performance levels. It is worth highlighting that only masonry infills will be considered as non-structural elements in this study, even if also other typologies of non-structural components (such as internal partitions, ceilings, electrical equipment and other building contents) can play a very important role in losses estimation.

For these purposes, existing analytical modeling techniques for RC frames' critical components are first reviewed and discussed.

Then, a deep investigation on the influence of infills on seismic performance at different limit states, also for new constructions, is carried out, in order to highlight the critical points that can interest also this kind of structures regarding infill presence.

The effect of infills on the global seismic behavior of RC frames is investigated, by analyzing their influence on global stiffness and strength, on the kind of collapse mechanism, on the displacement capacity and, consequently, on seismic capacity and seismic fragility at different performance levels (or Limit States (LSs)), depending on the main characteristics of the RC frame, such as the design typology and the number of stories.

Recognized the importance of infills especially at lower seismic intensity and the widespread of linear analysis methodology among practitioner, new procedures are proposed as tools to better taking into account damage to infills also in linear analyses with or without the explicit modeling of infills in the numerical model. The attention has been focused both on the design of new constructions and the assessment of existing structures, providing a contribution towards desirable more comprehensive future code prescriptions - that depend on mechanical properties of infills and proper displacement capacity thresholds - at lower seismic intensity within the context of linear analyses.

In particular, when infills take explicitly part of the numerical model, the attention is focus on the evaluation of an effective stiffness to assign to infill panels, to perform linear analyses. If infill panels are not included into the numerical model, limitation of damage to infills should be pursued through a proper limitation of displacement demand to the structure.

From the point of view of the bare structure (without infills in the structural

model) and in particular referring to higher intensity levels, proceeding from Damage Limitation (DL) LS towards Near Collapse (NC) LS, the analysis of RC frames different for design typology has highlighted the vulnerability points of such frames, already pointed out by experimental tests and past seismic events.

In particular the influence of beam-column joints (in particular exterior joints) is deeper investigated.

In fact, in literature there is not yet a commonly accepted approach for the determination of the shear strength and for nonlinear modeling of RC beam-column joints in moment resisting RC frames. In many studies, beam-column connections are modeled as rigid. However, many nonlinear joint models are available, but most of them may be unsuitable for modeling all sources of nonlinearity for the assessment of older concrete buildings. Some of them were developed and calibrated for confined beam-column joints or they are too complicated to implement.

On the basis of an extensive and critical review of previous experimental tests and existing joint modeling approaches, a new cyclic shear constitutive relationship is proposed for exterior unreinforced joints, different for failure typology, in order to describe nonlinear behavior of joint panels, to be used in conjunction with an explicit bond-slip spring, thus taking into account all sources of nonlinearity and different possible kinds of deficiencies.

Then, the influence of joint behavior on seismic performance at different performance levels, also taking into account the record-to-record variability, was investigated in nonlinear dynamic analysis of under-designed frames both in terms of strength and deformability contribution, while shear failure detected in columns, other critical points of such frames, is post-processed.

Finally, investigated the sensitivity of joint response to the main mechanical and geometrical properties of beam-column sub-assemblages, two experimental tests with deformed bars and different failure typology were designed and conducted under cyclic loading to improve the understanding of exterior joints seismic performance without transverse reinforcement in existing RC buildings. Experimental results are analyzed herein and compared with numerical results carried out through the adoption of the proposed numerical model.

1.3 Dissertation outline

Firstly, analytical modeling techniques for frame's critical components in non-ductile RC structures are reviewed and discussed. An overview on analytical modeling of the salient components of RC frames, namely flexural or shear-dominated beams and columns, and more in detail, beam-column joints and masonry infills, is carried out in **Chapter 2**.

Then, focusing the attention on elements that are commonly defined as non-structural, the influence of infill panels on seismic performance of RC buildings, different for design typology and infills configuration, has been investigated in **Chapter 3** at different performance levels within a static nonlinear framework. A simple modeling of RC elements was adopted in lumped plasticity approach and nonlinear behavior of beam-column connection is not taken into account.

Recognized the great importance of infills and their mechanical properties especially at low level of seismic demand, a deeper investigation on the role of infills at Damage Limitation Limit State was carried out, developing new procedures to account for infill presence directly or indirectly via linear analyses, as shown in **Chapter 4**.

As far as the critical points in the bare structure are concerned, in **Chapter 5** a deep investigation on joint behavior and related modeling issues is carried out, leading to a new proposal for modeling nonlinear behavior of exterior joints without transverse reinforcement.

In **Chapter 6**, the proposed joint model was applied in nonlinear dynamic analyses of RC frames, in conjunction with modeling proposals from literature for interior joints and beam/column behavior, considering the record-to-record variability and also highlighting the importance of column shear failures in under-designed RC buildings.

Finally, analysis results of experimental quasi-static tests conducted on two beam-column joint specimens with deformed bars and different failure typology are shown and commented in **Chapter 7**.

References

- Aycardi LE, Mander JB, Reinhorn AM (1992). Seismic resistance of reinforced concrete frame structures designed only for gravity loads: Part II — Experimental performance of subassemblages, Technical Report NCEER-92-0028, National Center for Earthquake Engineering Research, State University of New York at Buffalo, Buffalo, NY.
- Aycardi LE, Mander JB, Reinhorn AM (1994). Seismic resistance of reinforced concrete frame structures designed only for gravity loads: Experimental performance of subassemblages, *ACI Structural Journal* 91(5): 552–563.
- Bayhan, B., Mochle, J. P., Yavari, S., Elwood, K. J., Lin, S. H., Wu, C. L., and Hwang, S. J. (2013). Seismic response of a concrete frame with weak beam-column joints. *Earthquake Spectra*.
- Beres A, Pessiki SP, White RN, Gergerly P (1996) Implications of experiments on the seismic behavior of gravity load designed RC beam-to-column connections, *Earthquake Spectra* (EERI) 12(2): 185–198.
- Beres A, White RN, Gergely P (1992). Seismic behavior of reinforced concrete frame structures with nonductile details: Part I — Summary of experimental findings of full scale beam-column joint tests, Technical Report NCEER-92-0024, National Center for Earthquake Engineering Research, State University of New York at Buffalo, Buffalo, NY.
- Cabañas, L., Carreño, E., Izquierdo, A., Martínez, J.M., Capote, R., Martínez, J., Benito, B., Gaspar, J., Rivas, A., García, J., Pérez, R., Rodríguez, M.A., Murphy, P. (2011). Informe del sismo de Lorca del 11 de mayo de 2011. IGN, UCM, UPM, IGME, AEIS, available at <http://www.ign.es/ign/resources/sismologia/Lorca.pdf> (in Spanish)
- Celik, Ozan Cem. (2007). Probabilistic assessment of non-ductile reinforced concrete frames susceptible to Mid-America ground motions.
- Deierlein, G. G., Krawinkler, H., and Cornell, C. A. (2003). A framework for performance-based earthquake engineering. In *Pacific conference on earthquake engineering* (pp. 1-8).
- Dolšek, M., Fajfar, P. (2001). Soft storey effects in uniformly infilled reinforced concrete frames. *Earthquake Engineering*, 5(1), 1-12.
- Elwood, Kenneth J. (2004). Modelling failures in existing reinforced concrete columns. *Canadian Journal of Civil Engineering* 31.5 2004: 846-859.
- Gómez-Martínez, F. , Pérez-García, A., De Luca, F. , Verderame, G.M. , Manfredi G. (2012). Preliminary study of the structural role played by masonry infills on RC building performances after the 2011 Lorca, Spain, earthquake, proceedings of 15th WCEE, Lisbon, 24-28 September 2012.
- Goula, X., Figueras, S., Irizarry, J., Macau, A., Barbat, A., Lantada, N., Carreño, M.L., Valcárcel, J., Combescure, D., Belvaux, M., Monfort, D., Bremond, S., Verrhiest, G., Camares, C., Bairrao, R. (2011). Rapport de la mission AFPS du séisme de Lorca, available at <http://www.afps-seisme.org/index.php/fre/Seismes-majeurs/Seisme-a-Lorca>. (in Spanish)
- Hassan WM (2011). Analytical and Experimental Assessment of Seismic Vulnerability of Beam-Column Joints without Transverse Reinforcement in Concrete Buildings, PhD Dissertation, University of California, Berkeley, California, USA.

- Morandi, Paolo, Sanja Hak, and Guido Magenes (2013). Simplified out-of-plane resistance verification for Slender clay masonry infills in RC frames. 15th National Conference ANIDIS. 2013.
- Pessiki SP, Conley CH, Gergely P, White RN (1990). Seismic behavior of lightly reinforced concrete column and beam-column joint details, Technical Report NCEER-90-0014, National Center for Earthquake Engineering Research, State University of New York at Buffalo, Buffalo, NY.
- Ricci P., De Luca F., Verderame G.M. (2010), 6th April 2009 L'Aquila earthquake, Italy: reinforced concrete building performance, *Bulletin of Earthquake Engineering*, 9(1), 285-305.
- Shing, P. Benson, and Armin B. Mehrabi (2002). Behaviour and analysis of masonry-infilled frames. *Progress in Structural Engineering and Materials* 4.3: 320-331.
- Verderame, G. M., De Luca, F., Ricci, P., and Manfredi, G. (2011). Preliminary analysis of a soft-storey mechanism after the 2009 L'Aquila Earthquake. *Earthquake Engineering & Structural Dynamics*, 40(8), 925-944.

Chapter 2

BACKGROUND AND CRITICAL ISSUES IN MODELING OF NON-DUCTILE RC BUILDINGS

Proper prediction of the nonlinear behavior of the component of RC frames and formulation of reliable analytical models are essential prerequisites for the evaluation of seismic performance of RC structures.

For this purpose, existing analytical modeling techniques for frames' critical components are first reviewed and discussed. In particular, an overview on analytical modeling of the salient components of RC frames, namely flexural or shear-dominated beams and columns, and more in detail, beam-column joints and masonry infills, the core of this work, is carried out.

These models are discussed herein and they will be applied in next chapters in the finite element models of RC frames for nonlinear analyses in different approaches depending on the objective that it is intended to pursue, and with the addition of new proposals.

2.1 Modeling of critical components

2.1.1. Beam/column elements

2.1.1.1 Classification issue

Nonlinear behavior of RC elements strictly depends on their failure typology and, thus, on the interaction between external force acting on them. Flexural response of a RC element can be “limited” because of the onset of a premature shear failure and, in reverse, shear capacity can decrease because of the cyclic degradation of shear resistance contributions due to the increase in ductility demand after yielding.

Three different failure modes can be identified for a RC column, as a result of the adoption of a degrading shear capacity model (Figure 2.1).

When the initial non degraded shear strength is lower than plastic shear capacity (Figure 2.1a), shear failure occurs limiting flexural response, namely deformation capacity or energy dissipation capacity, and causing a significant sudden strength reduction.

When the degraded shear strength is higher than the plastic shear (Figure 2.1c), the flexural response can completely develop, without interaction with shear, exhibiting high ductility capacity up to the onset of degrading phenomena as bar buckling or concrete crushing and cover spalling.

In all the other cases, the element can reach yielding, but the inelastic flexural response is modified by the onset of a post-yielding shear failure (Figure 2.1b).

Anyway, after shear failure, the behavior of the element becomes strongly degrading up to the loss of axial load carrying capacity.

Thus, the behavior of a RC element can be classified on the basis of the ratio between plastic shear capacity and degrading shear strength. Several models have been developed to represent the degradation of shear strength with increasing inelastic ductility demand (Priestley et al. 1994, Biskinis et al., 2004; Sezen and Moehle, 2004). Nevertheless, further literature researches (Zhu et al., 2007, Elwood et al., 2007) and some code prescriptions (e.g. ASCE/SEI 41 – Supplement 1) proved that the failure mode classification cannot be adequately carried out on the basis only on the shear strength capacity and introduced a classification based also on other key parameters, e.g. transverse reinforcement ratio or stirrups-spacing-to-section-depth ratio.

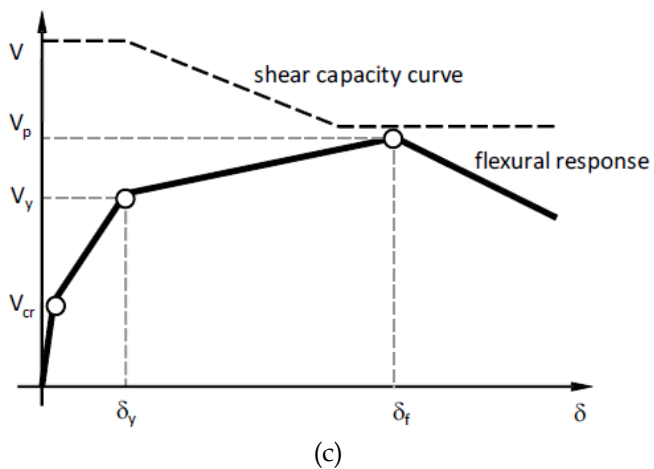
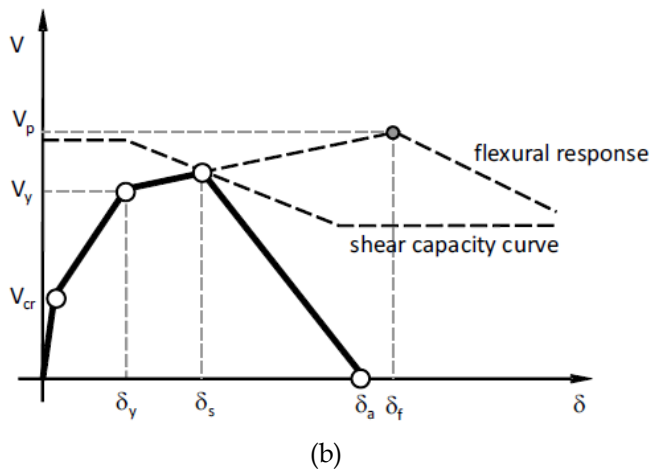
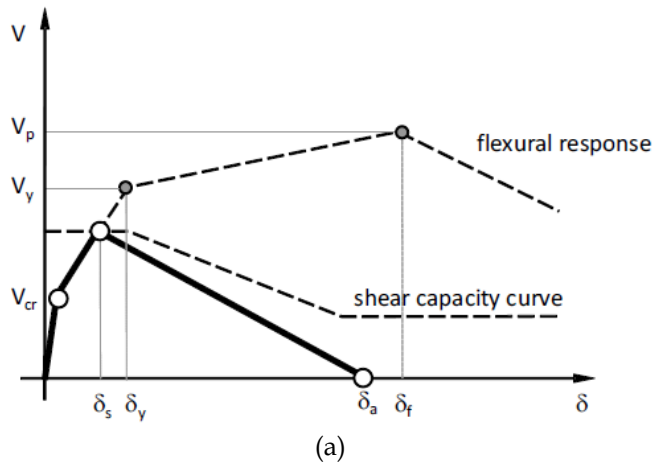


Figure 2.1. Classification: shear (a), flexure-shear (b), and flexural behavior (De Luca and Verderame 2015)

2.1.1.2 Flexural behavior

Inelastic structural component models can be differentiated depending on how plasticity is distributed along the member length and through the member cross section.

The most complex models discretize the element along its length and through the cross sections into micro- finite elements (Figure 2.2a) with nonlinear hysteretic constitutive properties that can have many input parameters, thus offering a great versatility, but also requiring a great effort in terms of model parameter calibration and computational resources.

Reducing the complexity level, the fiber formulation models distribute plasticity by numerical integrations through the member cross sections and along the member length (Figure 2.2b). Uniaxial material models are adopted to define the nonlinear hysteretic axial stress-strain behavior in the cross sections. The Bernoulli hypothesis on plane section is assumed, and uniaxial material “fibers” are numerically integrated over the cross section to obtain stress resultants (axial force and moments) and incremental moment-curvature and axial force-strain relations. The cross section parameters are then integrated numerically at discrete sections along the member length, using displacement or force interpolation functions (Kunnath et al. 1990, Spacone et al. 1996). Distributed fiber formulations provide strains in the steel and concrete cross section fibers, instead than plastic hinge rotations, and the calculated strain demands can be quite sensitive to element length, integration method, and strain hardening parameters.

A further step to reduce complexity and computational efforts is represented by the “finite length hinge model” (Figure 2.2c). This modeling approach is an efficient distributed plasticity formulation where hinge zones at the member ends are pre-defined. Cross sections in the inelastic hinge zones are characterized through either nonlinear moment-curvature relationships or explicit fiber-section integrations assuming Bernoulli hypothesis on plane section. If hinge length is well designed, integration of deformations along the hinge length captures the spread of yielding more realistically than the concentrated hinges, and the finite hinge length facilitates calculation of hinge rotations.

The simplest models concentrate the inelastic deformations at the ends of the element, such as through a rigid-plastic hinge or an inelastic spring with hysteretic properties (Figure 2.2d and Figure 2.2e). These elements have

numerically efficient formulations thanks to the concentration of the plasticity in zero-length hinges with moment-rotation model parameters.

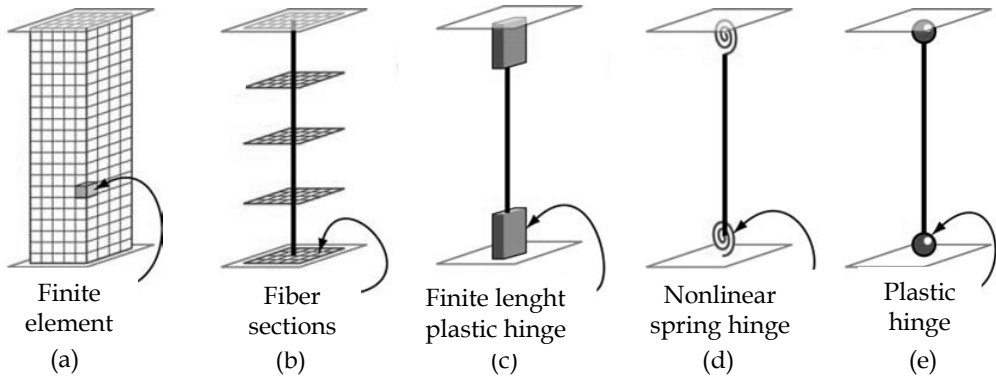


Figure 2.2. Flexural modeling - adapted from Dierlein (2010)

Fiber and finite element models capture the axial force-moment (P-M) interaction directly, while concentrated and finite length hinge models may consider the P-M response through yield surfaces. On the other hand, the detailed fiber and finite element models are not necessarily capable of modeling effects such as degradation due to reinforcing bar buckling and fracture that can be captured by simpler phenomenological models.

In fact, distributed plasticity formulations are able to model stress and strain variations through the section and along the member accurately, but important local phenomena, such as strength degradation due to local buckling of reinforcing bars, or the nonlinear interaction of flexural and shear, are difficult to capture without sophisticated and numerically intensive models. Vice-versa, models based on empirically-defined concentrated hinge may be more suitable to capture the nonlinear degrading response of members through the calibration of phenomenological moment-rotation relationships and hysteresis rules, using member test data, with the same or lower approximation of more sophisticated formulations.

Concentrated hinge models obviously require a pre-determination of backbone relationships between characteristic forces and deformations of structural components, together with the associated hysteresis rules, to define component behavior, demand parameters, and acceptance criteria.

In the adoption of such pre-defined backbones, when a nonlinear analysis

have to be performed, it is important to distinguish between “monotonic” and “cyclic envelope” curves. The former represents the response that would be observed for a component tested under monotonic loading, the latter represents the forces-displacements behavior under cyclic loading, depending on the applied cyclic loading history.

When the cyclic effects of earthquake loading are not modeled directly in the analysis, e.g. in nonlinear static analyses, the nonlinear component models should be defined based on the degraded cyclic envelope. For nonlinear dynamic analysis, the choice of components curves depends on how cyclic degradation is modeled. Direct modeling of cyclic degradation begins with a monotonic backbone curve and degrades this relationship as the analysis proceeds (Ibarra et al. 2005, Haselton et al. 2007). In indirect modeling approach, the component backbone curve does not degrade and it is defined as the cyclic envelope, already including cyclic strength degradation.

Additional springs can be added to the flexural model in order to take into account also shear behavior, as explained in next Section, or bond-slip of longitudinal reinforcing bars.

Since its computational efficiency and its capability to capture flexural behavior up to the loss of vertical loads carrying capacity, and also other deformability contributions as fixed-end-rotation or shear deformability, a lumped plasticity approach will be adopted in next Chapters..

2.1.1.3 Shear behavior

As explained above, to develop flexural behavior, the member shear strength must be larger than the flexural strength, which is the condition typically required in capacity design provisions for seismic design. Where the shear strength is not sufficient to preclude shear failure (such as in most of the existing buildings), shear effects must be considered in the analysis model in addition to flexural and axial load effects.

RC columns in buildings designed for gravity loads only or according to old seismic codes provisions are in most cases shear-dominated columns.

Once this shear failure is triggered before or after flexural yielding, shear and deformation capacities are progressively lost. Existing column’s shear failure models are briefly presented and discussed herein.

Simpler attempts to capture the shear failure in columns were based on a

post-processing of analyses results in which only flexural behavior is explicitly modeled (Otani and Sozen, 1972, Spacone et al., 1996, Liel et al. 2010). This approach is able to detect shear failure in a force-approach, but it does not properly estimate inelastic shear deformations and degrading behavior after shear failure.

A fairly straightforward approach to model shear effects is represented by the introduction of a nonlinear shear spring in series with the axial-flexural model (Pincheira et al. 1999, Lee and Elnashai 2001, Sezen and Chowdhury 2009, Jeon et al 2015). The definition of the backbone curve characterizing this shear spring can be based on the modified compression field theory (MCFT) (Vecchio and Collins, 1986) or on drift capacity at shear failure.

When the MCFT is adopted, only the backbone curve of shear model up to the point of maximum strength can be analytically predicted, and therefore additional assumptions to define the shear strength degradation are required. Pincheira et al. (1999) added a zero length shear spring that can account for the strength and stiffness degradation with increasing deformation demand (Figure 2.3a). The model is able to represent flexure or shear failure under monotonically increasing or reversed cyclic loading and stiffness degradation with cyclic loading can also be represented. Although the procedure they suggested to solve the convergence issue, it can be very computationally demanding and may not predict the dynamic characteristics of a softening structure.

Lee and Elnashai (2001) also utilized the MCFT to define the backbone curve of the shear spring and developed hysteretic rules including the variation of column axial loads (Figure 2.3b).

Sezen and Chowdhury (2009) developed the hysteretic model including the flexure-shear-axial interaction based on the backbone curve obtained from the MCFT, and also employed the bond-slip model developed by Sezen and Moehle (2003).

Jeon et al. (2015) simulated shear response by means of a zero-length shear spring located at one end of the column (Figure 2.3c). Shear failure begins once the column shear demand exceeds the column shear not-degraded capacity. The adopted shear strength prediction derives from the ASCE 41-06 shear strength model but it does not take into account the possible degradation of shear strength capacity with increased ductility demand.

Some shear strength models (Sezen 2002, Biskinis et al. 2004) calibrated on empirical data are useful for estimating the column shear strength as a function of inelastic ductility demand. However, they do not provide a reliable estimate of the drift capacity at shear failure (Elwood and Moehle 2005). Nevertheless, models that predict drift capacity for columns experiencing shear failure prior to or after than flexural yielding can be found in literature (Pujol et al. 1999, Elwood and Moehle 2005).

Pujol et al. (1999) proposed a drift capacity model for shear-critical columns by means of a statistical evaluation of an experimental database of 92 columns, also including columns with quite high transverse reinforcement ratios (higher than 0.01), thus not suitable for non-ductile columns.

Elwood and Moehle (2005) proposed an empirical drift capacity model, more inherent to non-ductile elements, by using a database of 50 flexure-shear-critical RC columns with configurations representative of those used in pre-1970s American buildings.

Later, on the basis of this drift capacity model, Elwood (2004) developed a drift-based shear failure model (the so-called “limit state material”) that can identify a shear failure associated with column shear and column’s total deformation by means of a shear spring in series with a nonlinear beam-column element (Figure 2.3d). The limit state material has a predefined tri-linear backbone curve and five parameters to define pinching and stiffness degradation; the limit state material changes the backbone of the material model to include strength degradation once the response of the beam-column element exceeds a predefined limit curve. However, a limited number of comparison studies with experimental results make it difficult to accurately validate the limit curve (Jeon 2013). Additionally, in an analytical model of a frame structure, where the column ends are not fully restrained against rotation, the computed interstory drift will include a rigid body rotation component not present in the experiments used to develop the shear and axial capacity models (Elwood and Moehle 2005).

LeBorgne (2012) extended the model of Elwood (2004) to estimate the lateral strength degrading behavior of RC columns prone to shear failure through a rotation-based shear failure model that triggers shear failure once either a shear capacity or a plastic hinge rotation capacity is reached. When shear failure is detected, a zero-length shear spring with a tri-linear backbone curve linked in series with the beam-column element modifies its constitutive properties to consider pinching and strength and stiffness degradation

determined through linear regressions from experimental data. Although the shear model offers very accurate results, the direct use of this shear model in the current software is not implemented making its applicability still too much complex.

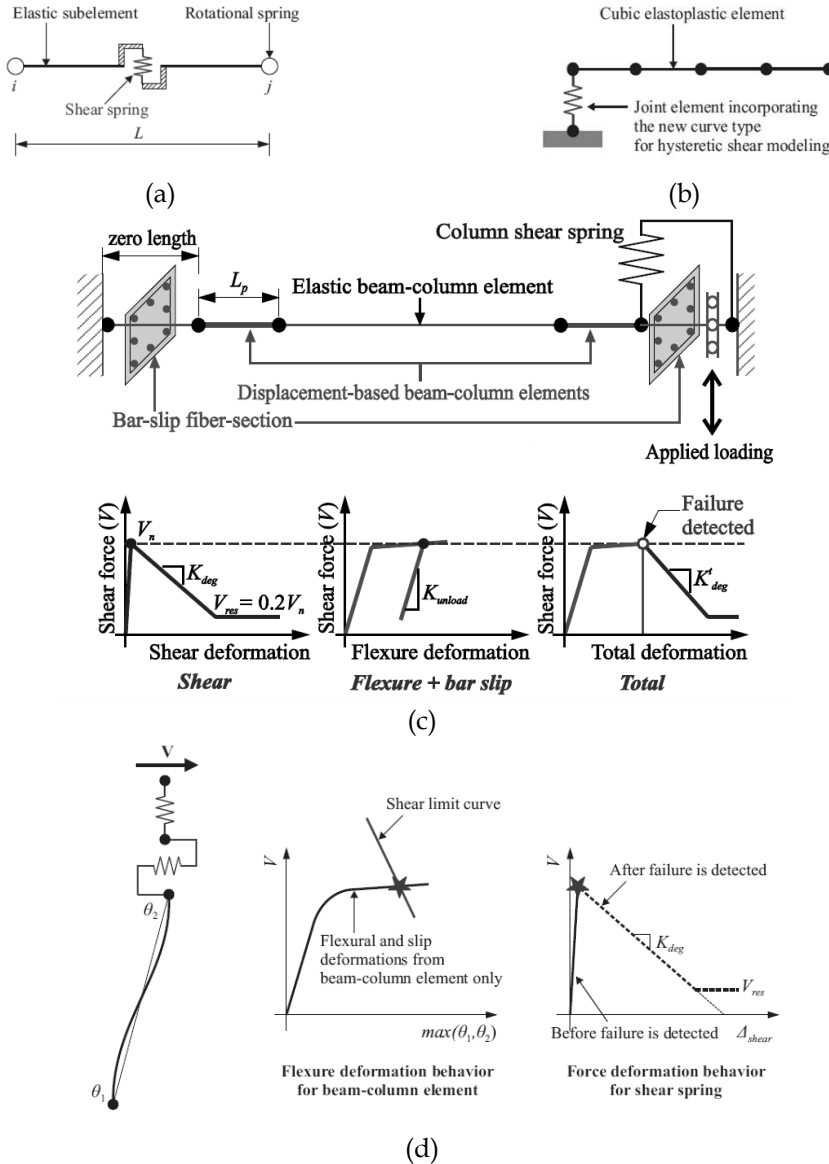


Figure 2.3. Examples of modeling of columns shear behavior – Pincheira et al.(1999) (a), Lee and Elnashai (2000) (b), Jeon et al. (2015) (c), Elwood (2004) (d)

A review of previous researches on the shear behavior of existing columns indicates that a reliable column shear failure model should be accurate, computationally efficient and compatible with existing software programs in order to practically conduct numerous nonlinear dynamic analyses. However, it is quite difficult that column shear models reviewed above satisfies all these requirements. Although the problem is still an open and important issue, in the present work the attention will be not directly focused on this topic.

More attention will be addressed to the influence of infills, in particular at lower performance level, and to the modeling issue related to RC beam-column connections.

2.1.2. Beam - column joints

A joint shear model that can account for the cyclic strength and stiffness deterioration is critically important in this work, especially for non-conforming RC buildings.

Different damage or failure modes can occur in the beam-column joint panel zone depending on the joint typology (exterior or interior, reinforced or unreinforced joint) and on structural details (e.g., use of plain round or deformed bars or bar anchorage solution), which ultimately affect the efficiency of the shear transfer mechanisms in the joint region and, thus, the post-cracking nonlinear behavior.

In particular, in the assessment of the performance of typical non-conforming buildings, seismic collapse safety might be significantly affected by the non-linear behavior of the joints that are involved in the failure mechanism because of poor structural detailing, as the lack of an adequate transverse reinforcement in the joint panel or deficiencies in the anchorage of beam reinforcement due to the absence of any capacity design principle or seismic design. Joint flexibility contributes significantly to overall story drift, especially in the nonlinear range. Basically, two contributions to overall deformability due to beam-column joints cannot be neglected: (i) the shear strain of the joint panel and (ii) the contribution of the fixed-end-rotation due to the slip of the longitudinal bars anchored into the joint (e.g., Cosenza et al. 2006).

Furthermore, under lateral seismic loading, high shear forces are generated in the joint core. Beam-column joints bear horizontal and vertical shear forces that are usually much larger than those acting within the adjacent beams and columns. Thus, joints can experience shear failures which should be avoided

by an appropriate design to ensure a ductile response of the whole frame. However, such a design does not regard typical non-conforming structures designed for gravity loads only or according to old seismic codes. In particular, exterior unreinforced RC joints often experience brittle failure under horizontal actions.

In literature there is not yet a commonly accepted approach for the determination of the shear strength and for nonlinear modeling of RC beam-column joints in moment resisting RC frames. Many nonlinear joint models are available, but most of them may be unsuitable for modeling all sources of nonlinearity for the assessment of older concrete buildings. Some of them were developed and calibrated for confined beam-column joints or they are too complicated to implement.

In this Section a revision of existing shear strength models and the main monotonic or hysteretic modeling techniques is carried out with a particular attention to exterior joints without transverse reinforcement, one of the main objective of this work.

2.1.2.1 Beam - column joints shear strength

As far as code prescriptions are concerned, ASCE-SEI 41 (2007) proposes recommendations for the shear strength for unreinforced joints for seismic rehabilitation purposes based on the pre-standard developed in FEMA 273 (1997) and FEMA 356 (2000). According to ASCE 41, nominal joint shear strength is defined according to Eq. (2.1), independently on the axial load ratio:

$$V_n = \gamma_n \sqrt{f_c} b_j h_c \quad (2.1)$$

		γ_n (MPa) ^{0.5}			
Transverse reinforcement ratio	Interior joint with transverse beams	Interior joint w/o transverse beams	Exterior joint with transverse beams	Exterior joint w/o transverse beams	Knee joint with or w/o transverse beams
< 0.003	1.0	0.8	0.7	0.5	0.3
≥ 0.003	1.7	1.2	1.2	1.0	0.7

Table 2.1. Joint shear coefficients according to ASCE-SEI 41 (2007)

In Eq. (2.1) f_c is the concrete compressive strength, b_j and h_c are the effective

joint width and the column cross-sectional height, respectively. The values of γ_n for joint shear strength are provided depending on the joint typology and the transverse reinforcement ratio, as shown in Table 2.1.

In literature, several authors have proposed analytical or empirical models to predict joint shear strength for interior or exterior, confined or unconfined joints. In this Section, a critical overview of the main modeling approaches presented in literature to evaluate shear strength for exterior unconfined joints is reported.

Models based on the Modified Compression Field Theory (MCFT) by Vecchio and Collins (1986), e.g. Lowes and Altoontash (2003), appeared to underestimate the shear strength of lightly reinforced joints (Shin and LaFave 2004a); thus they are unsuitable for prediction of shear strength of unreinforced joints.

Other strength models proposed in literature are based on an empirical or semi-empirical approaches (Bakir and Boduroglu 2002, Celik and Ellingwood 2008, Hassan 2011, Hegger et al.2003). Most of the empirical models proposed in literature have been developed based on statistical regression analysis with large scatter or small size or non-homogeneous, in terms of beam reinforcement anchorage or reinforcement typology (deformed/plain), experimental data sets.

Bakir and Boduroglu (2002) included the beam reinforcement ratio and the joint aspect ratio in the proposed equation for evaluating the contribution of concrete to joint shear strength, and anchorage details were included by an empirical factor.

Based on the analysis of an experimental database from literature, Celik and Ellingwood (2008) proposed to evaluate maximum joint shear strength according to ASCE-SEI approach, but re-calibrating the coefficient γ_n in Eq. (2.1) on the basis of collected experimental tests. In this way, for example for exterior unconfined joints, γ_n is found to belong to the range (0.83÷1.00), when anchorage failure does not occur, and to the range (0.42-0.62), in the case of anchorage failure.

Hassan (2011) proposed an empirical strength model including the effect of joint aspect ratio and axial load ratio for J-mode of failure. Moreover, an empirical bond strength model was also proposed to evaluate the joint shear strength for exterior and corner joints with short embedment length of beam bottom reinforcement in the case of pullout failure before rebar yielding,

showing a mean and coefficient of variation values of the ratio of experimental and calculated joint shear strength coefficient equal to 0.94 and 0.14, respectively.

Hegger et al. (2003) developed an empirical model including the effects of column reinforcement ratio and joint aspect ratio.

An extensive database of RC joints test specimens (136 and 18 experimental sub-assemblages with and without joint transverse reinforcement, respectively) was collected by Kim and LaFave (2007a). Influence parameters for joint shear strength were assessed, concluding that the most important influence parameters on joint shear behavior were found to be somewhat different by connection type and failure mode sequence. In Kim et al. (2007b) joint shear stress at peak response has been developed by a Bayesian parameter estimation method based on the collected database. All test specimens included in the database have at least a minimum amount of joint transverse reinforcement. For ductile joints, they constructed the joint shear strength model by performing a step-wise removal process to extract key parameters among ten parameters (namely, spacing ratio, ratio of recommended to provided amount of joint transverse reinforcement, ratios of beam depth to column depth and beam width to column width, joint transverse reinforcement index, beam reinforcement index, joint eccentricity, in-plane and out-of-plane geometry, concrete compressive strength). For joints without transverse reinforcement, a probabilistic joint strength model was established by modifying that related to ductile joints. The ductile joint shear strength model provides reliable estimates, while the non-ductile joint shear strength model should be improved because of the limited size of non-ductile joints in the database. Jeon (2013) later proposed a specialization of the regression formulation proposed by Kim and LaFave (2007b) for exterior and interior joints without transverse reinforcement.

Another "family" of models proposed in literature to evaluate joint shear strength are the principal-tensile-stress-based models. Paulay and Priestley (1992) first proposed a comparison between the average principal tensile stress of the unconfined joint with some critical values, namely shear cracking and shear failure. Priestley (1997) suggested limiting to $0.42\sqrt{f_c}$ the value of the principal tensile stress. Eurocode 8 (CEN 2005) and Italian provisions (D.M. 2008) adopt this approach for unreinforced joints.

Other authors proposed a similar approach, introducing an upper bound of such critical values in the case of ineffective anchorage (Sharma et al. 2011) or in the case of plain bars as longitudinal reinforcement of the adjacent beam and bar end hooks (Pampanin et al. 2003).

Such approaches allows to explicitly take into account the (beneficial) effect of the axial load ratio on joint shear strength, but the analysis of the experimental results – carried out on specimens with identical geometrical and mechanical properties and different axial load ratio level – showed that such an influence is quite negligible. More tests are necessary to investigate about the influence of the axial load on joint shear strength, especially for high level of axial load ratio (Park and Mosalam, 2012a).

Moreover, the deterioration of the shear strength of beam-column joints under cyclic displacement was experimentally observed (Wong 2005, Hakuto 2000). The diagonal tension cracking of the joint core in alternative directions during seismic loading causes the reduction of the diagonal compressive strength of the concrete; the joint shear strength may degrade with the increase in ductility demand in the adjacent members during cyclic loading.

Some models in literature attempted to capture this effect proposing a joint shear strength that decreases when ductility demand in the adjacent beam increases (Park 1997, Hakuto 2000). The relationship between the reduction of joint shear strength and the ductility demand – which can be expressed through a ductility factor – is empirically proposed in these models, but they cannot be accurately generalized because the ductility factor is uncertain and it takes also into account the deformation of the members adjacent to the joint.

Shiohara (2004) proposed a mathematical model to determine the joint shear strength of interior, exterior, and knee beam-column joints. The quadruple flexural resistance within a joint panel played an important role in defining joint shear failures. Joint shear strength was calculated from force equilibrium in four rigid segments within the joint panel. However, the model validation based on experimental results was not provided by the Author.

Successively, experimental tests were conducted on exterior unreinforced beam-column connections aimed at the definition of the main parameters having the greatest influence on joint shear strength. Park and Mosalam (2012a) investigated the effects of three main parameters, namely (i) joint aspect ratio, (ii) beam longitudinal reinforcement ratio, and (iii) column axial load, and confirmed that joint aspect ratio and beam longitudinal tension

reinforcement ratio and its strength mainly influence joint shear strength.

Park and Mosalam (2012b), based on the results of parametric studies, proposed another approach to evaluate joint shear strength and its degradation after beam yielding without any ductility factor; their model directly provides a definition of the failure mode (J- or BJ-failure mode) and it is formulated using a mechanical approach based on the strut-and-tie mechanism (Park and Mosalam, 2012b).

The strut-and-tie approach was already proposed and adopted in other literature studies (Hwang and Lee 1999, Vollum and Newman 1999, Tsonos 2007). Most of the “strut-and-tie-based” models have a conceptual limitation, because the average equilibrium and compatibility equations they are based on are not suitable to reproduce the real behavior of unreinforced beam-column joints – for which the joint shear failure is generally localized (Park and Mosalam, 2012a). Moreover, the accuracy of the strut-and-tie approach highly depends on the estimation of the diagonal strut area that strictly affects the joint shear strength.

Nevertheless the shear strength model proposed by Park and Mosalam (2012b) is based on a modified strut-and-tie approach, it shows a good agreement with experimental tests.

2.1.2.2 Modeling of joint shear behavior

In literature there are several models available to reproduce joint shear behavior into numerical analyses of RC frames. On the other hand, there are only a few technical codes that provide prescriptions in this sense.

ASCE/SEI 41 first suggests that beam-column joint in monolithic construction should be represented as a rigid zone having horizontal dimensions equal to the column cross-sectional dimensions and vertical dimension equal to the beam depth. Successively, ASCE 41 suggests a complete backbone curve for joint shear stress-strain modeling in nonlinear analyses, but recommended values for joint shear strength coefficient and plastic shear strain appear to be quite conservative (Hassan, 2011).

ACI 369-R11 defines an implicit beam-column joint using centerlines models with semi-rigid joint offsets: only a portion of the beam and column, or both, within the joint panel zone, is defined as rigid.

Many researchers have attempted to model the behavior of beam-column

joints in more realistic approaches, basically lumped plasticity approaches, multi-spring macro-models or finite element simulations. A brief discussion about the main modeling approaches existing in literature is reported in this Section.

One of the first approaches to joint modeling was to reproduce the deformability contribution due to bond slip of tensile reinforcement anchored into the joint core (as in Otani 1974). Filippou et al. (1983) also proposed a model consisting in a rotational spring at beam end connected with a rigid bar to the adjacent joint spring in order to consider the bond deterioration on the hysteretic behavior of RC joints.

Nevertheless, such models do not consider also joint shear deformability contribution.

Successively, a very simple model was first suggested by Krawinkler and Mohasseb (1987) for steel beam-column connections and successively by Alath and Kunnath (1995) for RC joints, the so-called “scissors”-model (see Figure 2.4a). It is composed by a rotational spring that models nonlinear behavior of the joint panel with rigid links spreading into the finite size of the panel and it is very easy to implement.

Then it was adopted by Pampanin et al. (2003) and Celik and Ellingwood (2008) for interior and exterior unconfined RC beam-column joints, as explained more in details in Section 2.1.2.3. Park and Mosalam (2013) also use such a model, but including joint panel shear deformability and beam bars bond slip contribution together in the definition of the unique spring that constitutes this kind of model.

Within the context of multi-spring modeling approaches, a distinction can be made between models that introduce multi-springs to model joint panel shear deformability (e.g., Sharma et al. 2011, Youssef and Ghobarah 2001), and models in which the multiple springs reproduce different deformability contributions (joint panel shear behavior, shear behavior of adjacent beam/column, slip contribution of bars anchored into the joint panel) (e.g., Biddah and Ghobarah 1999, Lowes and Altoontash 2003, Shin and LaFave 2004b).

Biddah and Ghobarah (1999) modeled the joint behavior with separate rotational springs for joint shear and bond-slip deformations (Figure 2.4b). The shear stress-strain relationship of the joint was simulated using a tri-linear idealization based on a softening truss model, while the cyclic response of the joint was captured with a hysteretic relationship with no pinching effects.

Youssef and Ghobarah (2001) proposed a more refined model in which the shear behavior of the joint panel was represented by four rigid elements enclosing the joint core pin-connected to one another and two nonlinear axial springs along the diagonals of the joint panel (Figure 2.4c).

Later, a model including four rigid elements enclosing the joint core pin-connected to one another, with a single rotational spring representing the joint panel shear behavior and additional springs modeling the other deformability contributions was successively suggested by Lowes and Altoontash (2003) and, similarly, by Altoontash (2004) and Shin and LaFave (2004b). In particular, Lowes and Altoontash (2003) proposed a 4-node 12-degree-of-freedom joint macro-model (Figure 2.4d) constituted by eight zero-length translational springs which simulate the bond-slip response of beam and column longitudinal reinforcement, a zero-length rotational spring that simulates the shear deformation of the joint, and four zero-length shear springs that simulate the interface-shear deformations. Shear stress-strain relationship of the panel zone is defined through the MCFT and, thus, it is not properly suitable for joints with no transverse reinforcement.

Altoontash (2004) proposed a simplified version of such a model by reducing the number of springs related to deformability contributions due to the adjacent beam/column elements, but with the same modeling approach and shear stress-strain definition for joint panel zone, as shown in (Figure 2.4e).

Similarly, Shin and LaFave (2004b) introduced two rotational springs in series at beam-joint interfaces to simulate beam bars bond slip deformability contribution and beam plastic rotation contribution, separately. Again the same modeling approach as Lowes and Altoontash (2003) for joint panel zone was adopted, but joint panel shear stress-strain definition was based on MCFT (for the envelope) and experimental data (for cyclic behavior).

Another multi-spring approach has been proposed by Sharma et al. (2011): the joint core region was modeled through shear springs in the column portion and a rotational spring in the beam region (Figure 2.4f); the backbones of these three springs were proposed for monotonic loading in principal stresses, and anchorage failure in the case of not sufficient beam bars anchorage length was also considered by reducing the critical principal stress.

It is worth noting that models with multiple nodes and multiple springs (e.g. Lowes and Altoontash, 2003; Shin and LaFave, 2004b; Sharma et al., 2011)

allow to capture more realistically the joint panel kinematic and simulate the horizontal translation that can occur between the centerlines of the columns above and below the joint. Vice-versa, scissors model does not capture this possible kinematic, but it is the simplest and computationally less demanding joint model and it seems to be sufficiently accurate in predicting the experimental beam-column joint panel response for simulating the seismic response of non-conforming RC frames for purposes of fragility assessment and performance-based earthquake engineering (Celik and Ellingwood, 2008).

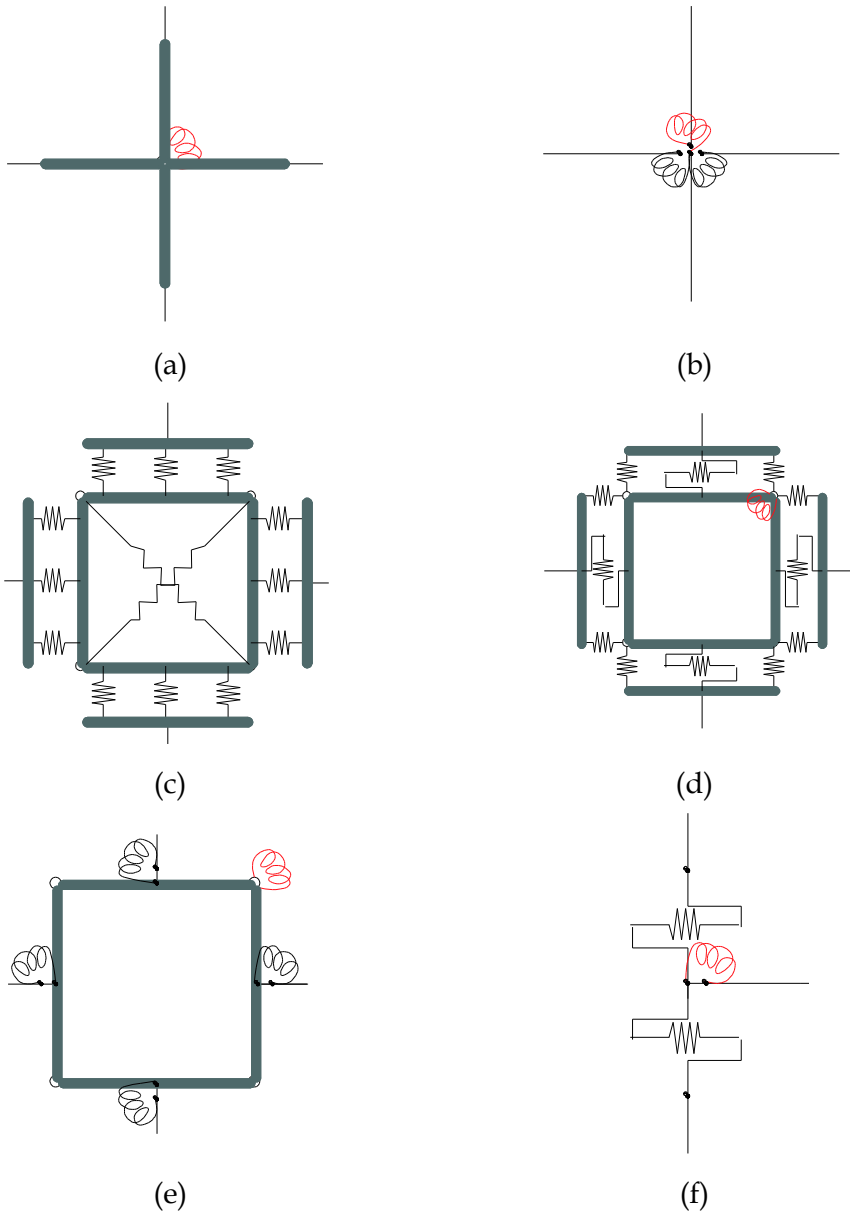


Figure 2.4. Models by Alath and Kunnath (1995)(a),Biddah and Ghobarah (1999) (b), Youssef and Ghobarah (2001)(c), Lowes and Altoontash (2003) (d),Altoontash (2004) (e), Sharma et al. (2011) (f)

2.1.2.3 Shear constitutive relationship of the joint panel

One of the critical issues to include joints into the structural model is the properly calibration of the shear stress-strain response of the joint panel.

A first distinction should be made between analytical and empirical constitutive relationship for joint panel behavior. Most of the analytical calibrations of such relationships in literature are more suitable for reinforced beam-column joints, for example models based on the MCFT, as explained in the previous Section.

In this Section, a critical review of the main constitutive relationships empirically calibrated, with a particular focus on exterior joint panels, proposed in literature is carried out.

In Alath and Kunnath (1995), the joint panel moments were computed from the column and beam moments, assuming the joint core was under pure shear, and joint panel shear properties were empirically defined and validated through experimental response of typical gravity load design (GLD) RC interior joints.

Pampanin et al. (2003) proposed a constitutive relationship for joint panel in terms of principal stresses versus joint shear strain started from strength degradation model for unreinforced joints proposed in literature by Priestley (1997) and extended it to poorly detailed with end-hooked plain bars through additional experimental tests on two tee-joints (Figure 2.5a). The cyclic behavior was modeled by a hysteresis rule able to represent the pinching effect due to slip of the reinforcement and shear cracking in the joint.

Sharma et al. (2011) started from a constitutive relationship similar to Priestley (1997), modifying it in terms of joint shear strain - on the basis of experimental tests with deformed bars by Clyde et al. (2000), Pantelides et al. (2002) and tests with plain bars by Pampanin et al. (2002) - and introducing a limitation in critical principal stress in the cases of anchorage failure (Figure 2.5b).

The constitutive relationship proposed by Celik and Ellingwood (2008) was based on a statistical analysis carried out on ten experimental tests – as far as external joints are concerned – non homogeneous for joint reinforcement ratio, anchorage conditions and failure mode (for some of these tests, only incomplete results were available). They suggested that the shear stress-strain backbone curve for the panel zone in typical non-conforming RC beam-column joints can be defined through four key points, which correspond to joint shear

cracking, reinforcement yielding, joint shear strength/adjoining beam or column capacity, and residual joint strength, respectively. The ordinates of the backbone points were reduced if the shear failure of the joint occurs before beams or columns reach their capacities. Shear failure of the joint is assumed to depend on the kind of joint (interior/exterior) and the anchorage conditions. Anchorage failure was taken into account through a reduced envelope for the joint shear stress-strain relationship. As far as strain capacity is concerned, they proposed a range of values for each characteristic point with a uniform probability distribution (Celik and Ellingwood, 2010). However, from the analysis of the experimental dataset they adopted, it can be observed that the proposed joint shear strain values for the four key points are related to interior joints tests only; such values are very high if compared with shear strain values obtained from experimental tests on exterior beam-column joints.

A multi-linear backbone curve representing the moment-rotation relationship of an unreinforced corner beam-column joint was also proposed by Park and Mosalam (2013), see Figure 2.5c. The modeling parameters of such a backbone curve were estimated on the basis of experimental results of four corner joint specimens tested by the authors with different joint aspect ratio and beam longitudinal reinforcement ratio. For strength prediction in the developed backbone curve, a simplified version of an analytical model proposed by Park and Mosalam (2012b) was adopted. Joint shear strain, γ_j , and rotation at the beam joint interface due to bar slip and/or crack opening, θ_s , were both measured during the tests, and the rotation of the proposed backbone for joint spring, θ_j , was defined as the sum of them, that is, $\theta_j = \gamma_j + \theta_s$. The analysis of the experimental tests by Park and Mosalam (2012c) shows that slip contribution to the overall deformability is higher if joint shear failure happens after beam yielding; however, when a single-spring approach with a unique joint rotation, θ_j -which includes both joint panel shear strain and slip rotation - is proposed (Park and Mosalam, 2013), the definition of the backbone does not depend at all on the failure typology. Thus, most of the shear constitutive relationships are empirically obtained from the few available (Pampanin et al. 2003, Park and Mosalam 2013) not homogeneous, in terms of beam reinforcement anchorage or reinforcement typology (deformed/plain), experimental tests, and independently on the failure typology (Celik and Ellingwood 2008, Sharma 2011).

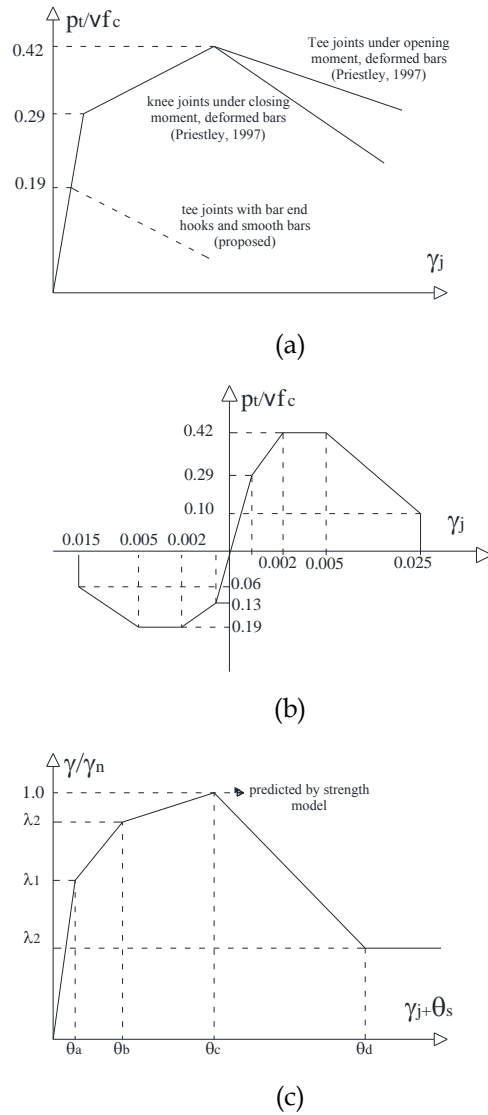


Figure 2.5. Constitutive relationship proposed in literature: Priestley (1997) and Pampanin (2003) (a), Sharma et al. (2011) if anchorage failure occurs (b), Park and Mosalam (2013) (c)

In this work, an attempt to obtain a new shear constitutive relationship, different for failure typology for exterior unreinforced joints, to be adopted in the context of scissors model for the joint panel and to use in conjunction with an explicit bond-slip spring, is formulated, as it will explained in Chapter 5.

Model proposed in literature by Celik and Ellingwood (2008) will be adopted for interior joints in dynamic analyses of RC frames, as explained in Chapter 6.

2.1.3. Infills

Several experimental and analytical investigations were performed on infilled RC structures, regarding both “local” effects - due to the interaction between infill panels and surrounding RC frames - and influence of infills on the global seismic performance of the analyzed structure, in order to investigate, on one side, on the increase in stiffness and strength provided by infills and, on the other side, on the possible localization of ductility demand depending on the infill distribution.

As far as the numerical investigation of the influence of infills on the global seismic behavior of RC frames is concerned, several studies have been developed from the second half of 1990s on.

Fardis and Panagiotakos (1997) and Kappos et al. (1998), following first code prescriptions about the consideration of infills in seismic design (CEN, 1995), evaluated the influence of infill walls and their configuration on RC frames designed for seismic loads according to contemporary earthquake engineering principles.

Other studies (Negro and Colombo, 1997; Fajfar and Drobnič, 1998) were developed based on full-scale experimental tests (Negro and Verzeletti, 1996; Pinto et al., 2002), focusing the attention on different issues such as the localization of displacement demand and the increase in stiffness and strength due to infill presence.

A wide and thorough series of numerical studies on infilled RC frames was carried out by Dolšek and Fajfar: first works were focused on the influence of infills on seismic demand depending on their mechanical characteristics and the design typology of the structure (2001) and on modeling issues (2002). Hence, an effort was made to develop simplified approaches allowing to carry out the seismic assessment of infilled RC frames within the N2 method (Fajfar and Gaspersic, 1996; Fajfar, 1999). To this end, a R- μ -T relationship accounting for the typical degrading force-displacement response of an infilled RC frame was proposed in (2004), and it was applied to two case-study structures in the companion paper (2005). In (2008a,b) the same seismic capacity assessment

procedure was applied to a case study structure in different infill configurations, and the influence of infills on the seismic performance at different Limit States was also evaluated in terms of failure probability, thus accounting for the influence of the inherent uncertainty in capacity and response of infill elements.

The influence of uncertainty on seismic capacity of infilled RC frames was also analyzed in (Celarec et al., 2012) and (Dymiotis et al., 2001), based on sensitivity and fragility analyses, respectively.

In these studies, modeling of infills was performed in different possible approaches. Infill walls can be modeled either by means of micro- (e.g., FEM) or macro- (e.g., single equivalent strut or multi-struts) models.

The detailed and computationally demanding modeling approach based on micro-models (Figure 2.6a) is generally not suitable for seismic analysis of multi-bay multi-story frames, whereas macro-models based on the equivalent strut approach are widely adopted, since they represent a good compromise between simplicity and accuracy.

In the early 1960s, Polyakov (1960) suggested the possibility to model infill panels as equivalent diagonal compressive strut (see Figure 2.6d). This modeling approach was later adopted by Holmes (1961) and Smith (1962), that, using additional experimental data, proposed the evaluation of the equivalent strut width as a function of the relative panel-to-frame-stiffness parameter.

Later, Mainstone (1971) and Liauw and Kwan (1984) also proposed more reliable empirical equations for the calculation of the equivalent strut width on the basis of experimental and analytical data.

However, it is clear that one single strut element is unable to model in detail the complex behavior of the infilled frames and, in particular, the possible local interaction between the infill panel and the surrounding RC frames. In last two decades, more complex macro-models were proposed, different in properties definition and number of diagonal struts.

Thiruvengadam (1985) proposed the use of a multiple-strut model to simulate the effect of an infill panel, that consists of a moment-resisting frame with a large number of pin-jointed diagonal and vertical struts. Initially, a perfect frame-infill bond condition is assumed, and the lateral stiffness of the infill by its shear deformation is modeled by a set of pin-ended diagonal struts - representing the shear and axial stiffness of the masonry infill - running in both directions.

Hamburger and Chakradeo (1993) proposed a multi-strut configuration that

can also account for the openings in a quite complex approach.

Chrysostomou (1991) and Chrysostomou et al. (2002) aimed to obtain the response of infilled frames under earthquake loading by taking into account both stiffness and strength degradation of infills. The infill panel was modeled through six compression-only struts (Figure 2.6b).

More recently, Crisafulli and Carr (2007) proposed a new macro-model to represent the effect of masonry-infill panels on the surrounding frame (Figure 2.6c). The model is implemented as a four-node panel element that is connected to the frame at the beam-column joints. Internally, the panel element accounts separately for the compressive and shear behavior of the masonry panel using two parallel struts and a shear spring in each direction. Such a model allows adequately considering the lateral stiffness and the strength of masonry panel, in particular if a shear failure along mortar joints or diagonal tension failure is expected.

Nevertheless multi-strut models allow to capture the local interaction between infill walls and adjacent structural elements, thus allowing to evaluate its effects, for example, in terms of local increase in shear demand in RC columns, the investigation of this kind of phenomena is beyond the scope of this work.

In next chapters, single strut models will be effectively used, as in the literature studies previously reported, in accordance with the aim to investigate the effect of infills on the global seismic behavior of RC frames, by analyzing their influence on global stiffness and strength, on the kind of collapse mechanism, on the displacement capacity and, consequently, on seismic capacity and seismic fragility at different performance levels (i.e., Limit States), depending on the main characteristics of the RC frame, such as the design typology and the number of stories.

Whatever the infill model that it is adopted, the structural response of an infilled RC frame is strongly nonlinear and thus it is difficult to predict. The positive or negative effects of infills still represents a controversial topic, with a critical need of further investigations for the seismic vulnerability assessment of extensive classes of existing buildings. Moreover, the interaction between unreinforced masonry infills and RC frames can lead to unexpected or peculiar effects when compared with the response of the bare frame, either at a local

level (e.g. shear failure in columns or damage to joint region) or on the global seismic response (e.g. soft story mechanism). The former aspect is not accounted for in this work, the latter will be better investigated in Chapter 3.

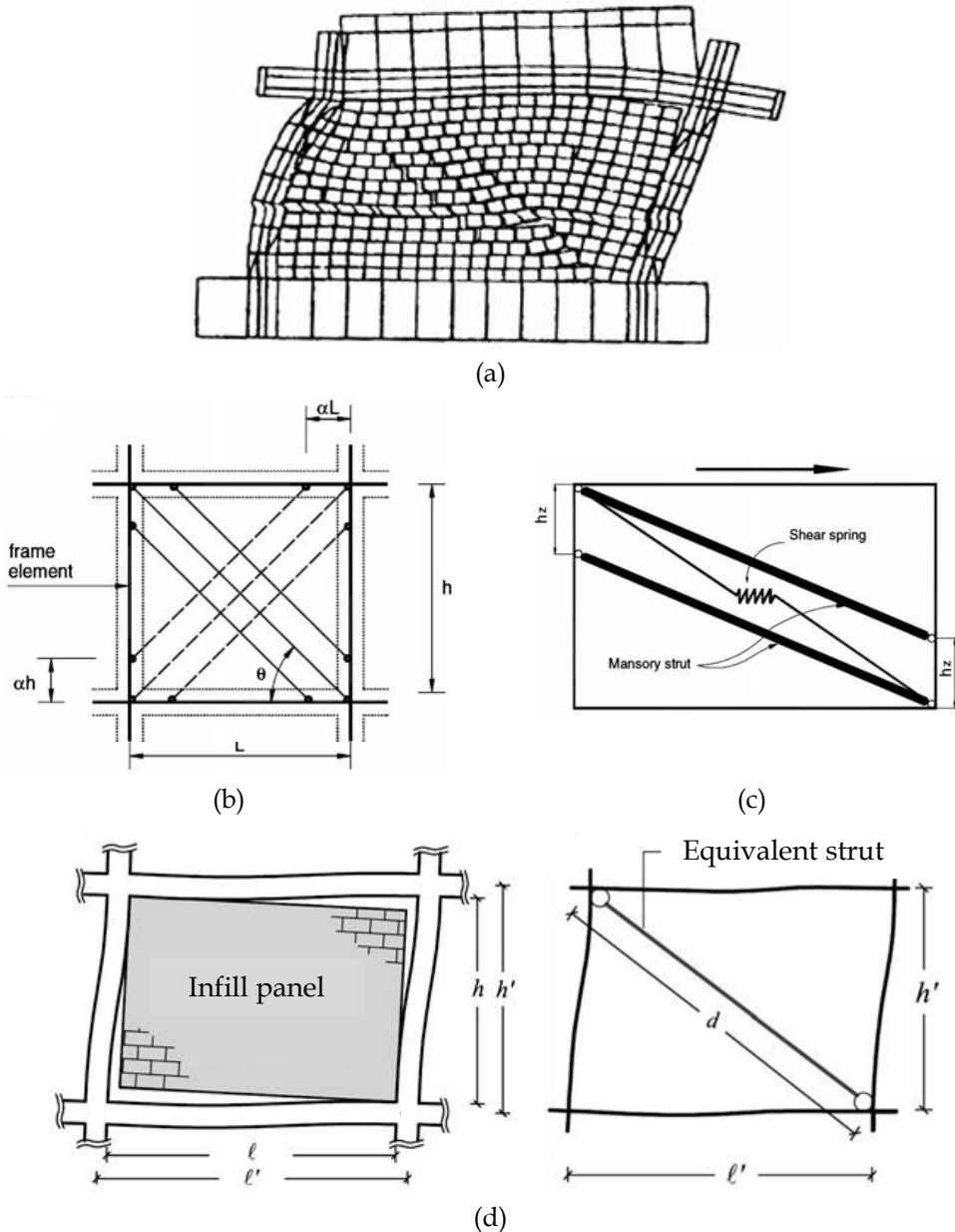


Figure 2.6. Examples of FEM modeling (b), multi-struts (b, c), and equivalent strut (d) models for infills

Moreover, uncertainty in several of the input parameters of the structural model – usually neglected in design and assessment procedures – can heavily affect the seismic response of infilled RC structures. Simulation studies have been performed in order to take into account the effects of uncertainty, as it will be shown in Chapter 3.

Recognized the great importance of infills and their mechanical properties especially at low level of seismic demand, the attention is then focused on the role of infills at Damage Limitation Limit State, developing new procedures to account for infill presence directly or indirectly via linear analyses, as reported in Chapter 4.

2.2 Structural performance levels

In this Section, a brief discussion on structural limit states or performance levels of interest in this study within the context of PBEE assessment framework, is carried out.

First of all, the four critical parameters that form the basis of a PBEE assessment framework are Intensity Measure, Engineering Demand parameters, Damage Measure and Decision Variables. The assessing process begins with the definition of a ground motion Intensity Measure (IM), which defines, in a probabilistic sense, the salient features of the ground motion hazard that affect structural response. Ground motion Intensity Measures are commonly defined by single parameter variables, such as peak ground acceleration/velocity or spectral acceleration/velocity, that correlate better with the resulting damage. Engineering Demand Parameter (EDP), describes the structural response in terms of deformations, accelerations, or other quantities calculated by simulations of the building to earthquake ground motions. Perhaps the most distinguishing aspect of the PBEE framework over traditional design methods is the explicit calculation of Damage Measures and Decision Variables (Dierlein et al. 2003). Damage Measures (DM) describe the physical condition of the structure and its components as a function of the imposed EDPs. Specific damage levels of the DMs are defined in terms of the consequences of the damage, such as necessary repairs to structural or non-structural components as a function of imposed deformations, life-safety

implications associated with falling hazards, fire, blocked egress, etc. Once the DMs are determined, the final step in the PBEE process is to calculate Decision Variables (DV), which translate damage measures into quantities that relate to risk management decisions concerning economic loss and life safety.

Within this framework, it can be identified a continuous function relating DMs with EDPs, and EDPs with IMs, that can be visualized by means of the “idealized” pushover shown in Figure 2.7.

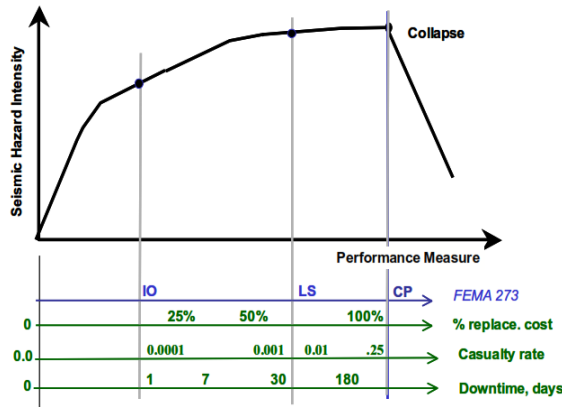


Figure 2.7. Idealized pushover curve (Dierlein et al. 2003)

Typically plotted in terms of earthquake-induced base shear (vertical axis) and interstory drift (horizontal axis), the static pushover concept can be generalized to relate earthquake input intensity to the resulting performance metrics.

For design or assessment purposes it is convenient to identify discrete levels of seismic performance for the major structural and other building components that significantly affect building function, property protection, and safety.

A way to “discretize” the continuous functions relating DMs with EDPs or and EDPs with IMs is the definition of Performance Levels (PLs) or, in European tradition, Limit States (LSs).

LSs depict the structural capacities at the thresholds of damage states and thus can be expressed through a threshold in damage measure (DM). LSs can be defined for structural or non-structural damage states, depending on the application, as monetary losses and downtime due to earthquake damage are controlled by a combination of those states.

In literature and code provisions PLs have typically been defined in different modes:

- (i) in “global terms”, as the achievement of a particular state in the global seismic response of the structure, for example, at 20% of base shear degradation after peak load in a static pushover curve (e.g. Fardis 2009), or when the tangent stiffness reduction overcomes a certain percentage threshold (e.g. Vamvatsikos and Cornell, 2002);
- (ii) in “local terms”, as the achievement of a defined condition on the element response, for example, the yielding or the ultimate flexural rotation capacity (e.g. Fardis 2009, CEN 2005, DM 2008), in the first element or in a certain percentage of elements (Celarec et al. 2012);
- (iii) in terms of “displacement threshold”, namely defining IDR or roof rotation limits related to the considered damage level (e.g. Aslani 2005 for RC components or Colangelo 2013 for infilled frames).

The second and, in particular, the third approaches are the most directly correlated to the structural damage. In particular, the second approach seems to be more easier to pursue since it is a direct consequence of the modeling choices; while the third one is more directly related to structural and non-structural losses (that is the primary goal of PBEE assessment), but it requires a strong effort to properly define displacement thresholds.

Several guidelines and codes worldwide qualitatively describe performance levels or damage states for purposes of building performance and seismic risk assessment. Generally speaking, modern seismic codes define performance levels aimed at avoiding collapse under major earthquakes and ensuring control and limitation of damage under more frequent but less severe earthquakes, in order to minimize economic and functionality losses.

ASCE 41 (ASCE 2007) provide guidance on three performance levels:

- immediate occupancy (IO) - Achieve essentially elastic behavior by limiting structural damage (e.g., yielding of steel, significant cracking of concrete, and nonstructural damage);
- life safety (LS) - Limit damage of structural and nonstructural components so as to minimize the risk of injury or casualties;
- collapse prevention (CP) - Ensure a small risk of partial or complete building collapse by limiting structural deformations and forces to the onset of significant strength and stiffness degradation.

ASCE 41 provides also acceptance criteria in terms of deformation and force demands on individual structural components.

Similarly, FEMA 273/356 (1997) defines three building performance levels: immediate occupancy (IO), life safety (LS), and collapse prevention (CP), and assigns inter-story drifts of 1%, 2%, and 4% to define these performance levels for RC frames.

Furthermore, SEAOC Vision 2000 defines five performance (damage) levels: fully operational (negligible), operational (minor or light), life safety (moderate), near collapse (major or severe), and collapse (complete), while European code (CEN 2005) traits with three main LSs, namely damage limitation (DL), significant damage (SD) and near collapse (NC) LSs.

The NC, SD, and DL LSs correspond to “Collapse Prevention”, “Life Safety”(the single performance level for which new structures are designed according to most current seismic design codes), and “Immediate Occupancy” levels, respectively, of NEHRP Guidelines and ASCE Pre-standards (CEB 2003).

In this work the definition of LSs in “local terms” and in terms of “displacement threshold” are adopted. First, the influence of infill distribution on seismic performance of RC buildings is estimated at DL LS and NC LS (defined in accordance with Eurocode 8 and NTC '08 approach), depending also on design typology. Then the influence of infills is better investigated at performance levels for which they are more influent, namely DL or IO LSs, proposing new procedures to account for infills in seismic performance evaluation of RC frames at DL LS via linear analyses.

Finally joint influence on seismic performance will be evaluated from IO to CP LSs, also considering some additional LSs, conventionally defined in “local terms”, namely in correspondence of the achievement of characteristic points of beam-column joints or beams/columns nonlinear response.

References

- .Kappos, A.J., Stylianidis, K.C., Michailidis, C.N., (1998). Analytical models for brick masonry infilled R/C frames under lateral loading. *Journal of Earthquake Engineering*, 2(1), 59-87.
- Alath S, Kunnath SK. (1995) Modeling inelastic shear deformations in RC beam–column joints. *Engineering mechanics proceedings of 10th conference*, May 21–24, University of Colorado at Boulder, Boulder, Colorado, vol. 2. New York: ASCE: p. 822–5.
- Altoontash A. (2004). Simulation and damage models for performance assessment of reinforced concrete beam–column joints. Ph.D. dissertation. Stanford (CA): Department of Civil and Environment Engineering. Stanford University.
- American Concrete Institute, Committee 369, ACI 369R-11. Guide for seismic rehabilitation of existing concrete frame buildings and commentary. Feb. 2011, U.S.A.
- American Society of Civil Engineers (ASCE), (2007). *Seismic Rehabilitation of Existing Buildings*, ASCE/SEI 41-06, Reston, Virginia
- Aslani, H. (2005). Probabilistic Earthquake Loss Estimation and Loss Disaggregation in Buildings, Doctoral Dissertation, Stanford University.
- Bakir PG, Bodurođlu HM (2002) A new design equation for predicting the joint shear strength of monotonically loaded exterior beam–column joints. *Engineering Structures*; 24:1105–17.
- Biddah A, Ghobarah A (1999), Modelling of shear deformation and bond slip in reinforced concrete joints. *Structural Engineering*; 7(4): 413–32.
- Biskinis DE, Roupakias GK, Fardis MN (2004). Degradation of shear strength of reinforced concrete members with inelastic cyclic displacement. *ACI Structural Journal* 2004;101(6):773–83.
- CEB, 2003. Seismic assessment and retrofit of reinforced concrete buildings. *Fib Bulletin No. 24*. International federation for structural concrete, task group 7.1. ISBN: 978-2-88394-064-2.
- Cosenza E, Manfredi G, Verderame GM (2006) A fibre model for push-over analysis of under-designed reinforced concrete frames, *Computers & structures*, 84(13): 904-916.
- Celarec D., Dolšek M., (2012). Practice-oriented probabilistic seismic performance assessment of infilled frames with consideration of shear failure of columns. *Earthquake Engineering and Structural Dynamics*, 42(9), 1339-1360.
- Celarec, D., Ricci, P., Dolšek, M. (2012). The sensitivity of seismic response parameters to the uncertain modelling variables of masonry-infilled reinforced concrete frames. *Engineering Structures*, 35, 165-177.
- Celik OC and Ellingwood BR (2008) Modeling Beam-Column Joints in Fragility Assessment of Gravity Load Designed Reinforced Concrete Frames, *Journal of Earthquake Engineering*. 12:357-381.
- CEN. European Standard ENV 1998-1-1/2/3. Eurocode 8: Design provisions for earthquake resistance of structures – Part I: General rules. Technical Committee 250/SC8, Comité Européen de Normalisation, Brussels, 2004.
- Chrysostomou, C. Z. (1991). Effects of degrading infill walls on the nonlinear seismic response of two-dimensional steel frames. Ph.D. thesis, Cornell Univ., Ithaca, NY.
- Chrysostomou, C. Z., Gergely, P., and Abel, J. F. (2002). A six-strut model for nonlinear dynamic analysis of steel infilled frames. *Int. J. Struct. Stab. Dyn.*, 2(3), 335–353

- Clyde C, Pantelides CP, Reaveley LD (2000). Performance-Based Evaluation of Exterior Reinforced Concrete Buildings Joints for Seismic Excitation, PEER Report, No. 2000/05, Pacific Earthquake Engineering Research Center, University of California, Berkeley, USA.
- Colangelo F. (2013). Drift-sensitive non-structural damage to masonry-infilled reinforced concrete frames designed to Euro-code 8. *Bulletin of Earthquake Engineering*, 11(6), 2151-2176, 2013.
- Crisafulli, F. J., and Carr, A. J. (2007). Proposed macro-model for the analysis of infilled frame structures. *Bull. New Zealand Soc. Earthquake Eng.*, 40(2), 69–77.
- De Luca F., Verderame G.M., (2015). Seismic Vulnerability Assessment: Reinforced Concrete Structures. In “Encyclopedia of Earthquake Engineering” edited by Michael Beer, Edoardo Patelli, Ioannis Kougoumtzoglou and Siu-Kui Au. Section Editors Fatemeh Jalayer and Carmine Galasso, Springer. (accepted for publication).
- Decreto Ministeriale del 14/1/2008. Approvazione delle nuove norme tecniche per le costruzioni. G.U. n. 29 del 4/2/2008, 2008. (in Italian)
- Deierlein, G. G., H. Krawinkler, and C. A. Cornell. "A framework for performance-based earthquake engineering." Pacific conference on earthquake engineering. 2003.
- Deierlein, G. G., Krawinkler, H., & Cornell, C. A. (2003). A framework for performance-based earthquake engineering. In Pacific conference on earthquake engineering (pp. 1-8).
- Dolšek, M., Fajfar, P. (2001). Soft storey effects in uniformly infilled reinforced concrete frames. *Earthquake Engineering*, 5(1), 1-12.
- Dolšek, M., Fajfar, P. (2004). Inelastic spectra for infilled reinforced concrete frames. *Earthquake Engineering and Structural Dynamics*, 33(15), 1395-1416.
- Dolšek, M., Fajfar, P. (2005). Simplified non-linear seismic analysis of infilled reinforced concrete frames. *Earthquake Engineering and Structural Dynamics*, 34(1), 49-66.
- Dolšek, M., Fajfar, P. (2008a). The effect of masonry infills on the seismic response of a four-storey reinforced concrete frame – a deterministic assessment. *Engineering Structures*, 30(7), 1991-2001.
- Dolšek, M., Fajfar, P. (2008b). The effect of masonry infills on the seismic response of a four-storey reinforced concrete frame – a probabilistic assessment. *Engineering Structures*, 30(11), 3186-3192.
- Dymiotis, C., Kappos, A.J., Chryssanthopoulos, M.K. (2001). Seismic reliability of masonry-infilled RC frames. *ASCE Journal of Structural Engineering*, 127(3), 296-305.
- Elwood KJ, Matamoros AB, Wallace JW, Lehman DE, Heintz JA, Mitchell AD, Moore MA, Valley MT, Lowes LN, Comartin CD, and Moehle JP (2007). Update to ASCE/SEI 41 Concrete Provisions. *Earthquake Spectra*: August 2007, Vol. 23, No. 3, pp. 493-523.
- Elwood, K.J. and Moehle, J.P. (2005) Drift capacity of reinforced concrete columns with light transverse reinforcement, *Earthquake Spectra*, Vol. 12, No. 1, pp. 71–89.
- Elwood, Kenneth J. Modelling failures in existing reinforced concrete columns. *Canadian Journal of Civil Engineering* 31.5 (2004): 846-859.
- Fajfar P., (1999), Capacity spectrum method based on inelastic demand spectra, *Earthquake Engineering and Structural Dynamics*, 28, 979-993.
- Fajfar P., Gaspersic P. (1996), The N2 method for the seismic damage analysis of RC buildings, *Earthquake Engineering and Structural Dynamics*, 25, 31-46.
- Fajfar, P., Drobnič, D. (1998). Nonlinear seismic analyses of the ELSA buildings. Proceedings of the 11th European Conference on Earthquake Engineering, Paris, France, September 6-11.

- Fardis, M.N., Panagiotakos, T.B. (1997). Seismic design and response of bare and masonry-infilled reinforced concrete buildings. Part II: infilled structures. *Journal of Earthquake Engineering*, 1(3), 475-503.
- Fardis, Michael N. Seismic design, assessment and retrofitting of concrete buildings: based on EN-Eurocode 8. Vol. 8. Springer Science & Business Media, 2009.
- Federal Emergency Management Agency (1997). FEMA 273, Guidelines for the seismic rehabilitation. Washington, D.C.
- Federal Emergency Management Agency (2000). FEMA 356, Prestandard and Commentary for the Seismic Rehabilitation of Buildings. Washington, D.C.
- FEMA (1997), NEHRP Guidelines for the Seismic Rehabilitation of Buildings, Federal Emergency Management Agency, Report 273, October 1997.
- Filippou F C, Popov E P, and Bertero VV, (1983) Effects of Bond Deterioration on Hysteretic Behavior of Reinforced Concrete Joints, Report No. UCB/EERC 83/19, University of California-Berkeley, Berkeley, CA, 184 pp.
- Hakuto S, Park R, Tanaka H. (2000) Seismic load tests on interior and exterior beam–column joints with substandard reinforcing details, *ACI Structural Journal*; 97(1):11–25.
- Hamburger, R. O., and Chakradeo, A. S. (1993). Methodology for seismic-capacity evaluation of steel-frame buildings with infill unreinforced masonry. Proc., National Earthquake Conf., Vol. 2, Central U.S. Earthquake Consortium, Memphis, TN, 173–191
- Haselton, C. B. and Deierlein, G. G. (2007). Assessing seismic collapse safety of modern reinforced concrete moment frame buildings, Blume Earthquake Engineering Center TR 156, Stanford University, Stanford, CA.
- Hassan WM (2011) Analytical and Experimental Assessment of Seismic Vulnerability of Beam-Column Joints without Transverse Reinforcement in Concrete Buildings, PhD Dissertation, University of California, Berkeley, California, USA.
- Hegger J, Sherif A, Roeser W (2003). Non-seismic design of beam–column joints. *ACI Structural Journal*; 100(5):654–64.
- Holmes, M. (1961). Steel frames with brickwork and concrete infilling. *ICE Proc.*, 19(4), 473–478.
- Hwang SJ, Lee HJ. (1999) Analytical model for predicting shear strength of exterior RC beam–column joints for seismic resistance. *ACI Structural Journal*; 96(5):846–57.
- Ibarra, L., Medina, R., and Krawinkler, H. (2005). Hysteretic models that incorporate strength and stiffness deterioration, *Earthquake Engineering and Structural Dynamics*, 34 (12), p. 1489-1511.
- Jeon, J. S., Lowes, L. N., DesRoches, R., & Brilakis, I. (2015). Fragility curves for non-ductile reinforced concrete frames that exhibit different component response mechanisms." *Engineering Structures* 85 (2015): 127-143
- Jeon, Jong-Su (2013). Aftershock vulnerability assessment of damaged reinforced concrete buildings in California.
- Kim, J., and LaFave, J. M.(2007a). Key influence parameters for the joint shear behavior of reinforced concrete (RC) beam-column connections, *Engineering Structures* 29, 2523–2539.
- Kim, J., LaFave, J. M., and Song, J. (2007b) A new statistical approach for joint shear strength determination of RC beam-column connections subjected to lateral earthquake loading, *Structural Engineering and Mechanics* 27, 439–456.

- Krawinkler, H. and Mohasseb, S. (1987), Effects of panel zone deformations on seismic response, *Journal of Construction Steel Research*, 8, 233-250.
- Kunnath, S. K., Reinhorn, A. M. and Park, Y. J. (1990). Analytical modeling of inelastic seismic response of R/C structures, *Journal of Structural Engineering*, American Society of Civil Engineers, 116 (4), p. 996-1017.
- LeBorgne, M.R. (2012) Modeling the post shear failure behavior of reinforced concrete columns, Ph.D. Thesis, The University of Texas at Austin, Austin, TX.
- Lee, D.H. and Elnashai, A.S. (2001) Seismic analysis of RC bridge columns with flexure-shear interaction, *ASCE Journal of Structural Engineering*, Vol. 127, No. 5, pp. 546–553.
- Liauw, T. C., and Kwan, K. H. (1984). Nonlinear behaviour of non-integral infilled frames. *Comput. Struct.*, 18, 551–560.
- Liel, Abbie B., Curt B. Haselton, and Gregory G. Deierlein (2010). Seismic collapse safety of reinforced concrete buildings. II: Comparative assessment of nonductile and ductile moment frames. *Journal of Structural Engineering* 137.4: 492-502.
- Lowes LN and Altoontash A. (2003) Modeling Reinforced-Concrete Beam-Column Joints Subjected to Cyclic Loading, *Journal of Structural Engineering*. 129:1686-1697.
- Mainstone, R. J. (1971). On the stiffnesses and strengths of infilled frames. *Proc., ICE Suppl.*, Vol. 4, Building Research Station, Garston, UK, 57–90.
- Negro, P., Colombo, A. (1997). Irregularities induced by nonstructural masonry panels in framed buildings. *Engineering Structures*, 19(7), 576-85.
- Negro, P., Verzeletti, G., (1997). Effect of infills on the global behaviour of R/C frames: energy consideration from pseudodynamic tests. *Earthquake Engineering and Structural Dynamics*, 25(8), 753-773.
- Otani S (1974) Inelastic analysis RC frame structures. *J StructDiv, ASCE*; 100(ST7):1433–49.
- Otani, S. and Sozen, M.A. (1972) Behavior of multistory reinforced concrete frames
- Otani, S. and Sozen, M.A. (1972) Behavior of multistory reinforced concrete frames during earthquakes, *Structural Research Series No. 392*, University of Illinois at Urbana-Champaign, IL.
- Pampanin S, Moratti M, Calvi GM. (2002) Seismic behaviour of RC beam–column joints designed for gravity loads. In: 12th European conference on earthquake engineering. Paper no. 726.
- Pantelides CP, Hansen J, Nadauld J, Reaveley LD (2002) Assessment of Reinforced Concrete Building Exterior Joints with Substandard Details, PEER Report, No. 2002/18, Pacific Earthquake Engineering Research Center, University of California, Berkeley, USA.
- Park R (1997) A static force-based procedure for the seismic assessment of existing reinforced concrete moment resisting frames. *Bulletin of the New Zealand National Society for Earthquake Engineering*, 30(3), 213-226.
- Park S and Mosalam KM (2013) Simulation of Reinforced Concrete Frames with Nonductile Beam-Column Joints, *Earthquake Spectra*, 29(1), 233-257.
- Park S and Mosalam KM, (2012a) Parameters for shear strength prediction of exterior beam–column joints without transverse reinforcement. *Engineering Structures*, 36, 198–209.
- Park S and Mosalam KM, (2012b) Analytical model for predicting the shear strength of unreinforced exterior beam–column joints, *ACI Structural Journal* 109, 149–159.
- Paulay T and Priestley M J N (1992) *Seismic design of reinforced concrete and masonry buildings*. John Wiley & Sons.

- Pincheira, J.A., Dotwiala, F.S., and D'Souza J.T. (1999) Seismic analysis of older reinforced concrete columns, *Earthquake Spectra*, Vol. 15, No. 2, pp. 245–272.
- Pinto, A.V., Verzeletti, G., Molina, J., Varum, H., Coelho, E., (2002). Pseudodynamic tests on non-seismic resisting RC frames (infilled frame and infill strengthened frame tests). Report EUR, EC, Joint Research Centre, Ispra, Italy.
- Polyakov, S. V. (1960). On the interaction between masonry filler walls and enclosing frame when loading in the plane of the wall. Translation in earthquake engineering, Earthquake Engineering Research Institute (EERI), San Francisco, 36–42.
- Priestley M. J. N., Verma, R., and Xiao, Y. (1994). Seismic shear strength of reinforced concrete columns. *Journal of Structural Engineering*, 120(8), 2310–2329.
- Priestley, M. J. N. (1997) Displacement-based seismic assessment of reinforced concrete buildings. *Journal of earthquake Engineering* 1: 157-192.
- Pujol, S., Ramirez, J.A., and Sozen, M.A. (1999) Drift capacity of reinforced concrete columns subjected to cyclic shear reversals, *Seismic Response of Concrete Bridges*, SP-187, American Concrete Institute, Farmington Hills, MI, pp. 255–274.
- Sezen, H. (2002) Seismic behavior and modeling of reinforced concrete building columns, Ph.D. Thesis, Department of Civil and Environmental Engineering, University of California at Berkeley, CA.
- Sezen, H. and Chowdhury, T. (2009) Hysteretic model for the lateral behavior of reinforced concrete columns including shear deformation, *ASCE Journal of Structural Engineering*, Vol. 135, No. 2, pp. 139–146.
- Sezen, H. and Mohele, J.P. (2004). Shear Strength Model for Lightly Reinforced Concrete Columns. *ASCE Journal of Structural Engineering*. 130(11), 1692-1703.
- Sharma A, Eligehausen R, Reddy GR (2011) “A new model to simulate joint shear behavior of poorly detailed beam–column connections in RC structures under seismic loads, part I: exterior joints”. *Engineering Structures*, 33(3), 1034-1051.
- Shin M and LaFave JM (2004a) “Testing and modelling for cyclic joint shear deformations in RC beam–column connections”. *Proceedings of the thirteenth world conference on earthquake engineering*. Paper no. 0301.
- Shin, M., and LaFave, J. M. (2004b) “Modeling of cyclic joint shear deformation contributions in RC beam-column connections to overall frame behavior” *Structural Engineering and Mechanics*, 18(5), 645-669.
- Shiohara, H. (2004) Quadruple flexural resistance in R/C beam-column joints, 13th world Conference on Earthquake Engineering, Paper No. 491, Vancouver, Canada.
- Smith, B. S. (1962). “Lateral stiffness of infilled frames.” *J. Struct. Div.*, 88(6), 183–199.
- Spacone, E., Filippou, F. C., and Taucer, F. F. (1996). “Fiber beam-column model for nonlinear analysis of R/C frames. 1: formulation,” *Earthquake Engineering and Structural Dynamics*, 25 (7), p. 711-725.
- Spacone, E., Filippou, F.C., and Taucer, F.F. (1996) Fibre beam-column model for nonlinear analysis of R/C frames: Part I Formulation, *Earthquake Engineering and Structural Dynamics*, Vol. 25, No. 7, pp. 711–725.
- Thiruvengadam, V. (1985). “On the natural frequencies of infilled frames.” *Earthquake Eng. Struct. Dyn.*, 13(3), 401–419

- Tsonos AG (2007) “Cyclic load behaviour of reinforced concrete beam–column sub-assemblages of modern structures”, *ACI Structural Journal*; 104(4):468–78.
- Vamvatsikos D., Cornell C.A. (2002), Incremental dynamic analysis. *Earthquake Engineering and Structural Dynamics*, 31(3), 491-514, 2002.
- Vecchio, F.J. and Collins, M.P. (1986) The modified compression field theory for reinforced concrete elements subjected to shear, *ACI Structural Journal*, Vol. 83, No. 2, pp. 219–231.
- Vollum RL and Newman JB (1999) “Strut and tie models for analysis/design of external beam–column joints.” *Mag Concr Res*;51(6):415–25.
- Wong HF (2005) “Shear strength and seismic performance of non-seismically designed RC beam–column joints”. Ph.D. thesis. Hong Kong University of Science and Technology.
- Youssef M, Ghobarah A (2001). “Modelling of RC beam–column joints and structural walls”. *Journal Earthquake Engineering*;5(1):93–111.
- Zhu L., Elwood K. & Haukaas T., 2007. Classification and seismic safety evaluation of existing reinforced concrete columns. *Journal of Structural Engineering*, (September), 1316–1330.

Chapter 3

INFLUENCE OF INFILL DISTRIBUTION AND DESIGN TYPOLOGY ON SEISMIC PERFORMANCE OF LOW- AND MID-RISE RC BUILDINGS

A growing attention has been addressed to the influence of infills on the seismic behavior of Reinforced Concrete buildings, also supported by the observation of damage to infilled RC buildings after severe earthquakes (e.g. L'Aquila 2009, Lorca 2011). In this Chapter, a numerical investigation on the influence of infills on the seismic behavior of four different case study buildings is carried out: four- and eight- story buildings, designed for seismic loads according to the current Italian technical code or for gravity loads only according to an obsolete technical code, are considered. Seismic capacity at two Limit States (Damage Limitation and Near Collapse) is assessed through static push-over analyses, within the N2 spectral assessment framework. Different infill configurations are considered (Bare, Uniformly Infilled, Pilotis), and a sensitivity analysis is carried out, thus evaluating the influence of main material and capacity parameters on seismic response, depending on the number of stories and the design typology. Fragility curves are obtained, through the application of a Response Surface Method. Seismic performance is also expressed in terms of failure probability, given a reference time period.

3.1 Introduction

During last decades, post-earthquake damage (e.g., Kocaeli 1999, L'Aquila 2009, Lorca 2011), numerical and experimental studies showed that a growing attention must be addressed to the influence of infills on the seismic behavior of Reinforced Concrete (RC) buildings. Currently, infills are generally considered in RC buildings as partition elements without any structural function, thus neglecting their significant influence on the increase in lateral stiffness and base shear, on the reduction in period of vibration, on possible brittle failure mechanisms in joints and columns due to local interaction between panels and the adjacent structural elements, and on the building collapse mechanism. As far as performance of RC structures during L'Aquila earthquake (2009) is concerned, the main damage involved non-structural elements such as infill panels and documented building collapses were essentially caused by irregularities in plan or elevation caused also by non-structural elements distribution (Ricci et al., 2010). Thus, infill panels have played an important role in the observed damage to RC structures (Verderame et al, 2010a). Moreover, during Lorca earthquake (2011), most of the losses were caused by non-structural damage (Cabañas et al., 2011; Goula et al., 2011) and masonry infills have provided an important additional strength to RC buildings - especially because no proper seismic principle was present in the design of most of Lorca RC buildings - avoiding in many cases the collapse of the structure (Gómez-Martínez et al., 2012).

In Chapter 2 (Section 2.1.3), it was shown that some experimental and analytical investigations were performed on infilled RC structures, regarding both "local" and "global" effects on the seismic performance. Many modeling proposals were also carried out in literature (as shown in Section 2.1.3).

In this Chapter, the effect of infills on the global seismic behavior of RC frames is investigated, by analyzing their influence on global stiffness and strength, on the kind of collapse mechanism, on the displacement capacity and, consequently, on seismic capacity and seismic fragility at different performance levels (i.e., Limit States), depending on the main characteristics of the RC frame, such as the design typology and the number of stories.

To this end, RC elements are modeled in one of the simpler approach (in lumped plasticity approach, as explained in Section 3.2), beam-column joints are rigid and a single strut model is adopted for infills, as in most of the

previous literature studies.

Simulation studies on the effect of uncertainty in several of the input parameters of the structural model – usually neglected in design and assessment procedures – on the seismic response of infilled RC structures are performed through sensitivity and fragility analyses.

Sensitivity analysis is a quite simple way to underline the effect of each of the input Random Variable (RV) on the seismic response of the infilled RC structure, thus identifying the input variables which produce the greatest impact (Celarec et al., 2012).

Fragility analysis is a higher step for uncertainty analysis which allows to take into account the effect of the contemporary in the variation of the input variables on the seismic response at a certain Limit State. Sensitivity and fragility analyses are performed, as explained in next sections.

Four- and eight- story buildings, designed for seismic loads according to the current Italian technical code or for gravity loads only according to an obsolete technical code, are considered. Infills are modeling through equivalent diagonal struts and the potential brittle failure mechanisms due to the local interaction between masonry infills and structural RC elements or out of plane failures are not accounted for herein.

Seismic capacity at two different Limit States, namely Damage Limitation (DL) and Near Collapse (NC), is assessed by means of Static Push-Over (SPO) analyses, within the N2 spectral assessment framework.

Different infill configurations are considered (Bare, Uniformly infilled and Soft-story infilled), and sensitivity analysis is carried out, thus evaluating the influence of main material and capacity parameters on seismic response at different Limit States, depending on the number of stories and the design typology.

Then, fragility curves are obtained through the application of a Response Surface Method and seismic performance is also expressed in terms of failure probability, given a reference time period.

A comprehensive comparison between seismic response related to different infill distributions in elevation, number of stories and design typology of the bare structure is performed, too, through the analysis of the case study structures, hence highlighting the difference in seismic performance at different Limit States and for each structure.

After comparing the expected (median) seismic capacity of the case study

structures, failure probabilities will be calculated – based on the results of the fragility analysis – and compared, thus highlighting the influence of uncertainty on the seismic performance at different Limit States and for each design typology and infill configuration.

It will be pointed out the great importance of infills and their mechanical properties, especially at low level of seismic demand, namely at Damage Limitation Limit State, both for structures designed only for gravity-loading or according to new seismic codes provisions, thus highlighting the necessity of a deeper investigation towards this direction in developing new procedures to account for infill presence directly or indirectly via the more widespread kind of analyses (linear analyses), as shown in Chapter 4.

Vice-versa at higher performance levels, mechanical parameters of RC elements have the major influence on seismic capacity.

3.2 Case study structures

The case study structures analyzed in this Chapter are symmetric in plan, both in longitudinal (X) and in transverse (Y) direction, with five bays in longitudinal direction and three bays in transverse direction. Interstorey height is equal to 3.0 m, bay length is equal to 4.5 m. Slab way is always parallel to the transverse direction; dead load from slab (without dead load related to beams and columns) is equal to 4.57 kN/m² for the last storey and 5.77 kN/m² for all of the other ones; live load is equal to 2 kN/m². So the four case study buildings are:

- two gravity load designed (GLD) buildings, a four-storey and an eight-storey building, defined by means of a simulated design procedure according to code prescriptions and design practices in force in Italy between 1950s and 1970s (Regio Decreto Legge n. 2229, 16/11/1939; Verderame et al., 2010b). The structural configuration follows the parallel plane frames system: gravity loads from slabs are carried only by frames in longitudinal direction. Beams in transverse direction are present only in the external frames. Element dimensions are calculated according to the allowable stresses method; the design value for maximum concrete compressive stress is assumed equal to 5.0 and 7.5 MPa for axial load and

axial load combined with bending, respectively. Column dimensions are calculated according only to the axial load based on the tributary area of each column, beam dimensions and reinforcement are determined from bending due to loads from slabs. Reinforcing bars are smooth and their allowable design stress is equal to 160 MPa. Section dimensions are (30x50)cm² for beams, whereas they are strongly variable for columns, depending on the design axial load, ranging from (40x75)cm² for the internal columns at the first story of the eight-story frame to (30x30)cm² at the top story. Longitudinal reinforcement ratio is between 0.5 and 0.9% in beams, whereas reinforcement in columns corresponds to the minimum amount of 0.8% of the section area, as prescribed by code (Regio Decreto Legge n. 2229, 16/11/1939);

- two seismic load designed (SLD) buildings, a four-storey and an eight-storey building, designed for seismic loads according to the current Italian code (Decreto Ministeriale del 14/1/2008) in Ductility Class High. Beams in transverse direction now are present also in the internal frames. The principles of the Capacity Design are applied. C25/30 concrete ($f_{cd} = 14.17$ MPa) and B450C steel ($f_{yd} = 391.3$ MPa) are used. Mean values for materials strength are assumed equal to 36 MPa and 550 MPa for concrete and steel respectively (Cosenza et al., 2009a,b). They are located in a high seismic city in Southern Italy (Avellino, Lon.: 14.793 Lat.: 40.915); soil type A (stiff soil) and 1st topographic category are assumed; the Peak Ground Acceleration (PGA) used for the design at Significant Damage Limit State (SLV) – corresponding to an exceeding probability of 10% in 50 years, that is, to a return period of 475 years – is equal to 0.19g. The 8-storey frame has both higher elastic period and higher mass with respect to the 4-storey frame, but base shear due to seismic loads is very similar in the two cases and, therefore, the analyzed frames have identical geometry and longitudinal reinforcement for beams and columns. Section dimensions are (30x50)cm² for beams and (30x60)cm² for columns. Longitudinal reinforcement ratio is about equal to 1.0% in beams and to 1.4 and 2.0% in external and internal columns, respectively.

The choice of these case study structures can be considered as representative of Italian building typologies because it is supported by in-situ

surveys carried out in different Italian cities (Cosenza et al., 2003; Pecce et al., 2004; Polese et al., 2008).

For each case study, three hypotheses are made about the infill configuration:

- Case 1: infill panels are uniformly distributed along the height (Uniformly Infilled frame, see Figure 3.1a).
- Case 2: first story is bare and upper stories are infilled (Pilotis frame, see Figure 3.1b).
- Case 3: no infill panel is present (Bare frame, see Figure 3.1c).

Infills panels, if present, are uniformly distributed in all the external frames of the building. Panel thickness is equal to 20 cm, corresponding to a double layer brick infill (120+80) mm thick, which can be considered as typical of a non-structural infill masonry wall (Bal et al., 2007). Presence of openings is not taken into account.

Nonlinear response of RC elements is modeled by means of a lumped plasticity approach: beams and columns are represented by elastic elements with rotational hinges at the ends. A three-linear envelope is used, where characteristic points are cracking, yielding and ultimate. Section moment and curvature at cracking and yielding are calculated on a fiber section, for an axial load value corresponding to gravity loads. The behavior is assumed linear elastic up to cracking and perfectly-plastic after yielding. Rotations at yielding and ultimate are evaluated through the formulations given in (Fardis, 2007). As far as ultimate rotation is concerned, consistent with the characteristics of tests included in the experimental database employed to obtain the formulation given in (Fardis, 2007), the proposed expression for the ultimate rotational capacity should be applied only to members with deformed bars, with seismic detailing and without lapping of longitudinal bars in the vicinity of plastic hinge region (typical of SLD structures). Nevertheless, this kind of formulation can be extended to members with different characteristics (non-conforming elements) through correction coefficients calibrated on the basis of experimental data on non-conforming members (Panagiotakos et al., 2002; Fardis and Biskinis, 2003; Fardis, 2009; Biskinis and Fardis, 2010; Verderame et al., 2010c), in order to take into account that non-conforming members have a lower mean rotational capacity. Notwithstanding, in (Verderame et al., 2010c) it is shown that the formulation proposed in (Fardis, 2007) is able to predict the deformation capacity at ultimate of non-conforming RC members with plain

bars, without the need for the application of any correction coefficient, based on experimental data about deformation capacity of this specific kind of elements.

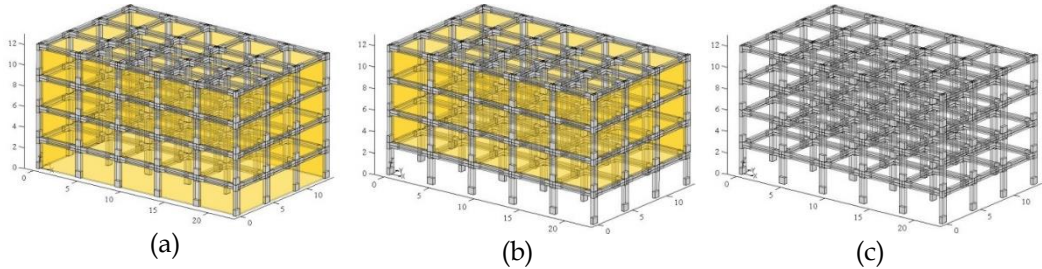


Figure 3.1. Uniformly infilled (a), Pilotis (b) and Bare (c) frames – four-storeys seismic loads design case-study structure

Infill panels are modeled by means of equivalent struts. Modeling infills through single compressed struts allows to investigate the effects of the panels on the global behavior of the analyzed structure. The adopted model for the envelope curve of the force-displacement relationship is the model proposed by Panagiotakos and Fardis (Panagiotakos and Fardis, 1996; Fardis, 1997). The proposed force-displacement envelope is composed by four branches, as shown in Figure 3.2.

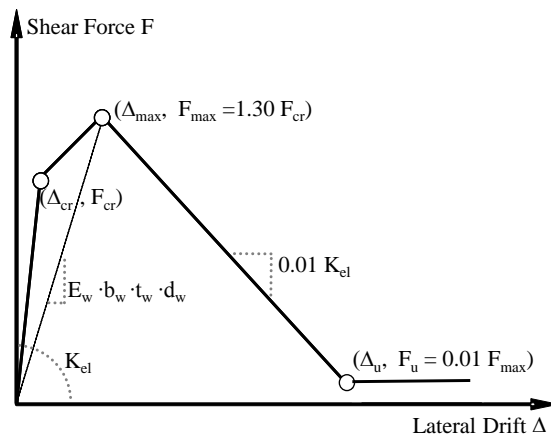


Figure 3.2. Panagiotakos and Fardis (1996): single-strut infill model

The first branch corresponds to the linear elastic behavior up to cracking;

the slope of this branch is the elastic stiffness of the infill panel k_{el} , and it can be expressed according to Equation (3.1), being A_w is the transversal area of the infill panel, G_w the shear elastic modulus and h_w its clear height. If τ_{cr} is the shear cracking stress, the shear cracking strength F_{cr} can be obtained according to Equation (3.2).

$$K_{el} = \frac{G_w A_w}{h_w} \quad (3.1)$$

$$F_{cr} = \tau_{cr} A_w \quad (3.2)$$

The second branch continues up to the maximum strength F_{max} , which can be calculated according to Equation (3.3). The corresponding displacement Δ_{max} is estimated according to the hypothesis that the secant stiffness up to maximum is provided by Mainstone's formulation (Mainstone, 1971), assuming that the width of the equivalent truss b_w can be evaluated according to Equation (3.4), being h_w and d_w the height and the diagonal length of the panel, respectively, and λ_h defined according to Equation (3.5). In Equation (3.5), E_w and E_c are the elastic Young modulus of the infill panel and of the surrounding concrete, respectively; θ is the diagonal slope of the equivalent truss to the horizontal; t_w is the infill thickness; I_c is the moment of inertia of the adjacent columns. Secant stiffness up to maximum is provided by the expression shown in Equation (3.6).

$$F_{max} = 1.30 \cdot F_{cr} \quad (3.3)$$

$$b_w = 0.175 (\lambda_h h_w)^{-0.4} d_w \quad (3.4)$$

$$\lambda_h = \sqrt[4]{\frac{E_w t_w \sin(2\theta)}{4E_c I_c h_w}} \quad (3.5)$$

$$K_{sec} = \frac{E_w b_w t_w}{\sqrt{L^2 + H^2}} \cos \theta \quad (3.6)$$

The third branch of the envelope is a degrading branch up to the achievement of a constant branch, i.e. up to the "infill residual strength point"; its slope (k_{deg}) depends on the elastic stiffness through the parameter α (Panagiotakos and Fardis, 1996), as shown in Equation (3.7). Authors suggest values in the range [0.005; 0.1] for the parameter α . Last branch is horizontal; it corresponds to a residual constant strength; residual-to-maximum strength

ratio β can be assumed equal to 1-2% (Panagiotakos and Fardis, 1996). In this Chapter, the ratio between post-capping degrading stiffness and elastic stiffness (parameter α) is assumed equal to 0.01. The ratio between residual strength and maximum strength (parameter β) is assumed equal to 0.01.

$$K_{deg} = -\alpha K_{el} \quad (3.7)$$

3.2.1. Analysis methodology

Nonlinear static push-over (SPO) analyses are performed on the case study buildings both in X and Y direction. The assumed lateral load pattern is proportional to the displacement shape of the first mode. Lateral response is evaluated in terms of base shear-top displacement relationship. Structural modeling, numerical analyses and post-processing of damage data, including the 3D graphic visualization of the deformed shape, are performed through the “PBEE toolbox” software (Dolšek, 2010), combining MATLAB® with OpenSees (McKenna et al., 2004), modified in order to include also infill elements (Ricci, 2010; Celarec et al., 2012). When the lateral response is characterized by a strength degradation due to the achievement of the degrading branch of the force-displacement relationship of the infills up to their “infill residual strength point”, a multi-linearization of the pushover curve is carried out by applying the equal energy rule respectively between the initial point and the maximum resistance point, between the maximum resistance point and the point corresponding to the achievement of the last “infill residual strength point”, between the point corresponding to the achievement of the last “infill residual strength point” and the point corresponding to the first RC element conventional collapse. Vice versa when the lateral response is not characterized by a strength degradation (because infill elements are not present or not involved in the collapse mechanism) an elasto-plastic bi-linearization is carried out by applying the equal energy rule between the initial point and the maximum resistance point.

Two Limit States (LSs) are investigated: Damage Limitation (DL) and Near Collapse (NC).

The definition of DL LS should take into account that the damage occurring at this LS has to be easily and economically repaired. As far as the infills are concerned, it can be assumed that the requirement corresponding to such a

criterion is that the infill panel has not achieved the inter-storey drift corresponding to its maximum resistance, as some experimental results pointed out (Colangelo, 2012; Hak et al., 2012), although at this stage some cracks have already occurred. In literature, different assumptions can be found regarding the diffusion of this kind of damage (that is, the proportion of panels reaching the maximum resistance displacement) to be assumed as corresponding to the attainment of this LS. As a matter of fact, according to different authors this LS occurs when the maximum resistance displacement is reached in first infill panel (Dolšek and Fajfar, 2006; Colangelo, 2012; Hak et al., 2012), in 50% of the infill panels at one story (Celarec and Dolšek, 2012), or in all of the infill panels at one story (Dolšek and Fajfar, 2008a). In this study, the first definition is conservatively adopted, thus assuming that DL LS in infills is attained at the displacement when the first infill panel reaches its maximum resistance thus starting to degrade; hence, taking into account also RC elements, the achievement of DL LS corresponds to the minimum between such displacement and the displacement when the first yielding in RC members occurs. However, in the case study structures analyzed in this Chapter (the clear span of each infill panel is almost the same) all the infills at the same story have the same displacement capacity and reach their maximum resistance at same time. However, this issue will be better discussed in Chapter 4 and it should deserve further discussion in the future.

NC LS is defined as the point corresponding to the first conventional collapse in RC members (i.e., the first RC member reaches its ultimate rotation), independent of the displacement demand on the infill panels. The definition of NC LS is consistent with the code-based approach (EC8-3, 2004), according to which, the failure of one RC member conventionally corresponds to structural failure. Such an approach is generally conservative when structural elements have a ductile behavior; in fact, also after the first conventional failure of a structural member, the structure is yet able to exhibit a further reserve of seismic capacity.

It should be noting that potential brittle failure mechanisms are not taken into account in this Chapter.

IN2 curves (Dolšek and Fajfar, 2004b; Dolšek and Fajfar, 2008b) for the equivalent SDoF systems are obtained by assuming as Intensity Measure both the elastic spectral acceleration at the period of the equivalent SDoF system (Sae(Teff)) and the Peak Ground Acceleration (PGA). Values of these seismic intensity parameters corresponding to characteristic values of displacement

(ductility) demand (including the considered LSs) are calculated, based on the R- μ -T relationships given in (Dolšek and Fajfar, 2004a) or in (Vidic et al., 1994) for degrading or non-degrading response, respectively.

Moreover, the procedure proposed in (Dolšek and Fajfar, 2005) to improve the accuracy of the displacement demand assessment in the case of low seismic demand is applied, by using specific R- μ -T relationships in this range of behavior, as proposed by the Authors.

Elastic spectra are the Uniform Hazard Newmark-Hall demand spectra adopted in Italian code (Decreto Ministeriale del 14/1/2008) – provided by (INGV-DPC S1, 2007) – for a high seismic city in Southern Italy (Avellino, Lon.: 14.793 Lat.: 40.915). Soil type A (stiff soil) and 1st topographic category are assumed (no amplification for stratigraphic or topographic effects). It is worth noting that a double iterative procedure is required to evaluate $S_{ae}(T_{eff})$ and PGA from the characteristic parameters of equivalent SDoF system – namely the ductility at the point of interest (μ), the period (T_{eff}) and for degrading systems also the ductility at the beginning of the degradation (μ_s) and the ratio between the residual strength and the maximum strength (r_u) – for the following reasons: (i) the spectral shape depends on some parameters, such as the corner period (T_C) and the ratio between the spectral acceleration on the constant branch and the PGA (F_0), which are not constant with the seismic intensity (i.e., with the return period), hence also the ratio between $S_{ae}(T_{eff})$ and PGA changes with the seismic intensity; (ii) some characteristic parameters of the elastic spectrum, such as T_C , are input parameters for the R- μ -T relationship, but also depends on the results obtained from the R- μ -T relationship since they depends on the seismic intensity. Due to the fact that the ratio between $S_{ae}(T_{eff})$ and PGA is not constant, the IN2 curves in terms of $S_{ae}(T_{eff})$ or in terms of PGA may have different shapes.

Demand spectra are provided by (INGV-DPC S1, 2007) in terms of parameters PGA, F_0 and T_C^* (which is multiplied by another coefficient depending on stratigraphic characteristics, C_C , to obtain T_C) for a range of return periods from 30 to 2475 years. For intermediate values of seismic intensity, an interpolation procedure is proposed (Decreto Ministeriale del 14/1/2008). Nevertheless, in this study there is the need to extend elastic demand spectra above and below the extreme values, as in (Liel et al., 2009). To this aim, the formulations proposed for the interpolation procedure are also

used to extrapolate the above mentioned parameters out of the given range of values.

3.3 Sensitivity analysis

In order to evaluate the influence of material characteristics and element capacity on the seismic response of the case study structure, a sensitivity analysis is carried out (Celarec et al., 2012; Celarec and Dolšek, 2010).

3.3.1. Selected random variables

In order to carry out a sensitivity analysis, the following parameters are selected as Random Variables (RVs):

- Concrete compressive strength, f_c ;
- Steel yield strength, f_y ;
- Chord rotation at yielding in RC members, θ_y ;
- Chord rotation at ultimate in RC members, θ_u ;
- "Loads" of load-displacement relationship of the infill trusses, F_{infill} ;
- "Displacements" of load-displacement relationship of the infill trusses, D_{infill} .

The variable F_{infill} is a vector whose components are $[F_{cr}; F_{max}]$, where F_{cr} and F_{max} are cracking and maximum strength of infills, respectively; similarly, the variable D_{infill} is the vector $[D_{cr}; D_{max}]$, where D_{cr} and D_{max} are cracking and maximum displacement of infills, respectively. Residual strength and corresponding displacement of infills are obtained from F_{infill} and D_{infill} according to the adopted model (Fardis, 1997). Loads and displacements of the load-displacement relationship of the infill trusses can thereby vary independently of each other. The variability of F_{infill} and D_{infill} includes both mechanical and modeling variability, as explained below.

A lognormal distribution is assumed for all of the RVs. Each distribution is defined through the central (median) value and the Coefficient of Variation (CoV) – see Table 3.1.

<i>RV</i>	<i>Distribution</i>	Seismic Load Design			Gravity Load Design		
		<i>Median Value</i>	<i>CoV</i>	<i>Reference</i>	<i>Median Value</i>	<i>CoV</i>	<i>Reference</i>
f_c	Lognormal	36.0 MPa	0.20	(Cosenza et al., 2009a)	25.0 MPa	0.31	(Verderame et al., 2001)
f_y	Lognormal	550.0 MPa	0.06	(Cosenza et al., 2009b)	369.7 MPa	0.08	(Verderame et al., 2012)
θ_y	Lognormal	$1.015 \times \theta_{y,calculated}$	0.331	(Fardis, 2007)	$1.015 \times \theta_{y,calculated}$	0.331	(Fardis, 2007)
θ_u	Lognormal	$0.995 \times \theta_{u,calculated}$	0.409	(Fardis, 2007)	$0.995 \times \theta_{u,calculated}$	0.409	(Fardis, 2007; Verderame et al., 2010c)
F_{infill}	Lognormal	$[F_{cr}; F_{max}]$	[0.30; 0.30]	(Fardis, 1997; Rossetto and Elnashi, 2005; Calvi et al., 2004)	$[F_{cr}; F_{max}]$	[0.30; 0.30]	(Fardis, 1997; Rossetto and Elnashi, 2005; Calvi et al., 2004)
D_{infill}	Lognormal	$[D_{cr}; D_{max}]$	[0.30; 0.70]	(Fardis, 1997; Rossetto and Elnashi, 2005; Calvi et al., 2004)	$[D_{cr}; D_{max}]$	[0.30; 0.70]	(Fardis, 1997; Rossetto and Elnashi, 2005; Calvi et al., 2004)

Table 3.1. Joint shear coefficient according to ASCE-SEI 41 (2007)

For the concrete compressive strength, reference values come from a statistical analysis on the mechanical properties of concrete employed in Italy (Verderame et al., 2001; Cosenza et al., 2009a). For the steel yield strength, values are referred to Aq50 steel typology (the most widely spread in Italy during 1960s) for GLD structures (Verderame et al., 2012), and to B450C for SLD structures (Cosenza et al., 2009b).

The determination of infill material characteristics is affected by high difficulties and uncertainties, and literature does not offer an enough large amount of experimental data. In this study, a median value of 1240 MPa for the shear elastic modulus G_w is adopted, based on wallette tests carried out at the University of Pavia on specimens made up of hollow clay bricks with a void ratio of 42%, selected as representative of typical light non-structural masonry (Fardis, 1997). Nevertheless, there are further infill mechanical characteristics to be determined in order to define, according to the adopted model, the load-displacement relationship of the infill trusses, namely the elastic Young's modulus E_w and the shear cracking stress τ_{cr} . A certain amount of correlation

certainly exists between these parameters, although it is not easy at all to be determined. In this study, the ratio between E_w and G_w is assumed equal to 10/3 based on the proposal of the Italian code (Circolare del Ministero dei Lavori Pubblici n. 617 del 2/2/2009), whereas τ_{cr} is assumed as independent on G_w , due to the independence between the RVs F_{infill} and D_{infill} .

Figure 3.3 shows the load-displacement relationships of the infill trusses related to (i) median values of F_{infill} and D_{infill} (red curve), (ii) the variation of F_{infill} only respect to median values (blue curves) and (iii) the variation of D_{infill} only respect to median values (green curves). These curves are obtained assuming median-minus-1.7-standard-deviation and median-plus-1.7-standard-deviation values for the two RVs.

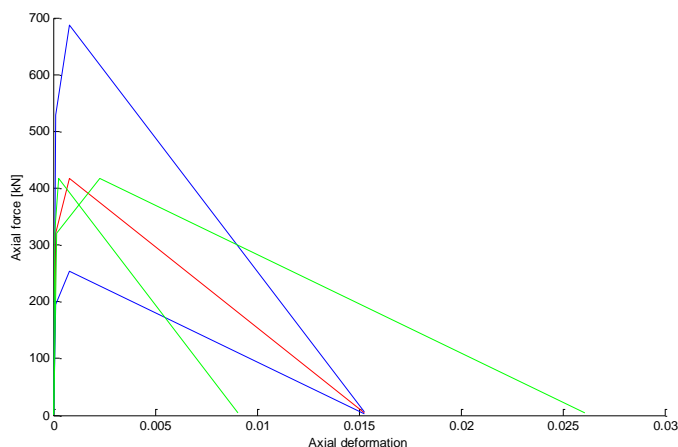


Figure 3.3. Load-displacement relationships of the infill trusses for median values of F_{infill} and D_{infill} (red), for the variation of F_{infill} respect to median values (blue) and for the variation of D_{infill} respect to median values (green)

As far as the modeling of uncertainty in infill mechanical properties is concerned, both mechanical (Young's modulus, shear elastic modulus, shear cracking strength) and modeling (maximum to shear cracking strength ratio, secant to peak stiffness) variability are considered based on experimental tests from literature and on experimental-to-predicted ratios obtained from the adopted infill model (Fardis, 1997). These two sources of variability are previously considered independently of one another: a CoV equal to 0.30 is assumed for both the elastic Young's modulus E_w (Calvi et al., 2004) – and consequently for the shear elastic modulus (Circolare del Ministero dei Lavori

Publici n. 617 del 2/2/2009) - and the shear cracking stress τ_{cr} (Calvi et al., 2004; Dymiotis et al., 2001); CoVs equal to 0.12 and 0.70 for the maximum-to-shear cracking strength ratio and the secant-to-peak stiffness, respectively, are used: they are obtained through the evaluation of the dispersion of the experimental-to-predicted ratio derived applying Fardis' model (Fardis, 1997) to the experimental tests from (Pires, 1990; Stylianidis, 1985), which the model itself is based on. The only variability of G_w , with equal all of the other variables, would lead to a CoV for D_{cr} and D_{max} equal to 0.30 according to the adopted infill model (Fardis, 1997); similarly, the only variability of τ_{cr} would lead to a CoV for D_{cr} , D_{max} , F_{cr} and F_{max} equal to 0.30; moreover, the only variability of maximum to shear cracking strength ratio would lead to a CoV for F_{max} and D_{max} equal to 0.12: thus modeling variability about maximum-to-shear cracking strength ratio is negligible. Finally, the only variability of secant to peak stiffness would lead to a CoV for D_{max} equal to 0.70. Therefore, the maximum CoVs for the parameters F_{cr} , F_{max} , D_{cr} and D_{max} - induced by the variation of mechanical and modeling variables - are obtained (0.30, 0.30, 0.30 and 0.70, respectively): the variability of the parameter D_{max} is governed by model variability due to secant-to-peak stiffness, whereas all of the other values of variability are given by variability of material properties.

As far as deformations at yielding and ultimate in RC members are concerned, median and CoV values are evaluated starting from the values calculated through the formulations proposed in (Fardis, 2007) and using median and CoV values of the experimental-to-predicted ratio, as illustrated by the author.

A sensitivity analysis is carried out to investigate the influence of each variable on the seismic capacity of each case study structure. The seismic capacity can be defined in terms of $S_{ae}(T_{eff})$ or PGA. The seismic capacity expressed in term of PGA - for a certain LS - is defined as the PGA corresponding to the demand spectrum under which the displacement demand is equal to the displacement capacity for that LS. PGA capacity at a certain LS is represented by the ordinate of the IN2 curves (expressed in terms of PGA) corresponding to the displacement capacity of the equivalent SDoF system S_d at that LS. In the same way, seismic capacity expressed in term of $S_{ae}(T_{eff})$ can be defined.

In order to carry out a sensitivity analysis, two models are generated for each RV assuming median-minus-1.7-standard-deviation and median-plus-1.7-

standard-deviation values for the considered variable, and median values for the remaining variables. The choice of these values will be better explained when the Response Surface Method (RSM) will be used in the fragility analysis carried out below. In addition, another analysis is carried out assuming median values for all of the variables (Model#1).

3.3.2. Analysis of results

In the following, obtained results are presented and discussed for Uniformly infilled, Pilotis and Bare frames, in both longitudinal and transverse directions and at DL and NC LSs in terms of $S_{ae}(T_{eff})$ or PGA. The $[S_d, S_{ae}(T_{eff})]$ and $[S_d, PGA]$ points on IN2 curves corresponding to DL and NC LSs are reported as yellow and red circles, respectively. The dashed horizontal branch in IN2 curves after the achievement of the NC LS conventionally represents the structural failure.

SPO (black), multi-linearized SPO (red) and IN2 in terms of $S_{ae}(T_{eff})$ (blue) curves and collapse mechanisms for Models#1 in both directions and for each infill configuration are shown in Figures 3.4 and 3.5 for the 4-storey SLD and the 4-storey GLD structures, respectively. SPO, multi-linearized SPO and IN2 curves and collapse mechanisms are also obtained for the 8-storey structures, but they are omitted in this Section for the sake of brevity.

Stories involved in all of the collapse mechanisms and stories involved in the achievement of DL LS for Models#1 in both X and Y direction and for each infill configuration of all the analyzed structures are reported in Tables 3.2 and 3.3, respectively.

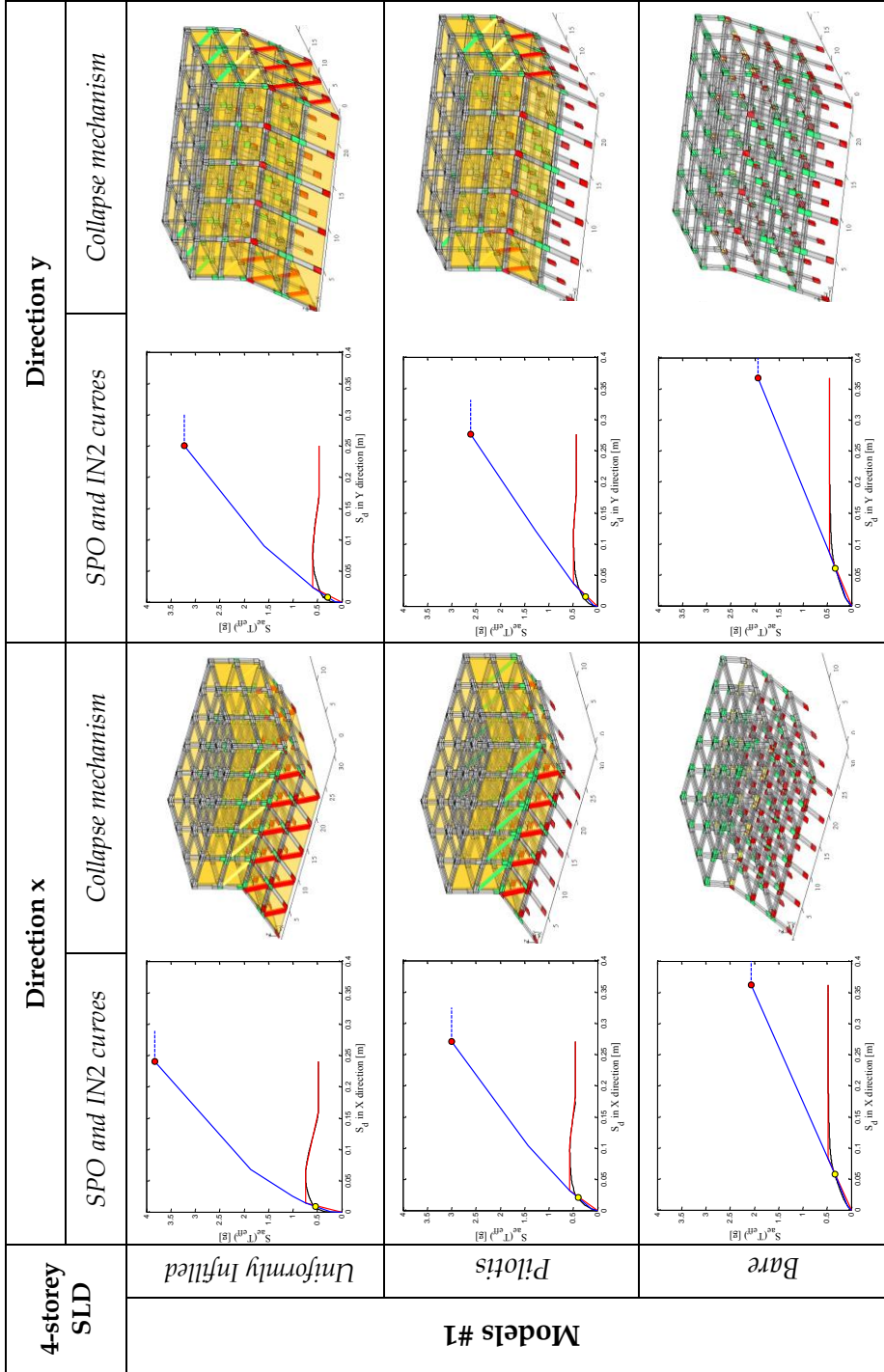


Figure 3.4. SPO (black), multi-linearized SPO (red) and IN2 in terms of $S_{ae}(T_{eff})$ (blue) curves, deformed shape and element damage at NC for Models#1 (4-storey SLD)

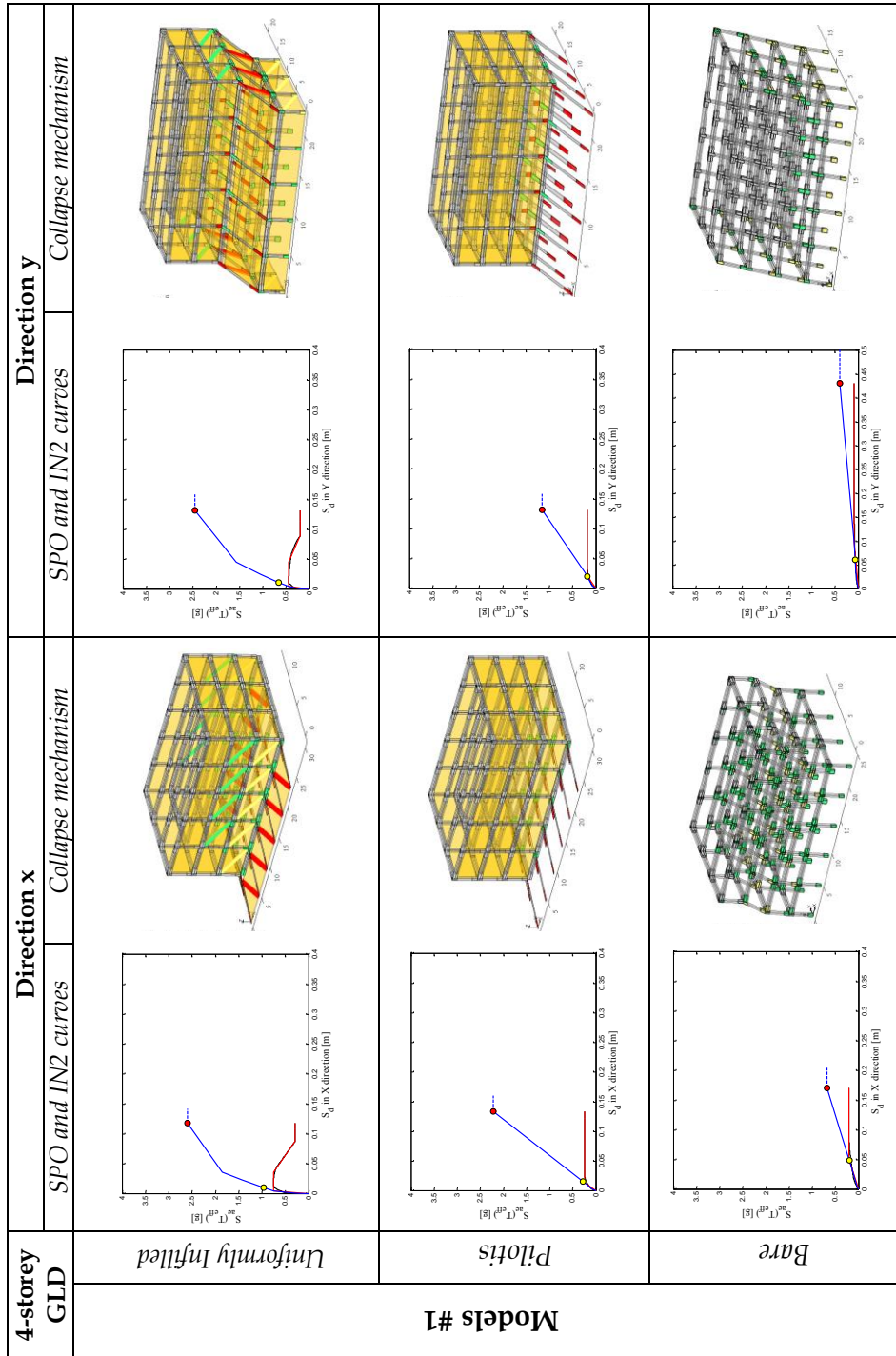


Figure 3.5. SPO (black), multi-linearized SPO (red) and IN2 in terms of Sae(Teff) (blue) curves, deformed shape and element damage at NC for Models#1 (4-storey GLD)

Infill config.	4- SLD		4- GLD		8- SLD		8- GLD	
	<i>x</i>	<i>y</i>	<i>x</i>	<i>y</i>	<i>x</i>	<i>y</i>	<i>x</i>	<i>y</i>
Uniformly Infilled	1+2	1+2	1	2	1+2+3	1+2+3+4	2+3	3+4
Pilotis	1+2	1+2	1	1	1+2	1+2+3+4	1+2	1+2+3
Bare	1+2+3	1+2+3	3	global	1+2+3+4+5	1+2+3+4+5	2+3+4+5+6	global

Table 3.2. Stories involved in the collapse mechanism for the Models#1 of each analyzed structure

Infill config.	4- SLD		4- GLD		8- SLD		8- GLD	
	<i>x</i>	<i>y</i>	<i>x</i>	<i>y</i>	<i>x</i>	<i>y</i>	<i>x</i>	<i>y</i>
Uniformly Infilled	1+2	2	1	1+2	2	2	2	2
Pilotis	1	2	1	1	2	2	2	2
Bare	2	2	2	4	2	2	3+4	3

Table 3.3. Stories involved in the achievement of DL LS for the Models#1 of each analyzed structure

As shown in Table 3.3, the achievement of DL LS can involve contemporary more than one story - despite the definition of DL LS itself - if the first yielding occurs contemporary in more than one RC member or if all of the infills in more than one story reach their maximum resistance thus starting to degrade.

SPO and IN2 curves in terms of $S_{ae}(T_{eff})$ or PGA and collapse mechanisms can be obtained for all of the other models - of each case study structure - generated through the only variation of one RV (while simultaneously holding the remaining RVs to their median values).

Through a comparison between Model#1 and the other models for each structure, change in SPO and capacity curve's parameters and PGA capacity at both LSs respect to Model#1 due to variations of the assumed RVs can be calculated.

It is to be noted that the influence of each single variable on PGA capacity, which will be illustrated through the sensitivity analysis, not only depends on the influence of the variable on the seismic response, but also depends on the dispersion assumed for that variable through the assigned CoV, which leads to consider values more or less distant from the central (median) value.

3.3.2.1 IN2 curves

Therefore, through the analysis of capacity curves' parameters and the application of a chosen R- μ -T relationship (Dolsek and Fajfar, 2004a; Vidic et al., 1994), the effect of the RVs on the seismic capacity can be discussed. Results of sensitivity analysis are reported from Figures 3.6 to 3.11 for GLD and SLD structures in terms of change in PGA capacity respect to Model#1 due to variations of the assumed RVs; the effect due to the variation of each RV on seismic capacity in terms of PGA is discussed in Table 3.4 and Table 3.5. Change in collapse mechanism that could be due to variation of infill mechanical properties respect to their median values, produce significant effects also on the PGA capacity, above all at NC LS, since that displacement capacity at NC LS depends on the number of stories involved in the collapse mechanism.

Uniformly Infilled

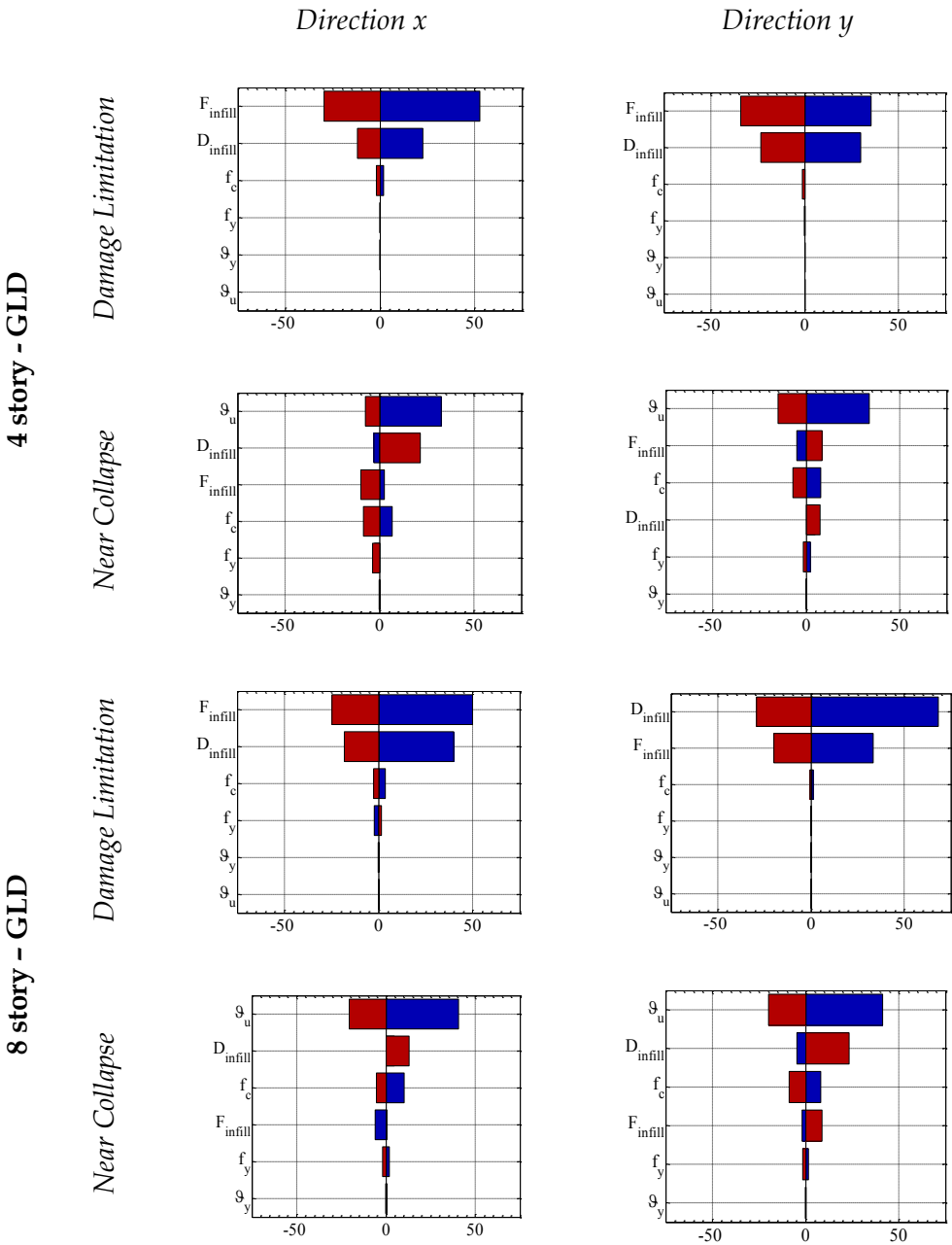


Figure 3.6. Change in PGA capacity (%) respect to Model#1 due to variations of the assumed RVs - GLD case study structures: Uniformly Infilled - Upper values (blue) and Lower values (red) of RVs

Pilotis

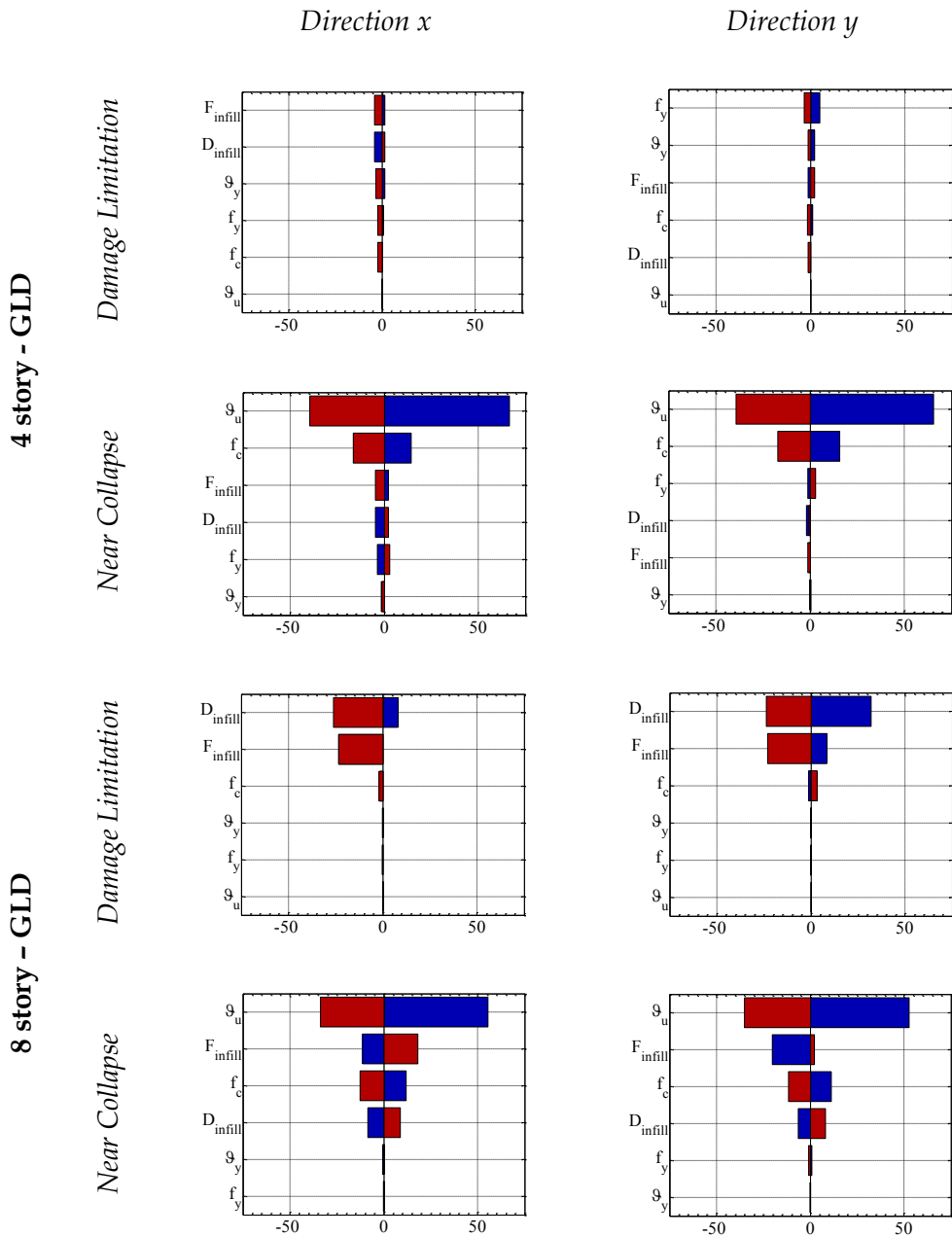


Figure 3.7. Change in PGA capacity (%) respect to Model#1 due to variations of the assumed RVs - GLD case study structures: Pilotis - Upper values (blue) and Lower values (red) of RVs

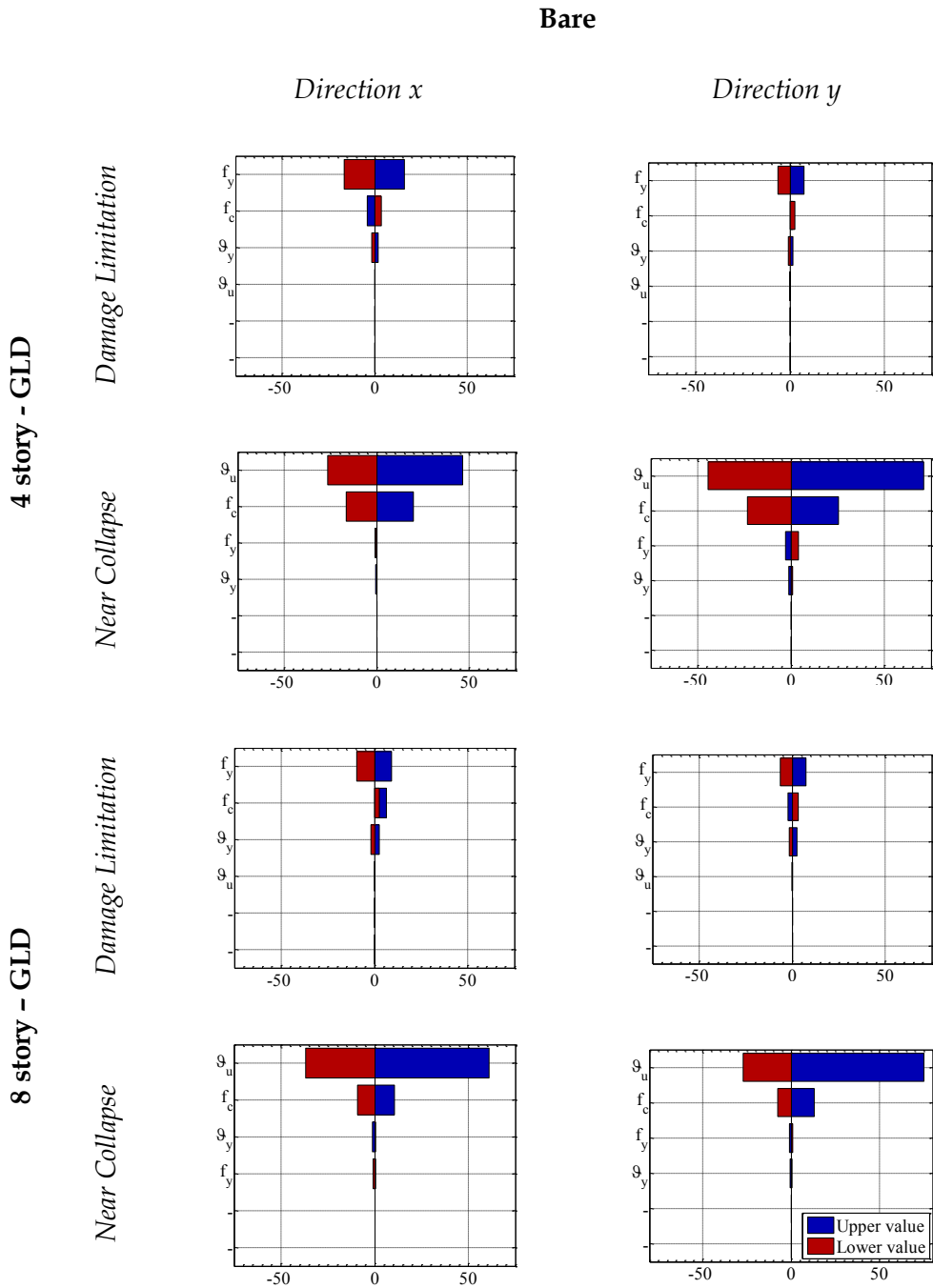


Figure 3.8. Change in PGA capacity (%) respect to Model#1 due to variations of the assumed RVs - GLD case study structures: Bare - Upper values (blue) and Lower values (red) of RVs

Uniformly Infilled

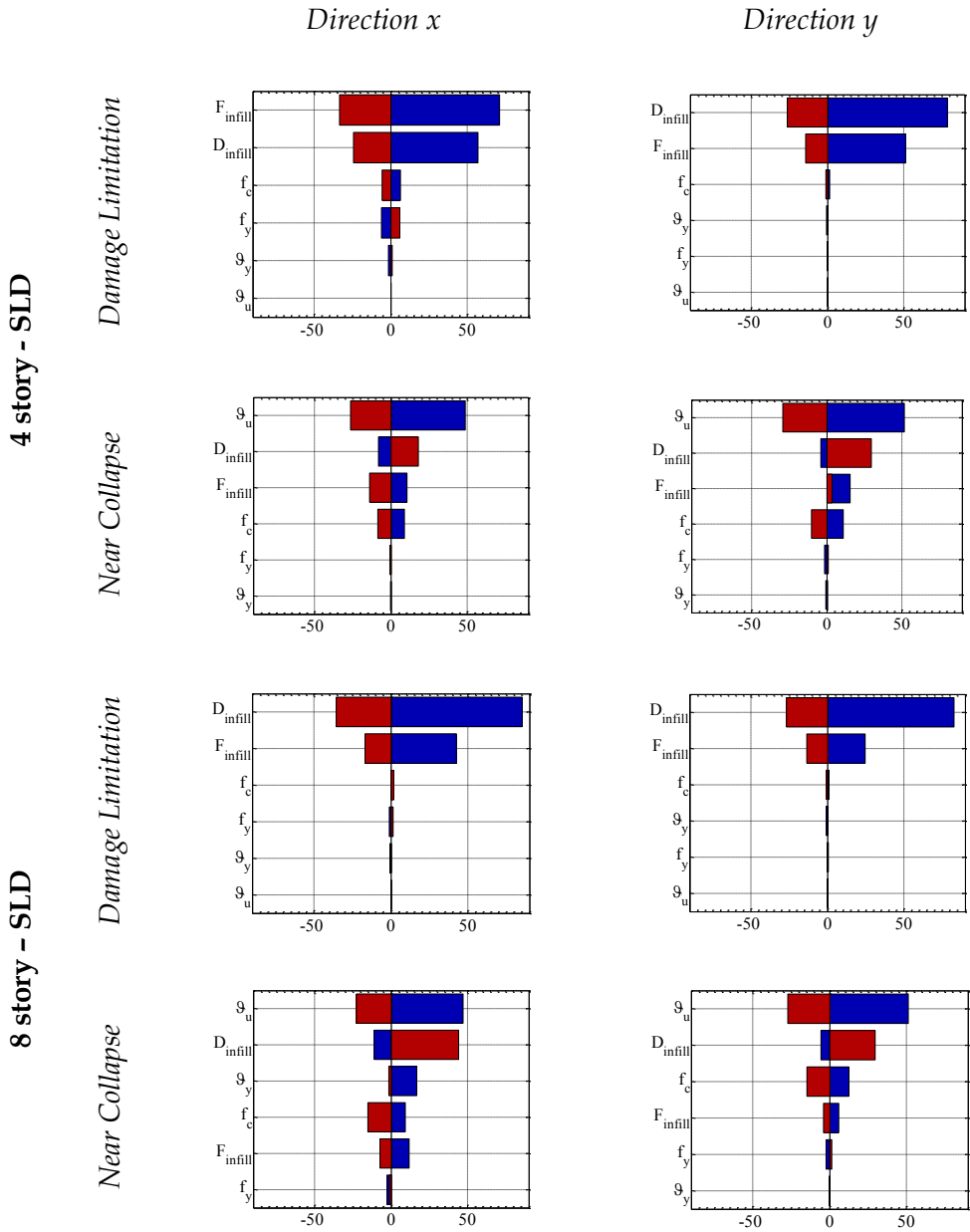


Figure 3.9. Change in PGA capacity (%) respect to Model#1 due to variations of the assumed RVs - SLD case study structures: Uniformly Infilled - Upper values (blue) and Lower values (red) of RVs

Pilotis

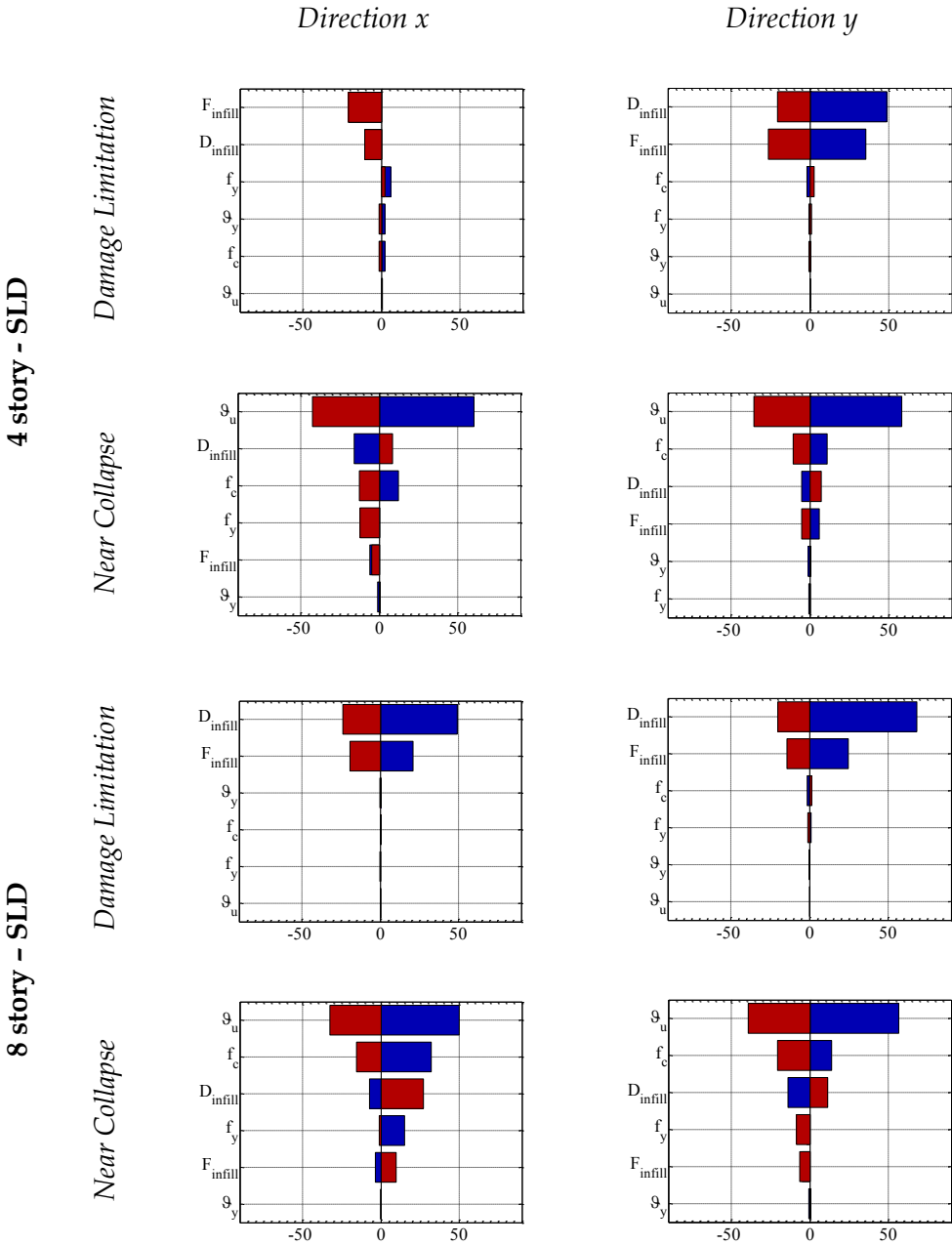


Figure 3.10. Change in PGA capacity (%) respect to Model#1 due to variations of the assumed RVs – SLD case study structures: Pilotis – Upper values (blue) and Lower values (red) of RVs

Bare

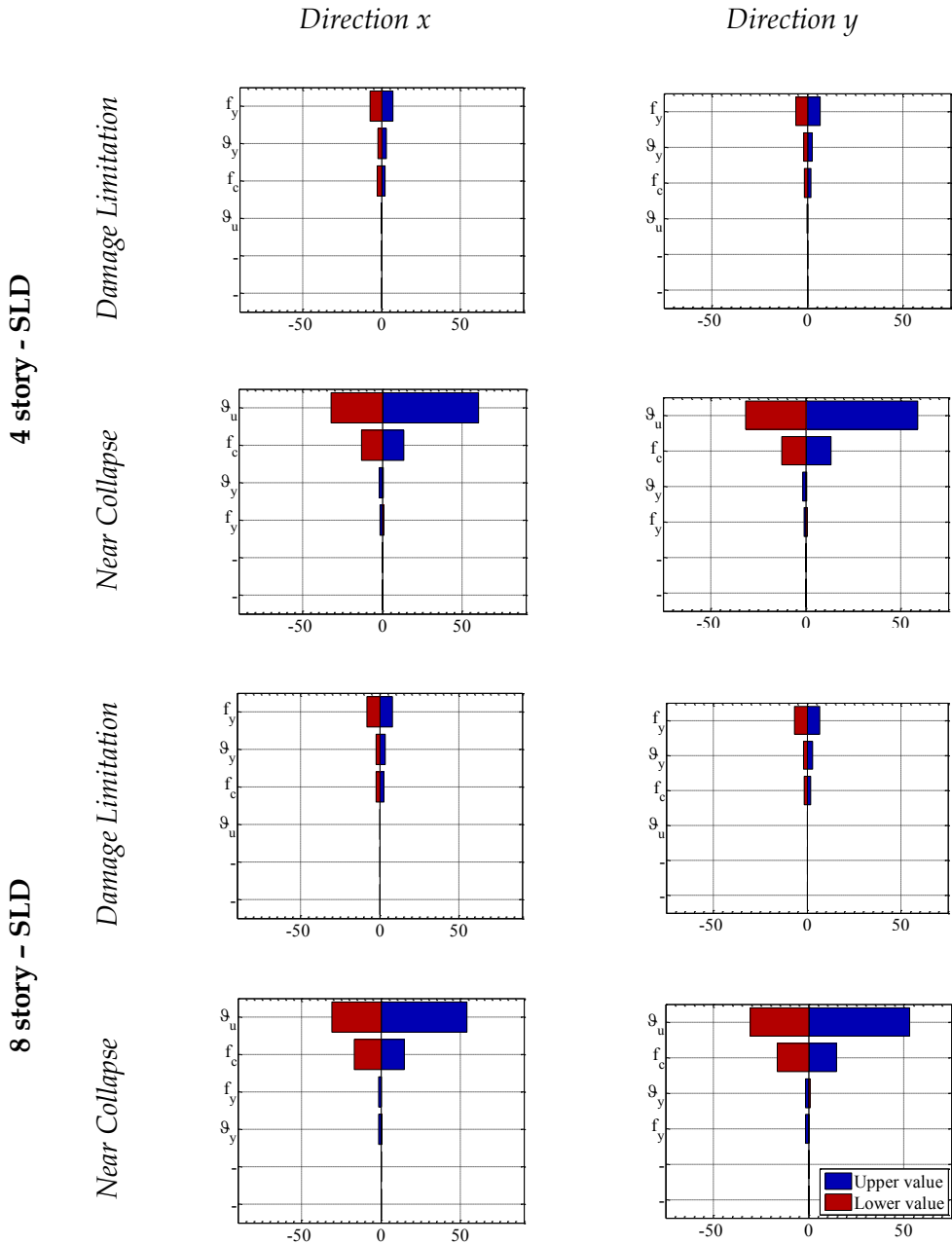


Figure 3.11. Change in PGA capacity (%) respect to Model#1 due to variations of the assumed RVs - SLD case study structures: Bare - Upper values (blue) and Lower values (red) of RVs

Gravity Load Design 4- and 8-storeys			
<i>RV</i>	<i>LS</i>	<i>Remarks</i>	
RC parameters	θ_u	NC	Parameter with the greatest influence in each case; if it increases, collapse ductility and PGA_{NC} increase.
		DL	No significant influence.
	θ_y	NC	No significant influence.
		DL	The achievement of DL LS is generally due to infills, if they are present in the model; for bare configurations, an increase in θ_y produces an increase both in displacement capacity and T_{eff} of the equivalent SDoF, thus resulting in no change of PGA_{DL} .
	f_c	NC	When it increases, the axial load ratio in columns decreases thus producing an increase in θ_u ; consequently ductility at collapse and PGA_{NC} increase.
		DL	No significant influence.
f_y	NC	No significant influence.	
	DL	Parameter with the greatest influence for bare configurations; an increase in f_y produces an increase in base shear strength C_s and displacement capacity Δ_{DL} , thus leading to an increase in PGA_{DL} ; not important for infilled configurations when the achievement of DL LS is due to infills.	
Infills parameters	F_{infill}	NC	Great influence on uniformly infilled configurations through the variation of collapse mechanism (i.e. 8-storey structures), of maximum strength $C_{s,max}$ and of T_{eff} ; its influence in terms of PGA_{NC} is smaller than θ_u and it is different depending on the case-study structure
		DL	Its influence is higher for Uniformly Infilled configurations rather than for Pilotis ones; in both cases if it increases a beneficial decrease in T_{eff} is produced, thus resulting in an increase in PGA_{DL}
	D_{infill}	NC	Except for variation of collapse mechanism (i.e., 8 stories-Uniformly Infilled-longitudinal direction), when it increases the yielding displacement of the equivalent SDoF S_{dy} increases too, whereas the maximum strength $C_{s,max}$ and the displacement capacity Δ_{coll} do not change, then ductility at collapse and PGA_{NC} decrease
		DL	Except for the 4 stories-Pilotis-longitudinal direction case-study structure, if it increases T_{eff} increases and displacement capacity Δ_{DL} increases more than yielding displacement of the equivalent SDoF S_{dy} , and so collapse ductility and PGA_{DL} increase

Table 3.4 Effects and remarks about sensitivity analysis –
GLD case study structures

Seismic Load Design 4- and 8-storeys				
<i>RV</i>	<i>LS</i>	<i>Remarks</i>		
RC parameters	θ_u	NC	Parameter with the greatest influence in each case; if it increases, collapse ductility and PGA_{NC} increase.	
		DL	No significant influence.	
	θ_y	NC	It becomes important just in one case-study (i.e. 8 stories-Uniformly Infilled-longitudinal direction) where, if it increases, a change in the collapse mechanism is produced and PGA_{NC} increases.	
		DL	The achievement of DL LS is generally due to infills, if they are present in the model; for Bare configurations, an increase in θ_y produces an increase both in displacement capacity and T_{eff} of the equivalent SDoF, thus resulting in no significant change in PGA_{DL} .	
	f_c	NC	When it increases, the axial load ratio in columns decreases and θ_u increases; consequently ductility at collapse and PGA_{NC} increase.	
		DL	No significant influence in general; only in one case (i.e. 4storeys-Uniformly Infilled-longitudinal direction), if it increases, an increase in base shear strength C_s is observed, thus leading to a beneficial decrease in T_{eff} and in PGA_{DL} .	
	f_y	NC	Important only for Pilotis configurations (i.e. 4- and 8- stories-Pilotis-longitudinal direction, 8 stories-Pilotis-transverse direction) where its change produces a variation of collapse mechanism.	
		DL	Parameter with the greatest influence for bare configurations due to an increase in base shear strength C_s and displacement capacity Δ_{DL} leading to an increase in PGA_{DL} ; not important for infilled configurations when the achievement of DL LS is due to infills.	
	Infill parameters	F_{infill}	NC	Except for variation of collapse mechanism, when it increases, the yielding displacement of the equivalent SDoF S_{dy} decreases and the maximum base shear strength $C_{s,max}$ increases, thus leading to an increase in PGA_{NC}
			DL	Except for variation of collapse mechanism in which displacement capacity Δ_{DL} decreases (i.e., 4 stories-Pilotis-longitudinal direction), if it increases, an increase in base shear strength C_s and a decrease in S_{dy} are produced, thus leading to a higher ductility capacity and PGA_{DL} .
D_{infill}		NC	When it increases, the yielding displacement of the equivalent SDoF S_{dy} increases too, whereas the maximum strength $C_{s,max}$ and the displacement capacity Δ_{coll} do not change, and then ductility at collapse and PGA_{NC} decrease.	
		DL	Except for variation of collapse mechanism (i.e. 4 stories-Pilotis-longitudinal direction), if it increases T_{eff} increases and displacement capacity Δ_{DL} increases more than yielding displacement of the equivalent SDoF S_{dy} , then ductility at collapse and PGA_{DL} increase.	

Table 3.5. Effects and remarks about sensitivity analysis – SLD case study structures

3.4 Comparisons and remarks: infill distribution, design typology and number of stories

In this Section, the influence of the infill configuration, the design typology and the number of stories on the seismic capacity of each case study building is evaluated. To this aim, IN2 curves are compared, always referring to the models where median values are assumed for all of the variables. The comparison is carried out in both directions through IN2 curves in terms of PGA: a comparison in terms of the elastic spectral acceleration capacity $S_{ae}(T_{eff})$ could be not realistic because of the high difference of effective period that exists between an infilled structure and the respective bare one.

3.4.1. Influence of the infill configuration

First of all, a comparison between three different infill configurations can be carried out about four-story and eight-story SLD or GLD case study structures.

If the four-story SLD structures (see Figures 3.12) are considered:

- (i) the Bare configuration shows the highest PGA capacity at DL LS (PGA_{DL}), both in longitudinal and transverse directions;
- (ii) Uniformly Infilled and Pilotis configurations have almost the same PGA_{DL} ;
- (iii) the Uniformly Infilled and the Pilotis configurations show the highest and the lowest PGA capacity, respectively, at NC LS (PGA_{NC}) in both directions.

If the four-story GLD structures (see Figures 3.12) are considered, instead:

- (i) the Uniformly Infilled and the Pilotis configurations show the highest and the lowest PGA capacity, respectively, at DL LS (PGA_{DL}) in both directions;
- (ii) Uniformly Infilled configuration has the highest PGA_{NC} .

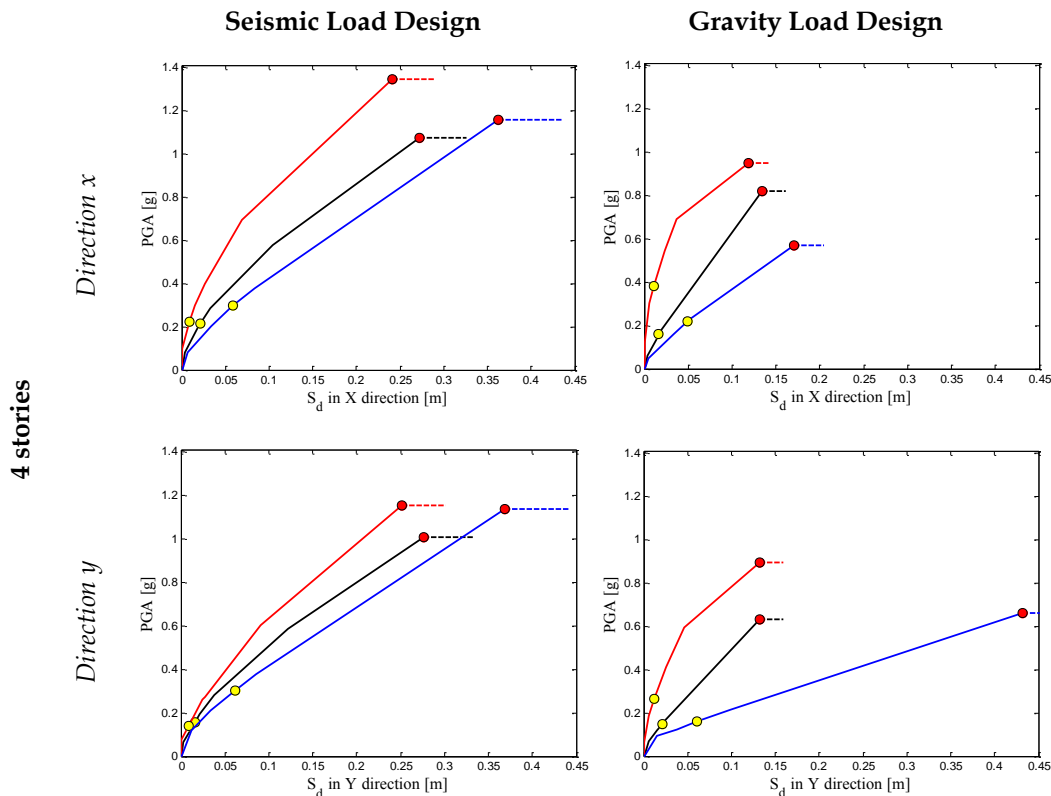


Figure 3.12. IN2 curves in terms of PGA – four-story SLD and GLD case study structures – Uniformly Infilled (red), Pilotis (black) and Bare (blue) configurations

Similar conclusions can be drawn for eight-story structures (see Figure 3.13), thus leading to the following general remarks:

- (i) at NC LS, a beneficial effect on PGA capacity generally exists when a regular distribution of infill panels is considered, whereas a detrimental effect is shown by structures with an irregular infill distribution;
- (ii) at DL LS, the above mentioned beneficial effect is not observed for SLD structures;
- (iii) displacement capacity, as expected, is higher for Bare structures both in longitudinal and transverse directions at each LS;
- (iv) ratios between Uniformly Infilled or Pilotis PGA capacity and Bare PGA capacity are higher for GLD structures whose seismic performances are more affected by infill presence respect to SLD structures;
- (v) in SLD structures the presence of infills changes also significantly the

collapse mechanism expected for the Bare configuration designed according to Capacity Design principles, thus influencing displacement, ductility and PGA capacities.

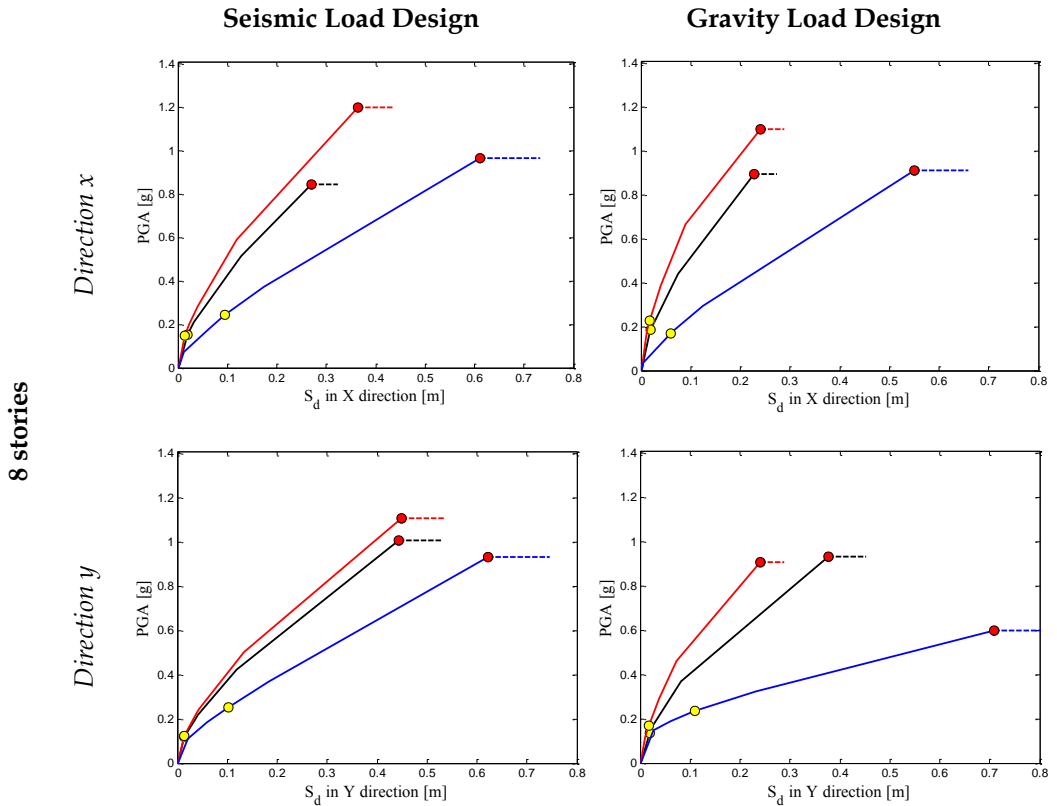


Figure 3.13. IN2 curves in terms of PGA – eight-story SLD and GLD case study structures – Uniformly Infilled (red), Pilotis (black) and Bare (blue) configurations

3.4.2. Influence of the design typology

A second kind of comparison can be carried out in order to show how the seismic capacity is affected by infills depending on the design typology of the structure.

IN2 curves in terms of PGA are reported in Figure 3.14 for four-story case study structures and discussed below.

At DL LS:

(i) in the Uniformly Infilled configuration, GLD structures show a concentration of displacement demand at the first story from early range of loading, resulting in a stiffening of the multi-linearized SPO curve and an increase in PGA_{DL} respect to SLD Uniformly Infilled structure;

(ii) in Pilotis and Bare configurations, SLD structures show the highest displacement capacity and PGA_{DL} ;

(iii) in Pilotis configurations, in transverse direction, the absence of internal beams for GLD structures leads to a higher deformability and displacement capacity.

At NC LS:

(i) SLD structures, respecting Capacity Design principles, show collapse mechanisms involving a greater number of stories and a higher collapse ductility and PGA_{NC} respect to GDL structures;

(ii) GLD Bare structure in transverse direction has a greater displacement capacity because in this case a global collapse mechanism is observed.

Similar conclusions can be drawn for eight-story structures (see Figure 3.15), thus leading to the following general remarks: (i) SLD structures generally show the best seismic performances at NC LS; (ii) as far as Uniformly Infilled configurations are concerned, GLD structures show the highest PGA_{DL} ; (iii) exceptions to the above conclusions are the cases (for eight-story structures) in which there is a concentration of displacement demand at bottom floors leading to an increase in PGA_{NC} due to a stiffening of the multi-linearized SPO curve (e.g., eight-story Pilotis in longitudinal direction).

4-story

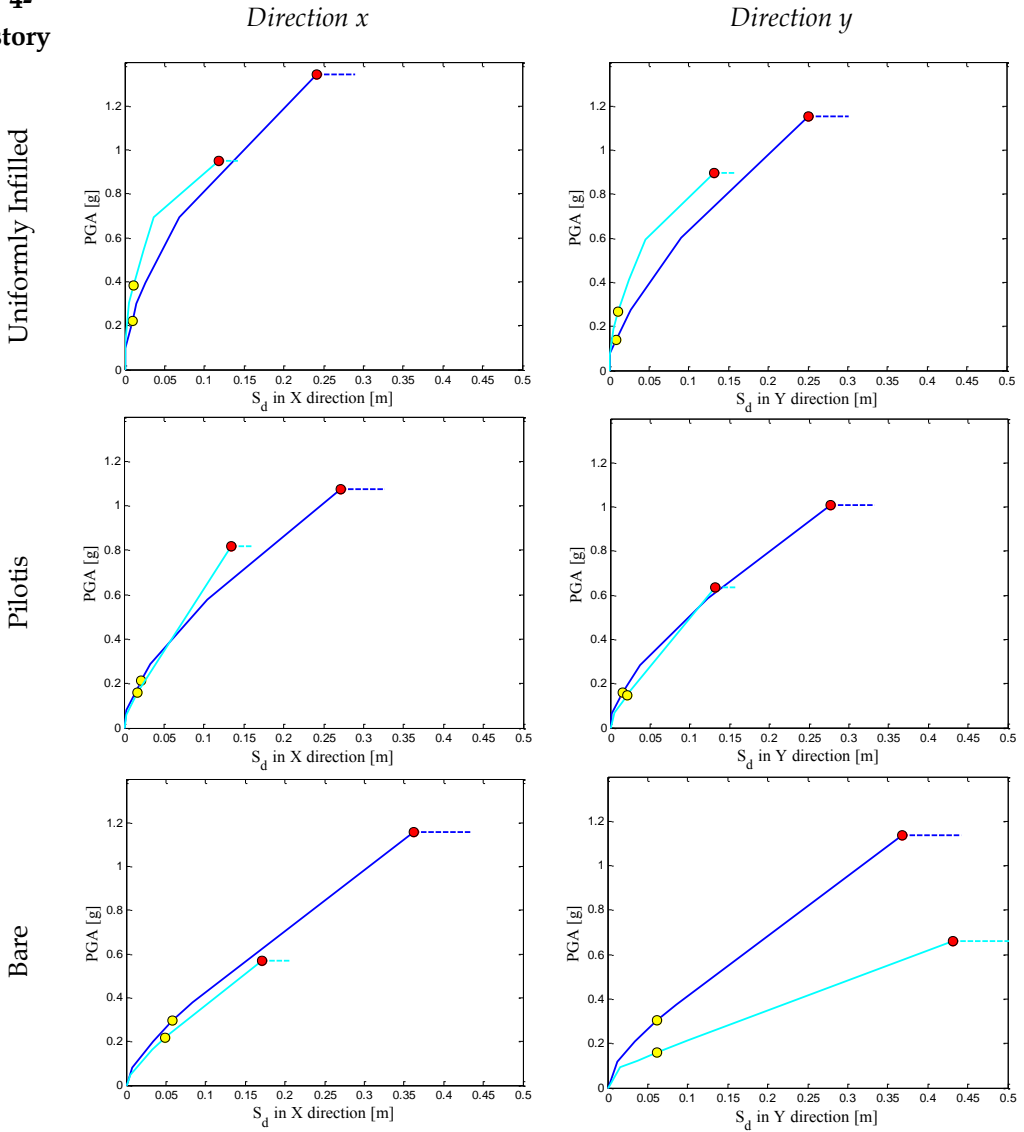


Figure 3.14. IN2 curves in terms of PGA – four-story case study structures – GLD (cyan) and SLD (blue)

8-
story

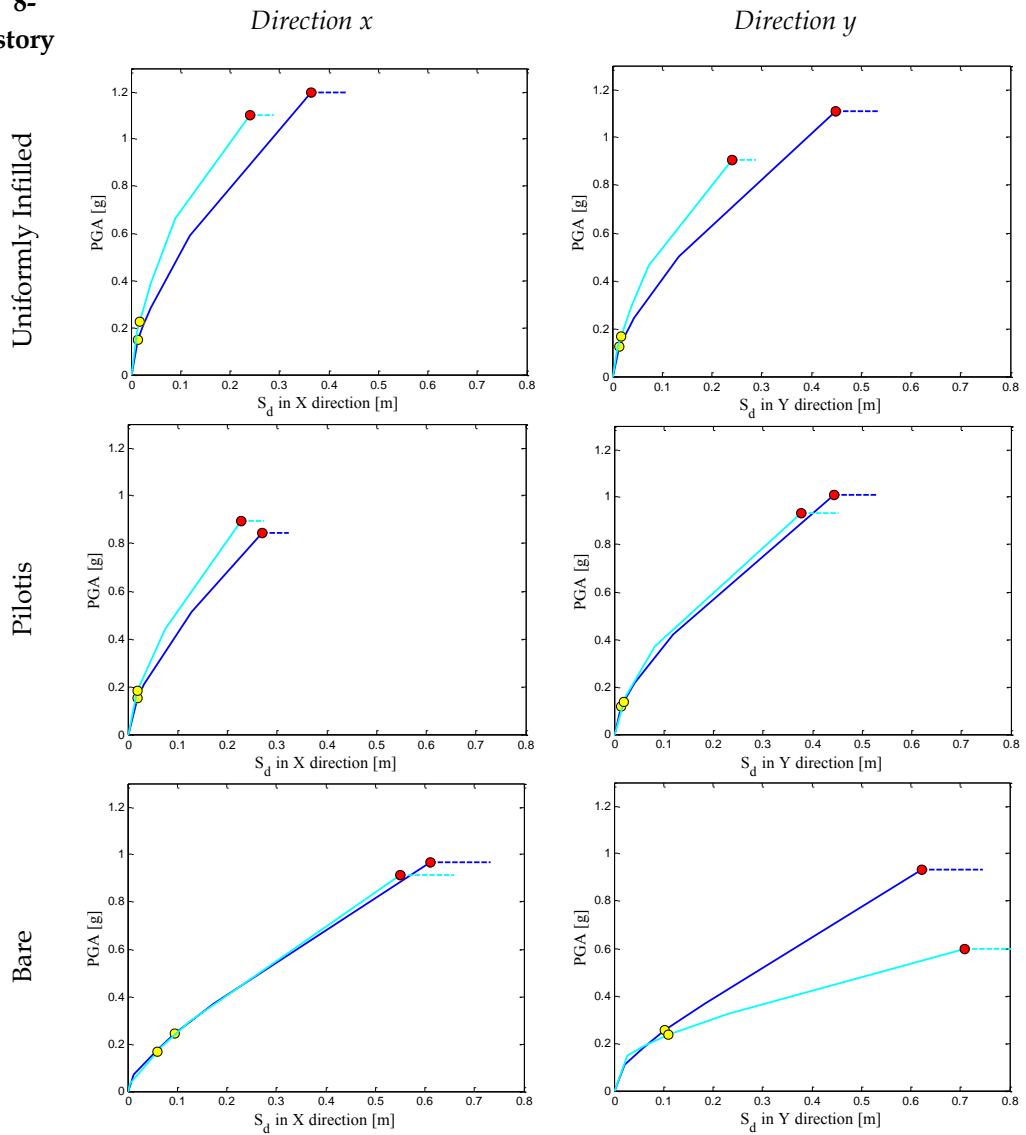


Figure 3.15. IN2 curves in terms of PGA – eight-story case study structures – GLD (cyan) and SLD (blue)

3.4.3. Influence of the number of stories

In this Section, a further analysis is carried out about structural seismic capacity depending on the number of stories.

The same trends are shown by four- and eight-story analyzed structures. It is worth noting that:

- (i) eight-story structures have a greater variability in collapse mechanisms depending on the infill configuration, input parameters and design typology;
- (ii) eight-story structures are less affected by infill presence in terms of PGA_{DL} .

3.4.4. A generalization attempt

A further effort was made in order to generalize the conclusions drawn from the above illustrated comparisons. To this end, the influence of infill panels on the seismic performance of the structure is explicitly evaluated in terms of percentage variation (r) between PGA capacity of the Uniformly Infilled model (PGA_{UI}) - or the Pilotis model (PGA_P) - and the PGA capacity of the Bare one (PGA_B).

In particular, the remarks carried out below are based on the parameter:

$$r = \frac{PGA_{UI} - PGA_B}{PGA_B} \quad (3.8)$$

For Models#1 of each case study structure, the PGA capacity of each model independent of the direction - at a given Limit State (LS) - can be assumed equal to the minimum PGA capacity at that LS between longitudinal and transverse direction and the Bare and the corresponding Uniformly Infilled models can be compared.

The percentage variation of PGA_{UI} respect to PGA_B has been obtained for each case study structure and reported in Figure 3.16 at DL and NC LSs, separately.

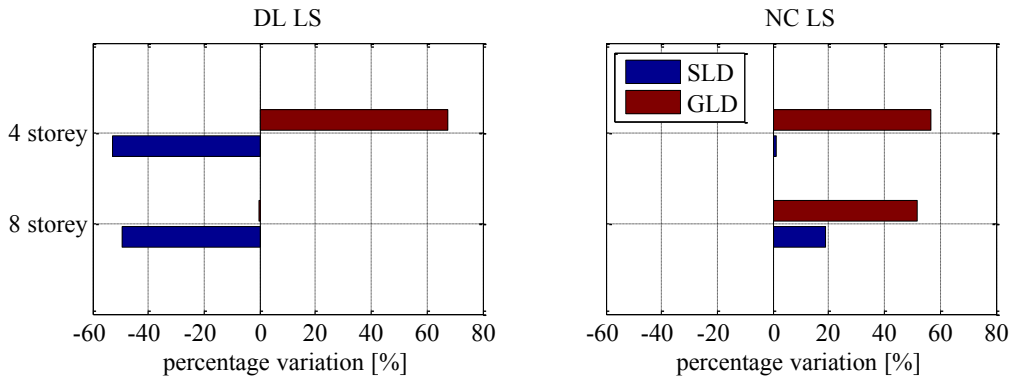


Figure 3.16. Percentage variation of PGA_{UI} with respect to PGA_B for GLD and SLD case study structures, at NC and DL LSs

From the analysis of Figure 3.16 some general considerations can be drawn:

- the percentage variation of PGA_{UI} respect to PGA_B at NC LS is higher for GLD structures than SLD structures, thus highlighting the higher influence of infill panels on GLD than SLD structures. Symbolically:

$$\left| \frac{PGA_{UI} - PGA_B}{PGA_B} \right|_{GLD} > \left| \frac{PGA_{UI} - PGA_B}{PGA_B} \right|_{SLD} \quad (3.9)$$

- the percentage variation is more relevant for low-rise structures, both at NC and DL LSs, especially for gravity load design typology;
- at DL LS, the presence of infill panels produce a detrimental reduction in PGA capacity for SLD structures (negative value of percentage variation), thus highlighting that for SLD structures, at low level of displacement demand, the detrimental reduction of the displacement capacity at DL LS due to the presence of infills is more important than the beneficial increase in stiffness and strength that infill panels produce respect to the bare structure designed according to new seismic code provisions, whereas an opposite trend is observed in GLD structures.

3.5 Fragility analysis

3.5.1. Methodology

First of all, the methodology used for the evaluation of fragility curves for the case study structures is illustrated.

A fragility curve represents a relationship between a seismic intensity parameter and the corresponding probability of exceedance of a given damage threshold (typically represented by a displacement capacity). If PGA capacity is “observed” in a population of buildings, according to a frequentist approach the cumulative frequency distribution of these observations provides the fragility curve (based on PGA seismic intensity measure) for that population of buildings and for that Limit State, based on the definitions themselves of fragility curve and PGA capacity. In this Chapter, such population of buildings is generated by a number of samplings of some Random Variables – which are input parameters to the determination of the PGA capacity (e.g., material characteristics or capacity parameters) – defined by Probability Density Functions describing the expected values and the corresponding variability, according to a Monte Carlo simulation technique. A stratified sampling of Random Variables is executed through the Latin Hypercube Sampling (LHS) technique (McKay et al., 1979), assuming a “median” sampling scheme (Vorechovsky and Novak, 2009). Nevertheless, it would be too computationally demanding to carry out a SPO analysis (for calculating the PGA capacity) for each sample of the chosen Random Variables. Hence, a RSM is applied (Pinto et al., 2004), assuming a second-order polynomial relationship between the PGA capacity, assumed as the scalar output variable, and the selected Random Variables, assumed as input variables. The design of experiments needed to determine such relationship is carried out according to the Central Composite Design (CCD) method. Hence, the number of experiments adds to $n=1+2k+2k$, if k input variables are assumed. In our case, the input variables are the Random Variables selected for the sensitivity analysis; in addition, the strength reduction factor R evaluated from $R-\mu-T$ relationship is assumed as a Random Variable, too. The estimate of the uncertainty in the evaluation of R – given a value of μ corresponding to the ductility capacity at a given LS – derives from the record-to-record variability observed in the results of the nonlinear dynamic analyses carried out on SDoF

systems (with several records) to obtain such R- μ -T relationships. Hence, the strength reduction factor R is treated as a Random Variable: the value of R calculated by means of the given R- μ -T relationship is assumed as the median value, and the corresponding variability is taken into account by assuming the lognormal standard deviation β_R as a function of μ , depending on the characteristics of the SDoF backbone, from (Vamvatsikos and Cornell, 2006). It is to be noted that the assumption of R as a Random Variable does not imply the execution of further SPO analyses. In order to apply the illustrated procedure, the considered input variables are represented by the Random Variables normalized to their median values (see Table 3.6).

Variable	Distribution	Median Value	CoV (SLD)	CoV (GLD)
\underline{f}_c	Lognormal	1	0.20	0.31
\underline{f}_y	Lognormal	1	0.06	0.08
$\underline{\theta}_y$	Lognormal	1.015	0.331	0.331
$\underline{\theta}_u$	Lognormal	0.995	0.409	0.409
\underline{E}_{infill}	Lognormal	[1;1]	[0.30;0.30]	[0.30;0.30]
\underline{D}_{infill}	Lognormal	[1;1]	[0.30;0.70]	[0.30;0.70]
\underline{R}	Lognormal	1	$f(\mu)$	$f(\mu)$

Table 3.6. Random Variables assumed to evaluated fragility curves

Hence, the number of experiments adds to $n=1+2 \cdot 7+2^7=143$ (if infills are present, as in Uniformly Infilled and Pilotis frames) or $1+2 \cdot 5+2^5=43$ (if infills are not present, as in Bare frame) for each case study, in each direction. Note that the results of the SPO analyses carried out with the sets of values corresponding to the 2 k “star points”, whose position is assumed at a distance of 1.7 times the standard deviation from the centre of design (Liel et al., 2009), was illustrated in the sensitivity analysis.

The resulting PGA capacity data allow to estimate the second-order polynomial relationship between the PGA capacity and the assumed Random Variables. Subsequently, a LHS of the $k=7$ considered Random Variables is carried out, thus obtaining m sets of values of these variables. In particular, $m=1000$ samplings are executed. The $m \times k$ obtained sampling matrix is used to estimate - through RSM - the corresponding m values of PGA capacity. This procedure is carried out 12 times for each case study structure (note that the same sampling matrix is always used; obviously in Bare frame only 5 of the 7

columns of the matrix are used). The corresponding cumulative frequency distributions of the obtained PGA capacity values provide the 12 fragility curves for Uniformly Infilled, Pilotis and Bare frames, in X and Y directions and at DL and NC LSs for each case study structure. Results are illustrated in the following. The comparison between the median values of the fragility curves reported herein has been actually already carried out through the observations reported above, when comparing the seismic capacities of Uniformly Infilled, Pilotis and Bare frames referring to Models#1 (median values for each Random Variable) for each case study. From a qualitative standpoint, the slope of the fragility curves - representing the variability associated with the seismic capacity - depends on the amount of variation in PGA capacity with the variation in each Random Variable, shown in the sensitivity analysis. Lower this amount, lower the change in PGA capacity with the change in Random Variables, less sensitive the PGA capacity to the modeled uncertainties, steeper the fragility curve (as often happens, for instance, at DL Limit State). Moreover, further variability due to the variability of the strength reduction factor R affects all of the fragility curves, but to a different extent: larger the ductility capacity at the LS of interest, larger the variability of the corresponding strength reduction factor R, larger the increase in the variability of PGA capacity.

3.5.2. Analysis of results

4-storey GLD: If fragility curves at NC LS in X direction are observed (see Figure 3.17a), a quite close median seismic capacity is noted between Uniformly Infilled and Pilotis frames, whereas the Bare frame results as the more vulnerable. Fragility curves at DL LS in X direction highlight the beneficial effect of uniformly distributed infills on the seismic capacity at this LS, that is, for relatively low seismic demand. Moreover, it is observed how in this case the detrimental effect of localization in displacement demand leads to a lower capacity of the Pilotis frame, compared with the remaining ones. Nevertheless, the relatively low slope of the fragility curve for the Uniformly Infilled frame reflects the particularly high influence of the uncertainty in mechanical properties of infill panels on the seismic capacity of this frame at DL. In Y direction the fragility curves at NC LS highlight that the best seismic performance is provided by the Uniformly Infilled frame. Moreover, also in Y

direction the beneficial effect of the increase in stiffness and strength provided by uniformly distributed infills on the seismic capacity at DL LS is clearly shown.

8-storey GLD: If fragility curves at NC LS in X direction are observed (see Figure 3.17b), a closer median seismic capacity respect to the previous case is noted between all the infilled configurations, thus highlighting the lower influence of infills on the 8-storey case study structures. Fragility curves at DL LS in X direction highlight the beneficial effect of uniformly distributed infills on the seismic capacity at this LS, similarly to the 4-storey GLD case study structure, whereas a quite close median seismic capacity is noted between Bare and Pilotis frames. Again, the relatively low slope of the fragility curve for the Uniformly Infilled frame reflects the particularly high influence of the uncertainty in mechanical properties of infill panels on the seismic capacity of this frame at DL. In Y direction, respect to the previous case, the fragility curves show that (i) at NC LS, seismic performance of Pilotis is better compared with the Bare frame and (ii) at DL LS, Bare frame is less vulnerable than the Uniformly Infilled frame.

4-storey SLD: Fragility curves at NC LS in X direction (see Figure 3.18a) highlight the beneficial effect of uniformly distributed infills on the seismic capacity and the detrimental effect of localization in displacement demand leading to a lower capacity of the Pilotis frame, compared with the remaining ones. At DL LS, in both directions, seismic performance of Bare frame is better compared with the other infilled frames.

8-storey SLD: Fragility curves at NC LS in both directions (see Figure 3.18b) highlight the beneficial effect of uniformly distributed infills on the seismic capacity whereas a quite close median seismic capacity is noted between Bare and Pilotis frames, at this LS. At DL LS, in both directions, seismic performance of Bare frame is better compared with the infilled frames.

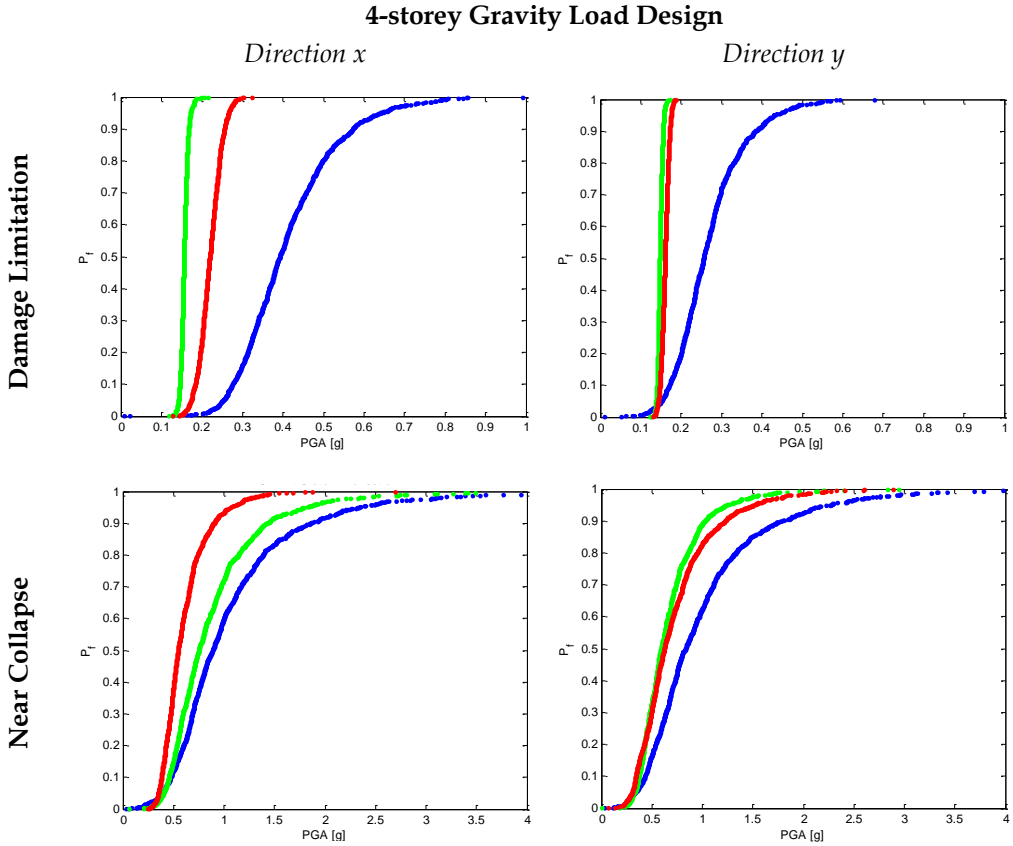


Figure 3.17. (a) Fragility curves – GLD case study structures

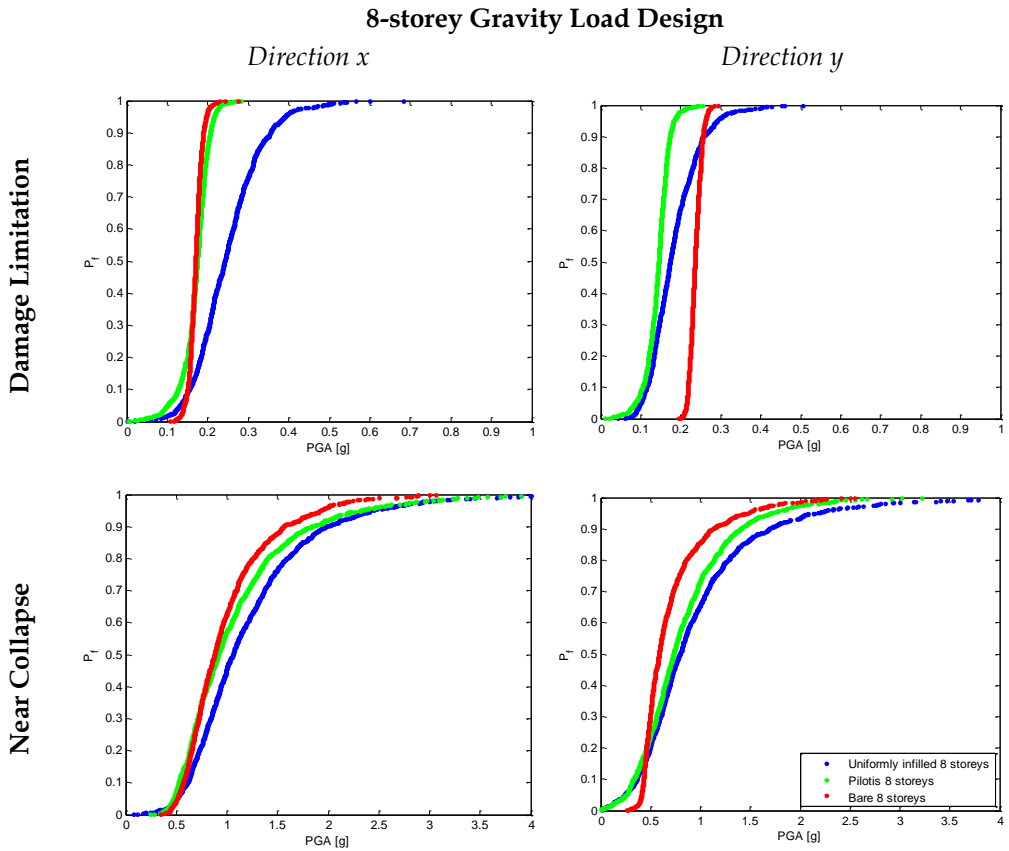
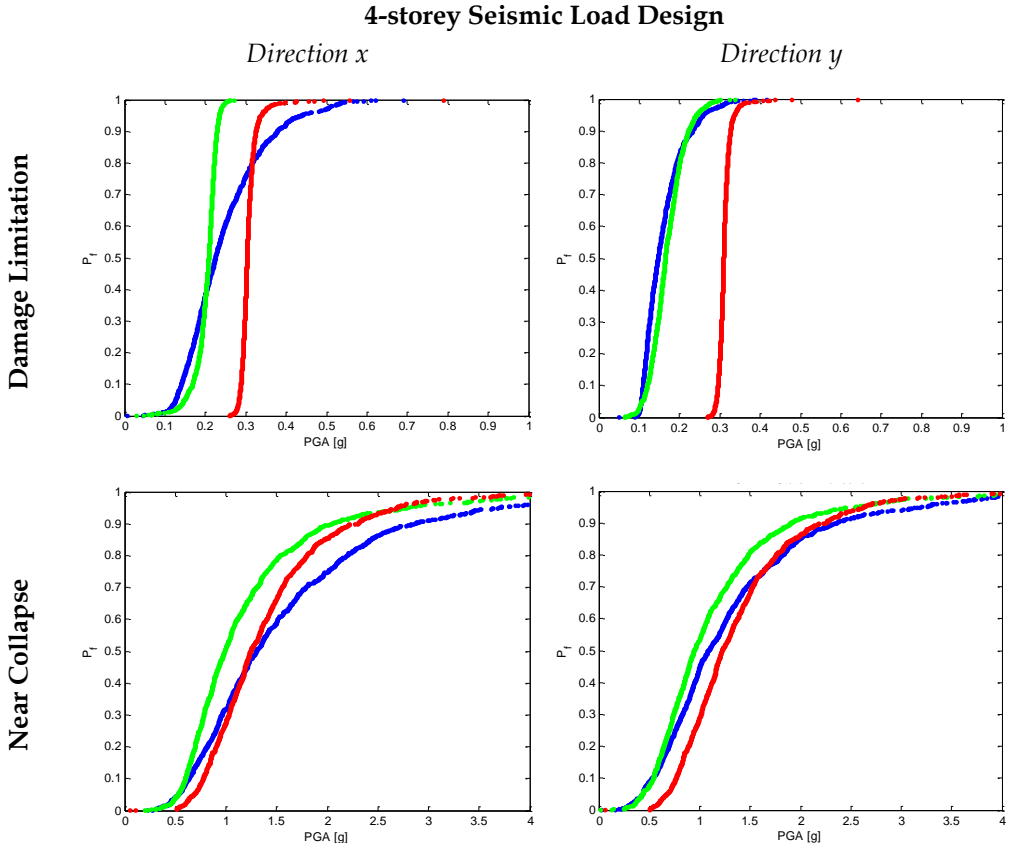


Figure 3.17. (b) Fragility curves – GLD case study structures



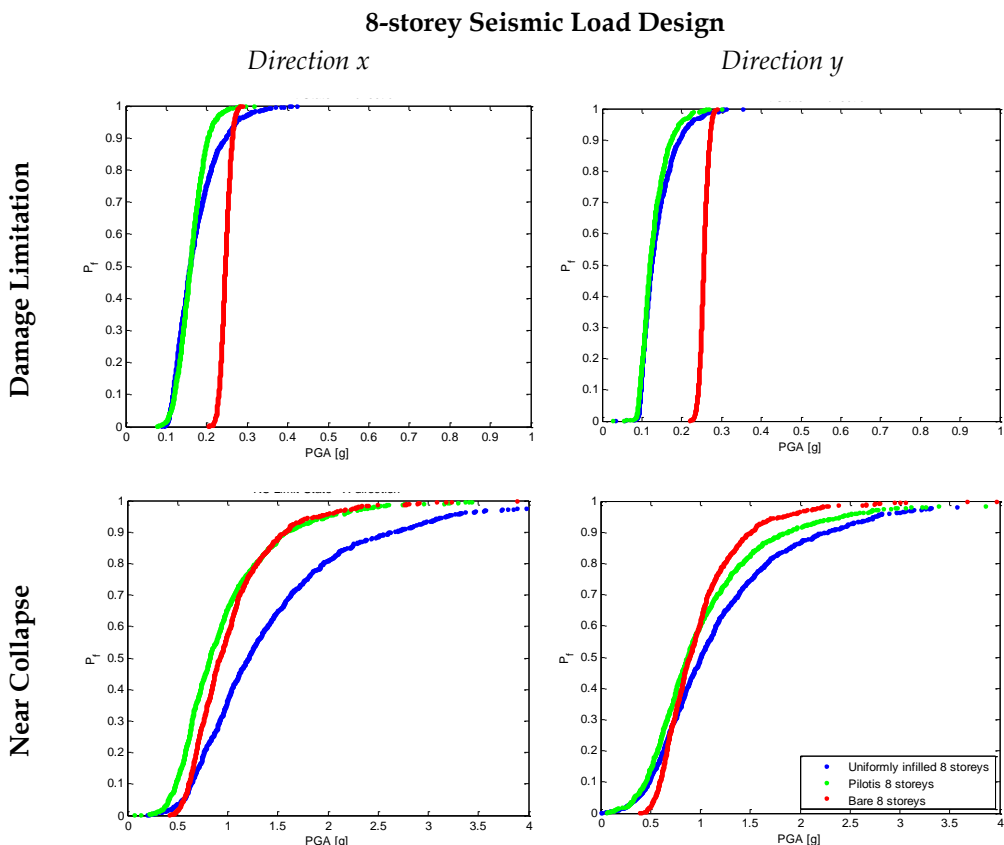


Figure 3.18. (b) Fragility curves – SLD case study structures

Fragility curves can be fitted by lognormal cumulative distributions: parameters are reported in Table 3.7, with $\overline{\text{PGA}}$ and β_{PGA} representing the estimated median (expressed in (g)) and logarithmic standard deviation of PGA capacity, respectively.

The latter provides an useful indication about the overall sensitivity of seismic capacity to the variability of the parameters mainly influencing the seismic response.

Table 3.7 Estimated parameters of the cumulative lognormal distributions fitting the fragility curve

		Seismic Load Design						Gravity Load Design									
		4 storeys			8 storeys			4 storeys			8 storeys						
		DL	NC	PGA	β_{PGA}	DL	NC	PGA	β_{PGA}	DL	NC	PGA	β_{PGA}	DL	NC	PGA	β_{PGA}
UJ	x	0.226	0.40	1.333	0.59	0.164	0.29	1.243	0.56	0.394	0.32	0.904	0.57	0.234	0.39	1.073	0.5
	y	0.152	0.29	1.108	0.61	0.131	0.28	0.999	0.67	0.254	0.34	0.848	0.58	0.173	0.33	0.763	0.71
P	x	0.199	0.18	1.052	0.52	0.158	0.21	0.851	0.49	0.156	0.06	0.786	0.47	0.164	0.31	0.955	0.49
	y	0.164	0.25	0.980	0.55	0.124	0.24	0.88	0.61	0.148	0.04	0.608	0.45	0.137	0.27	0.684	0.73
B	x	0.306	0.07	1.282	0.43	0.245	0.05	0.955	0.38	0.218	0.13	0.571	0.34	0.169	0.1	0.911	0.4
	y	0.310	0.05	1.262	0.42	0.255	0.04	0.92	0.37	0.16	0.06	0.639	0.49	0.236	0.06	0.641	0.39

3.5.2.1 A comparison between fragility analysis and observed damage

The most recent Italian earthquakes could be considered in order to carry out a comparison between observed damage and fragility analysis, e.g. L'Aquila (6th April 2009) event.

The most representative case of existing structures in Italian building stock among those analyzed in this Chapter could be the 4-storey GLD Uniformly Infilled or Pilotis structures.

As far as the fragility analysis is concerned, a unique fragility curve for each LS independent of the direction can be obtained (for each experiment carried out to obtain the fragility curve the minimum PGA capacity between longitudinal and transverse directions is considered) and the failure probability P_f at each LS corresponding to the PGA of the event can be evaluated.

On the other hand, damage observed during L'Aquila earthquake can be analyzed through AeDES forms ("scheda di 1° livello di rilevamento danno, pronto intervento e agibilità per edifici ordinari nell'emergenza post-sismica - AeDES 05/2000", Presidenza del Consiglio dei Ministri Dipartimento Nazionale della Protezione Civile) filled immediately after the 6th April 2009 event. Such forms contain information about geometry, structural typology, structural and non-structural damage of the surveyed buildings in the epicentral area and they express a "safety judgment": "A" (practicable building); "B" (temporally impracticable building); "C" (partially impracticable building); "D" (building requiring a deeper investigation); "E" (impracticable building), "F" (impracticable building because of external danger).

In particular, the case of Pettino (AQ) is analyzed, taking a sample of 305 RC surveyed structures (Pitilakis, 2012).

Pettino (AQ) is very close to the stations ID AQV-Recorder identifier GX066- and ID AQG-Recorder identifier FA030- that recorded the highest PGA values in the epicentral area of L'Aquila earthquake, equal to 0.61 g and 0.43, respectively (Iervolino et al., 2010).

The comparison between the observed damages and fragility analysis is more appropriate at DL LS, thanks to the most evident damage that occurred in infill panels during the event and also because the greatest part of the collapses identified in L'Aquila buildings after the event can be classified as

brittle failure mechanisms (Ricci et al, 2010; Verderame et al, 2010a) – neglected in the present study.

Thus, at DL LS, for the Uniformly Infilled structure, P_f – obtained from the related fragility curve – ranges from 0.92 to 0.99 (Figure 3.19a) when the PGA ranges from 0.43 g to 0.61 g. Moreover, an equivalence between the achievement of the conventional DL LS and the AeDES result “B” is assumed, based on the description of the damage associated to this “safe judgment” (“Manuale per la compilazione della scheda di 1° livello di rilevamento danno, pronto intervento e agibilità per edifici ordinari nell’emergenza post-sismica (AeDES)”, Presidenza del Consiglio dei Ministri Dipartimento Nazionale della Protezione Civile). In a frequentist approach, the failure probability at DL LS related to 4 storey RC buildings observed during the earthquake can be compared with the percentage of the 4-storey RC buildings that obtained an AeDES result equal to “B”, “C” or “E” (“D” result is never assigned to the sample structures). This percentage is equal to 95% (Figure 3.19b). It is worth noting that only 4-storey RC structure with regularity in plan and infill distribution are considered among the sample of surveyed structures (Pitilakis, 2012) in order to carry out a comparison with the case study structure analyzed in the Chapter. In conclusion, the observation of damage produced during L’Aquila earthquake – evaluated through AeDES forms – seems to be in agreement with the estimated P_f – derived from the fragility analysis for the considered LS.

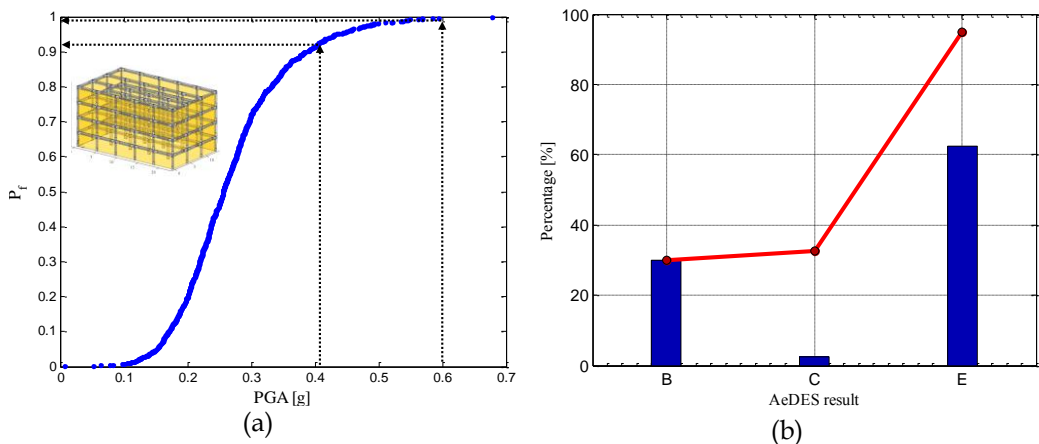


Figure 3.19. Fragility curve at DL LS structure independent on direction – 4 storey GLD (a); AeDES results – 4 storey RC structures with regularity in plan and infill distribution (b)

3.5.3. Evaluation of failure probability

A comparison between DL and NC LSs can be carried out also in terms of failure probability. The failure probability (P_f) of a structural system characterized by a resistance R under a seismic load S can be evaluated as

$$P_f = \int_0^{+\infty} f_S(S) F_R(S) dS \quad (3.10)$$

where $f_S(S)$ is the Probability Density Function (PDF) of the seismic intensity parameter and $F_R(S)$ is the probability that the resistance R is lower than a level S of seismic intensity. Hence, $F_R(S)$ is represented by a fragility curve, whereas the PDF of the seismic intensity S - in a given time window - is obtained from seismic hazard studies: based on the seismic hazard data provided by (INGV-DPC S1, 2007) for the Italian territory, if the coordinates of the site of interest are given, PGA values corresponding to different return periods (T_R) can be determined. Hence, given a PGA value, the corresponding $T_R(\text{PGA})$ can be calculated. Finally, given a time window (V_R), the exceeding probability of the same PGA is given by the Poisson process:

$$P_{V_R}(\text{PGA}) = 1 - e^{-\frac{V_R}{T_R(\text{PGA})}} \quad (3.11)$$

In the procedure described herein, PGA is assumed as seismic intensity parameter S , $F_R(S)$ is represented by the calculated fragility curves (assuming a linear interpolation between subsequent values of PGA) and $f_S(S)$ is derived from $P_{V_R}(\text{PGA})$, by calculating the PDF of PGA corresponding to the Complementary Cumulative Distribution Function (CCDF) of PGA represented by $P_{V_R}(\text{PGA})$. Hence, the failure probability P_f is calculated through Eq (3.10), by means of a numerical integration based on Simpson quadrature. Failure probabilities at DL and NC LSs are calculated for each frame, based on the fragility curves previously obtained and the seismic hazard described by the PGA exceeding probability in 50 years, obtained from (INGV-DPC S1, 2007) for the site of interest (Lon.: 14.793, Lat.: 40.915).

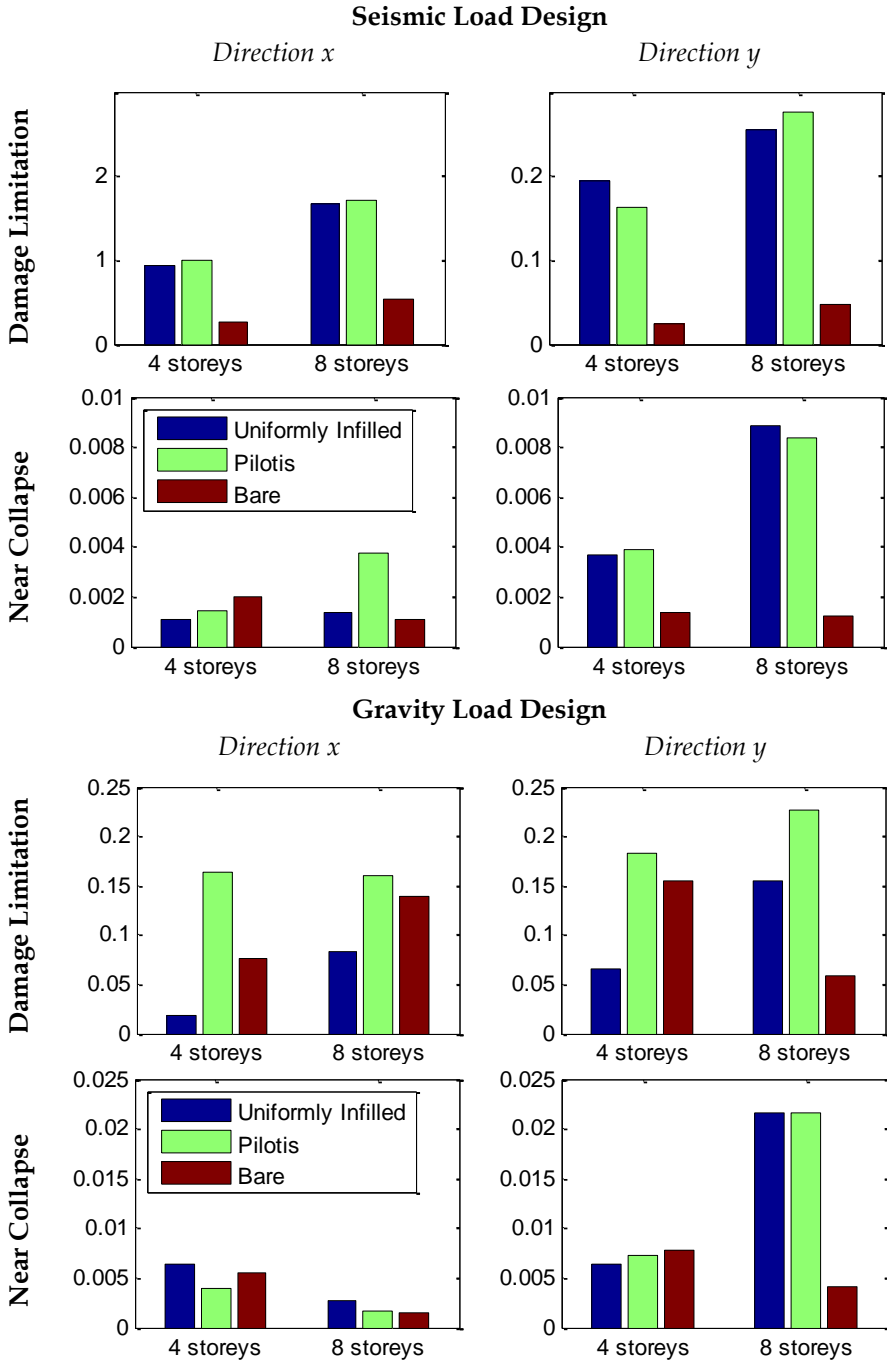


Figure 3.20. Failure probabilities P_f in 50 years for SLD and GLD case study structures

The failure probabilities P_f calculated for a time window of 50 years are reported in Figure 3.20 and in Table 3.8 for each case study structure, showing a direct comparison between different infill configurations, number of stories, considered directions and LSs.

It is worth noting that the effect of the uncertainties on the seismic capacity can be clearly observed when the comparison between seismic capacities in terms of median PGA capacity at a certain LS is not reflected by the comparison between the corresponding failure probabilities at that LS. For example, 8-storey SLD case study structure at NC LS in longitudinal direction can be considered: even if the expected (median) PGA capacity of the Uniformly Infilled model at NC LS is higher than the corresponding PGA capacity of the Bare model (see Table 3.7), the failure probability at NC LS is higher for the Uniformly Infilled (see Table 3.8), because of the lower slope of the fragility curve, that is, the higher logarithmic standard deviation of PGA capacity (see Table 3.7) characterizing this model.

Table 3.8. Failure probabilities P_f in 50 years for SLD and GLD case study structures

		Seismic Load Design						Gravity Load Design					
		4 storeys			8 storeys			4 storeys			8 storeys		
		DL	NC	DL	NC	DL	NC	DL	NC	DL	NC	DL	NC
UI	x	0.0939	0.0011	0.166	0.0014	0.0187	0.0064	0.0187	0.0064	0.0827	0.0027	0.0027	
	y	0.1934	0.0037	0.2551	0.0089	0.0653	0.0063	0.0653	0.0063	0.155	0.0216	0.0216	
P	x	0.0998	0.0015	0.1711	0.0037	0.1626	0.0039	0.1626	0.0039	0.1601	0.0017	0.0017	
	y	0.1625	0.0039	0.2751	0.0084	0.1826	0.0073	0.1826	0.0073	0.2267	0.0215	0.0215	
B	x	0.0264	0.002	0.0526	0.0011	0.076	0.0055	0.076	0.0055	0.1389	0.0014	0.0014	
	y	0.0249	0.0014	0.047	0.0012	0.1549	0.0078	0.1549	0.0078	0.0588	0.004	0.004	

3.6 Summary

In this Chapter, the effect of main parameters influencing the seismic capacity of the case study structures has been investigated through a sensitivity analysis. Such analysis has shown that the rotational capacity of columns, directly influencing the displacement capacity, has the highest influence on the PGA capacity at NC for all of the investigated structures. Concrete compressive strength significantly influences the capacity at collapse, too, through its influence on the rotational capacity of columns. As far as PGA capacity at DL LS is concerned, mechanical characteristics of infills have the highest influence on the response of the Uniformly Infilled frame, which is assumed to attain the DL LS when the first infill in a storey reaches its maximum resistance, whereas for Pilotis and above all for Bare frames also steel yield strength has a relatively high influence on PGA capacity at DL, since this LS can be due to the first yielding in RC members. Presence of infills significantly influences the collapse mechanism even if the Bare structure is designed according to Capacity Design principles.

As far as the comparison between three different infill configurations is concerned, some conclusions can be drawn:

- at NC LS, a beneficial effect on PGA capacity generally exists when a regular distribution of infill panels is considered, whereas a detrimental effect is shown by structures with an irregular infill distribution;
- at DL LS, the above mentioned beneficial effect is not observed for SLD structures;
- displacement capacity, as expected, is higher for bare structures both in longitudinal and transverse directions at each LS;
- in SLD structures the presence of infills can significantly change the (global) collapse mechanism expected for structures designed according to Capacity Design, thus influencing displacement, ductility and PGA capacities.

The following conclusions can be drawn from a comparison between different design typologies:

- seismic performances of GLD structures are more affected in terms of PGA capacity by infill panels respect to SLD structures, especially for low-rise structures;
- SLD structures generally show the best seismic performances at NC LS;
- as far as Uniformly Infilled configurations are concerned, GLD structures show the highest PGA_{DL} ;

▪ exceptions to the above conclusions are the cases (for eight-story structures) in which there is a concentration of displacement demand at bottom floors leading to an increase in PGA_{NC} due to a stiffening of the multi-linearized SPO curve.

Moreover, the same trends are shown by four- and eight-story structures. It is worth noting that eight-story structures

▪ have a greater variability in collapse mechanisms depending on infill configuration, input parameters and design typology;

▪ they are less affected by infill presence in terms of PGA_{DL} .

It has been pointed out the great importance of infills and their mechanical properties, especially at low level of seismic demand, namely at Damage Limitation Limit State, both for structures designed only for gravity-loading or according to new seismic codes provisions, thus highlighting the necessity of a deeper investigation towards this direction in developing new procedures to account for infill presence directly or indirectly via the more widespread kind of analyses (linear analyses), as it will be shown in Chapter 4.

Fragility curves were obtained for each case study structure, through the application of a Response Surface Method. In order to apply this procedure, the considered input variables were represented by the same Random Variables already used for the sensitivity analysis in addition to the strength reduction factor R , whose variability was taken into account by assuming the logarithmic standard deviation as a function of the ductility. Moreover, fragility curves were fitted by cumulative lognormal distributions. Analysis of seismic vulnerability and its dependence on the Random Variables' variability was performed in detail for each case study structure. Then, failure probabilities in the reference time period of 50 years were evaluated in order to underline the difference between seismic performances of each case study structure.

Moreover, it should be pointed out that special attention should be addressed to the potential brittle failure mechanisms due to the local interaction between masonry infills and structural RC elements and potential out of plane failures - which have not been accounted for herein - especially for existing RC buildings that have not been designed adopting general principles and detailing rules prescribed by modern seismic codes according to Capacity Design philosophy.

References

- Bal I.E., Crowley H., Pinho R., Gulay F.G., (2007). Structural characteristics of Turkish RC building stock in Northern Marmara region for loss assessment applications. ROSE Research Report No. 2007/03, IUSS Press, Pavia, Italy.
- Biskinis, D.E., Fardis, M.N. (2010). Flexure-controlled ultimate deformations of members with continuous or lap-spliced bars. *Structural Concrete*, 11(2), 93-108.
- Cabañas, L., Carreño, E., Izquierdo, A., Martínez, J.M., Capote, R., Martínez, J., Benito, B., Gaspar, J., Rivas, A., García, J., Pérez, R., Rodríguez, M.A., Murphy, P. (2011). Informe del sismo de Lorca del 11 de mayo de 2011. IGN, UCM, UPM, IGME, AEIS, available at <http://www.ign.es/ign/resources/sismologia/Lorca.pdf> (in Spanish)
- Calvi, G.M., Bolognini, D., Penna, A. (2004). Seismic Performance of masonry-infilled RC frames – Benefits of slight reinforcements. Invited lecture to “Sismica 2004 - 6° Congresso Nazionale de Sismologia e Engenharia Sísmica”, Guimarães, Portugal, April 14-16.
- Celarec, D., Dolšek, M. (2010). The influence of epistemic uncertainties on the seismic performance of RC frame building. *Proceedings of the 14th European Conference on Earthquake Engineering*, Ohrid, Macedonia, August 30-September 3. Paper No. 534.
- Celarec D., Dolsek M., (2012) Practice-oriented probabilistic seismic performance assessment of infilled frames with consideration of shear failure of columns, *Earthquake Engineering and Structural Dynamics*
- Celarec, D., Ricci, P., Dolšek, M. (2012). The sensitivity of seismic response parameters to the uncertain modelling variables of masonry-infilled reinforced concrete frames. *Engineering Structures*, 35, 165-177.
- CEN (1995). European Standard ENV 1998-1-1/2/3. Eurocode 8: Design provisions for earthquake resistance of structures – Part I: General rules. Technical Committee 250/SC8, Comité Européen de Normalisation, Brussels.
- CEN (2005) European standard EN1998-3. Eurocode 8: design provisions for earthquake resistance of structures – Part 3: assessment and retrofitting of buildings. European Committee for Standardisation, Brussels
- Circolare del Ministero dei Lavori Pubblici n. 617 del 2/2/2009. Istruzioni per l'applicazione delle “Nuove norme tecniche per le costruzioni” di cui al D.M. 14 gennaio 2008. G.U. n. 47 del 26/2/2009. (in Italian)
- Colangelo F. (2012). A simple model to include fuzziness in the seismic fragility curve and relevant effect compared with randomness. *Earthquake Engineering and Structural Dynamic*; 41:969–986.
- Cosenza E., Festa G., Manfredi G., Polese M., Realfonzo R., Verderame G.M., Zollo A., (2003). Comportamento strutturale in fase pre-eruttiva: il caso Vesuvio. In: *Il Rischio Vesuvio - Strategie di prevenzione e di intervento*. Pp. 315-394. Giannini, Naples, Italy. (in Italian)
- Cosenza, E., Galasso, C., Maddaloni, G. (2009a). Resistenza del calcestruzzo: modellazione probabilistica e risultati sperimentali, *Atti del XXV Convegno Nazionale AICAP “La progettazione e l'esecuzione delle opere strutturali nell'ottica della sostenibilità”*, Pisa, Italy, May 14-16. Paper No. 59. (in Italian)
- Cosenza, E., Galasso, C., Maddaloni, G. (2009b). Analisi statistica delle caratteristiche sismiche degli acciai da cemento armato, *Atti del XXV Convegno Nazionale AICAP “La progettazione*

- e Peseecuzione delle opere strutturali nell'ottica della sostenibilità", Pisa, Italy, May 14-16. Paper No. 57. (in Italian)
- Chrysostomou, C.Z., Gergely, P., Abel, J.F., (2002). A six-strut model for nonlinear dynamic analysis of steel infilled frames. *International Journal of Structural Stability and Dynamics*, 2(3), 335-353.
- Crisafulli, F.J., (1997). Seismic behaviour of reinforced concrete structures with masonry infills. Ph.D. Thesis, University of Canterbury, Christchurch, New Zealand.
- Decreto Ministeriale del 14/1/2008. Approvazione delle nuove norme tecniche per le costruzioni. G.U. n. 29 del 4/2/2008. (in Italian)
- Dolšek, M. (2010). Development of computing environment for the seismic performance assessment of reinforced concrete frames by using simplified nonlinear models. *Bulletin of Earthquake Engineering*, 8(6), 1309-1329.
- Dolšek, M., Fajfar, P. (2001). Soft storey effects in uniformly infilled reinforced concrete frames. *Earthquake Engineering*, 5(1), 1-12.
- Dolšek, M., Fajfar, P. (2002). Mathematical modelling of an infilled RC frame structure based on the results of pseudo-dynamic tests. *Earthquake Engineering and Structural Dynamics*, 31(6), 1215-1230.
- Dolšek, M., Fajfar, P. (2004a). Inelastic spectra for infilled reinforced concrete frames. *Earthquake Engineering and Structural Dynamics*, 33(15), 1395-1416.
- Dolšek, M., Fajfar, P. (2004b). IN2 - A simple alternative for IDA. *Proceedings of the 13th World Conference on Earthquake Engineering*, Vancouver, B.C., Canada, August 1-6. Paper No. 3353.
- Dolšek, M., Fajfar, P. (2005). Simplified non-linear seismic analysis of infilled reinforced concrete frames. *Earthquake Engineering and Structural Dynamics*, 34(1), 49-66.
- Dolšek M., Fajfar P., (2006). Simplified seismic assessment of infilled reinforced concrete frames, *Proceedings of the First European Conference on Earthquake Engineering and Seismology*, Geneva, Switzerland, 3-8 September 2006. Paper Number 888.
- Dolšek, M., Fajfar, P. (2008a). The effect of masonry infills on the seismic response of a four-storey reinforced concrete frame – a deterministic assessment. *Engineering Structures*, 30(7), 1991-2001.
- Dolšek, M., Fajfar, P. (2008b). The effect of masonry infills on the seismic response of a four-storey reinforced concrete frame – a probabilistic assessment. *Engineering Structures*, 30(11), 3186-3192.
- Dymiotis, C., Kappos, A.J., Chryssanthopoulos, M.K. (2001). Seismic reliability of masonry-infilled RC frames. *ASCE Journal of Structural Engineering*, 127(3), 296-305.
- Fajfar P., (1999), Capacity spectrum method based on inelastic demand spectra, *Earthquake Engineering and Structural Dynamics*, 28, 979-993.
- Fajfar, P., Drobnič, D. (1998). Nonlinear seismic analyses of the ELSA buildings. *Proceedings of the 11th European Conference on Earthquake Engineering*, Paris, France, September 6-11.
- Fajfar P., Gaspersic P. (1996), The N2 method for the seismic damage analysis of RC buildings, *Earthquake Engineering and Structural Dynamics*, 25, 31-46.

- Fardis, M.N. (1997). Experimental and numerical investigations on the seismic response of RC infilled frames and recommendations for code provisions. Report ECOEST-PREC8 No. 6. Prenormative research in support of Eurocode 8.
- Fardis, M.N. (2007). LESSLOSS – Risk mitigation for earthquakes and landslides. Guidelines for displacement-based design of buildings and bridges. Report No. 5/2007, IUSS Press, Pavia, Italy.
- Fardis, M.N., Biskinis, D.E. (2003). Deformation capacity of RC members, as controlled by flexure or shear. In: Performance-Based Engineering for Earthquake Resistant Reinforced Concrete Structures: A Volume Honoring Shunsuke Otani. Pages 511-530.
- Fardis, M.N., (2009). Seismic design, assessment and retrofitting of concrete buildings based on EN-Eurocode 8, Springer.
- Fardis, M.N., Panagiotakos, T.B. (1997). Seismic design and response of bare and masonry-infilled reinforced concrete buildings. Part II: infilled structures. *Journal of Earthquake Engineering*, 1(3), 475-503.
- Gómez-Martínez, F. , Pérez-García, A., De Luca, F. , Verderame, G.M. , Manfredi G. (2012), Preliminary study of the structural role played by masonry infills on RC building performances after the 2011 Lorca, Spain, earthquake, proceedings of 15th WCEE, Lisbon, 24-28 September
- Goula, X., Figueras, S., Irizarry, J., Macau, A., Barbat, A., Lantada, N., Carreño, M.L., Valcárcel, J., Combescure, D., Belvaux, M., Monfort, D., Bremond, S., Verrhiest, G., Camares, C., Bairrao, R. (2011). “Rapport de la mission AFPS du séisme de Lorca”, available at <http://www.afps-seisme.org/index.php/fre/Seismes-majeurs/Seisme-a-Lorca> (in Spanish)
- Hak, P. Morandi, G. Magenes, T. J. Sullivan, (2012). Damage Control for Clay Masonry Infills in the Design of RC Frame Structures, *Journal of Earthquake Engineering*, 16:sup1, 1-35
- Iervolino, I. , De Luca, F. , Chioccarelli, E., Dolce, M. (2010), L'azione sismica registrata durante il mainshock del 6 aprile 2009 a L'Aquila e le prescrizioni del D.M.14/01/2008 V.1, available at <http://www.reluis.it>
- INGV-DPC S1 (2007). Progetto S1. Proseguimento della assistenza al DPC per il completamento e la gestione della mappa di pericolosità sismica prevista dall'Ordinanza PCM 3274 e progettazione di ulteriori sviluppi. Istituto Nazionale di Geofisica e Vulcanologia – Dipartimento della Protezione Civile, <http://esse1.mi.ingv.it> (in Italian)
- Kappos, A.J., Stylianidis, K.C., Michailidis, C.N., (1998). Analytical models for brick masonry infilled R/C frames under lateral loading. *Journal of Earthquake Engineering*, 2(1), 59-87.
- Liel, A.B., Haselton, C.B., Deierlein, G.G., Baker, J.W. (2009). Incorporating modeling uncertainties in the assessment of seismic collapse risk of buildings. *Structural Safety*, 31(2), 197-211.
- Mainstone, R.J. (1971). On the stiffnesses and strengths of infilled frames. *Proceedings of the Institution of Civil Engineering*, Supplement IV, 57-90.
- McKay, M.D., Conover, W.J., Beckman, R.J. (1979). A comparison of three methods for selecting values of input variables in the analysis of output from a computer code. *Technometrics*, 21(2), 239-245.
- McKenna, F., Fenves, G.L., Scott, M.H. (2004). OpenSees: Open System for Earthquake Engineering Simulation. Pacific Earthquake Engineering Research Center. University of California, Berkeley, CA, USA. <http://opensees.berkeley.edu>

- Negro, P., Colombo, A. (1997). Irregularities induced by nonstructural masonry panels in framed buildings. *Engineering Structures*, 19(7), 576-85.
- Negro, P., Verzeletti, G., (1997). Effect of infills on the global behaviour of R/C frames: energy consideration from pseudodynamic tests. *Earthquake Engineering and Structural Dynamics*, 25(8), 753-773.
- Panagiotakos, T.B., Fardis, M.N. (1996). Seismic response of infilled RC frames structures. 11th World Conference on Earthquake Engineering, Acapulco, México, June 23-28. Paper No. 225.
- Panagiotakos, T.B., Kosmopoulos, A.J., Fardis, M.N. (2002). Displacement-based seismic assessment and retrofit of reinforced concrete buildings. Proceedings of the 1st fib Congress, Osaka, Japan, October 13-19. Pages 269-278.
- Pecce M., Polese M., Verderame G.M., (2003). Seismic vulnerability aspects of RC buildings in Benevento, Proceedings of the Workshop on Multidisciplinary Approach to Seismic Risk Problems. September 22, Sant'Angelo dei Lombardi, Italy. In: Pecce M., Manfredi G., Zollo A., 2004. The many facets of seismic risk. Pp. 134-141. CRdC AMRA.
- Pinto, P.E., Giannini, R., Franchin, P. (2004). Seismic reliability analysis of structures. IUSS Press, Pavia, Italy.
- Pinto, A.V., Verzeletti, G., Molina, J., Varum, H., Coelho, E., (2002). Pseudodynamic tests on non-seismic resisting RC frames (infilled frame and infill strengthened frame tests). Report EUR, EC, Joint Research Centre, Ispra, Italy.
- Pires, F., (1990). Influencia das paredes de alvenaria no comportamento de estruturas reticuladas de betao armado subjectas a accoes horizontaes. Ph.D. Thesis, LNEC, Lisbon, Portugal. (in Portuguese)
- Polese M., Verderame G.M., Mariniello C., Iervolino I., Manfredi G., (2008). Vulnerability analysis for gravity load designed RC buildings in Naples – Italy, *Journal of Earthquake Engineering*, 12(S2), 234-245.
- Pitilakis, K. (Project coordinator) (2012). Deliverable D4.6: Validation and Benchmarking socio-economic indicators determined in D4.1-4.4 (e.g., L'Aquila event) using empirical data and surveys with experts (Updated version: 22 February 2012). Systemic Seismic Vulnerability and Risk Analysis for Buildings, Lifeline Networks and Infrastructures Safety Gain (SYNER-G) Project.
- Regio Decreto Legge n. 2229 del 16/11/1939. Norme per la esecuzione delle opere in conglomerate cementizio semplice od armato. G.U. n. 92 del 18/04/1940. (in Italian)
- Ricci, P. (2010). Seismic vulnerability of existing RC buildings. Ph.D. Thesis, University of Naples Federico II, Naples, Italy.
- Ricci P., De Luca F., Verderame G.M. (2010), 6th April 2009 L'Aquila earthquake, Italy: reinforced concrete building performance, *Bulletin of Earthquake Engineering*, 9(1), 285-305.
- Rossetto, T., Elnashai, A. (2005). A new analytical procedure for the derivation of displacement-based vulnerability curves for populations of RC structures. *Engineering Structures*, 7(3), 397-409.
- Stylianidis, K.C., (1985). Experimental investigation of the behaviour of the single-story infilled R.C. frames under cyclic quasi-static horizontal loading (parametric analysis). Ph.D. Thesis, University of Thessaloniki, Thessaloniki, Greece.

- Vamvatsikos, D., Cornell, C.A. (2006). Direct estimation of the seismic demand and capacity of oscillators with multi-linear static pushovers through IDA. *Earthquake Engineering and Structural Dynamics*, 35(9), 1097-1117.
- Verderame, G.M., De Luca, F., Ricci, P., Manfredi G. (2010a). Preliminary analysis of a soft storey mechanism after the 2009 L'Aquila earthquake. *Earthquake Engineering Structure*, 40(8), 925-44.
- Verderame, G.M., Manfredi, G., Frunzio, G. (2001). Le proprietà meccaniche dei calcestruzzi impiegati nelle strutture in cemento armato realizzate negli anni '60. Atti del X congresso nazionale ANIDIS "L'ingegneria Sismica in Italia", Potenza-Matera, Italy, September 9-13. (in Italian)
- Verderame, G.M., Polese, M., Mariniello, C., Manfredi, G. (2010b). A simulated design procedure for the assessment of seismic capacity of existing reinforced concrete buildings. *Advances in Engineering Software*, 41(2), 323-335.
- Verderame, G.M., Ricci, P., Manfredi, G., Cosenza, E. (2010c). Ultimate chord rotation of RC columns with smooth bars: some considerations about EC8 prescriptions. *Bulletin of Earthquake Engineering*, 8(6), 1351-1373.
- Verderame, G.M., Ricci, P., Esposito, M., Manfredi, G. (2012). STIL v1.0 – Software per la caratterizzazione delle proprietà meccaniche degli acciai da c.a. tra il 1950 e il 2000, available at <http://www.reluis.it/>
- Vidic, T., Fajfar, P., Fischinger, M. (1994). Consistent inelastic design spectra: strength and displacement. *Earthquake Engineering and Structural Dynamics*, 23(5), 507-521.
- Vorechovsky, M., Novak, D. (2009). Correlation control in small-sample Monte Carlo type simulations I: A simulated annealing approach. *Probabilistic Engineering Mechanics*, 24(3), 452-462.

Chapter 4

LIMITATION OF DAMAGE TO INFILL PANELS IN SEISMIC DESIGN AND ASSESSMENT OF RC FRAMES VIA LINEAR METHODS

Recent earthquakes and numerical studies have demonstrated that the presence of infills in Reinforced Concrete buildings cannot be disregarded. In this Chapter the attention is focused on the limitation of damage to infill panels at Damage Limitation Limit State.

Nonlinear Incremental Dynamic Analyses are carried out on structural models with infills in order to evaluate the intensity measure level corresponding to the achievement of Damage Limitation Limit State. Then, the results of such analyses are used as a reference to propose modeling and analysis tools to be used for seismic design or assessment of infilled Reinforced Concrete frames at Damage Limitation Limit State, both in the case in which infills are explicitly modeled or not.

First, the estimation of the “equivalent” Interstorey Drift Ratio capacity on the corresponding bare model is carried out. Then, the effective stiffness of infill panels to be used in linear analysis (which nowadays is still a widespread method, especially for seismic design of new structures) for seismic assessment at Damage Limitation Limit State is evaluated. The estimation of a displacement limit capacity for a bare model in the context of linear analyses and the research of the effective stiffness of infills in the “true” infilled model are carried out through two procedures described in this Chapter.

The results of the application of these procedures for four- and eight-story infilled frames, designed for seismic loads - according to the current Italian technical code - and for gravity load only - according to an obsolete technical code - are presented and discussed.

4.1 Introduction

The observation of damage to infilled RC buildings after recent earthquakes (e.g. L'Aquila 2009, Emilia 2012) and numerical studies such as those reported in the previous Chapter, have demonstrated that the presence of infills in Reinforced Concrete (RC) buildings cannot be disregarded. Infills are usually assumed as partition elements without any structural function, but they have a significant influence on the increase in lateral stiffness and, consequently, on the reduction in period of vibration, on base shear capacity, on possible brittle failure mechanisms in joints and columns due to local interaction between panels and the adjacent structural elements, and on the building collapse mechanism.

This issue was investigated during last years (see Section 2.1.3) supported by numerical (Dolsek et al. 2001, 2002, 2004, 2006, 2008a, 2008b, Celarec et al 2012, Dymiotis et al 2001, Celarec and Dolsek 2009, Ricci et al. 2012a, 2012b, 2013) and experimental analyses (Negro and Colombo 1997, Fajfar and Drobic 1998, Negro and Verzelletti 1997, Pinto et al. 2002, Hak et al. 2012, Mehrabi et al. 1994, Crisafulli et al. 1997, Colangelo et al 2005), regarding both the influence of infills on the global seismic performance of infilled structures and local effects due to the interaction between infill panels and surrounding RC frames.

In Chapter 3, the effect of mechanical properties of infills and RC influencing the seismic capacity of infilled RC structures has been investigated also through sensitivity analyses (see also Celarec et al, 2012, Ricci et al 2012a, Ricci et al 2013). Such analyses have shown that the rotational capacity of RC columns and concrete compressive strength have the highest influence on the seismic capacity at high level of displacement demand; whereas, as far as seismic capacity at low level of displacement demand is concerned, e.g. at Damage Limitation (DL) Limit State (LS), mechanical characteristics of infill panels have the highest influence on the response of uniformly infilled frames (Ricci et al 2012a, Ricci et al 2013). Thus, the contribution of infills to the lateral seismic response in terms of strength and stiffness significantly changes with the displacement demand: displacement and drift demand significantly decrease if infills are explicitly taken into account in the numerical model with respect to the corresponding bare frame, but such a reduction depends on strength and stiffness properties of infills and it is more significant at DL LS

than at Ultimate LS (when infills are already extensively damaged). At DL LS the presence of infill panels produces a reduction in displacement capacity compared with the corresponding bare structure, due to the assumption of displacement capacity limits accounting for the damage affecting these elements; if such detrimental reduction is not counterbalanced by the beneficial increase in stiffness and strength provided by infill panels, a reduction in seismic capacity can be observed (Ricci et al. 2012b).

Since the great importance of infills at low level of displacement demand, it is worth deeper investigating about their influence on seismic performance of RC frames under seismic action characterized by low return periods.

In particular, in this Chapter, the attention is focused on DL LS. DL LS is intended to limit the costs of reparability and, therefore, the damage which occurs at this LS to elements designed without any structural function, such as infill panels, should be properly limited.

If infills were explicitly included into the structural model, the limitation of damage which occurs to them could be obtained directly limiting the IDR demand of the “true” infilled structure to the IDR capacity of the infill panels. To this end, a definition of such a IDR capacity is necessary. In literature, there are several experimental studies conducted on infilled RC frames that can allow to draw a qualitative description of damage occurring to infills at DL LS and to translate the degree of damage to unreinforced masonry infill panels into an IDR threshold (or IDR range).

Vice-versa, if the presence of infill panels is neglected in the structural model – as generally happens in the design of a new structure – damage occurring to infills can be limited in structural analyses through the limitation of the IDR demand on the bare structure.

In particular, if there are no non-structural elements that follow the deformations of the structural system, no damage to infills can be due to the deformation of the surrounding frame; therefore, it is expected that IDR threshold can be completely independent on infill properties. On the opposite side, if infill panels are rigidly connected to the surrounding structural frame, IDR threshold should be strictly related to their properties and, in particular, to their displacement capacity.

In accordance with this simple reasoning, seismic codes throughout the world (CEN 2005, Decreto Ministeriale 2008, ASCE-SEI/41) propose an IDR

threshold at DL LS on the bare structure whose value depends on the kind of partitions, and, in particular, on the relative degree of connection between structural and non-structural elements. In particular, the lower the degree of connection between non-structural elements and structural frame, the larger the IDR threshold; moreover, the more “ductile” the behavior of non-structural elements, the larger the IDR threshold.

It can be supposed that such IDR thresholds proposed by codes for a bare structure are defined on the basis of an implicit equivalence between the “true” infilled structure and the “equivalent” bare structure. Actually, from a theoretical point of view, the limit of IDR demand on the bare structural model can be interpreted as “equivalent” to the IDR directly evaluable on the “true” infilled structure; such “equivalent” IDR is the IDR capacity that should be assumed when using a numerical bare model in order to obtain a reliable estimate of intensity measure (IM) capacity at DL LS, that is, the same IM capacity obtained using a “true” infilled model.

Therefore, seismic capacity assessment or design at DL LS can be performed on the “true” infilled numerical model or, alternatively, on the “equivalent” bare structural model. Depending on the numerical model which is adopted, the displacement threshold at DL LS should be different, and, in particular, higher for the bare structural model, intensity measure capacity at the investigated LS being equal, because of its lower strength and stiffness with respect to the corresponding infilled model.

Moreover, if the designer would explicitly introduce infills in the structural model to perform linear analyses to account for their damage level, infills have to be properly modeled – especially in terms of stiffness – and a displacement limit directly correlated to their damage should be assumed.

Information and provisions about these aspects provided by technical codes are quite poor. In particular, further efforts to extend the concept of drift limitation to obtain some comprehensive design criteria for RC structures, explicitly depending on strength and stiffness properties of infill panels, should be produced.

In this Chapter, a more realistic way to perform the design of new structures – including the evaluation of damage occurring to infill panels – but also in the assessment of the existing structures – when assessment at DL LS is explicitly required – is proposed within the context of linear analyses.

The first issue which is investigated is related to the assessment of bare structural models: a procedure is proposed and applied aiming at the estimation of the “equivalent” displacement limit capacity on the bare model depending on the mechanical properties of the infilled frame.

The second issue is related to the assessment of infilled structural models: a procedure is proposed for the estimation of an effective stiffness of infill panels to be used in linear analysis for seismic assessment at DL LS, thus allowing to explicitly include these elements also within this kind of analysis approach, which nowadays is still a widespread method, especially for seismic design of new structures.

Finally, the results of the application of these procedures for four- and eight-story infilled frames, designed for seismic loads according to the current Italian technical code, and for gravity load only, according to an obsolete technical code, are presented and discussed.

4.2 Code provisions and literature review

According to a performance-based approach, modern seismic codes define performance levels aimed at avoiding collapse under major earthquakes and ensuring control and limitation of damage under more frequent but less severe earthquakes, in order to minimize economic and functionality losses. The latter objective is addressed by serviceability requirements expressed by Damage Limitation Limit State and Immediate Occupancy Performance Level (PL) in European and US standards, respectively (CEN 2005, ASCE-SEI/41, CEN 2004). DL LS and IO PL can be considered as corresponding to each other; both of them, for an ordinary building, should be verified for a 225yrs return period earthquake (CEB 2003).

In the following, performance requirements and acceptance criteria provided by seismic codes are illustrated; then, drift capacity limits are analyzed. To this end, data from literature are reported and discussed.

4.2.1. Code provisions on infill modeling and acceptance criteria

According to Eurocode 8 provisions for new buildings CEN 2004 at Damage Limitation LS the costs of damage should not be “disproportionately high” in

comparison with the costs of the structure itself; for existing buildings CEN 1998 non-structural components, such as partitions and infills, may show distributed cracking but the damage could be economically repaired, permanent drifts should be negligible, and the structure should not need any repair measures.

According to ASCE/SEI 41 provisions for existing concrete buildings ASCE-SEI/41 Immediate Occupancy PL is assumed to be reached in unreinforced masonry infill walls when minor ($< 1/8$ -in. width) cracking of masonry infills and veneers and minor spalling in veneers at a few corner openings occur; 0.1% is provided as an indicative value of the typical range of drift corresponding to such damage; permanent drifts should be negligible (Section §C1.5.1). According to FEMA 274 (1997) at 0.1% drift minor cracking along bed joints develops for weaker mortars, or diagonal cracks form across a panel for stronger mortars; these cracks may be noticeable, but no structural repair would be necessary.

Such requirements need to be translated in acceptance criteria for individual masonry infill panels when carrying out a seismic assessment. Two alternative approaches are adopted:

- a "direct" approach, based on the explicit modeling of masonry infills by means of elements added to the numerical model, usually consisting of equivalent struts; in this case, drift demand on infill panels is compared with the corresponding capacity provided by acceptance criteria;
- an "equivalent" approach, allowing to carry out the seismic assessment on a bare numerical model; in this case, an "equivalent" IDR capacity is assumed, that should ideally provide the same results - in terms of seismic safety check - obtained when using the "direct" approach.

If a "direct" approach is adopted, Eurocode 8 does not provide full indications for infill modeling, nor for drift capacity limits, whereas the Italian "Circolare Esplicativa" (§C8.7.2.1) allows to assume the IDR capacity at DL LS equal to the value provided for masonry (i.e., 0.3% for unreinforced masonry). On the contrary, ASCE/SEI 41 (§7.4) provides much more complete guidelines to model and assess the response of unreinforced masonry infill walls. The lateral stiffness of the wall is evaluated according to Mainstone's formula (Mainstone, 1971); for nonlinear analysis procedures, the load-drift response of

the wall is assumed to be perfectly plastic after shear strength is reached. Deformation capacity is assumed to increase with the ratio of frame to infill strengths, and with the slenderness of the infill wall. Acceptance criteria for linear analysis procedures indicate that at IO PL some inelastic deformations can occur, thus allowing some minor cracking of the infill panels (FEMA 274, §C7.5.2.3(A)).

If an “equivalent” approach is adopted (that is, if stiffness and strength contributions of infill walls are neglected in the numerical analysis) all of the above mentioned seismic codes provide equivalent IDR capacity values fictitiously higher than the actual deformation capacity of the infill wall. Eurocode 8 - part 1 suggests to limit the IDRs to 0.5%, if the story has brittle non-structural elements attached to the structure (notably, ordinary masonry infills), or 0.75%, if the story’s non-structural elements are “ductile”, or 1%, when there are no non-structural elements that follow the deformations of the structural system. Very similar provisions are provided by Italian seismic code Decreto Ministeriale 2008.

In ASCE/SEI 41 (§11.9.2) nonstructural (that are not explicitly modeled and assessed as structural elements) “heavy” masonry partitions are checked at IO PL for 0.5% IDR.

It is worth highlighting that, both in “direct” and “equivalent” approaches, another important modeling issue arises if a linear method of analysis is adopted, that is the choice of the stiffness assumed for structural (both in “direct” and in “equivalent” approaches) and non-structural (in “direct” approaches) elements in order to take into account, also in linear analyses, at Serviceability LSs, the influence of first cracking which occurs also for low level of seismic demand. In particular, in the “direct” approach, literature and code provisions regarding this issue for non-structural elements are much more limited in comparison with provisions related to RC members. Generally speaking, the estimation of such “effective” stiffness should depend on displacement demand on the structural elements, and thus it should be different for each element in the structure, depending on the level of displacement demand involving each of them. However, this kind of - necessarily iterative - procedure should require a computational demand which seems to be not compatible with the level of approximation that

implicitly characterizes a linear analysis. Hence, for a RC structure, when an effective stiffness is employed for a linear analysis, a unique value of degradation of the elastic stiffness (pre-cracking) is usually applied to RC members.

As far as RC structural members are concerned, several indications are provided. Some authors (e.g., Panagiotakos and Fardis, 1999) suggest to use the secant-to-yielding stiffness in order to predict displacement and forces demand with a good approximation with respect to a nonlinear analysis, as far as ultimate limit states are concerned. EC8-part 1 CEN 2004 prescribes an effective stiffness equal to one-half of the corresponding elastic one, often overestimating the secant-to-yielding stiffness (Fardis, 2009); such an overestimation obviously implies a non-conservative underestimation of the displacement demand. Thus, in EC8-part 3 CEN 1998 the adoption of a secant-to-yielding stiffness is explicitly suggested for checks in terms of displacements. ASCE-SEI 41/06 - Supplement I ASCE-SEI/41 suggests to use the secant-to-yielding stiffness, too, and the value of the effective stiffness for RC members depends on the kind of element and the axial load ratio. New Zealand standards (NZS 3101, 2006) prescribe a value of effective stiffness which not only depends on the kind of element and the axial load ratio, but also on the considered LS, on the ductility capacity at Ultimate LS, and on the steel yield strength.

In the “direct” approach context, when infills are modeled for a linear analysis, the evaluation of their stiffness is a key point. Such “effective” stiffness should ideally account for stiffness degradation due to first cracks and detachments between the infill and the surrounding frame. Nevertheless, quite poor provisions can be obtained from literature or technical codes about this issue for infills.

If an equivalent strut approach is adopted, the problem of evaluating the stiffness assumed for the infill panel is translated into the determination of the strut width. EC8-part 1 CEN 2004 does not provide a specific value of width-to-length ratio for the equivalent strut. Paulay and Priestley (1992) suggest a value of this ratio equal to 0.25 in order to estimate the secant stiffness corresponding to a lateral load equal to 50% of the maximum load capacity of the infilled frame; in Fardis (2009) a width-to-diagonal length ratio equal to 0.20 is proposed at DL LS, whereas a lower value (namely, 0.10-0.15) is suggested at Significant Damage LS. Moreover, as reported above, according

to ASCE/SEI 41 (§7.4), infills can be represented with equivalent diagonal compression struts, whose lateral stiffness should be evaluated according to Mainstone's formula (Mainstone, 1971).

4.2.2. Literature review on drift capacity of unreinforced masonry infill panels

The degree of damage to unreinforced masonry infill panels reported previously should be translated in drift (or drift range) provided by literature studies. Many difficulties arise from the fact that descriptions of damage levels reported by different authors are not fully consistent with each other, nor with performance levels provided by seismic codes. Moreover, any definition of limit state in terms of physical damage and feasibility of repair inherently is imprecise, qualitative, and open to individual judgment (e.g., "minor" cracks or "economically" repairable damage) (Colangelo, 2012, 2013a, 2013b).

In the following, main literature studies investigating this issue are reported, in an attempt to draw conclusions as general as possible on typical range drift corresponding to the investigated performance level.

In Rossetto and Elnashai (2003) a relationship between a Damage Index and the corresponding maximum IDR demand is proposed, based on dynamic experimental tests from literature; for infilled RC MRF, "Light" damage - starting from cracking at wall-frame interfaces, followed by cracking at corners of openings up to diagonal cracking of walls with limited crushing of bricks at beam/column connections - occurs for Damage Index values corresponding to a drift range between 0.08% and 0.31%.

In Gu and Lu, (2005), based on 140 specimens collected from literature, a "Functional" performance level is defined, corresponding to "limited to minor cracks and falling of small pieces of plaster [...] many noticeable cracks with limited length and width along the diagonal and around the foot corner [...] only local repair work needed [...] small economic loss"; such damage is attained at a drift level equal to 0.25% and corresponding to the peak lateral load of the wall.

Dolšek and Fajfar (2008) assume that Damage Limitation Limit State is attained when the last infill in a story reaches its peak load. Such condition is assumed to be reached at a story drift between 0.1% and 0.2%, depending on the slenderness of the panel and the presence of openings, these values being

in good agreement with the observed behavior in the pseudo-dynamic experimental test of the frame studied by the Authors (Pinto et al. 2002).

In Hak et al. (2012) a masonry infill model is proposed, calibrated on the experimental results provided by Calvi and Bolognini (2001). The Damage Limitation Limit State, at which “some infills are damaged but can be easily and economically repaired”, is assumed to be attained between 0.2% and 0.3%, the latter drift corresponding to the peak load in the infill. In the reference work by Calvi and Bolognini (2001), > 2mm wide cracks and damage to brick units at corners were observed at 0.2% (see Figure 4.1a).

In Özcebe et al. (2012) a numerical study on several different case-study existing RC frames with infills is carried out. Three Limit States for infills are defined, based on the attainment of different strain values in the equivalent struts. These values are based on literature studies providing typical material properties of Turkish type infill walls (Bal et al. 2007, 2008). The attainment of the strain at maximum stress in the infill is assumed as corresponding to the onset of non-negligible cracks, leading to “relevant” financial loss. Such Limit State is found to be attained for a drift ratio equal to 0.10%. According to the Authors, this value is in line with the values reported by Griffith (2008) for the drift at which masonry infill cracks, i.e., between 0.07% and 0.3%, based on several data collected from literature.

Behavior of masonry infilled RC frames and corresponding damage levels were widely investigated by Colangelo (2001, 2003, 2005, 2012, 2013, 2013a, 2013b), through experimental and numerical studies. During last years, the Author focused his attention on the uncertainty in drift capacity at different damage states, accounting for the influence of qualitative and individual judgment on damage evaluation through a fuzzy-based approach. In Colangelo, 2013a and 2013b, 1st (Slight) and 2nd (Moderate) damage states, consisting of “Onset of cracking in the bricks, associated with the first noticeable reduction of stiffness” and “Extended, wide cracks in the infill wall, before its peak strength is reached” are attained at 0.03% and 0.35%, respectively. If fuzziness is accounted for, leading to a decrease in fragility, such drift limits increase to 0.04% and 0.49%.

A summary of the analyzed drift ranges for DL LS from literature is reported in Figure 4.1b.

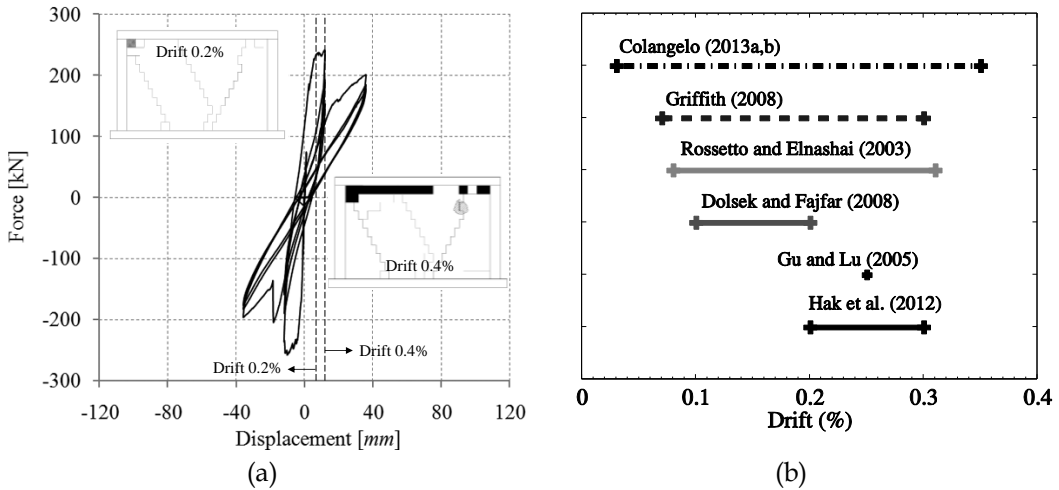


Figure 4.1. Example of experimental response of the unreinforced infilled RC frame (by Calvi and Bolognini, 2001) (a); IDR values corresponding to DL LS from literature (b)

In this study, the following description of damage to unreinforced masonry infill walls is assumed as corresponding to the investigated performance level:

“Minor (< 3mm) but distributed and visible cracks occur along mortar bed joints and/or brick units. The damage is more than aesthetic, but it is easily and economically repairable.”

Based on the reported literature data, it can be concluded that such kind and extent of damage occurs for a typical drift range approximately between 0.1% and 0.3%, close to the peak load of the infill panel.

ASCE/SEI 41 provisions, illustrated previously, appear in line with this conclusions, on the safe side.

4.3 Methodology

As explained in the previous Sections, seismic capacity assessment or design at DL LS can be performed on the “true” infilled numerical model or, alternatively, on the “equivalent” bare structural model.

It appears clear that the most widespread typology of numerical models which are used to approach structural analysis problems are bare structural models. Hence, the need to consider damage occurring to infills at DL LS also when using bare structural models leads to an “equivalent” approach: an

“equivalent” displacement threshold at this LS – to be used with bare models – has to be evaluated, depending on infills’ and RC members’ properties.

On the other hand, when infills are modeled in a linear analysis approach, i.e. in the context of the “direct” approach, the need to include infills into the numerical model leads to the research of the effective stiffness which should be assigned to such elements, or, if an equivalent strut approach is adopted, the determination of the strut width.

The research of the equivalent displacement capacity, on one side, and of the effective stiffness of infills, on the other side, in the context of linear analyses is carried out through two procedures, proposed and described herein starting from Incremental Dynamic Analyses (IDAs) (Vamvatsikos and Cornell, 2002, 2004).

In IDAs the non-linear infilled structural model is investigated through time history analyses under the action of a set of ground motion records; the non-linear time-history analysis is repeated increasing the scale factor of the record, for each record, thus obtaining a relationship between a ground motion intensity measure (PGA or spectral acceleration $S_a(T_{1,5\%})$) and an engineering demand parameter (maximum IDR in this case) for the structural model. IDAs are carried out on structural models explicitly including infills in order to evaluate the intensity measure level corresponding to the achievement of DL LS.

Starting from IDAs, the procedure aiming at the estimation of the IDR threshold on the corresponding bare model is described in Section 4.3.1.

Then, the research of the effective stiffness of infill panels to be used in linear analyses for seismic assessment at DL LS is analyzed in Section 4.3.2, thus allowing to explicitly include these elements also within this kind of analysis approach, which nowadays is still a widespread method, especially for seismic design of new structures.

In the proposed methodology, a great importance is assumed by the definition of the investigated LS. The definition of DL LS has to be considered still an open issue (see Section 4.2); however, based on the analysis of the literature review on the drift capacity of unreinforced masonry infill panels (see Section 4.2.2), in this study, DL LS is assumed to occur when the peak displacement is reached in the first infill panel, thus starting to degrade, consistent with the damage level and IDR range characterizing this LS, as discussed in Section 4.2.2. It is worth noting that, even if a different definition

of IDR capacity at DL LS is adopted, the procedures described below are still valid.

4.3.1. Bare model: equivalent IDR capacity

In this Section, the procedure aiming at the estimation of a displacement limit capacity - in terms of IDR - on the bare model is described. Results from nonlinear IDAs are used as a reference, and a principle of equivalence between nonlinear analyses on infilled models and linear time histories on the corresponding bare ones in terms of PGA capacity at DL LS is applied.

First of all, the non-linear infilled structural model is investigated through time history analyses under the action of the selected set of ground motion records, thus obtaining an IDA curve for each record in terms of peak IDR demand versus PGA.

The attention is focused on the DL LS defined as dependent on a displacement capacity limit directly related to the damage to infill panels and, in particular, to the IDR corresponding to the achievement of the maximum strength in the first infill, IDR_{DL} , as explained above. Thus the median value of PGA corresponding to this IDR threshold can be evaluated from the previously obtained set of IDAs. This value of PGA is the Intensity Measure (IM) capacity at DL LS of the infilled frame, PGA_{DL} (Step 1).

Then, Linear Time-History (LTH) analyses are performed on the corresponding bare structural frame for each selected record (Step 2). Finally the median value of the maximum IDR is estimated at the IM level equal to PGA_{DL} , namely $IDR_{DL,equiv}$ is obtained (Step 3). Such a IDR represents the maximum interstory drift demand on the bare model at DL LS and it represents the goal of this procedure, hereinafter referred to as “equivalent” IDR.

In Figure 4.2 a schematic example of the procedure explained above is reported. The described procedure can be repeated for different values of effective stiffness chosen to model RC members in LTH analyses, thus obtaining different values of “equivalent” IDR, depending on the stiffness adopted in the modeling of RC elements. Such an effective stiffness can be estimated as a rate (α_{RC}) of the elastic (pre-cracking) stiffness of each RC member, e.g. 50% (EC8-part 1).

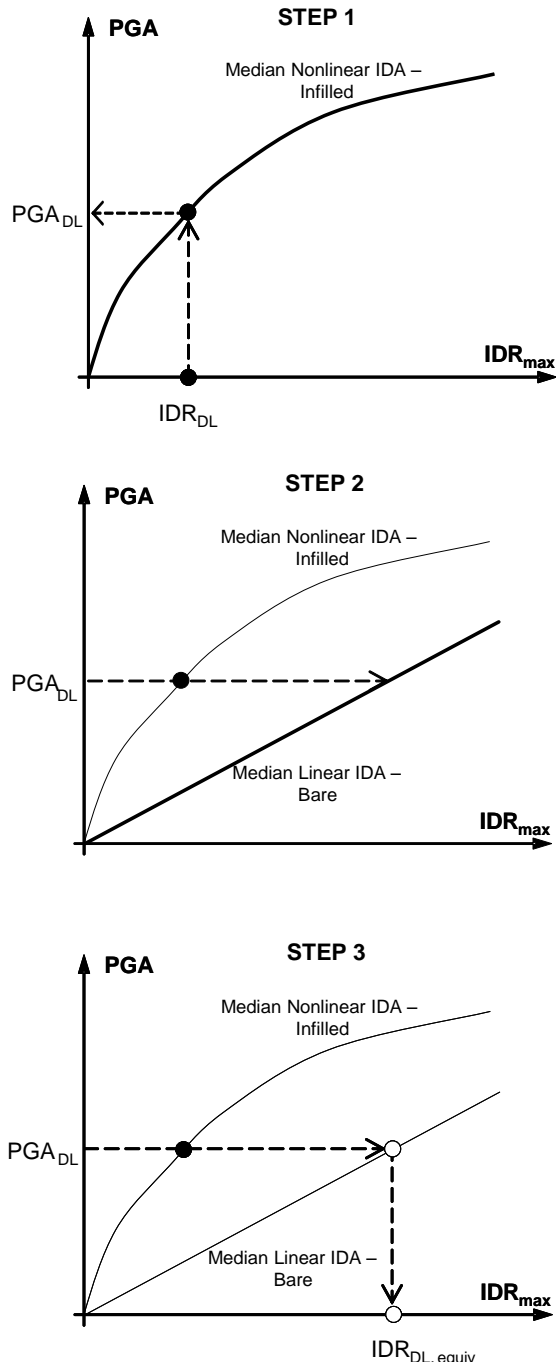


Figure 4.2. Schematic example of the procedure: research of the equivalent IDR capacity ($IDR_{DL, equiv}$)

It is worth noting that such an equivalence is imposed in terms of PGA capacity (instead than in terms of first period spectral elastic acceleration) because of the high difference in first period of vibration between an infilled frame and the corresponding bare one.

4.3.2. Infilled model: effective stiffness of infill panels

If the designer introduces infills in the structural model to perform linear analyses, infills have to be properly modeled. Information and provisions about such a modeling provided by technical codes are generally quite poor.

Generally speaking, effective stiffness for infill panels should be intermediate between the initial elastic stiffness and the stiffness secant to the capacity point, i.e. the secant-to-maximum stiffness, according to the definition of the achievement of DL LS adopted in this study.

In this Section, a procedure aiming at the estimation of the effective stiffness of infill panels to be used in linear analysis for seismic assessment at DL LS is proposed.

First of all, the same IDAs obtained as described before for the infilled frame are considered, in terms of peak IDR demand versus elastic spectral acceleration $S_a(T_1, 5\%)$, where T_1 is the fundamental period of the infilled frame. Thus the median value of $S_a(T_1, 5\%)$ corresponding to this IDR threshold, $\eta_{S_a(T_1, 5\%) | IDR}$, can be evaluated from the previously obtained set of IDAs. This value of $S_a(T_1, 5\%)$ is the IM capacity at DL LS, $S_a(T_1, 5\%)_{DL}$.

Then, LTH analyses are performed, assuming a linear behavior for both RC members and infill panels, and assuming a reduction factor (α) of the initial elastic stiffness of all the infill trusses. As shown in Figure 4.3, an iterative procedure is applied, varying the coefficient α between 0 (infinitely flexible infills) and 1 (infills with initial elastic stiffness). For each α value, LTH analyses for all of the selected records are performed, and the median value of the maximum IDR demand, $\eta_{IDR | S_a(T_1, 5\%)}$, is estimated at the IM level equal to $S_a(T_1, 5\%)_{DL}$. The iterative procedure stops when the value of $\eta_{IDR | S_a(T_1, 5\%)}$ is equal to IDR_{DL} ; the corresponding α factor, α_w , is the reduction factor of the initial elastic stiffness of infills providing an effective stiffness of infill panels such that a linear dynamic analysis on the infilled numerical model leads to a displacement demand in terms of maximum IDR at DL LS which is

approximately equal to the maximum IDR demand evaluated through nonlinear dynamic analysis on the same model.

In Figure 4.4 a schematic example of the result of the procedure explained herein is reported.

It is worth noting that, since that it is not possible to know a-priori which story is involved in the achievement of DL LS, the reduction factor is applied to all of the infill panels. Such a procedure allows to calibrate the factor α that provides the “real” maximum IDR demand – at a certain level of IM – through a linear analysis, but an error may occur in the estimation of the corresponding top displacement. This could be considered as an unavoidable approximation due to the limitation of a linear analysis itself, which is not able to capture the effects of a concentration of post-elastic displacement demand. However, this error could be considered not of a primary importance, since DL LS check is performed in terms of another displacement demand parameter, namely maximum IDR.

Nonlinear behavior of RC members can be considered, too, by repeating the described procedure for different value of effective stiffness of RC members, i.e. for different values of the rate (α_{RC}) of the elastic (pre-cracking) stiffness of each RC member. For each value of α_{RC} , a α_w factor can be estimated.

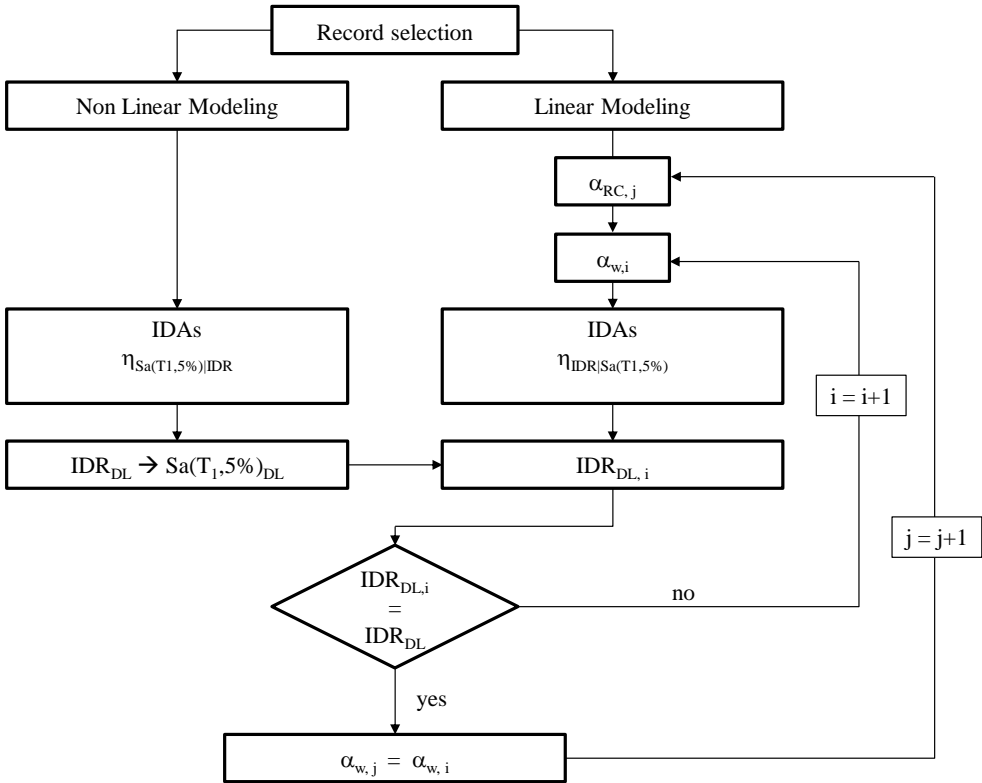


Figure 4.3. Steps of the procedure: research of the effective stiffness for infill panels

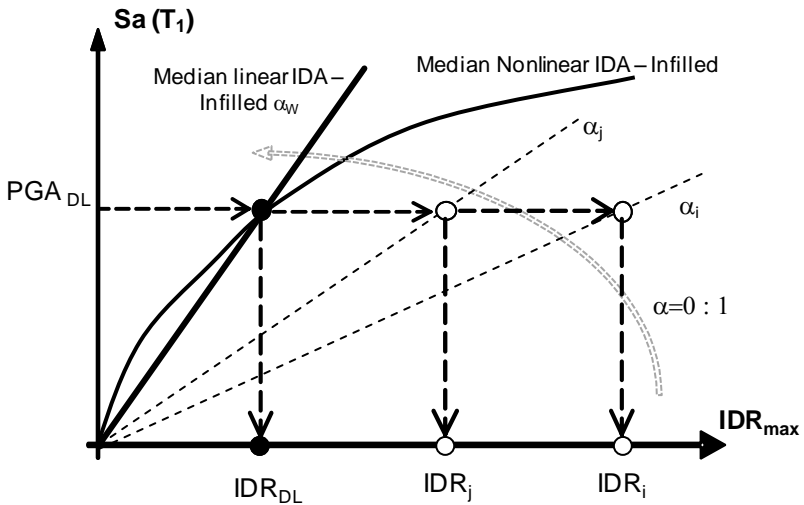


Figure 4.4. Schematic example of the result of the procedure: research of the effective stiffness for infill panels

4.4 Application examples

The methodology proposed in the previous Section is applied for four case study frames. Mechanical and geometrical properties of such frames and their modeling are described below. The results are presented and discussed herein.

4.4.1. Case study frames

The case study structures analyzed herein are infilled RC planar frames with five equal-length bays, with a bay length equal to 4.5 m and an interstory height equal to 3.0 m. The analyzed frames are extracted from the 3-D structures analyzed in Chapter 3; they are symmetric in plan, both in longitudinal and in transverse direction, with five bays in longitudinal direction and three bays in transverse direction. Slab way is always parallel to the transverse direction.

Thus, starting from different design typologies and number of stories, four case study frames are extracted and analyzed:

- two gravity load designed (GLD) frames, a four-story and an eight-story frame, defined by means of a simulated design procedure according to code prescriptions and design practices in force in Italy between 1950s and 1970s (Regio Decreto Legge n. 2229, 16/11/1939; Verderame et al., 2010b);
- two seismic load designed (SLD) frames, a four-story and an eight-story frame, designed for seismic loads according to the current Italian code (D.M. 2008) in Ductility Class High; hence, the principles of the Capacity Design are applied.

A more detailed description of these structures is reported in Chapter 3.

In each frame, infill panels are uniformly distributed along the height (see Figure 4.5). Panel thickness is equal to 200 mm, corresponding to a double layer brick infill (120+80) mm thick, which can be considered as typical of a non-structural infill masonry wall (Bal et al. 2007). Presence of openings is not taken into account.

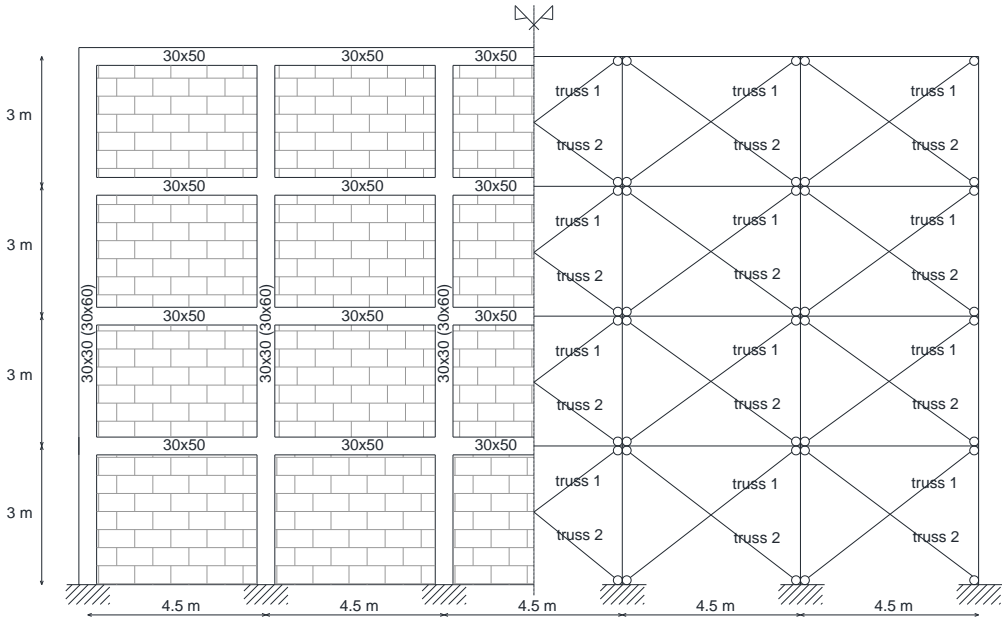


Figure 4.5. Four story case-study infilled RC GLD (SLD) frame

4.4.2. Modeling and analysis

Nonlinear response of RC elements is modeled by means of a lumped plasticity approach: beams and columns are represented by elastic elements with rotational hinges at the ends. A three-linear envelope is used, with cracking and yielding assumed as characteristic points. Section moment and curvature at cracking and yielding are calculated on a fiber section, for an axial load value corresponding to gravity loads. The behavior is assumed linear elastic up to cracking and perfectly-plastic after yielding. Rotation at yielding is evaluated through the formulations given in (Biskinis and Fardis, 2010). It is worth noting that displacement demand in RC members is typically low at the investigated LS, and in the analyses carried out in this paper no yielding of RC members was observed (for this reason the behavior after yielding is represented by a dashed line in Figure 4.6a). As far as the hysteretic behavior of RC members is concerned (see Figure 4.6a), no pinching of force and deformation is introduced, no damage due to ductility and energy, or degradation in unloading stiffness based on ductility are taken into account. Strength deterioration becomes an important factor when the structural

response approaches the collapse limit state; at earlier steps of inelastic behavior, both deteriorating and non-deteriorating systems exhibit similar responses (Ibarra et al. 2005). Since the inelastic demand in RC member is expected to be very low at the investigated LS, these hypotheses are not reasonably expected to introduce any significant lack of generality. Moreover, in new structures, with detailing of members for ductility, cyclic degradation of strength appears to be negligible (Fardis, 2009).

Infill panels are modeled by means of equivalent struts. Modeling infills through single compressed struts allows to investigate the effects of the panels on the global behavior of the analyzed structure, consistent with the purpose of this study.

The adopted model for the envelope curve of the force-displacement relationship is the model proposed by Panagiotakos and Fardis (1996). In literature, there are different models developed for infills in monotonic and cyclic conditions, based on the results of different experimental tests. If a single strut model is adopted, a simple way to model the behavior of such a compressive strut was proposed by Panagiotakos and Fardis (1996) based on experimental tests performed by Stylianidis (1985) and Pires (1990) and characterized by mechanical and geometrical properties representative of European built. It was observed that such a model appeared to be consistent also with other experimental results, described in Section 4.2.2, offering a quite good prediction of the deformability of the infill (Biondi et al. 2000).

The adopted force-displacement envelope is composed by four branches, as shown in Figure 4.6b and explained in details in Chapter 3. Due to the definition itself of DL LS (given in Section 4.2), the field of behavior after the peak is not investigated; thus the behavior after the peak is represented by a dashed line in Figure 4.6b.

As far as the response of the equivalent masonry strut due to cyclic loading is concerned, no strength and stiffness cyclic degradation is considered, as shown in Figure 4.6b, basically due to lack of data leading to high uncertainties and modeling difficulties (Fajfar et al. 2001, Zarnic and Gostic 1997, Sattar and Liel 2010). However, further studies should also consider this degradation investigating on the influence of hysteresis rules on the seismic behavior at the analyzed LS.

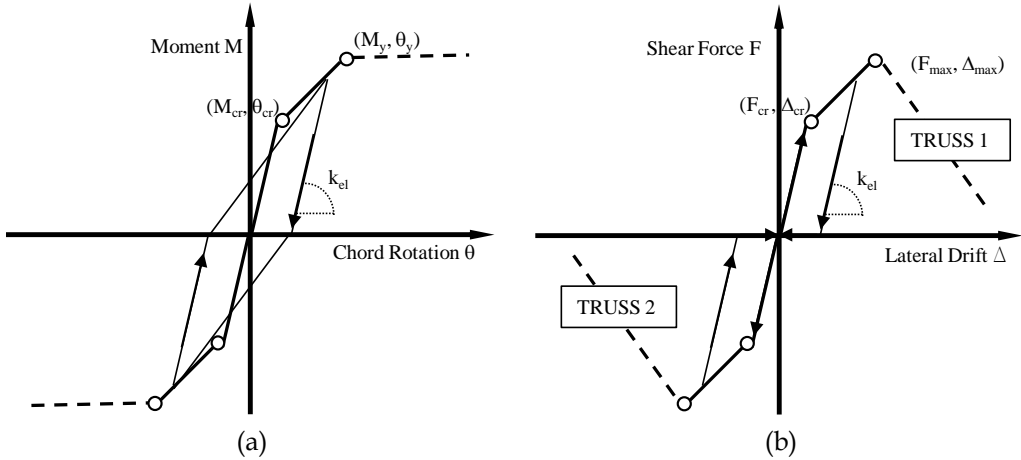


Figure 4.6. Hysteretic behavior of RC members (a) and “simple hysteresis rule” (Fajfar et al. 2001) of infill panels (b)

Through the adoption of this model for the case study structures, the IDR corresponding to the peak load of infills – which is the parameter of interest since the definition of DL LS adopted herein – is equal to 2.2‰, thus belonging to the typical drift range characterizing the extent of damage to infills associated with DL LS (see Figure 4.7). Moreover, infill panels have identical clear length and the same displacement capacity in the same story, thus reaching their peak load at same time.

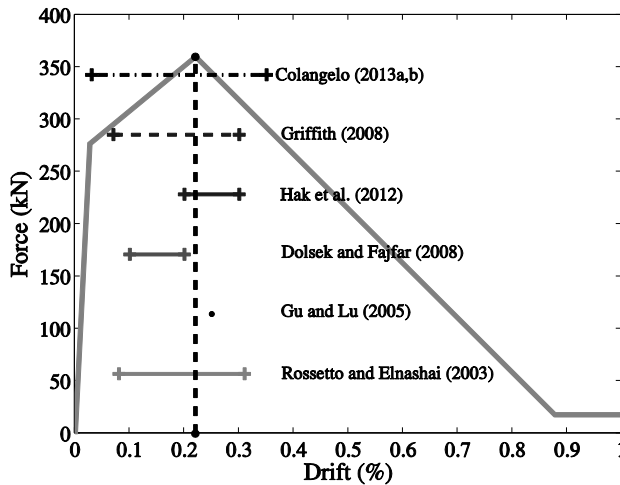


Figure 4.7. Force-drift envelope for infills in the case-study frames and drift ranges from literature (see Section 4.2)

The viscous damping is modeled with a mass- and tangent stiffness-proportional Rayleigh damping, assuming 2% damping for the first and the third modes.

A summary of the mechanical properties of both RC and infills is reported in Table 4.1.

		Mechanical property		References
RC	Concrete compressive strength, f_c	20.0 MPa	30.0 MPa	Based on Verderame et al. (2001) and Cosenza et al. (2009a)
	Steel yield strength, f_y	369.7 MPa	550.0 MPa	Verderame et al. (2012) and Cosenza et al. (2009a)
Infill	Shear elastic modulus, G_w	1240 MPa		Fardis (1997)
	Young elastic modulus, E_w	4133 MPa		Fardis (1997)
	Shear cracking stress, τ_{cr}	0.33 MPa		Fardis (1997)
	“Peak” IDR (IDR_{DL})	2.2‰		from model by Panagiotakos and Fardis (1996)

Table 4.1. Mechanical properties of RC and Infill

Structural modeling and numerical analyses are performed through the “PBEE toolbox” software (Dolsek, 2010), combining MATLAB® with OpenSees (McKenna et al. 2004), modified in order to include also infill elements (Ricci 2010, Celarec et al. 2012). A solution algorithm has been introduced in PBEE toolbox in order to solve non-converging problems, trying different possible solution algorithms, or reducing integration time step, or reducing tolerance as suggested in (Haselton et al. 2009). Moreover the “hunt and fill” procedure suggested in Vamvatsikos and Cornell (2002, 2004) is adopted to trace IDA curves.

4.4.3. Ground motion records selection

Natural records are selected and scaled to different level of seismicity in order to obtain IDA curves. The record selection has been performed by using REXEL software (Iervolino et al. 2010), from the European Strong-motion

Database, with earthquakes characterized by a magnitude which ranges between 6 and 7, with a source-to-site distance ranging between 0 and 30 km, and recorded on soil class A. A summary of the main properties of the two components of the seven selected records is reported in Table 4.2. On the whole, 14 records are used in the dynamic analyses.

Earthquake Name	M_w	Fault Mechanism	Epicentral Distance (km)	PGA_x (m/s ²)	PGA_y (m/s ²)	EC8 Site class
Campano Lucano	6.9	normal	25	0.588	0.588	
South Iceland	6.4	strike slip	22	0.513	0.386	
South Iceland	6.4	strike slip	28	0.199	0.274	
South Iceland	6.4	strike slip	15	1.248	1.132	A
Bingol	6.3	strike slip	14	5.051	2.918	
Montenegro	6.2	thrust	30	0.667	0.754	
Campano Lucano	6.9	normal	26	0.903	0.778	

Table 4.2. Selected ground motion records

4.4.4. Results

The results of the application of the procedures are presented and discussed herein in terms of equivalent IDR capacity related to bare structural models (in Section 4.4.4.1) and effective stiffness of infills for infilled numerical models (Section 4.4.4.2).

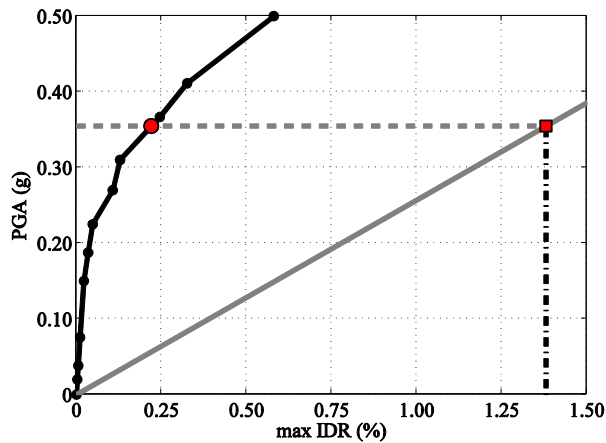
First of all, in Table 4.3, fundamental periods, PGA and $S_a(T_1, 5\%)$ capacity at DL LS are reported for each case study infilled model.

	T_1 (s)	PGA_{DL} (g)	$S_a(T_1)_{DL}$ (g)
SLD 4-story	0.114	0.44	0.43
SLD 8-story	0.241	0.28	0.40
GLD 4-story	0.122	0.35	0.36
GLD 8-story	0.271	0.26	0.38

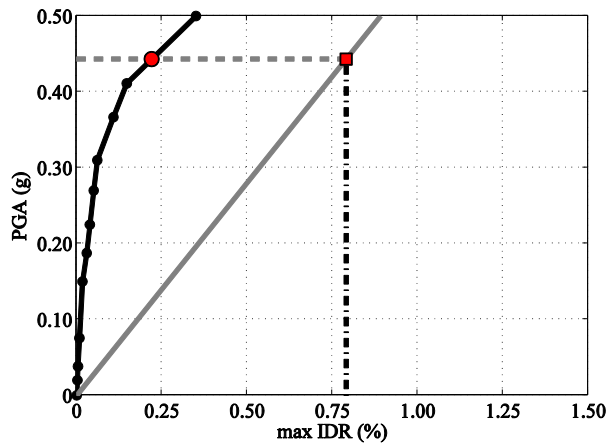
Table 4.3. Elastic periods of infilled frames; PGA and $S_a(T_1)$ capacity at DL LS

4.4.4.1 Analysis of results: equivalent IDR

The results of the procedure aiming at the research of the equivalent IDR capacity in terms of median nonlinear IDA curves and LTH results (in the case of $\alpha_{RC}=1$) are reported in Figure 4.8; IDR values corresponding to the achievement of DL LS (rep point), PGA capacity at DL LS, and equivalent IDR capacity on the bare models (red square) are also represented.



(a)



(b)

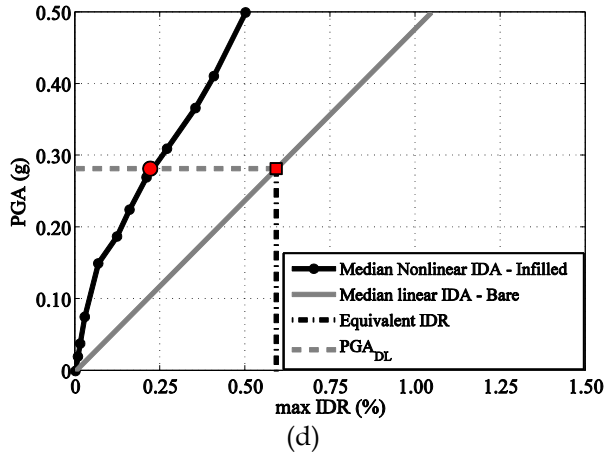
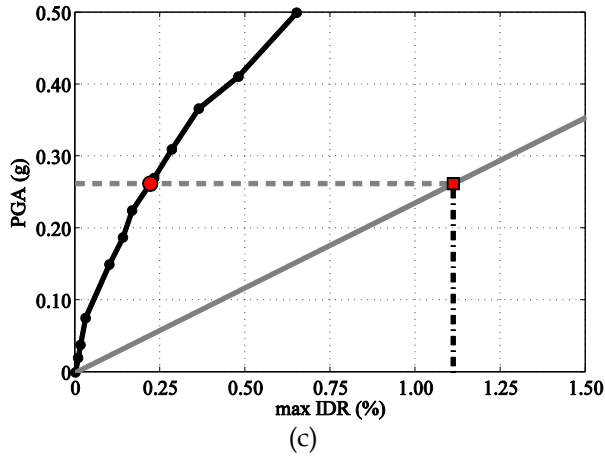
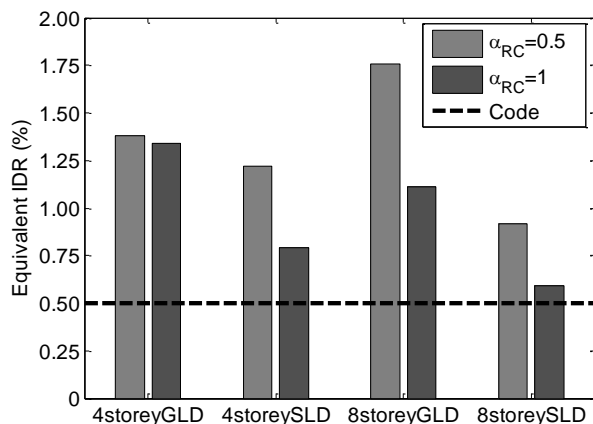


Figure 4.8. Equivalent IDR capacity (for $\alpha_{RC}=1$): 4-story GLD (a) and SLD (b) frames 8-story GLD (a) and SLD (b) frames

Moreover, Figure 4.9 and Table 4.4 show the trend of such equivalent IDR for the analyzed case study frames when an effective stiffness equal to one-half of the elastic stiffness ($\alpha_{RC}=0.5$) or equal to the elastic stiffness ($\alpha_{RC} = 1$) is assumed for RC members. It can be observed that the equivalent IDR is generally higher for GLD frames rather than for the corresponding SLD frames, for 4-story rather than for 8-story structures (except for one case).


 Figure 4.9. Equivalent IDR depending on the parameter α_{RC}

Equivalent IDR (%)			
N° story	α_{RC}	GLD	SLD
4	0.5	1.38	1.22
	1	1.34	0.79
8	0.5	1.76	0.92
	1	1.11	0.59

 Table 4.4. Equivalent IDR if $IDR_{DL}=2.2\%$

Generally speaking, equivalent IDR depends on (i) IDR capacity of infills at DL LS and on (ii) stiffness/strength contribution of these elements to the response of the RC frame up to this LS (that can be quantified by means of the comparison between infill lateral strength and plastic shear of RC columns at each story). Given equal the former, the higher the latter, the higher the equivalent IDR.

In particular, concerning SLD frames, RC members and infills have exactly the same geometrical and mechanical properties, and the absolute contribution of infills to the overall lateral strength of a story is identical in the two cases (four- and eight- story); nevertheless, in the 8-story frame axial load ratio and then plastic shear of RC columns (at the same story) are higher, resulting in a lower percentage contribution of infills to the overall lateral strength and to the post-RC cracking stiffness. Hence, the equivalent IDR for the 8-story frame is generally lower than the equivalent IDR for the 4-story frame.

In the same way, GLD frames are characterized by a higher percentage contribution of infills to the overall lateral strength and to the post-RC cracking

stiffness and, consequently, they presents higher equivalent IDRs rather than the corresponding SLD frames.

The same trends can be observed also from Figure 4.8: starting from non-linear IDA curves and corresponding capacity points at DL LS, the equivalent IDR increases with the IM (PGA) capacity and decreases with the slope of LTH IDA curves for the bare frame (i.e., the lower the stiffness of such numerical model). In SLD frames, the higher IM capacity of the 4-story frame is not counterbalanced by the lower stiffness of the 8-story bare numerical model, thus leading to a higher equivalent IDR for the former.

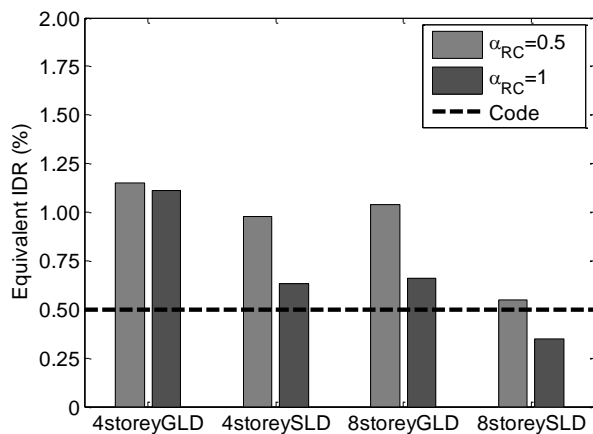
This trend is in agreement with a previous study (Ricci et al., 2012), in which it was tentatively expressed through the use of a parameter that takes into account both the strength and deformation capacity of infills, on a side, and lateral strength of RC members, on the other side.

Moreover, it could be expected that, the higher the IDR threshold (IDR_{DL}), the higher the PGA_{DL} , the higher the equivalent IDR for the bare frame. Such a concept is quantified in Table 4.5 and Figure 4.10, where equivalent IDR is calculated for a IDR_{DL} values equal to 1‰ (Figure 4.10a) or 3‰ (Figure 4.10b), close to the peak load of the panel.

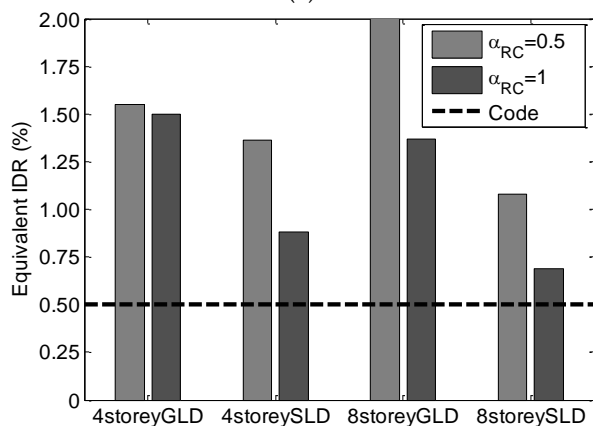
Equivalent IDR (%)					
		IDR _{DL} =1 ‰		IDR _{DL} =3 ‰	
N° story	α_{RC}	GLD	SLD	GLD	SLD
4	0.5	1.15	0.98	1.55	1.36
	1	1.11	0.63	1.5	0.88
8	0.5	1.04	0.55	2.16	1.08
	1	0.66	0.35	1.37	0.69

Table 4.5. Equivalent IDR if $IDR_{DL}=1$ ‰ or $IDR_{DL}=3$ ‰

Furthermore, in the hypothesis of identifying the achievement of DL LS with the achievement of the peak strength of infill panels, if infills are more “ductile”, the equivalent IDR should be higher; on the contrary, if infills are more “brittle”, such a IDR should be lower. Such a trend is also in agreement with Eurocode 8 prescription.



(a)



(b)

Figure 4.10. Equivalent IDR when IDR_{DL} is assumed equal to 1‰ (a) or 3‰ (b)

By observing Figure 4.9 and Figure 4.10, it should be noted that the IDR limit value proposed for bare models in most of the code prescriptions (e.g. Eurocode 8 and Italian D.M. 2008) – namely 5‰, in the hypothesis of buildings having non-structural elements of brittle materials attached to the structure – appears to be conservative in the case study frames analyzed herein.

From a qualitative standpoint, the higher the load and displacement capacity of infills with respect to RC members, the higher the equivalent IDR, the higher the conservatism of this code prescription. From a quantitative standpoint, a more comprehensive study – on the basis of the proposed procedures – should be carried out in order to attempt to provide a simple prediction formula for the equivalent IDR, depending on strength and

deformation capacity of infills and lateral strength of adjacent RC columns, to be used in DL LS check for models which do not take explicitly into account infill panels.

If the issue is regarded from the opposite standpoint, the IDR_{DL} value that should be assumed as a threshold at DLLS on the infilled model in order to obtain an equivalent IDR equal to 5‰ (proposed by many codes) on bare model can be calculated. Table 4.6 and Figure 4.11 shows the results of this calculation, proving that IDR_{DL} threshold should be generally lower than 1‰, namely infills should reach not even their peak strength point.

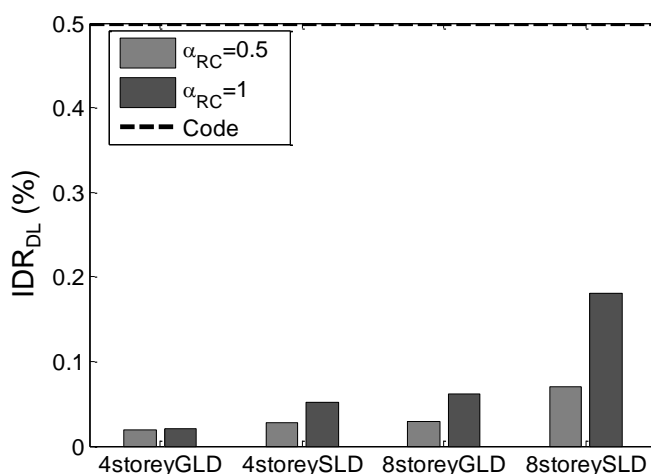


Figure 4.11 - IDR_{DL} to be assumed to obtain 5‰ equivalent IDR

N° story	IDR threshold (%)		
	α_{RC}	GLD	SLD
4	0.5	0.02	0.03
	1	0.02	0.05
8	0.5	0.03	0.07
	1	0.06	0.18

Table 4.6. IDR_{DL} to be assumed to obtain 5‰ equivalent IDR

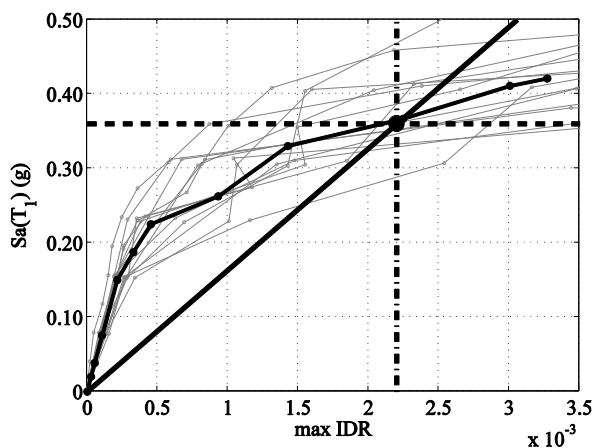
4.4.4.2 Analysis of results: effective stiffness for infill panels

The results of the procedure aiming at the estimation of effective stiffness of infills in terms of nonlinear IDA curves and LTH analyses are reported in Figure 4.12; $S_a(T_1, 5\%)$ capacity at DL LS and the IDR corresponding to the

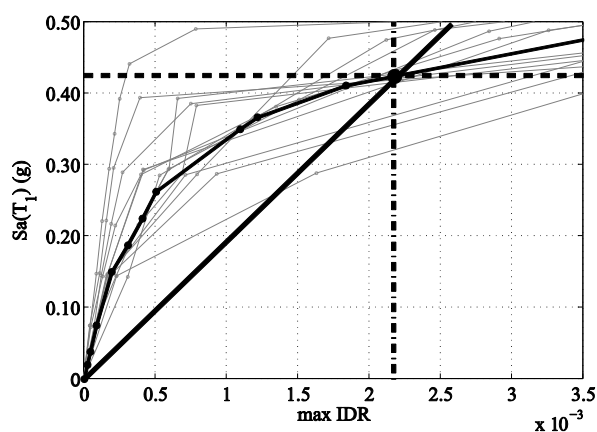
achievement of DL LS are also represented. The values obtained for α_w and the corresponding elastic periods of the case-study frames are reported in Table 4.7.

	α_w	$T(\alpha_w)$ (s)
SLD 4-story	0.21	0.25
SLD 8-story	0.28	0.42
GLD 4-story	0.23	0.24
GLD 8-story	0.32	0.41

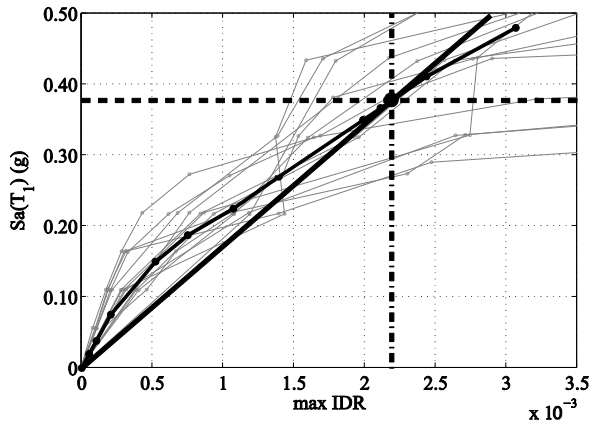
Table 4.7. Obtained values of α_w (with $\alpha_{RC}=1$) and corresponding elastic periods



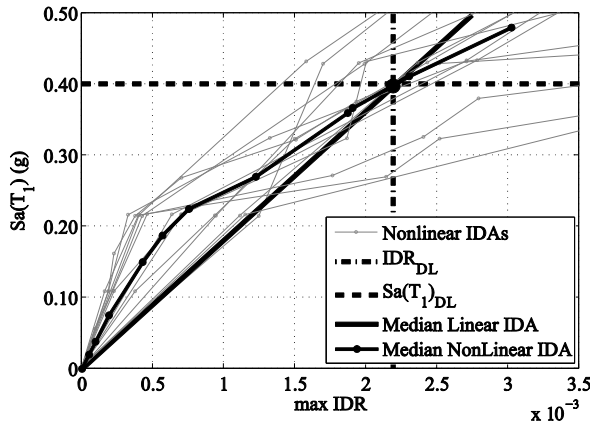
(a)



(b)



(c)



(d)

Figure 4.12. Nonlinear IDAs and Linear IDA for α_w : 4-story GLD (a) and SLD (b) frames; 8-story GLD (c) and SLD (d) frames

Moreover, the distribution of IDR demand corresponding to the achievement of DL LS can be evaluated through the nonlinear analyses as the median of the IDR demand at each story for all of the records when an IM value equal to the IM capacity at DL LS is considered. A concentration of IDR demand is shown at lower stories both for 4- and 8-storey frames, as shown in Figure 4.13. It is worth noting that the maximum IDR demand could also be a bit lower than the value of IDR_{DL} because of the procedure by which it is estimated: if the IDR_{DL} was achieved at different stories when different records are analyzed, the median value of the maximum IDR demand at each story for all of the records will result lower than IDR_{DL} .

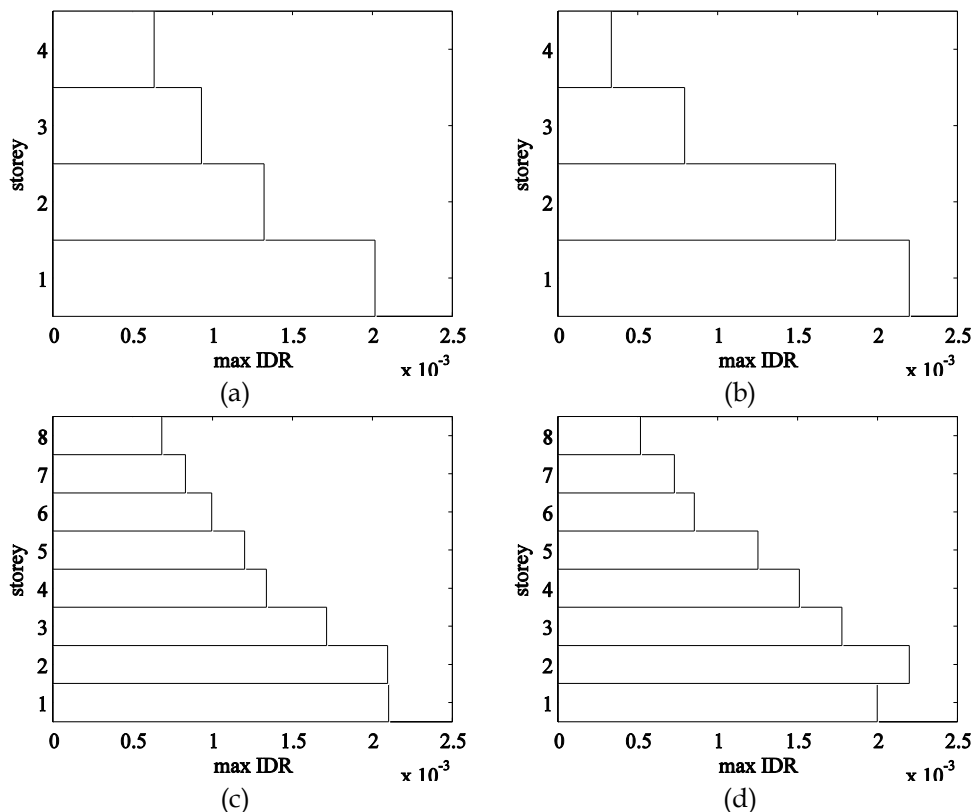
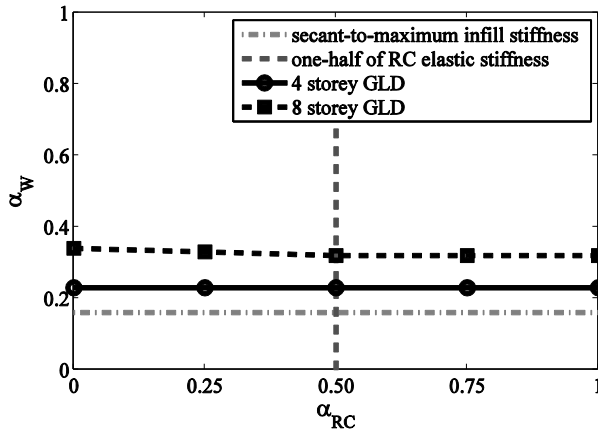


Figure 4.13. IDR demand at each story - 4-story GLD (a) and SLD (b) frames, 8-story GLD (c) and SLD (d) frames

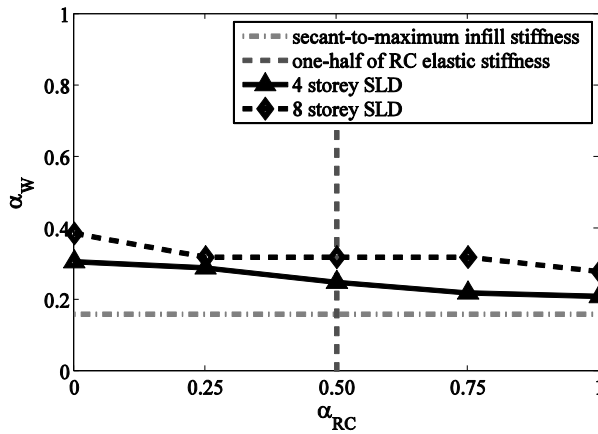
When the procedure is repeated for different value of effective stiffness that can be chosen to model RC members, i.e. for different values of α_{RC} , an array of α_w values can be estimated. In Table 4.8 and in Figure 4.14 the variation of α_w depending on the investigated values of α_{RC} is reported for each frame.

α_{RC}	α_w			
	4-story GLD	8-story GLD	4-story SLD	8-story SLD
0	0.23	0.34	0.31	0.39
0.25	0.23	0.33	0.29	0.32
0.50	0.23	0.32	0.25	0.32
0.75	0.23	0.32	0.22	0.32
1	0.23	0.32	0.21	0.28

Table 4.8. Variation of α_w depending on α_{RC}



(a)



(b)

Figure 4.14. Variation of α_w depending on α_{RC} for GLD (a) and SLD (b) frames

Obviously, a zero-stiffness for RC elements (namely $\alpha_{RC}=0$), makes no sense: it should be intended as representative of a frame in which RC members have free rotational hinges at their ends, that is not a realistic condition for a moment resisting RC frame. Herein, this case is just the extreme of a complete range of effective stiffness ratio, from 0 to 1.

Figure 4.14 clearly shows that if α_{RC} decreases, a higher effective stiffness has to be assumed for infill panels in order to obtain the same displacement demand, as expected. However, the curves representing the variability of α_w depending on α_{RC} have a very low slope. If frames with the same number of stories are considered, a stronger dependence of α_w on α_{RC} is observed for SLD

frames with respect to GLD frames. For example, comparing the 4-story SLD frame with the 4-story GLD frame, a higher contribution to lateral strength and stiffness of RC members is present in SLD case: the higher this contribution, the more sensitive the variation of the effective stiffness of infills with respect to the effective stiffness chosen to model RC members.

The value of α_w is higher in the case of the 8-story frames with respect to the 4-story frames, whichever α_{RC} value is considered. As a matter of fact, note that the reduction of stiffness corresponding to the use of α_w is assumed for all of the infill panels in the linear infilled model, whereas IDR demand up to DL LS is achieved only in one story, i.e. the one at which IDR_{DL} is attained first. Thus, the higher the number of stories, the lower should be such a uniform reduction adopted throughout all the stories (i.e., the higher should be α_w).

When a value of α_{RC} equal to 0.50 is adopted for RC members (as suggested in EC8), α_w changes from 0.25 to 0.32 for SLD frames and it ranges between 0.23 and 0.32 for GLD frames (see Table 4.8); since DL LS check is performed in terms of displacement, a conservative value of α_w to estimate the effective stiffness of infills for those specific case-study frames is the lower value of this range, i.e. 0.23. Moreover, Figure 4.14 shows that effective stiffness of infills estimated through α_w is always higher than the secant-to maximum stiffness (Mainstone's stiffness), i.e. α_w equal to 0.16 in the analyzed infilled frames. Hence, if an effective stiffness equal to the secant-to maximum stiffness is adopted for infills, DL LS check could be too conservative (being equal IDR capacity, namely IDR_{DL}). Note that Mainstone's stiffness is proposed by ASCE/SEI 41 provisions for modeling of infills. Details about the conservativeness of such a prescription will be provided in Section 4.4.4.3.

Furthermore, in the hypothesis of identifying the achievement of DL LS with the achievement of the peak strength of infill panels, it can be expected that, if infill panels are more "ductile", the effective stiffness should be lower, being equal elastic stiffness; vice-versa, when infills are more brittle, such an effective stiffness should be higher.

Considering geometrical and mechanical properties of the infill panels modeled in the case-study frames (Table 4.1), a α_w value equal to 0.23 implies a width-to-diagonal length ratio (b_w/d_w) equal to 0.16, a bit lower than the value proposed in Fardis (2009), where a width-to-diagonal length ratio equal to 0.20

is suggested at DL LS. The variation of that width-to-diagonal length ratio depending on α_{RC} is shown in Figure 4.15.

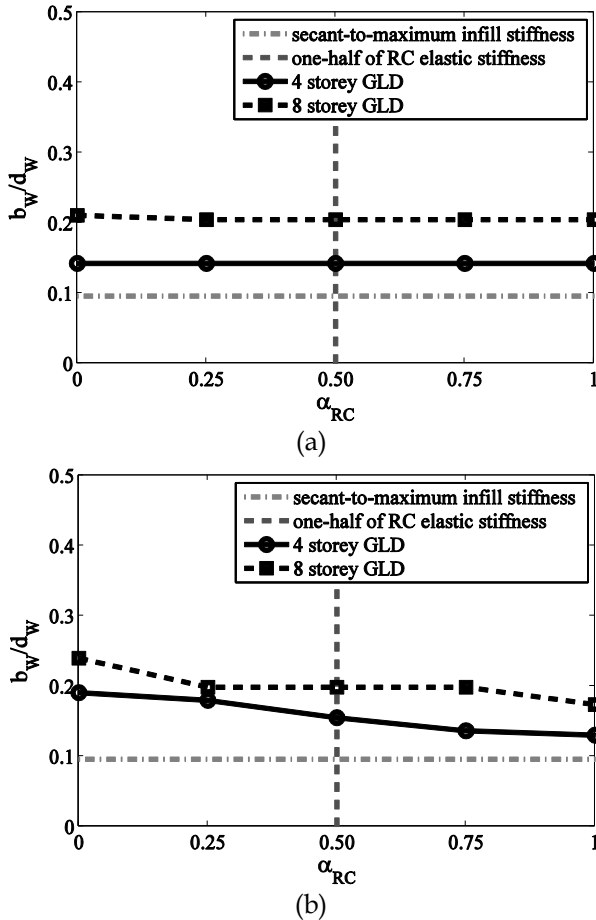


Figure 4.15. Variation of width-to-diagonal length ratio depending on α_{RC} for GLD (a) and SLD (b) frames

4.4.4.3 Analysis of ASCE/SEI 41 approach

ASCE/SEI 41 - American Code for Seismic Rehabilitation of Existing Buildings - suggests (§ C7.4.2.1) to assume that the width of the equivalent truss used to model infill panel (b_w) depends on the height and the diagonal length of the panel, h_w and d_w respectively, and on the parameter λ_h (Eq. 4.1); the latter parameter depends on the elastic Young modulus of the infill panel E_w and of the surrounding concrete E_c , the diagonal slope of the equivalent

truss to the horizontal θ , the infill thickness t_w , the moment of inertia of the adjacent columns I_c (see Eq. 4.2). Moreover, the equivalent strut shall have the same thickness and modulus of elasticity as the infill panel it represents. Hence, the equivalent strut will be characterized by an effective stiffness equal to the Mainstone's stiffness.

$$b_w = 0.175(\lambda_h h_w)^{-0.4} d_w \quad (4.1)$$

$$\lambda_h = \sqrt[4]{\frac{E_w t_w \sin(2\theta)}{4E_c I_c h_w}} \quad (4.2)$$

Since the definition itself of achievement of DL LS (given in Section 4.2), the "real" effective stiffness will be always lower than the elastic one and higher than the secant-to-maximum stiffness (Mainstone's stiffness) for each infill panel.

From a qualitative standpoint, if an effective stiffness equal to the secant-to maximum stiffness is adopted for infills in an infilled numerical model, DL LS check is too conservative. Hence it was necessary to calibrate a proper effective stiffness for infills to perform a more accurate analysis at DL LS, as shown in the previous Section.

From a quantitative standpoint, a simple procedure can be applied in order to evaluate the entity of such conservativeness in terms of PGA capacity.

First of all, the same median IDA curve obtained before for the infilled model is considered, in terms of maximum IDR versus PGA. The PGA value corresponding to IDR_{DL} on this IDA curve represents the "true" PGA capacity at DL LS, i.e. PGA_{DL} , related to the infilled frame. Then, LTH analyses are performed on the same infilled structural frame for all of the selected records assuming an effective stiffness equal to Mainstone's stiffness for all of the infill panels and the median value of PGA is estimated at a maximum IDR level equal to IDR_{DL} , namely adopting a displacement limit capacity directly correlated to the infill damage (i.e. IDR_{DL}). Such an IM level represents the PGA capacity at DL LS of the infilled numerical model in which Mainstone's stiffness is adopted as effective stiffness for infills, hereinafter referred to as $PGA_{DL,MS}$. The comparison between PGA_{DL} and $PGA_{DL,MS}$ provides the entity of the conservativeness of the ASCE code prescription. In Figure 4.16 a schematic example of the procedure explained herein is reported.

Nonlinear behavior of RC members can be considered, too, by repeating the described procedure for different values of effective stiffness of RC members, thus obtaining different values of $PGA_{DL,MS}$. The higher the effective stiffness adopted for RC members, the lower the conservativeness of such a prescription.

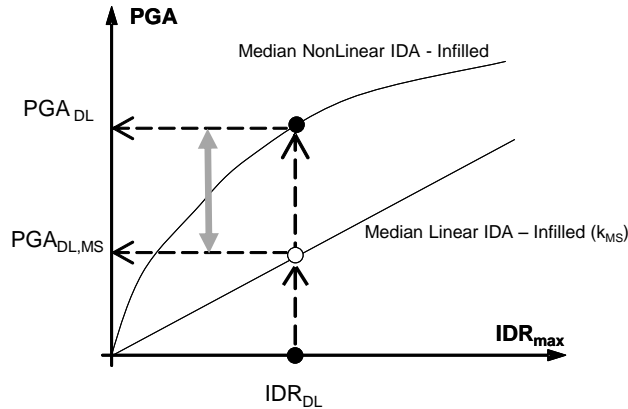
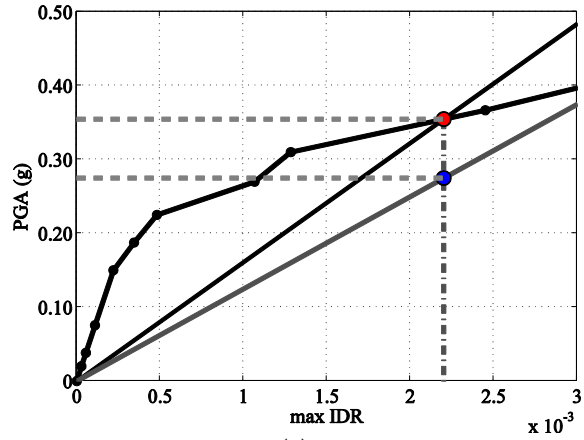
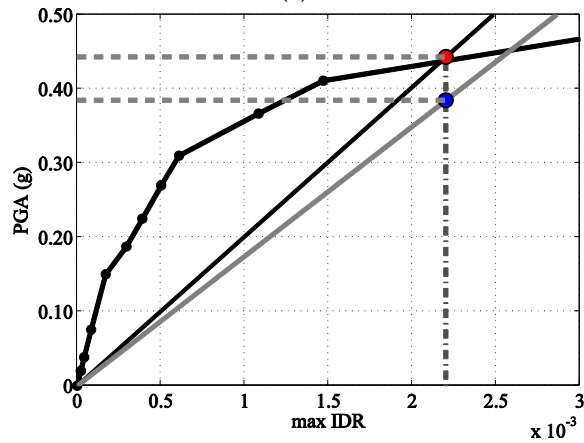


Figure 4.16. Schematic example of the analysis of conservativeness of ASCE/SEI 41 approach

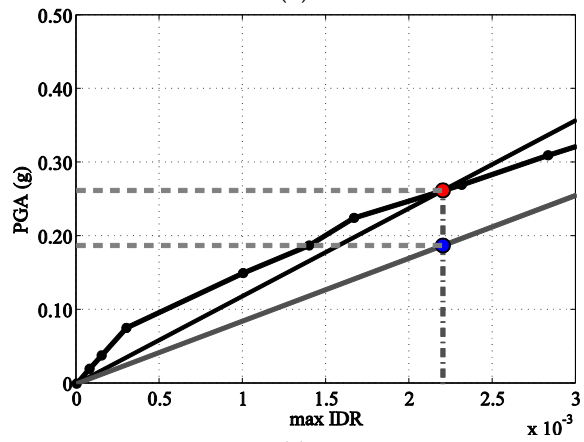
The results of the procedure aiming at the analysis of the conservativeness of the ASCE/SEI 41 approach are reported in Figure 4.17 for each case study frame, in terms of nonlinear IDA curves (used as a reference) and LTH analyses (in the case of $\alpha_{rc}=1$) when an effective stiffness equal to the secant-to-maximum stiffness is adopted (median linear IDA_{MS}). The IDR value corresponding to the achievement of DL LS (IDR_{DL}), PGA capacity at DL LS (PGA_{DL}), and PGA capacity corresponding to IDR_{DL} when Mainstone's stiffness is adopted for infills ($PGA_{DL,MS}$) are represented, too.



(a)



(b)



(c)

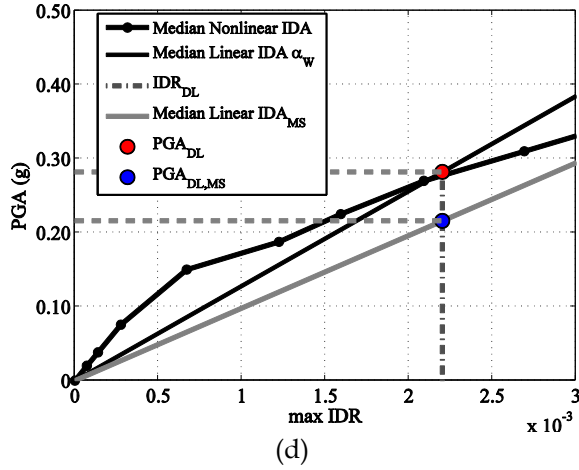


Figure 4.17. Analysis of the conservativeness of ASCE/SEI 41 approach (with $\alpha_{RC}=1$): 4-story GLD (a) and SLD (b) frames; 8-story GLD (a) and SLD (b) frames

The same results are reported in Table 4.9 in the cases of α_{RC} equal to 0.5 and 1 for each case study frame.

The ratio between $PGA_{DL,MS}$ and PGA_{DL} clearly shows that the adoption of an effective stiffness equal to the Mainstone's stiffness for infills leads to a very conservative estimate of the PGA capacity at DL LS when a displacement limit capacity directly correlated to the infill damage (i.e. IDR_{DL}) is adopted.

		GLD			SLD		
		PGA _{DL}	PGA _{DL,MS}	PGA _{DL,MS} / PGA _{DL}	PGA _{DL}	PGA _{DL,MS}	PGA _{DL,MS} / PGA _{DL}
α_{RC}		(g)	(g)	(%)	(g)	(g)	(%)
4	0.5	0.35	0.274	78.3	0.44	0.316	71.8
	1		0.275	78.6		0.385	87.5
8	0.5	0.26	0.171	65.8	0.28	0.198	70.7
	1		0.188	72.3		0.216	77.1

Table 4.9. Analysis of the conservativeness of ASCE/SEI 41 approach depending on the parameter α_{RC}

4.5 Summary

In this Chapter, modeling and analysis of infilled RC frames at DL LS was investigated. To this aim, starting from the analysis of performance criteria and associated drift capacity limits for infill panels, procedures were proposed and applied in order to provide modeling tools to be used in seismic assessment via linear analyses.

Nonlinear IDAs were carried out on structural models explicitly including infills in order to evaluate the IM level corresponding to the achievement of DL LS. Then, the results of such analyses were used as a reference.

First, the “equivalent” displacement limit capacity – in terms of IDR – to be used in “bare” numerical models (without infills) was obtained. Then, the effective stiffness of infill panels to be used in infilled models was evaluated, thus allowing explicitly including these elements also within this kind of analysis approach.

The methodologies aimed at the estimation of such parameters were proposed and applied to 4- and 8-story infilled frames, designed for seismic loads (according to the current Italian technical code) or for gravity loads only (according to an obsolete technical code). The results of this application were presented and discussed.

Equivalent IDR values highlight a general conservatism of code provisions, increasing with the contribution of infill panels to stiffness/strength of the RC frame.

Effective stiffness values, based on the adopted model for infill panels, highlight the need for a reduction of initial elastic stiffness of infills from 68% to 77% (when an effective stiffness equal to one-half of the elastic stiffness is assumed for RC elements, as suggested in EC8), in order to take into account first cracking prior to the attainment of DL limit, but also the conservatism of the widespread Mainstone’s model, which is also proposed by technical codes.

Foreseen developments include the analysis of the sensitivity of estimated parameters to further characteristics of the infilled RC frames and of their response under seismic action up to DL LS, namely displacement capacity and hysteresis rules for infills or post-cracking stiffness of RC members, infill-to-RC stiffness and strength ratio, and design criteria of RC elements. More generally, a comprehensive study could be carried out in order to attempt to provide predictive formulations both for equivalent IDR and effective stiffness,

depending on geometrical and mechanical characteristics of infill and RC elements. Finally, proposed approaches to linear modeling and analysis of infilled RC frames at DL LS could be evaluated within the Response Spectrum Analysis approach, since the latter is the most widespread method of analysis, especially for seismic design of new structures.

References

- ASCE/SEI 41 (2007). Seismic rehabilitation of existing buildings. American Society of Civil Engineers, Reston, VA, USA.
- Bal I.E., Crowley H., Pinho R., Gulay F.G. (2007). Structural characteristics of Turkish RC building stock in Northern Marmara region for loss assessment applications. ROSE Research Report No. 2007/03, IUSS Press, Pavia, Italy, 2007.
- Bal I.E., Crowley H., Pinho R., Gulay F.G. (2008). Detailed assessment of structural characteristics of Turkish RC building stock for loss assessment models. *Soil Dynamics and Earthquake Engineering* 28.10: 914-932, 2008.
- Biondi S., Colangelo F., and Nuti C. (2000). La risposta sismica dei telai con tamponature murarie. Gruppo Nazionale per la Difesa dai Terremoti, Rome. (in Italian)
- Biskinis D.E., Fardis M.N. (2010). Flexure-controlled ultimate deformations of members with continuous or lap-spliced bars. *Structural Concrete*, 11(2), 93-108, 2010.
- Calvi G.M., Bolognini D. (2001). Seismic response of reinforced concrete frames infilled with weakly reinforced masonry panels, *Journal of Earthquake Engineering* 5.02: 153-185, 2001.
- CEB, 2003. Seismic assessment and retrofit of reinforced concrete buildings. *Fib Bulletin* No. 24. International federation for structural concrete, task group 7.1. ISBN: 978-2-88394-064-2.
- Celarec D., Dolšek M. (2012). Practice-oriented probabilistic seismic performance assessment of infilled frames with consideration of shear failure of columns, *Earthquake Engineering and Structural Dynamics*, DOI: 10.1002/eqe.2275, 2012.
- Celarec D., Ricci P., Dolšek M. (2012). The sensitivity of seismic response parameters to the uncertain modelling variables of masonry-infilled reinforced concrete frames. *Engineering Structures*, 35, 165-177, 2012.
- CEN. European standard EN 1998-3. Eurocode 8: design provisions for earthquake resistance of structures – Part 3: assessment and retrofitting of buildings. European Committee for Standardization, Brussels, 2005.
- CEN. European Standard ENV 1998-1-1/2/3. Eurocode 8: Design provisions for earthquake resistance of structures – Part I: General rules. Technical Committee 250/SC8, Comité Européen de Normalisation, Brussels, 2004.
- Circolare del Ministero dei Lavori Pubblici n. 617 del 2/2/2009. Istruzioni per l'applicazione delle "Nuove norme tecniche per le costruzioni" di cui al D.M. 14 gennaio 2008. G.U. n. 47 del 26/2/2009, 2009. (in Italian)
- Colangelo F. (2001). Seismic-damage quantification for brick infills of RC frames, *Earthquake Resistant Engineering Structures III*, WITpress, DOI 10.2495/ERES010301, 2001.
- Colangelo F. (2003), Experimental evaluation of member-by-member models and damage indices for infilled frames. *Journal of earthquake engineering*, 7(1), 25-50, 2003.
- Colangelo F. (2005). Pseudo-dynamic seismic response of reinforced concrete frames infilled with non-structural brick masonry, *Earthquake Engineering and Structural Dynamics* 34(10), 1219-1241, 2005.
- Colangelo F. (2012). A simple model to include fuzziness in the seismic fragility curve and relevant effect compared with randomness. *Earthquake Engineering and Structural Dynamics*, 41(5), 969-986, 2012.

- Colangelo F. (2013), Quantificazione del danno delle tamponature di muratura non strutturale tramite lo spostamento relativo e la riduzione della rigidità, ANIDIS 2013, Padova, 30 giugno – 4 luglio 2013. (in Italian)
- Colangelo F. (2013a), Probabilistic characterisation of an analytical fuzzy-random model for seismic fragility computation. *Structural Safety*, 40, 68-77, 2013.
- Colangelo F. (2013b), Drift-sensitive non-structural damage to masonry-infilled reinforced concrete frames designed to Euro-code 8. *Bulletin of Earthquake Engineering*, 11(6), 2151-2176, 2013.
- Cosenza E., Galasso C., Maddaloni G. (2009a), Resistenza del calcestruzzo: modellazione probabilistica e risultati sperimentali, Atti del XXV Convegno Nazionale AICAP “La progettazione e l’esecuzione delle opere strutturali nell’ottica della sostenibilità”, Pisa, Italy, May 14-16. Paper No. 59, 2009. (in Italian)
- Cosenza E., Galasso C., Maddaloni G. (2009b), Analisi statistica delle caratteristiche sismiche degli acciai da cemento armato, Atti del XXV Convegno Nazionale AICAP “La progettazione e l’esecuzione delle opere strutturali nell’ottica della sostenibilità”, Pisa, Italy, May 14-16. Paper No. 57, 2009b. (in Italian)
- Crisafulli F.J. (1997), Seismic behaviour of reinforced concrete structures with masonry infills. Ph.D. Thesis, University of Canterbury, Christchurch, New Zealand.
- D.M. 2008, Decreto Ministeriale del 14/1/2008. Approvazione delle nuove norme tecniche per le costruzioni. G.U. n. 29 del 4/2/2008, 2008. (in Italian)
- Dolšek M. (2010), Development of computing environment for the seismic performance assessment of reinforced concrete frames by using simplified nonlinear models. *Bulletin of Earthquake Engineering*, 8(6), 1309-1329, 2010.
- Dolšek M., Fajfar P. (2001), Soft story effects in uniformly infilled reinforced concrete frames. *Earthquake Engineering*, 5(1), 1-12, 2001.
- Dolšek M., Fajfar P. (2002), Mathematical modelling of an infilled RC frame structure based on the results of pseudo-dynamic tests. *Earthquake Engineering and Structural Dynamics*, 31(6), 1215-1230, 2002.
- Dolšek M., Fajfar P. (2004), Inelastic spectra for infilled reinforced concrete frames. *Earthquake Engineering and Structural Dynamics*, 33(15), 1395-1416, 2004.
- Dolšek M., Fajfar P. (2006), Simplified seismic assessment of infilled reinforced concrete frames, Proceedings of the First European Conference on Earthquake Engineering and Seismology, Geneva, Switzerland, 3-8 September 2006. Paper Number 888, 2006.
- Dolšek M., Fajfar P. (2008a), The effect of masonry infills on the seismic response of a four-story reinforced concrete frame – a deterministic assessment. *Engineering Structures*, 30(7), 1991-2001, 2008.
- Dolšek M., Fajfar P. (2008b), The effect of masonry infills on the seismic response of a four-story reinforced concrete frame – a probabilistic assessment. *Engineering Structures*, 30(11), 3186-3192, 2008.
- Dymiotis C., Kappos A.J., Chryssanthopoulos M.K. (2001), Seismic reliability of masonry-infilled RC frames. *ASCE Journal of Structural Engineering*, 127(3), 296-305, 2001.
- Fajfar P., Dolšek M., Žarnić R., Gostič S. (2001), Development of numerical methodologies for infilled frames. Towards European integration in seismic design and upgrading of building structures, Euroquake-project, Final report.
- Fajfar P., Drobnič D. (1998), Nonlinear seismic analyses of the ELSA buildings. Proceedings of the 11th European Conference on Earthquake Engineering, Paris, France, September 6-11, 1998.

- Fardis M.N. (1997), Experimental and numerical investigations on the seismic response of RC infilled frames and recommendations for code provisions. Report ECOEST-PREC8 No. 6. Prenormative research in support of Eurocode 8.
- Fardis M.N. (2009), Seismic design, assessment and retrofitting of concrete buildings based on EN-Eurocode 8, Springer, 2009.
- Federal Emergency Management Agency–ASCE. FEMA 274—NEHRP commentary on the NEHRP guidelines for the seismic rehabilitation of buildings. Washington, DC: Federal Emergency Management Agency–ASCE, 1997.
- Gu X., and Lu Y. (2005), A fuzzy–random analysis model for seismic performance of framed structures incorporating structural and non-structural damage. *Earthquake engineering & structural dynamics* 34.10: 1305-1321, 2005.
- Hak S., Morandi P., Magenes G., Sullivan T. J. (2012), Damage Control for Clay Masonry Infills in the Design of RC Frame Structures, *Journal of Earthquake Engineering*, 16:sup1, 1-35, 2012.
- Haselton C.B., Liel A.B., Deierlein G.G. (2009), Simulating structural collapse due to earthquakes: model idealization, model calibration, and numerical solution algorithms. ECCOMAS Thematic Conference on Computational Methods in Structural Dynamics and Earthquake Engineering (COMPdyn 2009), Rhodes, Greece, June 22–24, 2009.
- Ibarra L.F., Medina R.A., Krawinkler H. (2005), Hysteretic models that incorporate strength and stiffness deterioration. *Earthquake Engineering and Structural Dynamics*, 34(12), 1489-1511, 2005.
- Iervolino I., Galasso C., Cosenza E. (2010), REXEL: computer aided record selection for code-based seismic structural analysis, *Bulletin of Earthquake Engineering*, 8(2), 339-362, 2010.
- Mainstone R.J. (1971), On the stiffnesses and strengths of infilled frames. *Proceedings of the Institution of Civil Engineering*, Supplement IV, 57-90.
- McKenna F., Fenves G.L., Scott M.H. (2004), OpenSees: Open System for Earthquake Engineering Simulation. Pacific Earthquake Engineering Research Center. University of California, Berkeley, CA, USA. <http://opensees.berkeley.edu>.
- Mehrabi A.B., Shing P.B., Schuller M.P., Noland J.L. (1994), Performance of masonry infilled R/C frames under in-plane lateral loads, Report No. CU/SR-94/6. Department of Civil, Environmental, and Architectural Engineering, University of Colorado at Boulder, Boulder, CO, USA.
- Negro P., Colombo A. (1997), Irregularities induced by nonstructural masonry panels in framed buildings. *Engineering Structures*, 19(7), 576-85, 1997.
- Negro P., Verzeletti G. (1997), Effect of infills on the global behaviour of R/C frames: energy considerations from pseudo-dynamic tests. *Earthquake Engineering and Structural Dynamics*, 25(8), 753-773, 1997.
- NZS 3101:2006, Commentary on the Concrete Design Standard, Part 2. Standards Association of New Zealand, Wellington, New Zealand, 2006.
- Özcebe S., Crowley H., Bal I. E. (2012), Distinction Between No and Slight Damage States for RC in Existing RC Buildings using a Displacement-Based Approach, *Proceedings of the 15th World Conference on Earthquake Engineering*, Lisbon, Portugal, September 24-28, 2012.
- Panagiotakos T.B., Fardis M.N. (1996), Seismic response of infilled RC frames structures. 11th World Conference on Earthquake Engineering, Acapulco, México, June 23-28. Paper No. 225, 1996.

- Panagiotakos T.B., Fardis M.N. (1999), Estimation of inelastic deformation demands in multistory RC frame buildings. *Earthquake Engineering and Structural Dynamics*, 28(5):501-528, 1999.
- Paulay T., Priestley M.J.N, Seismic design of reinforced concrete and masonry buildings. John Wiley & Sons, New York, USA, 1992.
- Pinto A.V., Verzeletti G., Molina J., Varum H., Coelho E. (2002), Pseudodynamic tests on non-seismic resisting RC frames (infilled frame and infill strengthened frame tests). Report EUR, EC, Joint Research Centre, Ispra, Italy.
- Pires F., Carvalho E. C. (1992). The behaviour of infilled reinforced concrete frames under horizontal cyclic loading, Proceedings of the Tenth World Conference on Earthquake Engineering, AA Balkema, Rotterdam, The Netherlands.
- Regio Decreto Legge n. 2229 del 16/11/1939. Norme per la esecuzione delle opere in conglomerate cementizio semplice od armato. G.U. n. 92 del 18/04/1940. (in Italian)
- Ricci P., (2010) Seismic vulnerability of existing RC buildings. Ph.D. Thesis, University of Naples Federico II, Naples, Italy.
- Ricci P., De Risi M.T., Verderame G.M., Manfredi G (2012a)., Influence of infill presence and design typology on seismic performance of RC buildings. Part I: sensitivity analysis. Proceedings of the 15th World Conference on Earthquake Engineering, Lisbon, Portugal, September 24-28, 2012.
- Ricci P., De Risi M.T., Verderame G.M., Manfredi G. (2012b), Influence of infill presence and design typology on seismic performance of RC buildings. Part II: fragility analysis and evaluation of code provisions at Damage Limitation Limit State. Proceedings of the 15th World Conference on Earthquake Engineering, Lisbon, Portugal, September 24-28, 2012.
- Ricci P., De Risi M.T., Verderame G.M., Manfredi G. (2013), Influence of infill distribution and design typology on seismic performance of low- and mid-rise RC buildings. *Bulletin of Earthquake Engineering*, Volume 11, Issue 5, Page 1585-1616, 2013.
- Ricci P., Verderame G.M., Manfredi G. (2011), Analytical investigation of elastic period of infilled RC MRF buildings. *Engineering Structures*, 33(2), 308-319, 2011.
- Rossetto T., and Elnashai A. (2003), Derivation of vulnerability functions for European-type RC structures based on observational data. *Engineering structures* 25.10: 1241-1263, 2003.
- Sattar S., Liel A.B. (2010), Seismic Performance of Reinforced Concrete Frame Structures With and Without Masonry Infill Walls. 9th US National and 10th Canadian Conference on Earthquake Engineering, Toronto, Canada.
- Stylianidis KC (1985), Experimental investigation of the behaviour of the single-story infilled R.C. frames under cyclic quasi-static horizontal loading (parametric analysis). Ph.D. Thesis, University of Thessaloniki, Thessaloniki, Greece.
- Vamvatsikos D., Cornell C.A. (2002), Incremental dynamic analysis. *Earthquake Engineering and Structural Dynamics*, 31(3), 491-514, 2002.
- Vamvatsikos D., Cornell C.A. (2004), Applied incremental dynamic analysis. *Earthquake Spectra*, 20(2), 523-553, 2004.
- Verderame G.M., Manfredi G., Frunzio G. (2001), Le proprietà meccaniche dei calcestruzzi impiegati nelle strutture in cemento armato realizzate negli anni '60. Atti del X congresso nazionale ANIDIS "L'ingegneria Sismica in Italia", Potenza-Matera, Italy, September 9-13, 2001. (in Italian)

- Verderame G.M., Ricci P., Esposito M., Manfredi G. (2012), STIL v1.0 – Software per la caratterizzazione delle proprietà meccaniche degli acciai da c.a. tra il 1950 e il 2000, available at <http://www.reluis.it>.
- Verderame, G.M., Polese, M., Mariniello, C., Manfredi, G. (2010b). A simulated design procedure for the assessment of seismic capacity of existing reinforced concrete buildings. *Advances in Engineering Software*, 41(2), 323-335.
- Žarnić R., Gostič S. (1997), Masonry infilled frames as an effective structural sub-assembly. In: Fajfar, Krawinkler, Ed. *Seismic design methodologies for the next generation of codes*. Rotterdam: Balkema, 335-46, 1997.

Chapter 5

A NONLINEAR MACRO MODEL OF EXTERIOR RC JOINTS WITHOUT TRANSVERSE REINFORCEMENT UNDER SEISMIC LOAD

In the assessment of the performance of typical non-conforming buildings, seismic collapse safety might be significantly affected by non-linear behavior of joints that are involved in the failure mechanisms. In fact, in typical non-conforming buildings, joints are characterized by poor structural detailing, as the lack of an adequate transverse reinforcement in the joint panel or deficiencies in the anchorage of beam reinforcement due to the absence of any capacity design principle.

Few reliable approaches for modeling all sources of nonlinearity are available for poorly designed beam-column joints because of relatively poor information from experimental tests.

Many nonlinear joint models are available, but most of them may be unsuitable for the assessment of older concrete buildings, either because they were developed and calibrated for confined joints or because they are complicated to use.

In this Chapter, the attention is focused on exterior joints with no transverse reinforcement and a possible approach to model them in RC frames is proposed.

First, an experimental database of cyclic tests available in literature on joints without transverse reinforcement that exhibited different modes of failure (shear joint failure and anchorage failure) is collected and analyzed.

Second, the joint panel constitutive parameters are defined to reproduce the experimental joint shear stress-strain relationships, when they were available.

Then, bond-slip is taken into account by introducing a slip spring whose properties are calculated using a bond-slip model and which explicitly

introduces a limitation of joint shear strength in the case of anchorage failure.

Finally, the proposed modeling approach is validated using the experimental tests included in the database.

5.1 Introduction

Damage observed after the most recent earthquakes and experimental investigations on the seismic performance of non-conforming RC buildings highlighted the vulnerability of the beam-column joint region (Ricci et al, 2010). The behavior of beam-column joints is a critical issue in the assessment of seismic performance of RC moment resisting frames; therefore, within the context of Performance-Based Earthquake Engineering, a growing attention should be addressed to the modeling of RC beam-column connections and the influence of failure of joints on the seismic performance of RC buildings.

In particular, in the assessment of the performance of typical non-conforming buildings, seismic collapse safety might be significantly affected by the non-linear behavior of the joints that are involved in the failure mechanisms because of poor structural detailing, as the lack of an adequate transverse reinforcement in the joint panel or deficiencies in the anchorage of beam reinforcement due to the absence of any capacity design principle or seismic design. Joint flexibility contributes significantly to overall story drift, especially in the nonlinear range. Basically, two contributions to overall deformability due to beam-column joints cannot be neglected: (i) the shear strain of the joint panel and (ii) the contribution of the fixed-end-rotation due to the slip of the longitudinal bars anchored into the joint (e.g., Cosenza et al. 2006).

Furthermore, under lateral seismic loading, high shear forces are generated in the joint core. Beam-column joints bear horizontal and vertical shear forces that are usually much larger than those acting within the adjacent beams and columns. Thus, joints can experience shear failures which should be avoided by an appropriate design to ensure a ductile response of the whole frame. However, such a design does not regard typical non-conforming structures designed for gravity loads only. In particular, exterior unreinforced RC joints often experience brittle failure under horizontal actions.

Basically, two main different modes of failure can be identified (Figure 5.1): (i) joint shear failure prior to (J-failure) or after than (BJ-failure) yielding of beam longitudinal reinforcement (in hypothesis of strong column-weak beam); (ii) anchorage failure of longitudinal reinforcement anchored into the joint panel (A-failure) in the case of insufficient bars anchorage length.

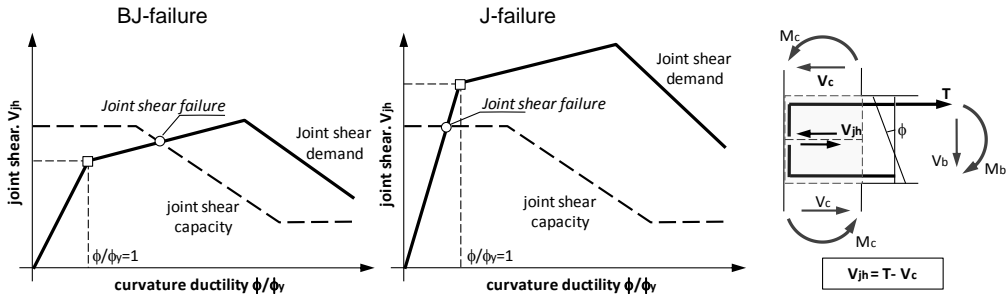


Figure 5.1. Schematic representation of joint shear failure typologies prior to (J) or after than (BJ) beam yielding

In literature there is not yet a commonly accepted approach for the determination of the shear strength and for nonlinear modeling of RC beam-column joints in moment resisting RC frames. Many nonlinear joint models are available, but most of them may be unsuitable for modeling all sources of nonlinearity for the assessment of older concrete buildings. Some of them were developed and calibrated for confined beam-column joints or they are too complicated to implement.

Shear stress-strain relationship proposed in models from literature was often calibrated independently on the failure typology, even if experimental tests can exhibit a joint stress-strain behavior which can be very different depending on the failure typology (pure shear failure of the joint panel or joint failure after beam yielding), especially as far as peak strength and post-peak behavior (softening slope and residual strength) are concerned. Therefore, the joint stress-strain envelopes for numerical modeling of RC joints should be calibrated depending on the failure typology. It is worth highlighting that a pre-classification of failure typology, and consequently of the stress-strain envelope, is always possible by knowing only material properties and geometry.

Moreover, especially in the context of displacement-based approaches for seismic assessment, another key point is the correct modeling of all the sources of deformability of the joint sub-assembly, and therefore the modeling of the slip contribution of longitudinal bars in addition to joint panel shear strain.

It can be very useful to calibrate only the joint panel deformability contribution on the basis of experimental tests and to calculate analytically the slip contribution. According to this approach one of the joint deformability

contributions (slip) can be easily generalized, even with a great accuracy (on the basis of consolidated models from literature), for different anchorage conditions of longitudinal bars, type of rebar (deformed or plain) and quality of bond between concrete and steel. The other contribution (joint panel shear strain) should be calibrated with a number of tests as greater as possible (tests in which the local stress-strain response has been explicitly measured and provided) and as homogeneous as possible for anchorage type.

A strong effort, especially towards a better calibration of the panel zone deformability, and, thus, a deeper analysis of experimental tests on unconfined joints on the basis of experimental tests, are still necessary.

The number of experimental tests performed in last years on unreinforced joints is increasing. Experimental databases were collected by some authors, e.g. Genesio (2012) or Celik and Ellingwood (2008), generally including tests not-homogeneous for anchorage type (effective/ineffective), reinforcement typology (deformed/plain), presence of transverse beams or concrete slab. Generally, only global force-displacement response was provided by Authors of tests; only in a few cases joint shear stress-strain response are available (e.g. Clyde et al 2000 and Pantelides et al. 2002 for planar exterior joints).

In Chapter 2, a deep overview on beam-column joint shear strength models and joint nonlinear modeling was carried out, with a particular attention to exterior unreinforced beam-column joints, that are the core of this Chapter. The attention is focused on exterior joints containing no transverse reinforcement and a possible approach to model beam-column joints in RC frames is proposed.

First, an experimental database of cyclic tests available in literature on joints without transverse reinforcement that exhibited different modes of failure (shear joint failure and anchorage failure, respectively) is collected and analyzed.

Second, the joint panel constitutive parameters are defined to reproduce the experimental joint shear stress-strain relationships, when they were available, depending on the failure typology. Then, bond-slip is taken into account by introducing a slip spring whose properties are analytically calculated using a bond-slip model and which explicitly introduces a limitation of joint shear strength in the case of anchorage failure of beam bars anchored into the joint panel.

Thus, the proposed model allows the mechanical definition of the bar slip contribution for each level of displacement demand (also covering joints in which the embedment length is not sufficient) and the adoption of a stress-strain relationship for the joint panel that is diversified for failure mode and calibrated on eight 2D experimental tests, homogeneous for anchorage type.

Finally, the proposed joint model is validated using other experimental tests included in the database.

5.2 Experimental database

In the past decades many researchers carried out experimental investigations in order to understand the nonlinear behavior of RC beam-column joints. In this Section, first a review of experimental investigations on monotonic and cyclic loading of beam-column joints is presented, in particular referring to those tests which are closely related to this work, i.e., 2D under-designed exterior joints; then a database is collected and analyzed, as shown in next Sections.

5.2.1. *Experimental investigations from literature*

The main aim of experimental tests is the evaluation of the joint shear strength of subassemblies built according to different code provisions and with different reinforcement detailing. Nevertheless, these tests usually do not provide sufficient information to completely evaluate seismic behavior, including joint shear deformability, ductility, energy dissipation and post peak behavior. Generally, only in a few cases joint shear stress-strain response are provided by the Authors of the tests (e.g. Clyde et al 2000 and Pantelides et al. 2002 for planar exterior joints).

Jirsa and Marques (1972) tested exterior beam-column connections with standard 90° and 180° hooks conforming to ACI 318-71 specifications under monotonic loading. Particular focus was given to different types of confinement of the core, axial load, hoops in the joint core, longitudinal column bars and concrete cover. The analysis of these tests pointed out that (i) the level of axial load does not significantly influence the behavior of the hooked anchorages, (ii) the hoops in the core have to be closely spaced

relatively to the anchorage's hooks in order to be effective, (iii) the thickness of the concrete cover does not influence the capacity of the anchorage.

Nilsson (1973) observed the effects of the difference in the detailing between exterior and interior joints by means of seven 2/3 scaled tests, with different anchorage configurations of beam bars in the joint panel and different joint aspect ratios. No hoops in the joints panel were provided. All the specimens failed due to diagonal tension cracking. It was highlighted that bar anchorage strictly influences joint shear capacity and that shear capacity increases with decreasing joint aspect ratio.

Taylor (1974) and Taylor and Clarke (1976) tested twenty-six 3/4 scaled exterior joints under monotonic loading, investigating the influence of the beam reinforcement ratio and different beam reinforcement anchorage. One or three few hoops were provided in the joint core. It was observed that for high beam flexural capacity the joint was not able to transfer shear forces. It was also observed that the configurations with 90°-hooks bent into and away from the joint, are preferable than U-bars under seismic loads.

Of the eight specimens tested in the investigation by Uzumeri (1977), three exterior RC beam-column joints not reinforced in the joint area were tested under constant axial compressive load. The presence of axial load was found to be beneficial at the early stages of loading; however, at the latter stages, it was pointed out that large axial load might be detrimental rather than helpful. In all cases, the beam remained not-damaged while the joint rapidly deteriorated with increasing displacements. The joints without transverse reinforcement were able to provide anchorage for the beam bars allowing the achievement of 98% of the theoretical ultimate moment capacity of the beams. The joint was unable, however, to sustain the anchorage of the beam bars in cycles subsequent to this load level.

The experimental study of three exterior beam-column joints by Paulay and Scarpas (1981) indicates that horizontal joint shear reinforcement may be reduced considerably. The amount of shear reinforcement varied between specimens; however, the vertical shear reinforcement (i.e., intermediate column bars) was the same in all specimens. The effect of the axial load was studied: a reduction in column axial load resulted in a dramatic reduction of the stiffness, strength, and energy dissipation of the specimen in the subsequent loading cycle.

Ehsani and Wight presented the results of six exterior RC beam-column

sub-assemblages that were tested in cyclic loading (1985). It was stated that the maximum joint shear stress in exterior connections should be limited to $1\sqrt{f_c}$ (MPa) to reduce excessive joint damage, column bar slippage, and beam bar pullout.

Limited experimental evidence suggests that increasing the column axial load tends to reduce the total lateral drift at yield (Kurose 1987). Although some researchers report that increased column axial load results in increased shear strength of joints without reinforcement, the data do not show a significant trend (Beres et al. 1992).

Bond and anchorage of bars in RC beam-column joints were studied by Kaku and Asakusa (1991). It was shown that the consequences of bond deterioration included pinching of the force story-drift hysteresis curves, increasing the slip deformation at the beam-column interface, changing the shear transfer mechanism in the joint core, and decreasing the flexural strength of the adjoining members.

Scott (1992), Scott et al. (1994) also evaluated the effect of different joint detailing on the shear capacity under monotonic loading through fifteen exterior joints, with a particular focus on strain distribution in bar anchorages. They concluded that the column axial load increases the joint shear capacity and confirmed that the configurations with 90°-hooks bent into and away from the joint, are preferable than U-bars.

Clyde et al. (2000) tested four half-scale RC exterior joints to investigate their behavior in a shear-critical failure mode. The joints were typical of building frames with non-ductile details in the beam-column joints. The joints were subjected to quasi-static cyclic loading, under two levels of axial load ratio. Specific performance levels for this type of RC joint were established and a comparison was made to current design and rehabilitation standards.

Hakuto et al. (2000) performed simulated seismic load tests on RC one way interior and exterior beam-column joints with substandard reinforcing details typical of buildings constructed before the 1970s. The exterior beam-column joints contained very little transverse reinforcement in the members and in the joint core. In one beam-column joint unit, the hooks at the end of the beam top bars were bent up and the hooks at the ends of the bottom bars were bent down. In the other beam-column joint unit the hooks at the ends of the bars were bent into the joint as in current practice. The improvement in performance of the joint with beam bars anchored according to current

practice, namely into the joint core, was demonstrated.

Pantelides et al. (2002) evaluated the seismic performance of exterior joints in existing non-ductile one-way RC building frames with three different details of beam and beam-column joint reinforcement. These reinforcement details were selected to satisfy the 1963 ACI Code (ACI 1963), but do not satisfy more recent provisions such as the ACI 352 Committee Report (ACI 1991). A total of six test units were tested. All of the test units had top bars bent into the joints with a 180° hook; two of the test units had bottom bars extending only 152 mm into the joint, two test units had the bottom bars extending all the way into the joint, and the remaining two test units had bottom bars bent up into the joint with a 180° hook. Two levels of axial compression load were investigated for each of the three details: 10% and 25% of the axial column capacity in compression.

Pampanin et al. (2002) carried out two tests and observed that joints with plain round bars and 180° hooks as anchorage of the beam bars in the joint panel usually exhibit a very poor joint shear capacity and ductility, exhibiting the so-called “concrete wedge” damage mechanism.

Wong (2005) and Wong and Kuang (2008) performed two different experimental test series on beam-column joints designed without transverse reinforcement in the joint core. The influence of the beam bar anchorage (Kuang and Wong, 2006) and the beam-column depth ratio on the joint shear behavior were evaluated (Wong and Kuang, 2008). It was shown that the form of beam anchorage significantly influenced the joint shear capacity. The need to include the effect of beam-column depth ratio in the design of the joint was also stated.

Further studies were performed on as-built beam-column joints in order to have a term of comparison with retrofitted joints, generally retrofitted by means of FRP material (Tsonos and Papanikolaou 2003, Antonopoulos and Triantafillou 2003, Di Ludovico 2012), RC jackets (Karayannis 2008), or post-installed anchors (Genesio 2012).

Anyway, in most of the tests the focus was generally given only to the ultimate shear strength of the joint. Only few authors have measured the joint shear deformation, e.g., Clyde, 2000; Pantelides, 2002, that are the main references in this study.

5.2.2. Analysis of the collected database

In the previous Section various experimental tests performed on unreinforced exterior RC beam-column joints and presented in literature by researchers in the past have been presented.

Thus, in this Section the collection and the analysis of an experimental database are carried out based on tests available in literature on joints without transverse reinforcement that were subjected to a range of displacement histories and joint shear stress demands, and which does not exhibited anchorage failure (see Table 5.1). This experimental database includes only planar unreinforced joints substantially homogeneous for beam bars anchorage type (with bar bent into the joint core), namely no loss of bond can be imputed to an anchorage failure.

Geometrical and mechanical properties are reported for all tests, together with axial load ratio (v), maximum experimental joint shear ($V_{j,max}$), and maximum non-dimensional joint shear stress ($\gamma_{n,max}$). All tests were performed through the application of a constant or variable axial load on column and a cyclic displacement history at the end of beam. No tests on 3D-corner joints specimens which include slab influence on joint behavior were considered.

In the collected database:

- axial load ratio ranges (v) between 0 and 0.31,
- concrete compressive strength (f_c) ranges between 16.4 and 67.3 MPa,
- steel yielding strength (f_y) belongs to the range 332÷585 MPa,
- and the joint aspect ratio (h_b/h_c) varies from 0.89 to 2.00.

Since the proposed model is an empirical model for joint shear stress-strain behavior, its applicability is intended to be limited in such ranges of mechanical and geometric parameters.

A separate database was collected for experimental tests characterized by anchorage failure. It can be noted that the number of such tests presented in literature is more limited, but expanding. In addition to geometrical and mechanical properties, fundamental data about beam bars anchorage length (l_b), experimental joint shear ($V_{j,Aexp}$) and non-dimensional joint shear stress ($\gamma_{j,Aexp}$) corresponding to anchorage failure are reported for such tests in Table 5.2.

5.2.3. Experimental versus predicted joint shear strength

First, joint shear strength related to experimental tests without anchorage failure is investigated.

In Table 5.1 maximum experimental joint shear ($V_{j,max}$) obtained from such tests is reported for each specimen, and a comparison between models by Park and Mosalam (2012b), referred to as P&M, Priestley (1997), Celik and Ellingwood (2008), referred to as C&E, and ASCE SEI-41/06, referred to as ASCE, versus experimental results is carried out.

In particular, as far as the model by Celik and Ellingwood (2008) is concerned, the mean value ($0.915 \text{ MPa}^{0.5}$) of the proposed range of shear strength coefficient γ_n is adopted (see Chapter 2).

Since the maximum experimental joint shear cannot be higher than joint shear corresponding to beam flexural capacity, the predicted joint shear strength was limited to the joint shear corresponding to the achievement of beam capacity (flexural capacity is evaluated in a fiber-approach as later explained in Section 5.4). This limitation is already implicit for models by Park and Mosalam (2012b), since their definition of joint shear strength (as explained in Chapter 2).

From Table 5.1 it can be observed that the code-based approach (ASCE SEI-41/06) in a seismic assessment is very conservative (31% on average) and characterized by the highest CoV (25%).

The model by Celik and Ellingwood (2008) appears to overestimate joint shear strength (the error is about +15% with a CoV of model-to-experimental strength ratio equal to 19%).

As far as model by Priestley (1997) is concerned, since joint capacity is expressed in terms of principal tensile stress, a simple equation was adopted to calculate the corresponding shear stress, taking into account the effective column axial load. This model provides a mean value of model-to-experimental strength ratio quite lower than unity (0.92 on average), and it also shows a quite high CoV of such a ratio (25%).

It can be observed that the mean of the model-to-experimental strength ratio is the closest to unity (1.02) and the CoV is the lowest (11%) when model by Park and Mosalam (2012b) is adopted to predict shear strength with respect to the adoption of code provisions or other models from literature.

The strength model proposed by Park and Mosalam (2012b) is adopted in

the model proposed in this study to define the ordinate of the peak point, as reported in Eq. (5.1) (in MPa):

$$V_n = k \left[\sqrt{f_c} b_j h_c \frac{\cos \theta}{\cos(\pi/4)} \right] \quad (5.1)$$

where θ is a function of the joint aspect ratio (beam height/column depth), b_j and h_c are the effective joint width and the column cross-sectional depth, respectively, f_c is the concrete compressive strength and “ k ” is a strength factor accounting for the effect of the beam longitudinal reinforcement ratio.

In addition, such a model directly provides the expected joint failure typology. When “ k ” is equal or higher than the unity, a J-failure occurs; the value of “ k ” is limited to 1.0 corresponding to which V_n in Eq. (5.1) assumes its maximum value. The minimum value of V_n is reached when “ k ” is equal to 0.4. When the parameter “ k ” ranges between 0.4 and 1.0 a BJ-failure occurs.

It can be argued that model by Park and Mosalam (2012b) takes into account the effect of the joint aspect ratio on joint shear strength, but it neglects the effect of column axial load, unlike models that provide critical principal stresses (e.g. Priestley, 1997). Starting from the comparison between model-to-experimental strength ratio results related to models by Park and Mosalam (2012b) and Priestley (1997), it seems that joint aspect ratio has a higher influence on joint shear strength with respect to column axial load.

On the other hand, it seems that any possible beneficial (or detrimental) effect of column axial compression on joint shear strength is not clearly highlighted from the analysis of literature studies or from the collected database. In particular, in the case of weak column - strong beam, an increase of the column axial load (up to the column cross-section balanced point) improves the column moment capacity and, in turn, joint shear strength (Park and Mosalam, 2009, 2012a). Vice-versa, in the case of strong column -weak beam, that is the case of most tests in the collected database, high column axial load might give both beneficial and detrimental effects to the joint shear strength (Park and Mosalam, 2009, 2012a). Column compression block depth obviously increases with the increase of the column axial load; thus the compressive diagonal strut width increases too, improving joint strength. Furthermore, high column axial load improves bond strength between the beam reinforcing bars and the surrounding concrete leading to increasing joint

shear strength. Meanwhile, the crack propagation is accelerated when the column axial load increases and consequently the joint has a lower shear strength. Moreover, P-Delta effects and buckling of the column bars – which are enhanced by high values of axial load ratio – lead to further negative effects on the joint shear strength (Park and Mosalam, 2009, 2012a).

Bonnaci and Pantazopoulou (1993) and Moiser (2000) concluded that column axial load has no important effect on joint strength by the analysis of a collected experimental database. Also Hassan (2011) highlighted that joints with higher axial load failed at lower principal tension stress, while joints at lower axial load failed at higher principal tension stress, suggesting that the principal tension stress model can overestimate the effect of axial load on joint shear strength. In particular, Hassan (2011) suggested that the beneficial effect of axial load is more pronounced if axial load ratio is higher than 0.2, while for lower axial load ratio, the joint shear strength enhancement due to increasing axial load is not so much significant. Similar conclusions were drawn by Kim and LaFave (2009, 2012), finding that all correlation coefficients between joint shear strength and column axial stress ratio were more closer to zero than unity.

In Figure 5.2 a comparison between experimental and predicted joint shear strength by ASCE SEI-41 (2006), Priestley (1997), Celik and Ellingwood (2008), Park and Mosalam (2012b) is carried out regarding tests collected in the experimental database. Black lines in Figure 5.2 represent regression lines passing from the origin of the axes. The comparison carried out in Figure 5.2 allows highlighting that, when model by Park and Mosalam is adopted, the regression line is closer to the bisector in this graph (with respect to the other models) and dispersion of points is quite restrained.

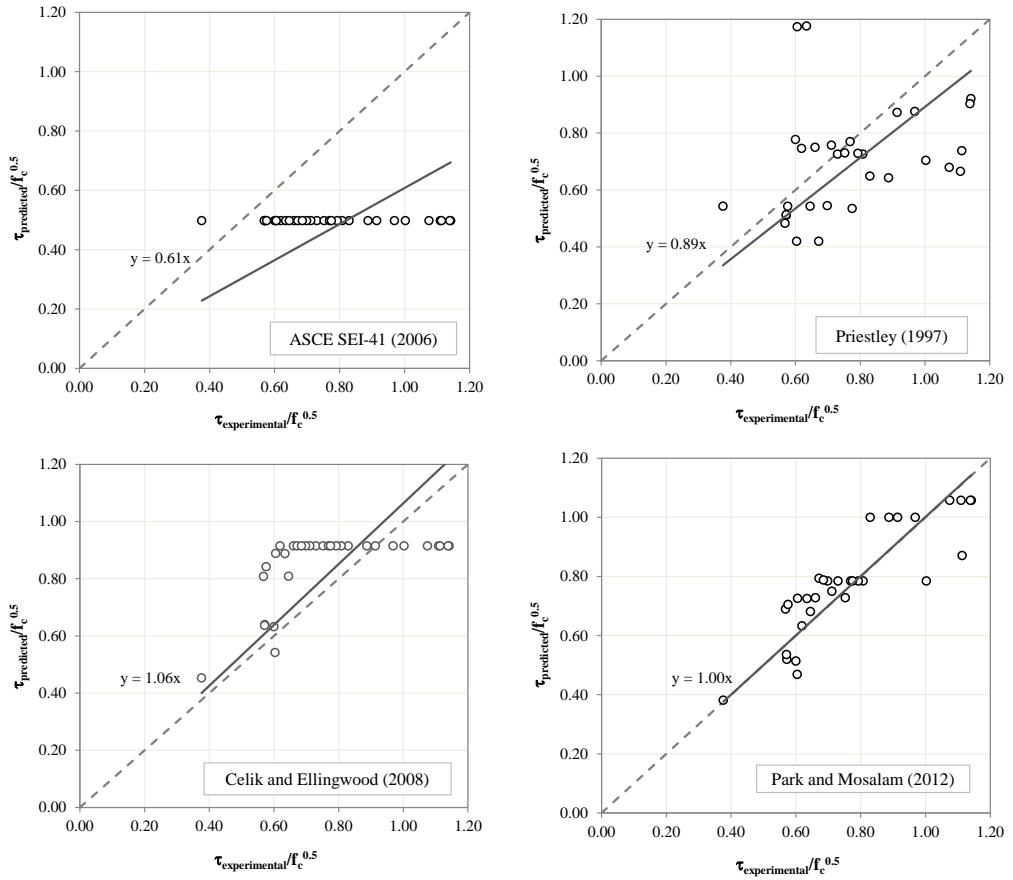


Figure 5.2. Comparison between experimental and predicted joint shear strength for tests from database

Reference	ID specimen	ν	$\gamma_{i,Ascp}$ (MPa) ^{0.5}	$V_{j,Ascp}$ (kN)	l_b (mm)	b_c (mm)	h_c (mm)	b_b (mm)	h_b (mm)	f_c	$f_{y,b}$	$f_{y,c}$	$A_{s,bif}$ (mm ²)	L_b (_{clear}) mm	L_c (_{clear}) mm	$V_{j,CSE}/$ $V_{j,Ascp}$	$V_{j,sham}/$ $V_{j,Ascp}$	$V_{j,propos}/$ $V_{j,Ascp}$
El-Amoury- Chobarah (2002)	T0	0.20	0.52	285.1	150	250	400	250	400	30.6	425	425	12566.6	1750	1300	1.01	0.95	1.12
Beres et al. (1992)	E-07	0.10	0.10	85.3	152	406.4	406.4	355.6	609.6	29.1	413.7	413.7	570.0	1549	1353	0.57	3.89	1.46
Genesio (2012)	J13-1	0.12	0.49	269.8	150	300	350	300	400	27.5	552	552	829.4	2350	1300	0.88	0.81	0.74
Shafaiei et al. (2014)	C3	0.15	0.37	112.0	75	250	250	220	250	23	460	460	461.8	1250	750	0.96	1.12	0.61
Pantelides et al. (2002)	1	0.10	0.44	416.3	152	406.4	406.4	406.4	406.4	33.1	458.5	469.5	2565.2	1676.4	1295.4	1.19	0.87	1.01
	2	0.27	0.63	569.0	152	406.4	406.4	406.4	406.4	30.2	458.5	469.5	2565.2	1676.4	1295.4	0.83	0.91	0.88
Murty et al. (2011)	S1	0	0.39	116.6	200	200	250	200	400	27.8	-	-	628.3	1150	550	1.18	0.43	1.11
															Mean	0.94	1.28	0.99
															CoV	0.23	0.91	0.28

Table 5.2. Experimental database of planar unreinforced RC beam-column joints - anchorage failure

5.2.4. Anchorage failure

In Table 5.2 maximum experimental joint shear ($V_{j,\Delta\text{exp}}$) obtained from experimental tests with anchorage failure is reported for each specimen. A comparison between experimental results and three models, (Celik and Ellingwood, 2008, Sharma et al., 2011 and the proposed one) is carried out; first two models are empiric models, while the proposed model is based on analytical formulations.

According to the model by Celik and Ellingwood (2008), the yield moment capacities of the beams related to ineffective anchorage length of bars are scaled by a factor α , which is reported to vary between 0.40 and 0.70, to account for anchorage failure. This moment can be converted in shear stress (see Eq. 5.5 presented below) so that a comparison with the joint shear strength ($\tau_{jh,\text{max}}$) can be carried out; shear stress corresponding to anchorage failure is the minimum shear stress obtained through such a comparison. In particular, for the exterior beam-column joints, the joint shear strength ($\tau_{jh,\text{max}}$) falls within the range $(0.42-0.62)\sqrt{f_c}$ (MPa). Mean values of the proposed ranges of values for factor α (=0.55) and joint shear strength $\tau_{jh,\text{max}}$ (=0.52 $\sqrt{f_c}$) are assuming in Table 5.2 for experimental versus numerical comparison. By observing mean value of numerical-to-experimental shear strength, it can be concluded that this model is a good proposal in terms of strength (mean=0.94, CoV=0.23).

Sharma et al. (2011) proposed a limitation of the principal tensile stress to the value of $0.19\sqrt{f_c}$ (MPa) in the cases of anchorage failure. Therefore, this limit is converted in shear stress for each test and compared with the corresponding experimental value. Mean value of numerical-to-experimental shear strength is quite higher than unity (1.28), and variability is also significant (CoV=0.98).

The mechanical approach adopted herein (referred to as “proposed” in Table 5.2) to account for deformability contribution due to slip and possible strength limitation due to anchorage failure is based on the local bond stress-slip relationship (τ_b -s) proposed by Model Code 2010. The local bond stress initially increases with slip until a plateau is reached; then, after a softening branch for increasing slip values, bond stress reaches a constant residual value. In Figure 5.3a the bond stress-slip relationship adopted herein is reported; it is related to the case of “other bond conditions” and pull-out failure (that is the failure typology exhibited in the analyzed experimental tests).

Such model is very similar to local bond stress-slip models previously

proposed in literature (e.g. Eligehausen et al., 1983) and it also allows to consider the effect of steel strains (when yielding strain is overcome) and transverse pressure on local bond stress-slip relationship, as shown in Figure 5.3b and c. In the analyzed experimental tests, yielding of bottom bars (with ineffective anchorage length) does not occur before anchorage failure; thus no degradation of bond stress due to steel strain is considered until the maximum strength is reached. The effect of transverse pressure is assumed to be due to column axial load; thus the higher axial load ratio, the higher local bond stress.

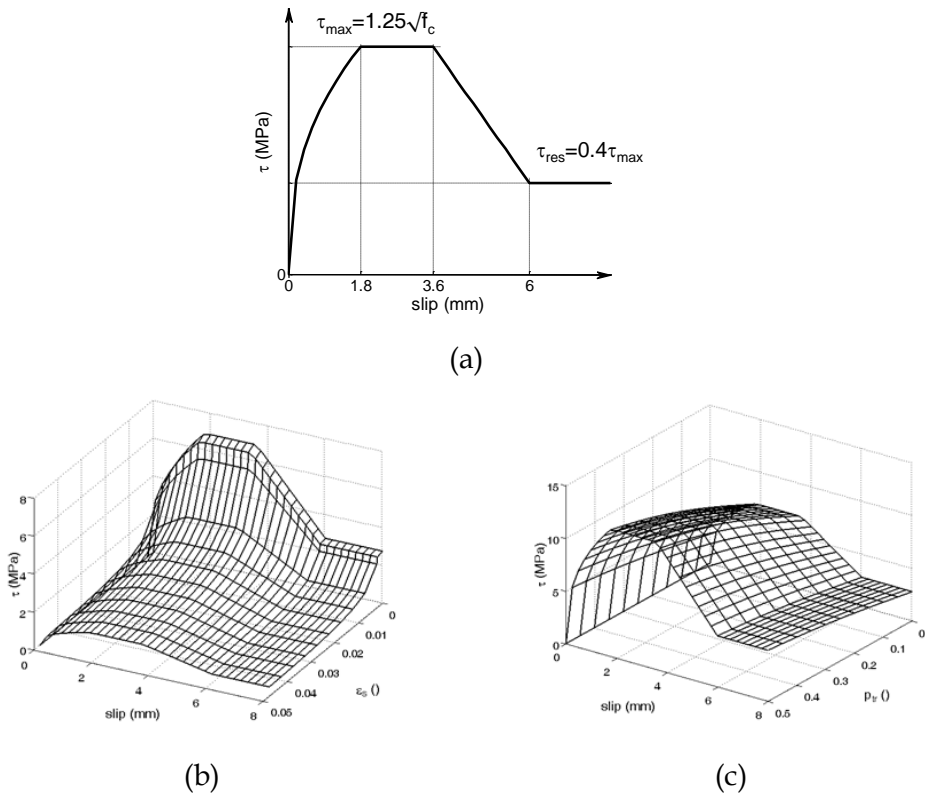


Figure 5.3. Bond stress-slip model by Model Code 2010: local bond stress-slip relationship in case of pull-out failure (“other bond conditions”) (a); influence of steel strains (b) and transverse pressure (expressed as axial load ratio) (c)

The anchorage failure condition is evaluated through the steel stress (σ_s) – slip (s) response of a straight bar (with abscissa x) with length l_b and diameter ϕ_b embedded in concrete (as in Figure 5.4). It is well known that the response of

the embedded bar is ruled by the equation of translational equilibrium of the bar in conjunction with the compatibility equation between steel bar and surrounding concrete, namely:

$$\frac{d\sigma_s}{dx} = \frac{4}{\phi_b} \tau_b(x) \quad (5.2a)$$

$$\frac{ds}{dx} = \varepsilon_s(x) \quad (5.2b)$$

where σ_s and ε_s are steel stress and strain, respectively. Eq. 5.2b is presented in the hypothesis of negligible tensile concrete strain.

Starting from the knowledge of steel stress-strain and bond stress-slip relationships, $\varepsilon_s(x)$ and $s(x)$ have to be obtained from the equations above, by defining two boundary conditions. The first boundary condition is defined in correspondence to the free end of the steel bar ($x=0$), for which $\varepsilon_s=0$. The second condition can be defined in terms of slip once again at section with abscissa equal to zero ($x=0$). The solution can be obtained through a numerical integration procedure (e.g. Cosenza et al, 2006).

Therefore, starting from the generic condition $s(x=0)=s^*$, the corresponding steel strain, $\varepsilon_s(x=l_b)$, and steel stress, $\sigma_s(x=l_b)$, can be calculated. When s^* increases, in turn $\sigma_s(x=l_b)$ increases, until the achievement of a peak value $\sigma_{s,max}$, beyond which bond slip increases while $\sigma_s(x=l_b)$ decreases, according to equilibrium equation and bond stress-slip relationship. On the basis of equilibrium and compatibility equations at beam-joint interface, the value of beam moment corresponding to $\sigma_{s,max}$, namely $M_b(\sigma_{s,max})$, can be univocally obtained.

The corresponding joint shear strength ($V_{j,A}$) is calculated as the difference between the tensile force in beam longitudinal bars (T) and column shear (V_c), both evaluated in correspondence to anchorage failure, namely when $\sigma_s=\sigma_{s,max}$:

$$V_{j,A} = T(\sigma_{s,max}) - V_c(\sigma_{s,max}) = \sigma_{s,max} \cdot A_{s,b} - \frac{M_b(\sigma_{s,max})}{2L_c} \quad (5.3)$$

where L_c is the column shear span and $A_{s,b}$ is the area of the beam bottom reinforcement layer. Such strength is compared with the experimental

maximum joint shear $V_{j, \text{Aexp}}$. The mean value of numerical-to-experimental shear strength related to the proposed model is very close to unity (0.99), even if CoV is quite high (0.28).

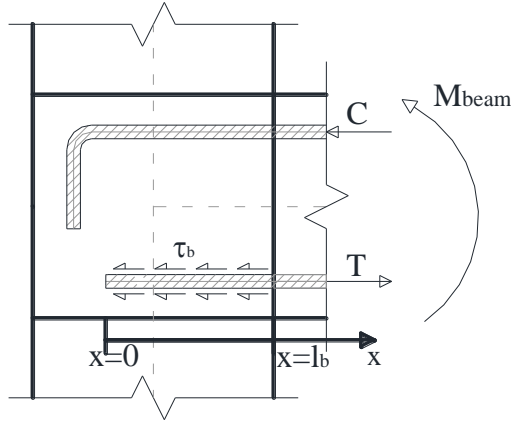


Figure 5.4. Longitudinal beam bar anchored into the joint core

5.3 Proposed joint modeling

The proposed model is based on the introduction of rigid links spreading through the panel zone dimensions and the adoption of two rotational springs in series: the first one is located in the centerline of the joint panel and it represents the shear behavior of the joint panel; the other one is located at the interface between the joint panel and the adjacent beam and it represents the bond-slip contribution (Figure 5.5).

The joint panel constitutive parameters are defined to reproduce the experimental joint shear stress-strain relationships on the basis of experimental tests for which they were available. Bond-slip rotational spring properties are calculated using an analytical bond-slip model.

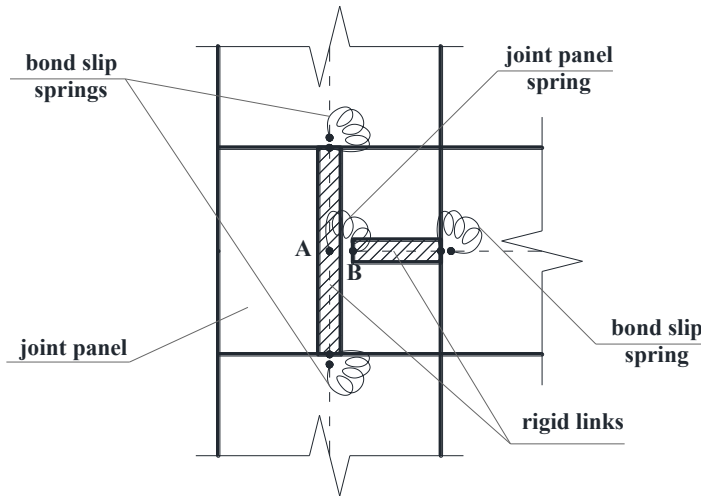


Figure 5.5. Proposed joint modeling

When a RC frame has to be modeled for nonlinear analyses including joint behavior, beams and columns will be modeled according to a distributed plasticity approach or a lumped plasticity approach, without the deformability contribution of fixed-end-rotation; in addition, rigid links spreading into the joint panel should be introduced (as in Figure 5.5) together with two rotational springs (joint panel spring and bond slip spring) defined as explained in Section 5.3.1 and 5.3.2.

5.3.1. Calibration of shear stress-strain relationship of the joint panel

The joint panel zone model was calibrated through tests well documented in the literature, different for the failure mode they exhibited, namely J-failure (by Pantelides et al., 2002) and BJ-failure (by Clyde et al., 2000), for which experimental stress-strain relationships for joint panel were available.

Pantelides et al. (2000) performed cyclic tests on six full-scale models of exterior beam-column joints with two different axial load ratio levels (10% and 25% of compressive strength of concrete f_c) and no transverse reinforcement within the joint core. All specimens had the same dimensions. Reinforcement bars in beam and columns were designed to prevent yielding, forcing a shear mode of failure in the joint (J-failure). Two specimens (test units 1 and 2) were designed with typical gravity load detailing and the bottom beam

reinforcement bars did not have adequate embedment inside the joint. Such specimens have been excluded from the analyzed database in Table 5.1 because a loss of bond due to anchorage failure occurred, but later they have been considered in Table 5.2, as explained in Section 5.2. The other four specimens (test units 3, 4, 5 and 6) had both top and bottom beam bars bent into the joint. Test units 5 and 6 presented a U-hook type of anchorage for both top and bottom beam bars.

Clyde et al. (2000) performed cyclic tests on four half-scale exterior unreinforced RC beam-column joints, with two different levels of axial load on the column, namely 10% and 25% of the compressive strength of concrete (f_c). All beam-column specimens had exactly the same dimensions and detailing. Both bottom and top beam reinforcements were bent up and down, respectively, into a hook in the joint. The yielding of beam longitudinal reinforcement bars before joint failure was documented by the authors (BJ-failure).

As shown in Figure 5.5, the proposed joint panel zone model is a scissors model.

It can be implemented by defining duplicate nodes, node A (master) and node B (slave), with the same coordinates at the center of the joint panel. Node A is connected to the column rigid link and node B is connected to the beam rigid link. A zero length rotational spring connects the two nodes and allows only relative rotation between them through a constitutive model which describes the shear deformation of the joint panel zone. Such a rotational spring (schematically represented in Figure 5.6) is defined as a quadri-linear moment (M_j) - rotation (γ_j) spring characterized by four points for J- and BJ-mode of failure, separately: cracking, pre-peak, peak and residual points. These key points are explained in details below.

Figure 5.7a and Figure 5.7b reports the shear stress-strain envelopes and their mean envelopes constituted by these four characteristic points that have been identified for joints tested by Clyde et al. (2000) and Pantelides et al. (2002), respectively; shear stress is intended to be calculated as $V_j / (A_j \sqrt{f_c})$.

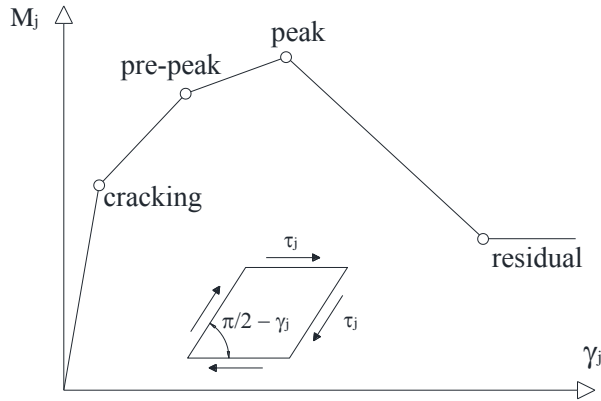


Figure 5.6. Schematic proposed stress-strain relationship for joint panel

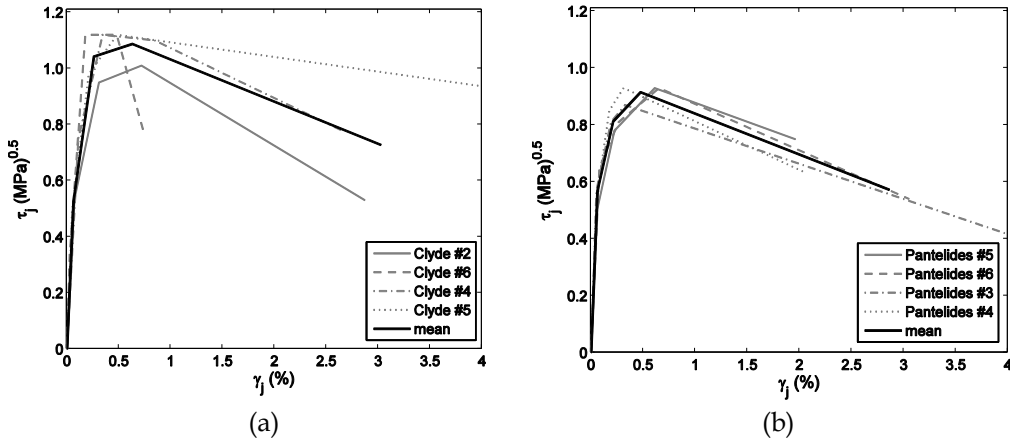


Figure 5.7. Shear stress-strain envelopes for joints tested by Clyde et al. (2000) – BJ-failure (a) and Pantelides et al. (2002) – J-failure (b)

Table 5.3 shows the values of shear strain and shear stress-to-peak strength ratios ($\tau_j/\tau_{j,peak}$) related to the experimental tests used for the calibration of the panel zone constitutive relationship for each characteristic point of the proposed backbone.

Clyde et al. (2000) - BJ-failure								
Backbone point	test #2		test #6		test #4		test #5	
	γ_j (%)	$\tau_j/\tau_{j,peak}$						
cracking	0.07	0.52	0.03	0.31	0.11	0.68	0.05	0.44
pre-peak	0.31	0.94	0.18	0.69	0.34	1.02	0.21	0.88
peak	0.72	1.00	0.48	1.00	0.85	1.00	0.48	1.00
residual	2.87	0.53	0.75	0.83	2.64	0.71	5.85	0.75

Pantelides et al. (2002) - J-failure								
Backbone point	test #5		test #6		test #3		test #4	
	γ_j (%)	$\tau_j/\tau_{j,peak}$						
cracking	0.06	0.54	0.08	0.69	0.05	0.65	0.06	0.59
pre-peak	0.23	0.84	0.27	0.95	0.19	0.93	0.18	0.92
peak	0.61	1.00	0.65	1.00	0.33	1.00	0.31	1.00
residual	1.96	0.81	3.05	0.46	4.37	0.42	2.07	0.68

Clyde et al. (2000) - BJ-failure						
Backbone point	min	max	mean	min	max	mean
	γ_j (%)			$\tau_j/\tau_{j,peak}$		
cracking	0.03	0.11	0.06	0.31	0.68	0.49
pre-peak	0.18	0.34	0.26	0.69	1.02	0.88
peak	0.48	0.85	0.63	1.00	1.00	1.00
residual	0.75	5.85	3.03	0.53	0.83	0.71

Pantelides et al. (2002) - J-failure						
Backbone point	min	max	mean	min	max	mean
	γ_j (%)			$\tau_j/\tau_{j,peak}$		
cracking	0.05	0.08	0.06	0.54	0.69	0.62
pre-peak	0.18	0.27	0.21	0.84	0.95	0.91
peak	0.31	0.65	0.48	1.00	1.00	1.00
residual	1.96	4.37	2.86	0.42	0.81	0.59

Table 5.3. Stress-strain relationships for joint panel for BJ- and J-mode of failure

Cracking point

The cracking point represents the onset of hairline cracks in the joint panel. Experimental tests adopted in this chapter to calibrate the stress-strain shear

behavior of the joint panel suggested that the corresponding shear strain (γ_j) is the same for J- and BJ-mode of failure and equal to 0.06%.

Cracking strength is calibrated on the basis of the stress-strain response of experimental tests in which they were available (4 J- and 4 BJ-failure). In particular, cracking strength has been compared with analytical formulations presented in literature (Park and Mosalam, 2013; Priestley, 1992; Uzumeri, 1977) and the expression suggested by Uzumeri (1977), which shows the lower mean error for the analyzed tests is adopted as reported in Eq. (5.4):

$$\tau_{j,cr} = 0.29\sqrt{f_c} \sqrt{1 + 0.29 \frac{P}{A_j}} \quad (\text{MPa}) \quad (5.4)$$

where P represents the column axial load and A_j the joint area (that can be calculated according to ACI-318-05 or ASCE SEI-41).

Pre-peak point

In the case of BJ-failure the pre-peak point corresponds to the yielding of longitudinal beam bars, thus the pre-peak strength is explicitly defined in a mechanical approach and it is calculated as the joint stress corresponding to the achievement of yielding in the adjacent beam. The corresponding joint shear strain obtained from tests is assumed equal to its mean value (0.26%).

In the case of J-failure, the pre-peak point corresponds to the widening of the main diagonal cracks and the developing of other cracks in the joint panel. The corresponding strength is assumed equal to 0.9 times the peak strength (defined below), in accordance with the observation of experimental tests by Pantelides et al (2002) (see Table 5.3) and other models proposed in literature, e.g. Park and Mosalam (2013). The corresponding joint shear strain obtained from tests is assumed equal to its mean value (0.21%).

Peak point

In the case of BJ-failure the peak point corresponds to a joint stress value not higher than the joint shear stress related to the achievement of the flexural strength in the adjacent beam; in the case of J-failure this point corresponds to the achievement of the maximum shear strength specifically inherent to the joint, independently on the stress demand in the adjacent beam. As explained in Section 5.2.1, the shear strength model proposed by Park and Mosalam

(2012b) directly provides joint shear strength and its failure typology, it shows a very good agreement with experimental tests and it is adopted in the proposed model.

The joint shear strain corresponding to the peak point obtained from tests is assumed equal to its mean value, i.e. 0.63% for BJ-failure and 0.48% for J-failure.

Residual point

Residual strength is calibrated on the basis of experimental tests, separately for J- and BJ-mode of failure. The softening branch is obtained by a straight line connecting the peak point and the ultimate point provided by the authors for each experimental test. In this study, a mean residual strength equal to 60% or 70% of the peak strength for J-failure mode and BJ-mode, respectively, is evaluated from the database. The joint shear strain corresponding to the residual point obtained from tests is assumed equal to its mean value, i.e. 3.03% for BJ-failure and 2.86% for J-failure. However, it is worth to highlight that there are very poor data regarding the achievement of this limit state and they are not always reliable because of the uncertainties in the experimental measurements of joint panel deformation for large displacement demand.

A summary of the coordinates of the characteristic points of the proposed backbone is reported in Table 5.4 and a graphic representation of such a backbone separately for J- and BJ-mode of failure is reported in Figure 5.8a.

Backbone point	J-failure		BJ-failure	
	τ	γ	τ	γ
cracking	From Eq. (5.3)	0.06%	From Eq. (5.3)	0.06%
pre-peak	0.9 τ_{peak}	0.21%	$\tau (M_{\text{yielding,beam}})$	0.26%
peak	From Eq. (5.2)	0.48%	From Eq. (5.2)	0.63%
residual	0.6 τ_{peak}	2.86%	0.7 τ_{peak}	3.03%

Table 5.4. Summary of the proposed backbone for the joint panel

In Figure 5.8b, c, d, the proposed constitutive relationship is also compared with other proposals of complete shear stress-strain backbone presented in literature and previously discussed in Chapter 2.

In Figure 5.8b, the model by Celik and Ellingwood (2008) is represented

in terms of mean values of shear stress and strain for the characteristic points of the backbone; such a backbone is characterized by shear strain values significantly higher than those related to the proposed backbone.

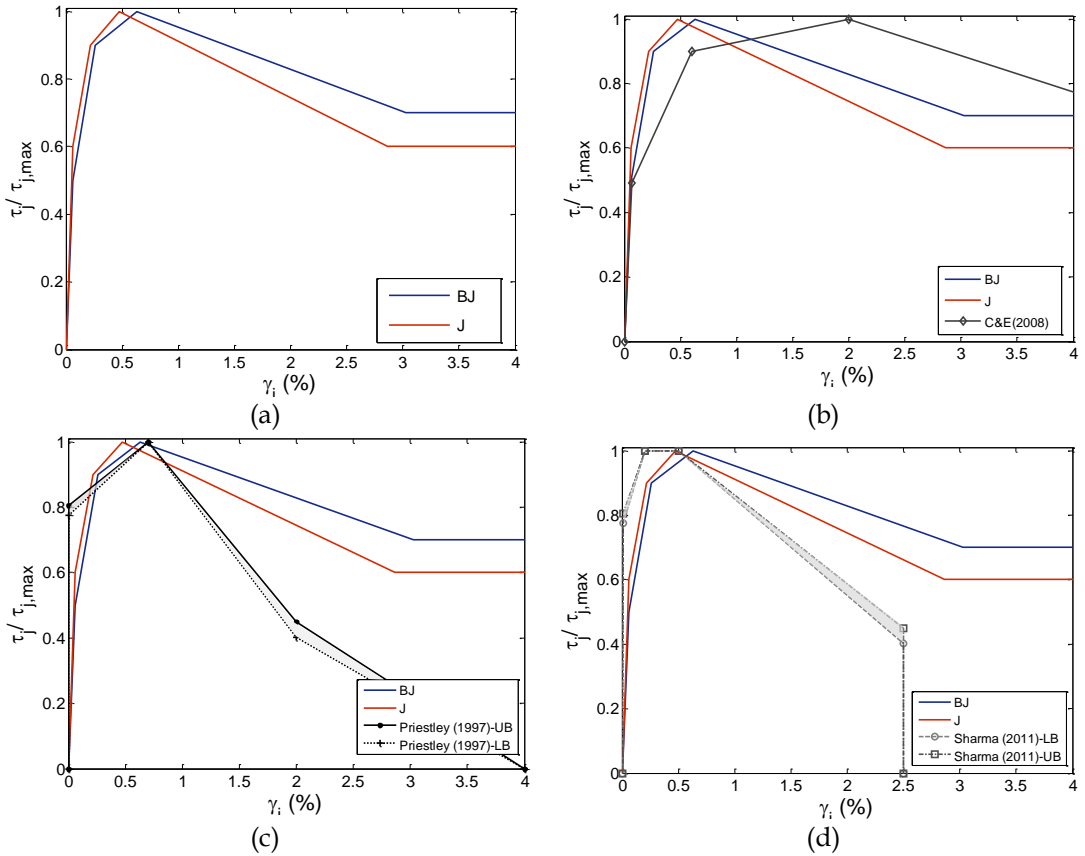


Figure 5.8. Proposed stress-strain relationship for joint panel (for J- and BJ-mode of failure) (a); comparison between proposed model and models by Celik and Ellingwood 2008 (b), Priestley 1997 (c), and Sharma et al. 2011 (d).

In Figure 5.8c and d, models by Priestley (1997) and Sharma et al. (2011) are presented through their upper bound (referred to as “UB”) and lower bound (referred to as “LB”). Since these two constitutive relationships are provided from the authors in principal stresses, the transformation in non-dimensional shear stress requires the knowledge of column axial stress. Therefore, such a transformation has been carried out for the eight tests adopted herein for the calibration of the joint panel shear behavior (Clyde et al. 2000, Pantelides et al. 2002) in order to obtain backbones that can be directly compared to the

proposed ones. Minimum and maximum values for non-dimensional shear stress – which define upper and lower bounds – were calculated. Non-dimensional stress – strain relationship related to models by Priestley (1997) and Sharma et al. (2011) appear to be stiffer in post-cracking branches; however, peak strains are not so different from the proposed ones. Vice-versa, the post-peak behavior related to these two models is characterized by stiffer softening branches with respect to the proposed stress-strain relationship.

It should be specified that Figure 5.8b and d, models by Celik and Ellingwood (2008) and Sharma et al. (2011) are presented in the cases of no anchorage failure to allow a direct comparison with the backbones of the joint panel proposed herein.

For each characteristic point of the backbone, from simple equilibrium equations (see Appendix 5), the moment transferred through the rotational spring M_j can be obtained as a function of the joint shear stress τ_j (Park and Mosalam, 2012b; Sharma et al., 2011) through the Eq. (5.5):

$$M_j = \tau_j A_j \frac{1}{\frac{1 - h_c / (2L_b)}{jd_b} - \frac{1}{2L_c}} \quad (5.5)$$

where L_b and L_c are the beam and column shear span, respectively, evaluated from the inflection point to the centerline of the joint panel, jd_b is the beam level arm, h_c the column height and A_j the effective joint area (defined according to ASCE SEI-41, Section 6.4.2.3.1).

It should be noted that the relationship between beam moment and joint shear stress (from which Eq. (5.5) is derived) is based on the assumption of a fixed inflection point at the mid-length of beam and columns. Such an assumption is correct in the cases of tests sub-assemblages belonging to the database, for which shear span is known without any ambiguity. In the context of the whole structure, actually the assumption becomes an approximation (because shear span in beams and columns is not known a-priori), but it is a modeling approach quite consolidated in literature (e.g. Celik and Ellingwood 2008, Hassan 2011) and it makes easier the implementation of joints in the structural model of a frame.

The abscissas of the backbone of such a spring are joint panel shear strain γ_j ,

because the joint rotation resulting from beam bar slip (θ_s) is explicitly defined by a separate zero-length rotational slip spring element located between the beam-joint interface section and the end of the beam rigid link (as explained in the next section).

A comparison with other models proposed in literature in terms of joint panel deformability is carried out and reported in Table 5.5.

	Cracking		Pre-peak		Peak		Residual	
	J	BJ	J	BJ	J	BJ	J	BJ
proposed model (mean)	0.06%		0.21%	0.26%	0.48%	0.63%	2.86%	3.03%
Celik and Ellingwood (2008)	0.01-0.13%		0.2-1.0%		1-3%		3-10%	
Genesio (2012)	0.10%		-		0.70%	0.50%	-	
Park and Mosalam (2012b)	-		-		$2\varepsilon_1^{(+)}$	$2\varepsilon_1^{(+)}$	-	
Sharma et al. (2011)	-		0.2%		0.5%		2.5%	

(-) means that information is not available from literature

(⁺) ε_1 is the principal tensile strain and it depends on the aspect ratio of the joint.

Table 5.5. Comparison between the proposed model and other models from literature in terms of γ_j

It can be noted that proposed values for shear strain are generally lower with respect to values proposed by other literature models for each characteristic point of the backbone.

Model by Celik and Ellingwood (2009) provides the higher values for joint shear strain; such values are very high if compared with shear strain values obtained from experimental tests on exterior unreinforced beam-column joints.

Genesio (2012) investigated only two “limit states” in terms of deformability, i.e. cracking and peak strength, thus a complete backbone cannot be defined; however, shear strain values are quite similar to the proposed ones.

Park and Mosalam (2013) proposed the adoption of a single spring including both slip and joint panel contributions to the overall deformability, as reported in Chapter 2. However, in a previous work (Park and Mosalam, 2012b) they proposed a distinct definition of joint panel shear strain, γ_j , and beam longitudinal rebar slip rotation, θ_s (in the hypothesis of strong column and weak beam), with regards to the definition of the joint peak strength point, assuming that

$$\gamma_{j,\text{peak}} = 2 \cdot \varepsilon_I = 2 \cdot (0.003 + 0.0005 \cdot h_b / h_c) \quad (5.6)$$

where $\gamma_{j,\text{peak}}$ represents the joint panel shear strain at peak strength and ε_I is the principal tensile strain (expressed as a function of the joint aspect ratio, h_b/h_c). Thus, $\gamma_{j,\text{peak}}$ does not depend on the failure typology and ranges between 0.65% and 0.8% when joint aspect ratio varies from 0.5 to 2; thus it is generally higher than the strain values proposed herein for the peak point.

Sharma et al. (2011) proposed shear strain values similar to the values proposed herein by the authors for the case of J-failure and introduced a reduction of shear strain related to the achievement of residual strength in the case of anchorage failure.

5.3.2. Bond slip spring

The second deformability contribution related to beam-column joints is the rigid rotation (known as fixed-end-rotation) produced by the slippage of the longitudinal bars anchored into the joint core due to the moment acting at the interface between element (beam or column) and joint (see Figure 5.9).

This deformability contribution can be computed and taken into account through different approaches. Between them, one of the approaches proposed in literature to account for slip deformation is the reduction of the effective stiffness of beams and columns, as recommended by ASCE/SEI 41 supplement. However, in general, the deformability contribution due to bond slip is explicitly evaluated, in an empirical approach, namely through its calibration based on experimental tests (e.g. Park and Mosalam, 2013), or in a mechanical approach, namely analytically calculated using a bond-slip model (e.g. Hassan, 2011).

In the latter approach, moment acting at the interface between element (beam or column) and joint (below referred to as interface section) can be directly related to the corresponding rotation due to the slippage of bars anchored into the joint panel.

In this study, a mechanical approach is adopted; the bond stress-slip relationship employed herein is that proposed by Model Code 2010 (as explained in Section 5.2.2).

The slip of steel bars at the joint-element (i.e., beam or column) interface is

evaluated by a procedure similar to that described above in Section 5.2.2; a translational equilibrium equation (Eq. 5.2a) for the bar and a compatibility equation (Eq. 5.2b) between steel and concrete in tension control the problem. The solution of the problem is univocally defined if the boundary conditions are provided in the two end sections of rebar.

At the interface between joint and element ($x=l_b$), the boundary condition is obtained using translational and rotational equilibrium equations. In fact, starting from axial load P and moment M_b acting at the interface section, tensile steel strain ε_s and neutral axis depth x can be calculated through equilibrium equations. Similarly, starting from tensile steel strain ε_s and axial load P , the corresponding neutral axis depth and moment M_b can be obtained.

In section at $x=0$, the boundary conditions depends on the behavior of the anchorage detail, see Figure 5.9. From a theoretical point of view, in this section, two limit conditions can be identified:

- if anchorage is rigid, slip at the inner end of the rebar is equal to zero ($s=0$), and a steel stress develops on the anchoring device;
- if the anchorage is not present, straight rebar is characterized by a free end, thus a unrestricted slippage occurs, so that $\varepsilon_s=0$.

In the first case, a pull-out of bars leads to the premature failure of the member end section (anchorage failure); conversely, rigid anchorage allows the full development of flexural capacity of the member end section (Fabbrocino et al. 2004).

Commonly, anchorage devices have a response that lies between the above boundaries, so that both slip and steel strain are not zero and are dependent on the response of the end anchorage.

When the rebar is terminated with an end hook, the steel element can be treated as composed by the hook plus the straight portion. Steel-concrete interaction in the straight region is described by the adopted τ - s bond relationship, while the hook can be modeled as a translational non-linear spring, whose behavior is governed by the stress-slip (σ_h - s_h) relationship computed in the common section between the hook and the straight part, as depicted in Figure 5.9a. In literature, there are several proposals for stress-slip of anchorage device, both for deformed bars (Soroushian et al., 1988, Alsiwat and Saatcioglu, 1992; Monti et al., 1993) and plain bars (Fabbrocino et al. 2004, Fabbrocino et al. 2005).

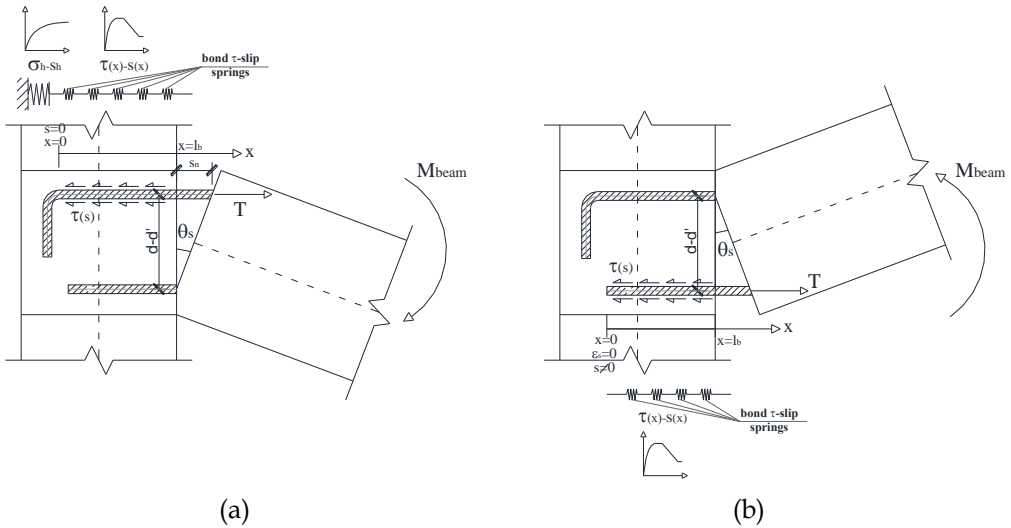


Figure 5.9. Rotation θ_s due to slip of end-hooked (a) and straight (b) longitudinal bars

Thus, given a certain value of steel strain ϵ_s , the corresponding beam (or column) moment M_b at the interface section and the corresponding slip can be univocally calculated. The rigid rotation θ_s related to the calculated value of slip (s) can be obtained as proposed by (Otani and Sozen, 1972), namely:

$$\theta_s = \frac{s}{d - d'} \tag{5.7}$$

where $(d-d')$ is the distance between tensile steel bars and compressive steel bars, and slip involving the compression rebar is considered negligible. Thus, it is possible to completely define the relationship between moment M_b acting at the interface and the corresponding slip rotation θ_s . Moreover, such a relationship appears to be different if hook is present or not at the end section of the embedded bar.

In the case of bar anchored through a terminal hook, it can be assumed that anchorage is effective allowing a complete development of the flexural response at the interface section. Therefore, $M_b-\theta_s$, slip spring can be defined in order to follow the flexural behavior at the interface section. In particular, the quadri-linear slip spring (see Figure 5.10a) is defined by four points.

The first point of the spring is identified by the cracking moment M_{cr} and no slip deformation is assumed ($\theta_s=0$); therefore, the first branch of the slip spring

is a rigid branch. The second and third points are defined by yielding moment M_y and beam flexural capacity, respectively; the corresponding θ_s can be calculated assuming a strain value in tensile bars which corresponds to the first yielding and the flexural capacity of the beam, respectively. The fourth point identifies the softening branch and it is defined from the beam softening branch.

Vice-versa, in the case of bar anchored without an end hook (see Figure 5.9b), an anchorage failure can occur. In this case, in M_b - θ_s slip spring, the point related to anchorage failure can be identified in the post-cracking phase, with rotation $\theta_{s,peak}$ and moment $M_{A-failure}$ corresponding to the attainment of the peak strength $\sigma_{s,max}$ in the stress-slip relationship at the free end of the straight bar (see Section 5.2.2 and Figure 5.10b). Post-peak phase is characterized by the reduction in steel strain of the embedded bar (related to the flexural unloading at interface section), on one hand, and the increase in the slippage of the bar, on the other hand, until a residual bond strength is achieved in correspondence to the complete pull-out of the bar, corresponding to $\theta_{s,res}$ and M_{res} (see Figure 5.10b). The latter point, corresponding to the complete pull-out, is identified in M_b - θ_s relationship assuming a slip at free end section of the bar equal to the slip corresponding to residual bond stress in the employed bond stress-slip relationship. In order to better define the slip spring response, a further point is defined between cracking and peak strength conditions (see point $\theta_{s,2}$ - M_2 in Figure 10b); in this study, it is evaluated assuming that bar slip at the free end section is equal to the slip corresponding to the beginning of the bond strength plateau in the employed bond stress-slip relationship.

Finally, it should be noted that slip spring is a multi-linear approximation of the “real” moment-slip rotation spring that could be computed as a continuous function (see dotted line in Figure 5.10b). The quadri-linear approximation (solid lines in Figure 5.10b) is proposed herein to make easier the implementation of such a spring in most common structural software, such as OpenSees (McKenna and Fenves, 2006).

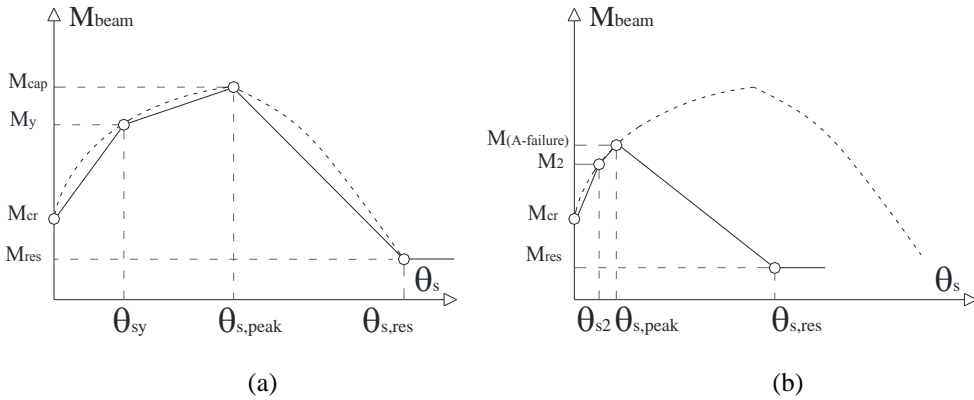


Figure 5.10. Quadri-linear springs without (a) and with (b) anchorage failure

5.4 Validation by experimental tests

The proposed joint model is validated using some of the experimental test data included in the database, reported in Table 5.1 and Table 5.2.

The comparison between numerical and experimental results is performed taking into account tests for which test setup, material and geometrical properties are completely known without any ambiguity. Numerical simulations are performed first on tests characterized either by a BJ- or by a J-failure mode, and then on tests which exhibited anchorage failure. The classification of the failure mode is carried out according to model by Park and Mosalam (2012a).

Tests with no anchorage failure for which strength predicted by Park and Mosalam (2012a) (adopted in the proposed model) does not differ from experimental strength more than 20% are reported in this Section. The total amount of tests (characterized by J or BJ failure mode) used in the validation phase is 17 (all characterized by strong column-weak beam hierarchy).

Tests by Clyde et al. (2000) and Pantelides et al. (2002), which have been used for the calibration of shear stress-strain relationship of the joint panel, were also considered in this validation step. Since geometry and test setup are not completely known for tests by Pantelides et al (2002), such tests are not taken into account in the comparison between the numerical and the experimental response of the sub-assemblages. As far as tests by Clyde et al. (2000) are concerned, it is worth to highlight that, according to Park and

Mosalam's strength model, these tests are in a limit range of behavior between J- and BJ-failure (i.e. k in Eq. (5.1) is close to 1), but the predicted mode of failure is a J-failure. Such a prediction does not reflect exactly what happens in the experimental tests because of the unavoidable error associated to a prediction model. However, the mean error associated to this strength model is the lower one between the models existing in literature for the analyzed database, as highlighted in Section 5.2.1. Thus, in the validation step, consistently with the adopted strength model, tests by Clyde et al. are simulated by using the stress-strain relationship related to J-failure mode.

Experimental tests with no anchorage failure (4 tests) for which numerical simulations have been carried out are reported below in this Section.

The finite element analyses of the specimens were performed using OpenSees (McKenna and Fenves, 2006); Figure 5.11 shows the structural model developed for analyses.

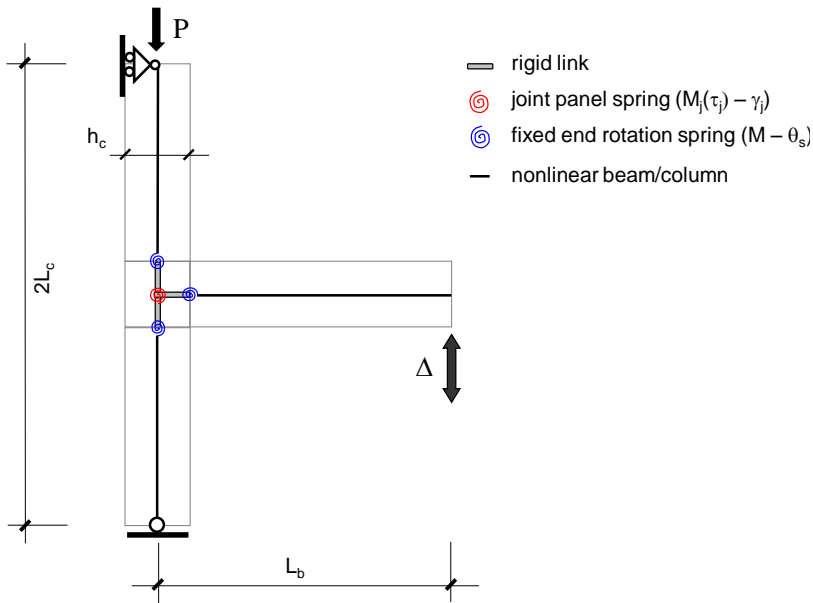


Figure 5.11. Numerical model for beam-column joint sub-assemblages simulations

In particular, flexural response of beam and column is modeled in a fiber approach. Concrete and steel properties were obtained from the analyzed test program reports; the Kent-Scott-Park model was adopted for concrete (Kent

and Park, 1971; Scott et al., 1982) and an elastic-plastic-hardening stress-strain relationship was adopted for steel (Concrete01 and ReinforcingSteel uniaxial materials in OpenSees software, respectively).

Beam-column joint response is modeled through the scissors model. $M_j-\gamma_j$ relationship for joint panel is obtained from constitutive relationships proposed by different models analyzed herein (Priestley 1997, Celik and Ellingwood 2008, Park and Mosalam 2013, ASCE SEI-41, “rigid joint” and the proposed joint model) and specialized for geometrical characteristics and load conditions related to each test.

As far as the model by Celik and Ellingwood (2008) is concerned, the characteristic points of the $M_j-\gamma_j$ relationship are related to the mean values of the proposed ranges of shear stress and strain of the joint panel.

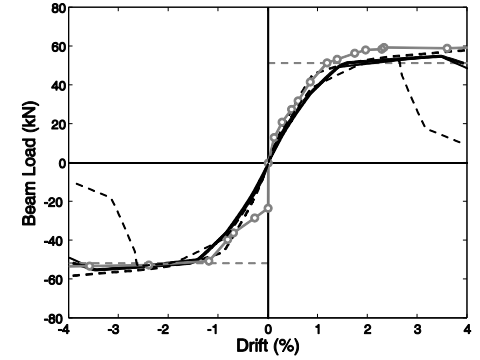
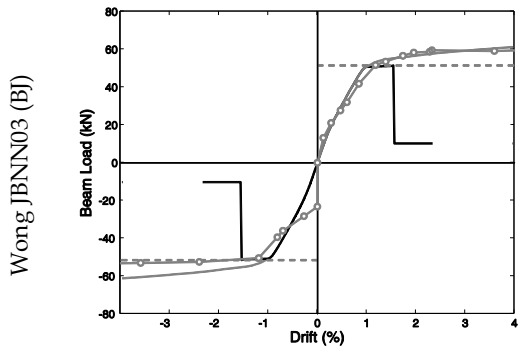
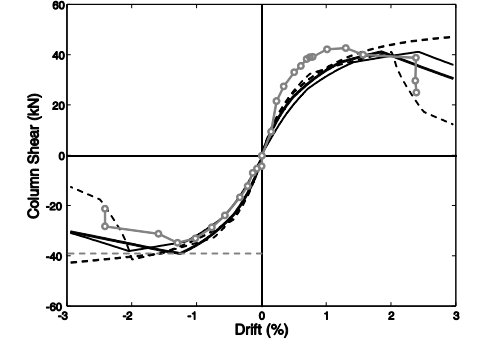
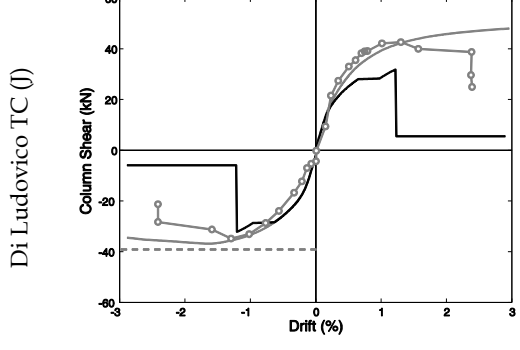
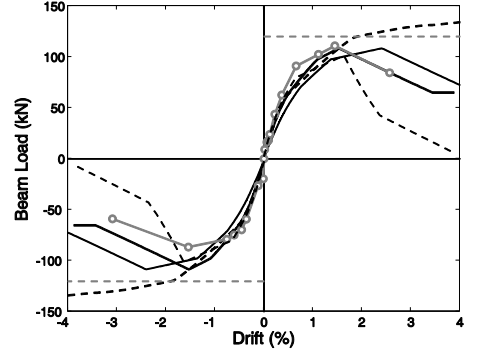
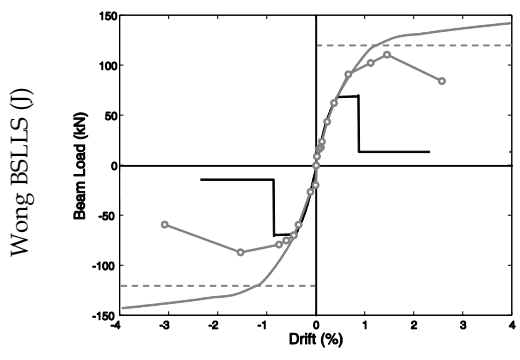
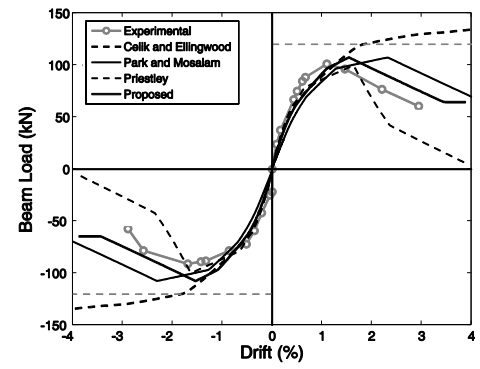
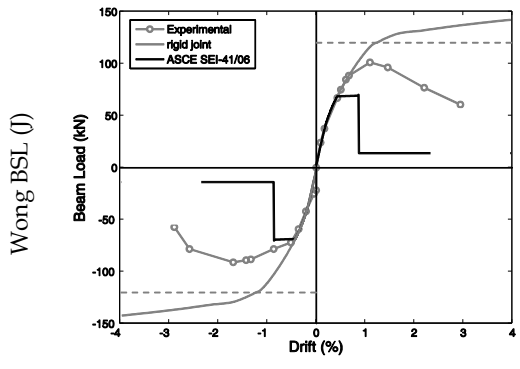
Beam-column joint response is implemented with a four-point backbone moment-rotation relationship (Pinching4 uniaxial material in OpenSees software).

Deformability contribution due to the slippage of beam longitudinal bars anchored into the joint core is reproduced through another zero-length element introduced at beam-joint interface. The related $M_b-\theta_s$ relationship is obtained as defined in Section 5.3.2, by specifying geometrical and mechanical properties for each tests.

When the model by Park and Mosalam (2013) is applied, since the deformability parameter of the relative constitutive relationship includes both joint panel shear strain and slip contribution due to the slippage of the beam bars, bond-slip spring is not introduced in the numerical model.

In the case of “rigid Joint” neither joint panel shear strain nor slip deformability contribution are considered. In the cases of models by ASCE/SEI 41, deformability contribution due to slip is not taken into account. Moreover, when model by Celik and Ellingwood (2008) is adopted slip contribution is neglected as proposed by the authors of the model.

Some of all the simulated tests with no anchorage failure (6 J-failures and 2 BJ-failures) are reported in Figure 5.12, which shows beam shear versus drift (calculated as the ratio between top displacement of beam and total length of beam). Grey dotted horizontal thin lines represent beam yielding.



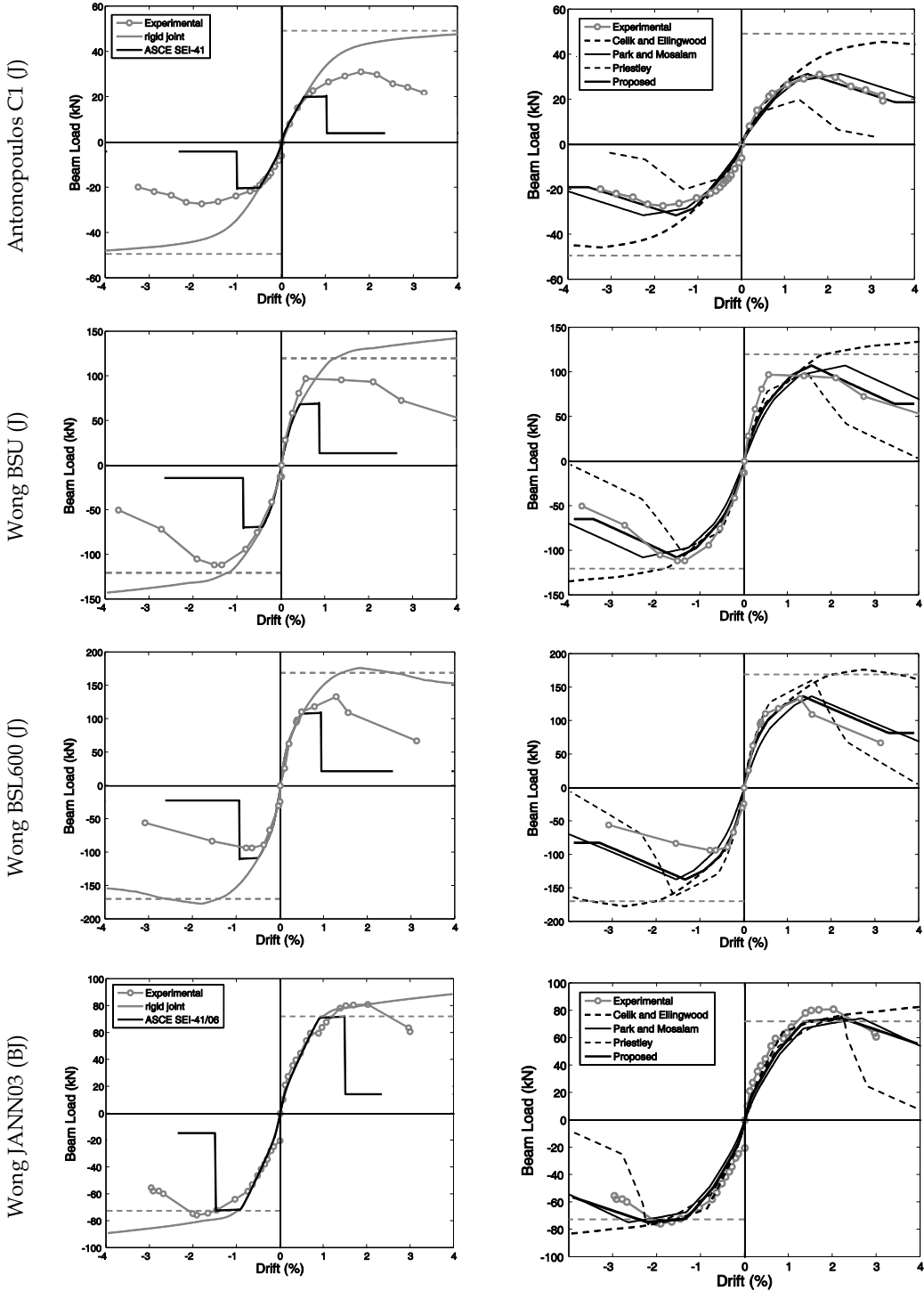


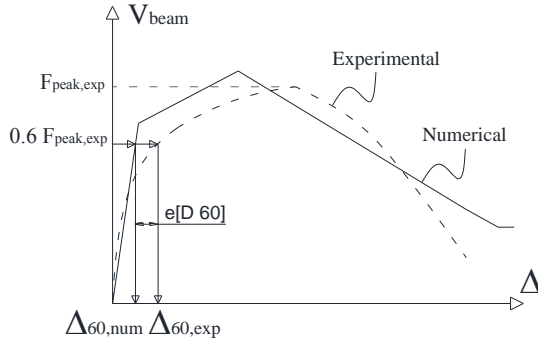
Figure 5.12. Comparisons between experimental and numerical results

In Figure 5.12, first column represents the comparison between experimental data, rigid joint model and ASCE SEI-41 model; second column represents the comparison between experimental data, model proposed herein and models by Priestley (1997), Celik and Ellingwood (2008), and Park and Mosalam (2013). It can be noted that the peak point and softening behavior are generally predicted quite well by adopting the proposed modeling approach, as it will be shown better later in Table 5.6, Table 5.7, Table 5.8 and Figure 5.14. Moreover, in general, models by Priestley and Celik and Ellingwood represent the lower and upper bounds, respectively, for the other models and the experimental response for the post-peak behavior.

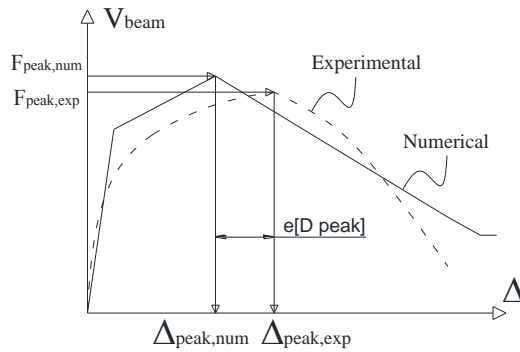
For all of the analyzed tests, the comparisons between numerical and experimental responses are performed for each model for three points, that are considered to be representative of the pre-peak behavior, peak response and post-peak behavior (see Table 5.6, Table 5.7 and Table 5.8). In particular:

- numerical drift corresponding to 60% of experimental peak force is evaluated for each model and compared with the experimental one; the corresponding error is referred to as $e[D_{60}]$;
- numerical drift corresponding to the predicted peak force is evaluated for each model and compared with the experimental peak drift (namely, drift at experimental peak force); the corresponding error is referred to as $e[D_{peak}]$;
- numerical force corresponding to the drift at the last point of the experimental response (“residual”) is evaluated for each model and compared with the experimental corresponding force; the corresponding error is referred to as $e[F_{res}]$.

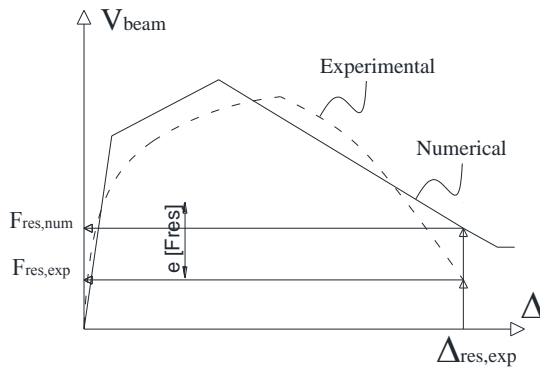
Figure 5.13 reports a schematically representation of the errors in terms of drift at 60% of the peak Force ($e[D_{60}]$), peak drift ($e[D_{peak}]$), and residual Force ($e[F_{res}]$).



(a)



(b)



(c)

Figure 5.13. Schematic sketch of the errors in terms of drift at 60% of the peak Force ($e[D_{60}]$), peak drift ($e[D_{peak}]$), and residual Force ($e[F_{res}]$).

It is worth noting that a direct comparison in terms of experimental-versus-numerical peak force is already presented in Table 5.1 (in terms of joint strength).

Table 5.6, Table 5.7, Table 5.8 show experimental values and percentage errors (e) of peak drift (D_{peak}), drift at 60% of the peak Force (D_{60}), and residual Force (F_{res}) for the proposed model (Prop.), models by Celik and Ellingwood (C&E), Park and Mosalam (P&M), Priestley (Priest.) and ASCE (related to the experimental behavior on the peak strength side). A negative value of the percentage error means that the model underestimates the experimental value.

It can be observed that on average model by Celik and Ellingwood better predicts drift at 60% of the peak force among models from literature (the related error is about 12%). The proposed model and model by Priestley provide a higher error on D_{60} (about 23% and 33% respectively). Moreover, for some of the analyzed tests, numerical simulation related to model by ASCE is characterized by a numerical peak force that is lower than 60% of the experimental peak force; thus, for these tests, in Table 5.7 no values of $e[D_{60}]$ are provided for model by ASCE. One similar case occurs also for model by Priestley (test Clyde#6).

As far as the post-peak behavior is concerned, in Table 5.8 it can be noted that the proposed model provides the lower error in terms of F_{res} , so that it describes better than other models from literature the softening behavior of the experimental response. Models by Priestley and above all the code approach (ASCE) significantly underestimate residual strength (errors equal to -55% and -100% respectively) and the corresponding joint deformability.

The peak response is described through numerical-versus-experimental comparison in terms of peak force (already presented in Table 5.1) and peak drift (in Table 5.6). Peak response is well described in terms of D_{peak} by the proposed modeling approach (the error is equal to 7%). Only model by Priestley provides a bit higher error in terms of D_{peak} (18.6%). The error evaluated according to other models from literature are higher than 60%.

In Figure 5.14 graphical representation of the relative errors of peak drift ($e[D_{\text{peak}}]$), drift at 60% of the peak Force ($e[D_{60}]$), and residual Force ($e[F_{\text{res}}]$) is shown for all of the simulated tests and for all of the analyzed models from literature.

Test	failure mode	$F_{peak, exp}$	$D_{peak, exp}$	e [D_{peak}] (%)				
		(kN)	(%)	Prop.	C&E	P&M	Priest	ASCE
WONG BS-L	J	100.50	1.1	41.2	473.8	113	48.5	-56.4
WONG BS-L600	J	134.58	1.3	2.6	105.2	17.9	65.4	-60.3
WONG BS-U	J	111.35	1.4	9.0	318.2	64.2	14.6	-66.4
WONG BS-L-LS	J	110.35	1.4	12.4	321.1	69.3	19.7	-65.3
WONG JA-NN03	BJ	81.96	2.0	12.1	276.9	36.5	12.1	-57.3
WONG JA-NN15	BJ	87.16	1.4	16.4	358.1	55.2	170.3	-59.5
WONG JB-NN03	BJ	58.18	2.3	50.5	167.7	48.8	12.4	-62.0
TSONOS L1	J	60.00	1.5	-18.3	64.8	36.2	-5.2	-66.4
ANTONOPUOLOS C1	J	31.30	1.8	-17.0	82.4	27.0	-25.6	-65.6
ANTONOPUOLOS C2	J	31.10	1.4	15.0	37.0	71.0	-5.0	-52.7
DI LUDOVICO TC	J	80.50	1.3	41.6	168.0	85.7	53.1	-50.4
DI LUDOVICO TC_2	J	76.50	1.3	57.6	142.2	69.2	99.2	-67.6
GENESIO JT_1	BJ	76.90	3.2	-35.4	145.8	95.6	-51.7	-60.6
CLYDE #2	J	290.00	2.0	-12.4	47.2	49.2	-41.9	-80.1
CLYDE #6	J	279.20	1.9	-30.2	-21.2	47.2	-41.1	-79.6
CLYDE #4	J	290.00	1.0	7.5	23.0	157	18.8	-75.7
CLYDE #5	J	275.00	1.6	-33.7	-31.7	56.3	-27.6	-85.2
mean value				7.0	157.6	64.6	18.6	-65.4

Table 5.6. Experimental values and percentage errors (e) of peak drift (D_{peak}), for the proposed model (Prop.), models by Celik and Ellingwood (C&E), Park and Mosalam (P&M), Priestley (Priest.) and ASCE

Test	failure mode	$F_{60,exp}$ (kN)	$D_{60,exp}$ (%)	e [D ₆₀] (%)				
				Prop.	C&E	P&M	Priest	ASCE
WONG BS-L	J	60.30	0.4	22.64	9.49	48.97	13.61	-8.34
WONG BS-L600	J	80.75	0.3	24.33	16.59	74.52	13.12	-3.23
WONG BS-U	J	66.81	0.3	82.14	70.14	111.18	60.26	33.05
WONG BS-L-LS	J	66.21	0.4	33.56	37.56	70.53	20.14	0.24
WONG JA-NN03	BJ	49.18	0.5	36.45	15.74	54.77	28.52	5.65
WONG JA-NN15	BJ	52.30	0.5	0.53	-17.91	31.73	-13.72	-29.03
WONG JB-NN03	BJ	34.91	0.7	19.42	-4.54	23.90	8.82	-12.48
TSonos L1	J	36.00	0.5	-25.98	-30.10	1.18	-34.28	-50.27
ANTONOPUOLOS C1	J	18.78	0.5	28.22	7.50	36.09	96.03	-8.80
ANTONOPUOLOS C2	J	18.66	0.3	110.36	79.19	125.92	167.45	57.67
DI LUDOVICO TC	J	48.30	0.3	92.22	68.58	124.44	72.67	69.15
DI LUDOVICO TC_2	J	45.90	0.3	38.28	30.68	79.95	15.74	10.04
GENESIO JT_1	BJ	46.14	0.5	48.18	12.80	38.16	143.17	0.89
CLYDE #2	J	174.00	1.0	-46.55	-42.60	-44.08	-0.09	-
CLYDE #6	J	167.52	0.9	-35.94	-34.34	-35.38	-	-
CLYDE #4	J	174.00	0.5	-2.21	11.90	8.15	-15.59	-
CLYDE #5	J	165.00	0.7	-30.28	-21.82	-30.81	-42.29	-
mean value				23.26	12.29	42.31	33.35	4.96

Table 5.7. Experimental values and percentage errors (e) of drift at 60% of the peak Force (D₆₀) for the proposed model (Prop.), models by Celik and Ellingwood (C&E), Park and Mosalam (P&M), Priestley (Priest.) and ASCE

Test	failure mode	$F_{res,exp}$ (kN)	$D_{res,exp}$ (%)	$e [F_{res}]$ (%)				
				Prop.	C&E	P&M	Priest	ASCE
WONG BS-L	J	60.61	2.9	24.85	113.91	53.93	-54.22	-100.
WONG BS-L600	J	67.31	3.1	29.44	157.52	38.29	-43.11	-100
WONG BS-U	J	51.94	4.1	24.21	159.43	29.55	-100.00	-100
WONG BS-L-LS	J	84.57	2.6	0.38	49.28	24.20	-55.93	-100
WONG JA-NN03	BJ	60.96	3.0	8.51	30.25	14.09	-68.43	-100
WONG JA-NN15	BJ	81.67	2.2	-16.03	-3.73	-9.39	1.50	-100
WONG JB-NN03	BJ	60.02	4.8	-28.36	-0.81	-34.43	-100.00	-100
TSonos L1	J	27.94	6.4	26.49	123.63	26.51	-100.00	-100
ANTONOPUOLOS C1	J	21.85	3.2	-4.85	108.84	16.90	-72.31	-100
ANTONOPUOLOS C2	J	19.39	3.2	26.41	80.56	54.31	-68.95	-100
DI LUDOVICO TC	J	73.59	2.4	-7.39	17.41	5.73	-44.39	-100
DI LUDOVICO TC_2	J	46.38	3.2	27.43	122.61	22.18	-11.17	-100
GENESIO JT_1	BJ	53.04	3.5	35.10	86.52	54.55	-92.91	-100
CLYDE #2	J	120.67	2.8	70.67	142.21	135.83	-57.98	-100
CLYDE #6	J	119.64	3.2	40.27	125.00	112.45	-73.40	-100
CLYDE #4	J	91.37	2.2	131.93	205.49	188.93	28.60	-100
CLYDE #5	J	100.00	2.8	75.70	159.19	75.44	-29.54	-100
mean value				27.34	98.66	47.59	-55.43	-100

Table 5.8. Experimental values and percentage errors (e) of residual Force (F_{res}) for the proposed model (Prop.), models by Celik and Ellingwood (C&E), Park and Mosalam (P&M), Priestley (Priest.) and ASCE

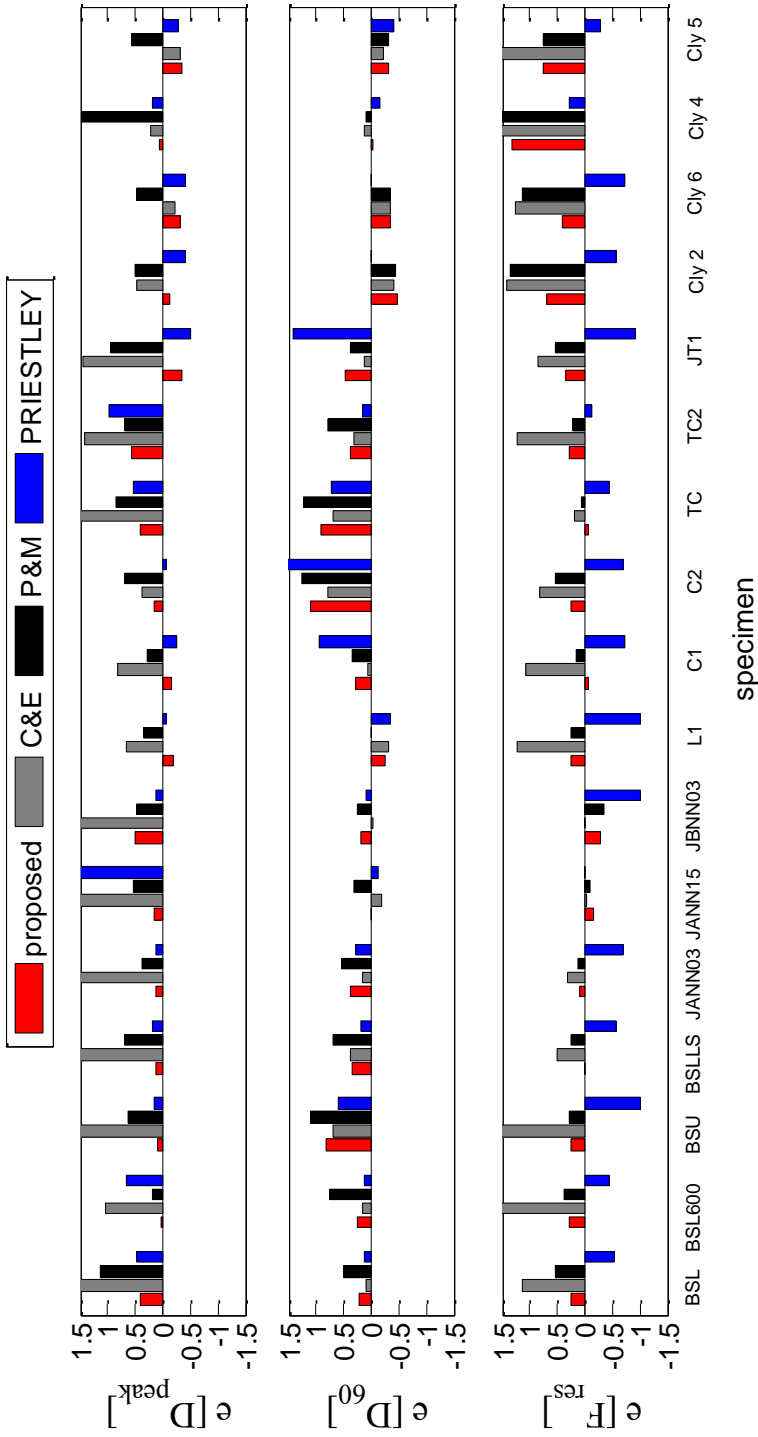


Figure 5.14. Relative error in terms of peak drift ($e[D_{peak}]$), drift at 60% of the peak Force ($e[D_{60}]$), and residual Force ($e[F_{res}]$).

An overview of numerical-versus-experimental comparisons can be carried out by summing up data provided in Table 5.1, Figure 5.12 and Figure 5.14.

From Figure 5.12 it can be observed that the rigid joint model generally overestimates the sub-assembly strength, especially for J-failure mode. In this model there is no limitation of strength due to joint failure and thus the adjacent elements can explicate their flexural strength (if shear failure is prevented, as in these cases).

On the contrary, for the selected tests, ASCE SEI-41 underestimates the strength (as it can be verified also in Table 5.1) and the displacement capacity of the sub-assembly. The mean percentage error related to ASCE SEI-41 model is always negative, both for peak force and peak displacement (see Table 5.1 and Tables 5.6-8); thus this code-approach appears to be very conservative.

Model proposed by Celik and Ellingwood (applied using the mean values of the proposed range of values for each characteristic point) generally overestimates maximum strength and displacement capacity for the analyzed experimental tests; the proposed joint strength ($0.83-1.00\sqrt{\text{MPa}}$ for exterior joints) seems to be too high. With respect to other simulations, such a model provides also higher values of peak drift because of the high values of joint drift capacity (mean of 2% at peak point). Mean relative error in terms of peak drift is almost always positive (see Table 5.6) and it overcomes the unity when model by Celik and Ellingwood is adopted in numerical simulations.

Model proposed by Priestley (1997) slightly underestimates peak load and overestimates peak drift on average; however it shows a good prediction of beam-column joint sub-assembly behavior, even if it often shows a softening branch that is quite steeper than the experimental response.

Finally, model by Park and Mosalam captures well the strength of the sub-assemblies, as shown also in Table 5.1, but not also their deformability. Since model by Park and Mosalam (2012b) is adopted herein for strength prediction, the mean error in terms of peak force for the proposed model and model by Park and Mosalam are overlapped in Figure 5.14.

Since the great spread of displacement-based approaches for seismic assessment, a very important role is assumed by the comparison between models from literature and experimental values in terms of drift capacity.

By comparing the mean errors in Table 5.6, it can be observed that model by Park and Mosalam generally overestimates the peak deformability of the sub-

assemblages, while the proposed model shows the lower mean error (see Tables 5.6 and 5.8) at peak drift and residual strength with respect to the other models from literature. Thus, the proposed model can be very suitable for seismic assessment in the context of displacement-based approaches.

It is worth noting that relative errors for almost all of the tests by Clyde et al. (Table 5.6) appear to be quite high in terms of peak deformability; these data could be considered unexpected since stress-strain envelope (for BJ-failure) of the joint panel has been calibrated just from tests by Clyde et al.. Actually relative errors for tests by Clyde et al. are due to the predicted mode of failure according to the adopted strength model (Park and Mosalam, 2012b), that is a J-failure mode and does not reflect exactly what happens in the experimental tests. However, in the validation step, consistently with the adopted strength model, tests by Clyde et al. are simulated by using the stress-strain relationship related to J-failure mode, i.e. a stress-strain envelope that is different from the envelope calibrated just on these test data, and, therefore, the peak deformability is generally underestimate (negative percentage error).

As far as the initial stiffness is concerned, for each test, results obtained from all joint models by numerical simulations are very similar to each other, and they are very close to experimental results. This outcome related to the elastic range of behavior is the evidence of a higher deformability of the adjacent beam/column elements with respect to the pre-cracking deformability of the joint panel.

A numerical versus experimental comparison is also carried out for tests that exhibited anchorage failure. Also in this case such a comparison is performed taking into account tests for which test setup, material and geometrical properties, and load-drift global response are completely known without any ambiguity.

In Figure 5.15 the experimental response is compared with numerical response obtained through the proposed model and by adopting a “rigid joint” model; the represented quarter is that characterized by anchorage failure of beam bars.

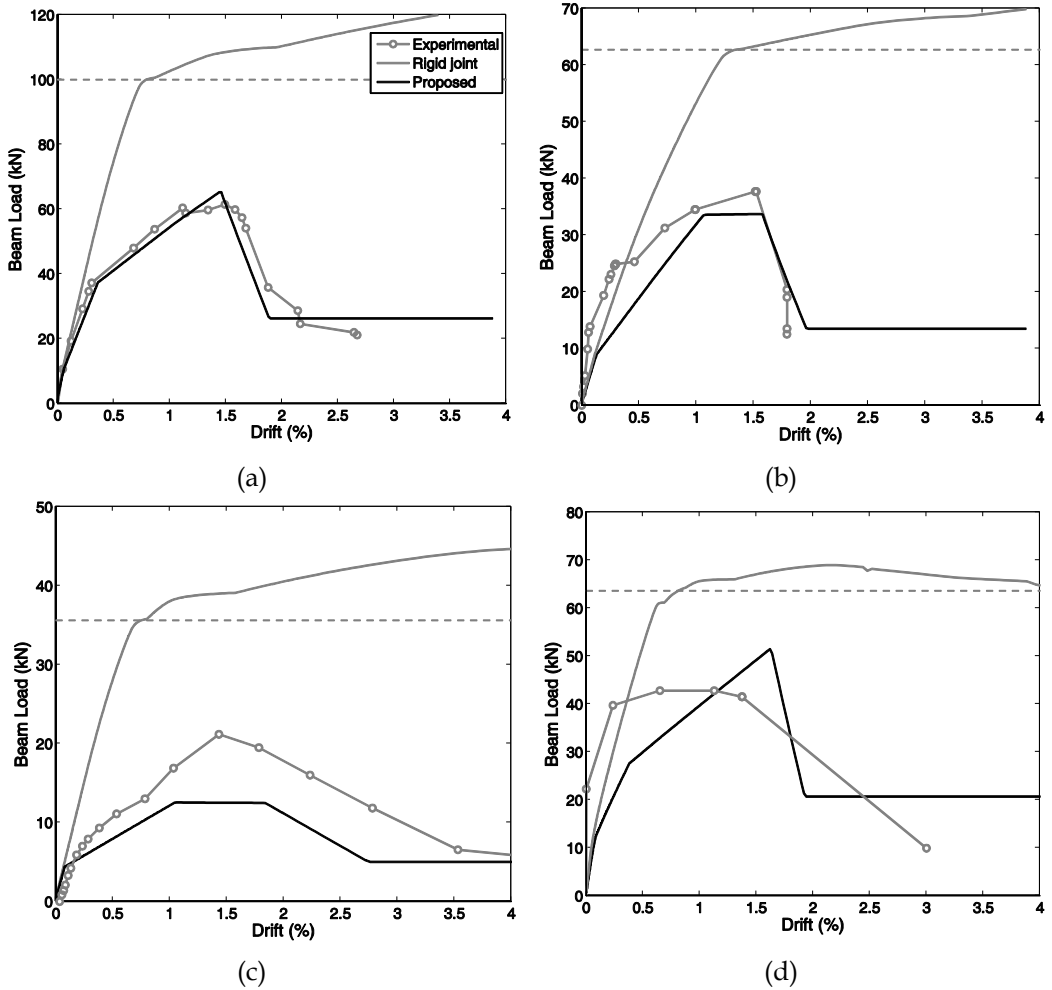


Figure 5.15. Comparisons between experimental and numerical results for tests which exhibited anchorage failure: El-Amoury-Ghobarah 2002 (a), Genesis JT1-3 2012 (b), Shafaei et al. 2014 (c), Murty et al. 2011 (d); gray dotted line identifies yielding of the beam

In Table 5.9 the experimental values and errors for peak force (shear in beam) (F_{peak}) and peak drift (Δ_{peak}) related to the proposed model are reported. A negative value of the percentage error means that the model underestimates the experimental value.

Test	failure mode	$F_{\text{peak,exper}}$	$\Delta_{\text{peak,exper}}$	$e [F_{\text{peak}}]$	$e [\Delta_{\text{peak}}]$
		(kN)	(%)	(%)	(%)
El-Amoury and Ghobarah T0	Anchorage failure	60.0	1.50	8.72	-2.67
Shafaei et al. C3		40.9	1.52	-17.73	3.95
Genesio JT1-3		21.1	1.43	-40.76	27.27
Murty et al. S1		43.2	1.13	19.17	43.36

Table 5.9. Experimental values and percentage errors (e) of peak force (F_{peak}) and peak drift (Δ_{peak}) for the proposed model (Prop.) – anchorage failure

Much more experimental data should be necessary to a proper calibration and validation of such a model in the cases of anchorage failure, but first comparisons shown herein appear to be quite promising.

5.5 Summary

In literature, there is not yet a commonly accepted approach for the determination of the shear strength and for nonlinear modeling of exterior unconfined beam-column joints in moment resisting RC frames. Many nonlinear joint models are available, but most of them may be unsuitable for modeling all sources of nonlinearity for the assessment of older concrete buildings, because they were developed and calibrated for confined beam-column joints, or on the basis of statistical regression analysis with quite small size and large scatter of experimental datasets, and independently on the joint failure typology.

In this Chapter, a macro-model for exterior unconfined joints has been proposed. It depends on the joint failure typology and it has been defined in a “semi-empirical” approach, according to the steps described as follows:

- An experimental database consisting of 39 tests on exterior unreinforced beam-column joints that exhibited J-, BJ- or Anchorage failure mode has been collected and illustrated.
- The joint panel constitutive parameters have been defined in order to reproduce the experimental joint shear stress-strain behavior, when they were available from tests. The proposed model for joint panel is a scissors model characterized by a quadri-linear Moment–Rotation spring with four points for J- and BJ-mode of failure, namely: cracking, pre-peak, peak, and residual point.
- The peak strength has been evaluated according to the model by Park and Mosalam (2012a), which directly provides joint shear strength depending on the failure typology and shows a very good agreement with analyzed experimental tests.
- Bond-slip has been taken into account by introducing an explicit slip spring (at the beam-joint interface) whose properties are analytically calculated using a finite difference model of the bar anchored into the joint panel.
- Cases of anchorage failure due to an insufficient embedment length of the straight longitudinal bar into the joint core (which represents typical anchorage conditions of bottom reinforcement layer at beam’s ends in non-conforming frames designed for gravity loads only) have been taken into account limiting the peak strength of the slip spring consistent with the maximum stress allowed in the bar.
- The proposed joint model has been validated using some of the

experimental tests included in the database, and a comparison between the proposed model and other models from literature and code provisions has been carried out. The proposed model conducts to the lower errors in terms of peak strength, peak drift and residual strength, if compared with the other models.

Future investigations shall be conducted to calibrate the cyclic behavior of interior joints, too, starting from the available cyclic experimental tests.

Moreover, joint axial failure should be better investigated and introduced into the model, starting from the analysis of some theoretical and empirical friction models that have been recently proposed in literature (Hassan and Moehle, 2013).

Appendix 5: M_j - τ_j relationship

Equilibrium equations to obtain the moment transferred through the rotational spring M_j as a function of the joint shear stress τ_j are reported in details in this Appendix. The symbology is the same adopted throughout the Chapter.

Exterior joints

$$V_n = T - V_c = \frac{M_b}{jd} - \frac{M_b}{\left(L_b - \frac{h_c}{2}\right)} L_b \frac{1}{2L_c} = \frac{M_b}{jd} - \frac{M_b}{\left(1 - \frac{h_c}{2L_b}\right)} \frac{1}{2L_c} = M_b \left(\frac{1}{jd} - \frac{1}{\left(1 - \frac{h_c}{2L_b}\right) 2L_c} \right)$$

$$\tau_j A_j = M_b \left(\frac{1}{jd} - \frac{1}{\left(1 - \frac{h_c}{2L_b}\right) 2L_c} \right)$$

$$\tau_j A_j \frac{1}{\frac{1}{jd} - \frac{1}{\left(1 - \frac{h_c}{2L_b}\right) 2L_c}} = M_b$$

$$\tau_j A_j \frac{1}{\frac{1}{jd} - \frac{1}{\left(1 - \frac{h_c}{2L_b}\right) 2L_c}} \left(\frac{1}{1 - \frac{h_c}{2L_b}} \right) = M_b \left(\frac{1}{1 - \frac{h_c}{2L_b}} \right) = M_j$$

$$\tau_j A_j \left(\frac{1}{\frac{1 - \frac{h_c}{2L_b}}{jd} - \frac{1}{2L_c}} \right) = M_b \left(\frac{1}{1 - \frac{h_c}{2L_b}} \right) = M_j$$

$$M_j = \tau_j A_j \frac{1}{\frac{1 - \frac{h_c}{2L_b}}{jd} - \frac{1}{2L_c}}$$

Interior joints

$$\begin{aligned}
 V_n = T + T' - V_c &= \frac{M_b + M'_b}{jd} - \frac{M_b + M'_b}{\left(L_b - \frac{h_c}{2}\right)} L_b \frac{1}{2L_c} = \frac{M_b + M'_b}{jd} - \frac{M_b + M'_b}{\left(1 - \frac{h_c}{2L_b}\right)} \frac{1}{2L_c} = \\
 &= (M_b + M'_b) \left(\frac{1}{jd} - \frac{1}{\left(1 - \frac{h_c}{2L_b}\right) 2L_c} \right) \\
 \tau_j A_j &= (M_b + M'_b) \left(\frac{1}{jd} - \frac{1}{\left(1 - \frac{h_c}{2L_b}\right) 2L_c} \right) \\
 \tau_j A_j \frac{1}{\frac{1}{jd} - \frac{1}{\left(1 - \frac{h_c}{2L_b}\right) 2L_c}} &= M_b + M'_b \\
 \tau_j A_j \frac{1}{\frac{1}{jd} - \frac{1}{\left(1 - \frac{h_c}{2L_b}\right) 2L_c}} \left(\frac{1}{1 - \frac{h_c}{2L_b}} \right) &= (M_b + M'_b) \left(\frac{1}{1 - \frac{h_c}{2L_b}} \right) = M_j \\
 \tau_j A_j \frac{1}{\frac{1 - \frac{h_c}{2L_b}}{jd} - \frac{1}{2L_c}} &= (M_b + M'_b) \left(\frac{1}{1 - \frac{h_c}{2L_b}} \right) = M_j \\
 M_j = \tau_j A_j \frac{1}{\frac{1 - \frac{h_c}{2L_b}}{jd} - \frac{1}{2L_c}} &
 \end{aligned}$$

References

- ACI 318-63. Building code requirements for reinforced concrete. Detroit, MI: American Concrete Institute (ACI), 1963
- ACI 318-71. Building code requirements for reinforced concrete (ACI 318-71) and commentary (ACI 318R-71). Detroit, MI: American Concrete Institute (ACI), 1971
- ACI Committee 352. 1991. Recommendations for design of beam-column joints in monolithic reinforced concrete structures (ACI 352R-91). American Concrete Institute, Farmington Hills, MI.
- Alath S, Kunnath SK. (1995). Modeling inelastic shear deformations in RC beam-column joints. Engineering mechanics proceedings of 10th conference, May 21–24, University of Colorado at Boulder, Boulder, Colorado, vol. 2. New York: ASCE: p. 822–5.
- Alsawat J M, and Saatcioglu M, (1992). Reinforcement Anchorage Slip under Monotonic Loading. Journal of Structural Engineering, ASCE, V. 118, No. 9, Sept. 1992, pp. 2421-2438.
- Altoontash A. (2004). Simulation and damage models for performance assessment of reinforced concrete beam-column joints. Ph.D. dissertation. Stanford (CA): Department of Civil and Environment Engineering. Stanford University.
- American Concrete Institute, Committee 369, ACI 369R-11. Guide for seismic rehabilitation of existing concrete frame buildings and commentary. Feb. 2011, USA.
- American Concrete Institute, Committee 369, ACI 369R-11. Guide for seismic rehabilitation of existing concrete frame buildings and commentary. Feb. 2011, U.S.A.
- Antonopoulos CP and Triantafillou TC (2003) Experimental investigation of FRP-strengthened RC beam-column joints. Journal of composites for construction, 7(1): 39-49.
- ASCE/SEI 41, Seismic rehabilitation of existing buildings. American Society of Civil Engineers, Reston, VA, USA, 2007.
- Bakir PG, Bodurođlu HM (2002). A new design equation for predicting the joint shear strength of monotonically loaded exterior beam-column joints. Engineering Structures; 24:1105–17.
- Beres, A., El-Borgi, S., White, R. N., & Gergely, P. (1992). Experimental results of repaired and retrofitted beam-column joint tests in lightly reinforced concrete frame buildings. In Technical Report NCEER (Vol. 92). US National Center for Earthquake Engineering Research.
- Beres, A., White, A.N., and Gergely, P. (1992). Seismic behavior of RC frame structures with nonductile details: Part I-Summary of experimental findings of full scale beam-column joint tests, Report NCEER-92-0024, NCEER, SUNY Buffalo, NY.
- Biddah A, Ghobarah A (1999), Modelling of shear deformation and bond slip in reinforced concrete joints. Structural Engineering; 7(4): 413–32.
- Celik OC and Ellingwood BR (2008). Modeling Beam-Column Joints in Fragility Assessment of Gravity Load Designed Reinforced Concrete Frames, Journal of Earthquake Engineering. 12:357-381.
- Celik, OC, and Ellingwood, BR (2010). Seismic fragilities for non-ductile reinforced concrete frames—Role of aleatoric and epistemic uncertainties, Structural Safety, 32(1): 1-12.

- CEN. European standard EN 1998-3. Eurocode 8: design provisions for earthquake resistance of structures – Part 3: assessment and retrofitting of buildings. European Committee for Standardisation, Brussels, 2005.
- Clyde C, Pantelides CP, Reaveley LD (2000). Performance-Based Evaluation of Exterior Reinforced Concrete Buildings Joints for Seismic Excitation, PEER Report, No. 2000/05, Pacific Earthquake Engineering Research Center, University of California, Berkeley, USA.
- Cosenza E, Manfredi G, Verderame GM (2006). A fibre model for push-over analysis of under-designed reinforced concrete frames, *Computers & structures*, 84(13): 904-916.
- Decreto Ministeriale del 14/1/2008. Approvazione delle nuove norme tecniche per le costruzioni. G.U. n. 29 del 4/2/2008, 2008. (in Italian)
- Di Ludovico M, Balsamo A, Prota A, Verderame GM, Dolce M, Manfredi G. Preliminary results of an experimental investigation on RC beam-column joints”, 6th International Conference on FRP Composites in Civil Engineering (CICE 2012), Rome, Italy, 13-15 June 2012, Paper 02-511.
- Ehsani, M.R., and Wight, J.K. (1985). Exterior reinforced concrete beam-to-column connections subjected to earthquake-type loading. *ACI Journal*, 82(4), 492-499.
- El-Amoury T, Ghobarah A (2002). Seismic rehabilitation of beam–column joint using GFRP sheets. *Engineering Structures*; 24:1397–407.
- Eligehausen R, Popov EP, and Bertero VV (1983) Local Bond Stress-Slip Relationship of a Deformed Bar Under Generalized Excitations, Report No. UCB/EERC 83/23, University of California-Berkeley, Berkeley, CA.
- Fabbrocino G, Verderame G, Manfredi G (2005) Experimental behaviour of anchored smooth bars in old type RC. buildings, *Engineering Structures*, 27(10): 1575-1585.
- Fabbrocino G, Verderame G M, Manfredi G, Cosenza E (2004) Structural models of critical regions in old-type RC frames with smooth rebars. *Engineering Structures* 26.14: 2137-2148.
- Federal Emergency Management Agency (1997). FEMA 273, Guidelines for the seismic rehabilitation. Washington, D.C.
- Federal Emergency Management Agency (2000). FEMA 356, Prestandard and Commentary for the Seismic Rehabilitation of Buildings. Washington, D.C.
- Filippou F C, Popov E P, and Bertero VV, (1983) Effects of Bond Deterioration on Hysteretic Behavior of Reinforced Concrete Joints, Report No. UCB/EERC 83/19, University of California-Berkeley, Berkeley, CA, 184 pp.
- Genesio G (2012) Seismic assessment of RC exterior beam-column joints and retrofit with haunches using post-installed anchors. Ph.D. thesis, University of Stuttgart, Germany.
- Hakuto S, Park R, Tanaka H. (2000) Seismic load tests on interior and exterior beam–column joints with substandard reinforcing details, *ACI Structural Journal*; 97(1):11–25.
- Hassan and Moehle (2013) Quantification of residual axial capacity of beam-column joints in existing concrete buildings under seismic load reversals, *Compdyn – Kos Island*, Greece, 12–14 June 2013.
- Hassan WM (2011) Analytical and Experimental Assessment of Seismic Vulnerability of Beam-Column Joints without Transverse Reinforcement in Concrete Buildings, PhD Dissertation, University of California, Berkeley, California, USA.

- Hegger J, Sherif A, Roeser W (2003). Non-seismic design of beam–column joints. *ACI Structural Journal*; 100(5):654–64.
- Hwang SJ, Lee HJ. (1999) Analytical model for predicting shear strength of exterior RC beam–column joints for seismic resistance. *ACI Structural Journal*; 96(5):846–57.
- Jirsa, O. J. and Marques, J. L. G. (1972). A study of hooked bar anchorages in beam-column joints. Austin, TX: University of Texas, 1972. Final Report - Reinforced Concrete Research Council, Project 33
- Kaku, T., and Asakusa, H. (1991). Bond and anchorage of bars in reinforced concrete beam-column joints. *ACI SP-123, Design of Beam-Column Joints for Seismic Resistance*, J.O. Jirsa, ed., American Concrete Institute, Detroit, MI., 401-423.
- Karayannis CG, and Sirkelis GM (2008) Strengthening and rehabilitation of RC beam–column joints using carbon-FRP jacketing and epoxy resin injection. *Earthquake Engineering & Structural Dynamics*, 37(5), 769-790.
- Kent D C, Park R. Flexural Members with Confined Concrete. *ASCE*,1971.97(ST7):1969-1990.
- Kim J. , and LaFave J.M. (2012) A simplified approach to joint shear behavior prediction of RC beam-column connections. *Earthquake Spectra* 28.3: 1071-1096.
- Kim, J., & LaFave, J. M. (2009). Joint shear behavior of reinforced concrete beam-column connections subjected to seismic lateral loading. Newmark Structural Engineering Laboratory. University of Illinois at Urbana-Champaign.
- Kim, J., and LaFave, J. M.(2007a) Key influence parameters for the joint shear behavior of reinforced concrete (RC) beam-column connections, *Engineering Structures* 29, 2523–2539.
- Kim, J., LaFave, J. M., and Song, J. (2007b) A new statistical approach for joint shear strength determination of RC beam-column connections subjected to lateral earthquake loading, *Structural Engineering and Mechanics* 27, 439–456.
- Krawinkler, H. and Mohasseb, S. (1987), Effects of panel zone deformations on seismic response, *Journal of Construction Steel Research*, 8, 233-250.
- Kurose, Y. (1987). Recent studies on reinforced concrete beam-column joints in Japan. Austin, TX: University of Texas, 1987. PMFSEL Report No. 87-8
- Lima C, Martinelli E., and Faella C. (2012) Capacity models for shear strength of exterior joints in RC frames: state-of-the-art and synoptic examination. *Bulletin of Earthquake Engineering* 10.3: 967-983.
- Lowes LN and Altoontash A. (2003) Modeling Reinforced-Concrete Beam-Column Joints Subjected to Cyclic Loading, *Journal of Structural Engineering*. 129:1686-1697.
- McKenna F, Fenves GL, Scott MH (2006) OpenSees: Open System for Earthquake Engineering Simulation. Pacific Earthquake Engineering Research Center. University of California, Berkeley, CA, USA. <http://opensees.berkeley.edu>.
- Model Code 2010-first complete draft (2010). Fédération Internationale du Béton fib/International Federation for Structural Concrete.
- Moiser, W.G. (2000). Seismic Assessment of Reinforced Concrete Beam–Column Joints, MSCE thesis, University of Washington. Seattle, WA.
- Monti G, Spacone E and Filippou E C (1993), Model for Anchored Reinforcing Bars under Seismic Excitations, Report UCB/EERC-93/08, University of California, Berkeley, Berkeley, CA, 1993,91 pp.

- Murty CVR, Rai D, Bajpai KK, Jain SK. (2003). Effectiveness of reinforcement details in exterior reinforced concrete beam–column joints for earthquake resistance. *ACI Structural Journal*;100(2):149–56.
- Nilsson, I. H. E. (1973). Reinforced concrete corners and joints subjected to bending moment. Stockholm: National Swedish Building Research, 1973.
- Otani S (1974) Inelastic analysis RC frame structures. *J StructDiv, ASCE*; 100(ST7):1433–49.
- Otani S, and Sozen MA (1972) Behavior of multistory reinforced concrete frames during earthquakes. University of Illinois Engineering Experiment Station. College of Engineering. University of Illinois at Urbana-Champaign.
- Pampanin S, Magenes G, Carr A (2003) Modelling of shear hinge mechanism in poorly detailed RC beam-column joints, Proceedings of the FIB 2003 symposium.
- Pampanin S, Moratti M, Calvi GM. (2002) Seismic behaviour of RC beam–column joints designed for gravity loads. In: 12th European conference on earthquake engineering. Paper no. 726.
- Pantazopoulou, S., and Bonacci, J. (1993). Consideration of questions about beam-column joints. *ACI Structural Journal*, 89(1).
- Pantelides CP, Hansen J, Nadeau J, Reaveley LD (2002) Assessment of Reinforced Concrete Building Exterior Joints with Substandard Details, PEER Report, No. 2002/18, Pacific Earthquake Engineering Research Center, University of California, Berkeley, USA.
- Park R (1997) A static force-based procedure for the seismic assessment of existing reinforced concrete moment resisting frames. *Bulletin of the New Zealand National Society for Earthquake Engineering*, 30(3), 213-226.
- Park S and Mosalam K M (2009). Shear Strength Models of Exterior Beam-Column Joints without Transverse Reinforcement. PEER report, 106.
- Park S and Mosalam KM (2013) Simulation of Reinforced Concrete Frames with Nonductile Beam-Column Joints, *Earthquake Spectra*, 29(1), 233-257.
- Park S and Mosalam KM, (2012b) Analytical model for predicting the shear strength of unreinforced exterior beam-column joints, *ACI Structural Journal* 109, 149–159.
- Park S, and Mosalam, KM, (2012c) Experimental investigation of nonductile RC corner beam-column joints with floor slabs, *Journal of Structural Engineering*, 139(1), 1-14.
- Park Sand Mosalam KM, (2012a) Parameters for shear strength prediction of exterior beam–column joints without transverse reinforcement. *Engineering Structures*, 36, 198–209.
- Park, S., and Mosalam, KM, (2012d) Experimental and Analytical Studies on Reinforced Concrete Buildings with Seismically Vulnerable Beam- Column Joints, PEER Report 2012/03.
- Paulay T and Priestley M J N (1992) Seismic design of reinforced concrete and masonry buildings. John Wiley & Sons.
- Paulay, T., and Scarpas, A. 1981. The behaviour of exterior beam-column joints. *Bulletin of the New Zealand National Society for Earthquake Engineering*, 14(3), 131-44.
- Priestley, M. J. N. 1 (1997) Displacement-based seismic assessment of reinforced concrete buildings. *Journal of earthquake Engineering* 1: 157-192.
- Ricci P, De Luca F, Verderame GM. 6th April 2009 L'Aquila earthquake, Italy: reinforced concrete building performance. *Bulletin of Earthquake Engineering* 9.1 (2010): 285-305.
- Scott (1992). Scott, R. H The effects of detailing on RC beam/column connection behaviour. In: *The Structural Engineer* 70 No. 18, pp. 318-324

- Scott B D, Park R, Priestley M J N. (1982), Stress-strain behavior of concrete confined by overlapping hoops at low and high strain rates. No 99-2, p. 13-27
- Scott, R. H., Feltham, I., Whittle R. T. (1994). Reinforced concrete beam-column connections and BS 8110. In: *The Structural Engineer* 72 (1994), No. 4, pp. 55-60
- Sezen H and Setzler EJ (2008) Reinforcement slip in reinforced concrete columns. *ACI Structural Journal*, 105(3).
- Shafaei, J., Hosseini, A., Marefat, M. S., and Ingham, J. M. (2014). Rehabilitation of earthquake damaged external RC beam-column joints. In *New Zealand Society for Earthquake Engineering Technical Conference and AGM*.
- Sharma A, Eligehausen R, Reddy GR (2011) A new model to simulate joint shear behavior of poorly detailed beam-column connections in RC structures under seismic loads, part I: exterior joints. *Engineering Structures*, 33(3), 1034-1051.
- Shin M and LaFave JM (2004a) Testing and modelling for cyclic joint shear deformations in RC beam-column connections. *Proceedings of the thirteenth world conference on earthquake engineering*. Paper no. 0301.
- Shin, M., and LaFave, J. M. (2004b) Modeling of cyclic joint shear deformation contributions in RC beam-column connections to overall frame behavior *Structural Engineering and Mechanics*, 18(5), 645-669.
- Soroushian P., Obaseki K., Nagi M.; and Rajas, M. C. (1988) Pullout Behavior of Hooked Bars in Exterior Beam-Column Connections. *ACI Structural Journal*, V. 85, No. 3pp. 269-276.
- Taylor, H. P. J. and Clarke, J. L. (1976). Some detailing problems in concrete frame structures. In: *The Structural Engineer* 54 No. 1, pp. 19-32
- Taylor, H. P. J. (1974). *The behaviour of in situ concrete beam-column joints*. London: Cement and Concrete Association, 1974. Technical Report
- Tsonos AG (2007) Cyclic load behaviour of reinforced concrete beam-column sub-assemblages of modern structures, *ACI Structural Journal*; 104(4):468-78.
- Tsonos AG and Papanikolaou KV (2003) Post-Earthquake Repair and Strengthening of Reinforced Concrete Beam-Column Connections (Theoretical & Experimental Investigation). *Bulletin-New Zealand society for earthquake engineering* 36.2: 73-93.
- Uzumeri SM (1977) Strength and ductility of cast-in-place beam-column joints. From the American Concrete Institute Annual Convention, Symposium on Reinforced Concrete Structures in Seismic Zones, San Francisco, 1974. No. SP-53.
- Vecchio FJ and Collins MP (1986) The modified-compression field theory for reinforced concrete elements subjected to shear. *J Amer Concr Inst*;83(2):219-31.
- Vollum RL and Newman JB (1999) Strut and tie models for analysis/design of external beam-column joints. *Mag Concr Res*;51(6):415-25.
- Wong, H. F.; Kuang, J. S.: Effects of beam-column depth ratio on joint seismic behaviour. *Structures and Buildings* 161 (2008); No. 2, pp. 91-101
- Wong HF (2005) Shear strength and seismic performance of non-seismically designed RC beam-column joints. Ph.D. thesis. Hong Kong University of Science and Technology.
- Youssef M, Ghobarah A (2001). Modelling of RC beam-column joints and structural walls". *Journal Earthquake Engineering*;5(1):93-111.

Chapter 6

INFLUENCE OF JOINT RESPONSE ON SEISMIC ASSESSMENT OF NON-CONFORMING RC FRAMES

In the seismic performance assessment of existing Reinforced Concrete buildings, non-ductile failures related to both columns and beam-column joint regions represent a critical issue.

A growing attention should be addressed to the behavior of non-ductile elements, starting from the classification of the failure typology of beams and columns and the analysis of the behavior of beam-column connections.

As explained in the previous Chapter, in typical existing buildings, seismic collapse safety might be significantly affected by the non-linear behavior of joints which are involved in the failure mechanisms because of poor structural detailing (e.g. lack of an adequate transverse reinforcement in joint panel, deficiencies in the anchorage or absence of any capacity design principle). Conventional modeling approaches consider only beam and column flexibility, although joints can provide a great contribution to the global deformability as well as a significant strength reduction.

In this Chapter, a numerical investigation on the influence of joint failures on the seismic performance at different performance levels of two RC case study frames - designed for gravity loads only and for seismic loads according to obsolete technical codes - is performed. A preliminary classification of joint failure typology within the frames and the definition of the corresponding nonlinear behavior are carried out. Structural models that explicitly include beam-column joints are built. In particular, the joint model proposed and presented in Chapter 5 was applied, in conjunction with modeling proposals from literature for interior joints and beam/column behavior.

A probabilistic assessment based on nonlinear dynamic simulations of the structural response is performed taking into account record-to-record variability and also highlighting the importance of column shear failure in under-designed RC buildings.

6.1 Introduction

Assessment of seismic performance of structures requires the development of nonlinear analysis models that can detect all possible local and global collapse modes.

Since, potential element deterioration and failure modes are a consequence of the design and detailing requirements, materials properties and structural system, once all failure typologies have been identified for a given structural system, the attention can be focused on a subset of likely collapse mechanisms by means of the analysis of experimental test data, engineering judgment, analytical models, and observations from past earthquakes. The identified collapse modes then serve as the basis for selecting appropriate simulation and damage models that can be used to predict structural seismic performance.

The building code requirements for modern special moment frames are designed to promote ductile and more desirable collapse modes, and to prevent the formation of the brittle collapse modes (ACI 2002; CEN 2005, DM 2008). The strong column – weak beam requirement promotes flexural hinging in beams before columns. Likewise, shear strength capacity design provisions for beams and columns should ensure that shear failure is highly unlikely in beam-column elements. Vice-versa, older RC moment frames, with minimal detailing requirements used in their design, are vulnerable to a wider range of possible collapse modes (Aycardi et al. 1994; Kurama et al. 1994; Kunnath et al. 1995; Kunnath et al. 1995; El-Attar et al. 1997; Filiatrault et al. 1998; Filiatrault et al. 1998). These structures have a demonstrated tendency to fail in soft story or column-hinging mechanisms (Liel, 2008), when they are designed for gravity loads only, or to exhibit joint failures (Celik and Ellingwood, 2008), also if old seismic codes are adopted for the design (Jeon et al. 2015). Moreover, column shear failure may occur, depending on the column's design and gravity loading (Elwood 2004). Less stringent detailing requirements may also promote lap-splice failure or pull-out of the bottom beam reinforcing bars anchored into the joint panel.

In particular, in seismic performance assessment of non-conforming (or “under-designed”) RC buildings, non-ductile failures related to both columns and beam-column joint regions represent a critical issue.

In this Chapter, a numerical investigation on the influence of joint failures on the seismic performance at different performance levels of two RC case study frames - designed for gravity loads only and for seismic loads according to an obsolete technical code - is performed. A preliminary classification of joint failure typology within the frames and the definition of the corresponding nonlinear behavior is carried out. Structural models that explicitly include beam-column joints are built. In particular, the joint model proposed and presented in Chapter 5 was applied, in conjunction with modeling proposals from literature for interior joints and beam/column behavior, as it will be explain in Section 6.2.

A probabilistic assessment based on nonlinear dynamic simulations of the structural response is performed taking into account record-to-record variability and also highlighting the importance of column shear failure in under-designed RC buildings.

6.2 Structural modeling

Analytical evaluation of seismic performance at different performance levels requires primarily the accurate modeling of nonlinear behavior and deterioration due to seismic loading for each of the constituent element in the structural system, such that all possible local and global collapse modes can be captured. Therefore, to ensure that the model faithfully represents the structure and its possible failure modes, accurate representation of material properties and deterioration of beam-column elements and joints is needed.

Nonlinear element models for RC beam-columns calibrated by Haselton et al. (2007) is adopted in this Chapter to capture the yielding, strain hardening, and spalling and rebar buckling that lead to degradation of strength and stiffness in the structure, as described in Section 6.2.1.

Modeling of joint shear behavior in beam-column joints is the focus of Section 6.2.2.

Dynamic analyses are performed in two conditions: (i) with “rigid joints”, assuming a very high stiffness and shear strength for beam-column connections and (ii) “with joints”, explicitly modeling the nonlinear behavior of joints.

An overview of the frame modeling is shown in Figure 6.1 and it will be described more in details in Sections 6.2.1 and 6.2.2.

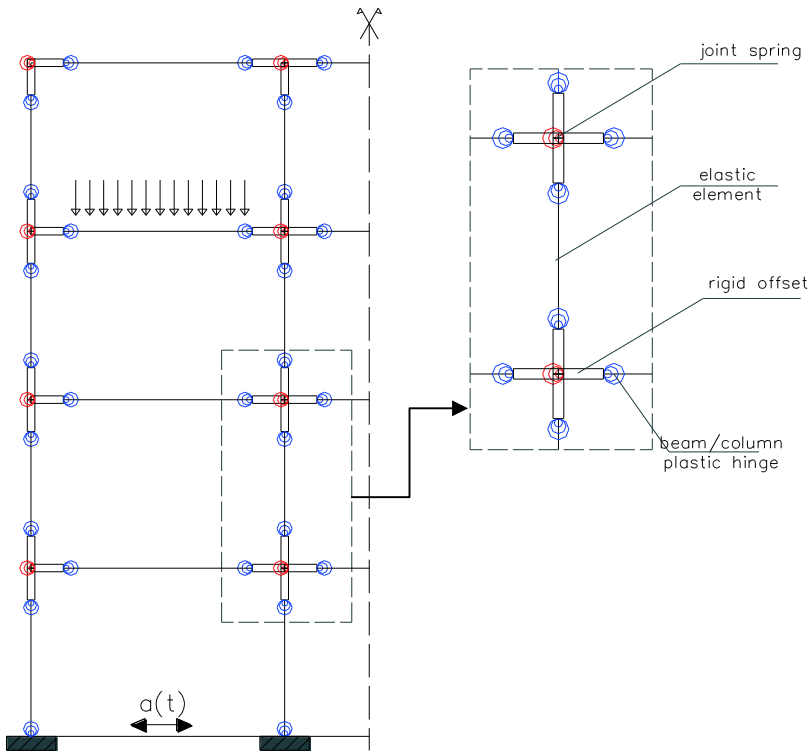


Figure 6.1. Adopted structural modeling

It is worth noting that, despite the care taken in developing nonlinear analysis models, the simulation model is not able to capture all possible collapse modes, in particular degrading behavior after shear failures in columns and axial load failure in beam-column joints. To avoid non-conservative under-prediction of collapse fragility, these non-simulated failure modes should be at least considered by post-processing the dynamic analyses results to determine whether these failure modes may occur before the conventional collapses that were explicitly simulated.

In particular, in non-ductile RC frame structures, columns are potentially vulnerable to brittle shear failure, a failure that may eventually cause collapse of a portion of the structure when the column loses its ability to carry gravity loads. In this study, for the columns which are expected to yield before failing in shear, the model described in Section 6.2.1 captures the important aspects of

strength and stiffness deterioration as the column yields and, subjected to increasing deformations, fails in shear. However, the model cannot capture explicitly the onset of shear failure and the subsequent axial collapse of column, because the column model does not incorporate axial-shear interaction. Post-processing for identifying this non-simulated failure mode is discussed in detail in Section 6.2.3.

Likewise, axial failure in beam-column joints regions will be detected in post-processing because of the lack of experimental data and reliable models that allow to capture this failure mode explicitly in the modeling.

6.2.1. Beams and columns modeling

The choice of the model for nonlinear response and deterioration related to beam-column flexural hinging is discussed in more detail in this Section.

Either fiber-type or lumped plasticity models could be used to model behavior associated with flexural deterioration, as discussed in Chapter 2. In this Chapter, a lumped plasticity model, calibrated to reproduce the effects of yielding, spalling and bar buckling, is used in the numerical model for RC elements.

While lumped plasticity models lack the detail and spread-plasticity capabilities of fiber models, they can be properly calibrated on the basis of data from experimental tests to capture the deterioration associated with rebar buckling and stirrup fracture leading to loss of confinement (Ibarra 2003, Haselton 2006). Fiber-type models were judged unsuitable for simulating structural collapse because available steel material models are not able to replicate the behavior of rebar as it buckles or fractures (Haselton, 2006).

Lumped plasticity models also account for bond-slip that occurs in regions of high bond stresses in beam-column joints. Also rebar pull-out and the resulting loss in strength could be accounted for by introducing an additional spring, defined similarly to the modeling approach suggested in Chapter 5. However, in the analyzed cases, the latter possible failure is excluded, by assuming that a sufficient anchorage length or efficient anchorage devices are guaranteed, as common construction practice provided for, especially for seismic designed structures.

The lumped plasticity model adopted herein to simulate plastic hinges in beam-column elements utilizes a nonlinear spring model developed by Ibarra,

Medina, and Krawinkler (2005), implemented in OpenSees by Altoontash (2004), and calibrated by Haselton et al. (2007).

Figure 6.2 shows the tri-linear monotonic backbone curve, together with associated hysteretic behavior of the model.

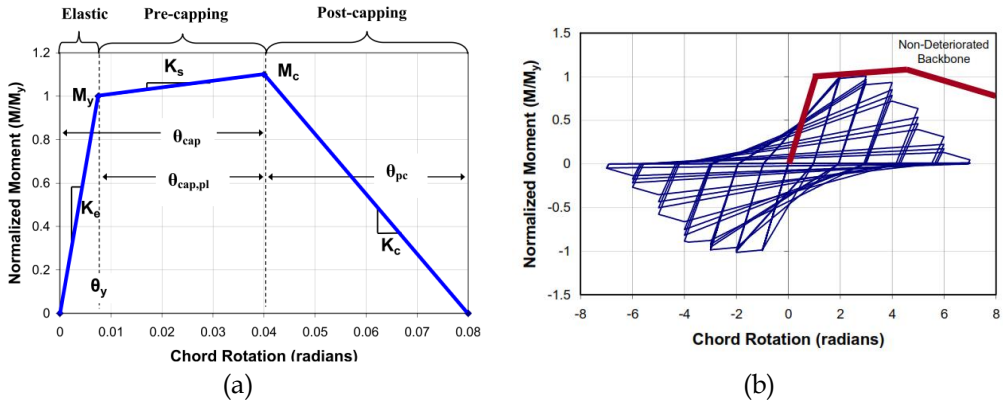


Figure 6.2. Monotonic backbone (a) and hysteretic degradation (b) in model by Haselton et al (2007)

Even if the model cannot capture the effect of the variation in axial load during the analysis (such as the majority of lumped-plasticity approaches), it simulates the post-peak response, modeling the strain softening behavior associated with concrete crushing, rebar buckling and fracture. The model also captures four modes of cyclic deterioration: strength deterioration of the inelastic strain hardening branch, strength deterioration of the post-peak strain softening branch, accelerated reloading stiffness deterioration, and unloading stiffness deterioration. Cyclic deterioration is based on an energy index that has two parameters: normalized energy dissipation capacity, λ , and an exponent term to describe how the rate of cyclic deterioration changes with accumulation of damage, c .

Direct modeling of cyclic degradation is adopted in this model, which begins with a monotonic backbone curve and degrades this relationship as the analysis proceeds (Ibarra et al. 2005, Haselton et al. 2007).

In total, the model requires the specification of seven parameters to control the monotonic and cyclic behavior (see Figure 6.2a): yielding moment (M_y), elastic stiffness (K_e), strength hardening ratio (M_c/M_y) - that is a measure of post-yield stiffness -, plastic rotation at peak strength ($\theta_{cap,pl}$), post-peak plastic rotation (θ_{pc}) - that is related to the post-capping stiffness -, and two parameters for cyclic degradation (λ and c). The model can also assign a

residual strength, as a function of the ultimate strength. In this research, 1% residual strength is used for all beams and columns to avoid problems with numerical convergence. It is likely that RC beams and columns actually have higher residual strength such that the model is quite conservative, but it is difficult to quantify on the basis of available experimental data (Liel, 2008).

In order to evaluate numerically each of the required parameters, the Ibarra model parameters have been calibrated to 255 experimental tests of RC columns by Haselton et al. (2007). The calibration of the beam-column element model to the data from each experimental test follows a standardized procedure, placing a particular emphasis on correct calibration of the capping point and post-capping strength deterioration, which can have a significant impact on structural collapse prediction.

These calibrations provided empirical equations relating the design parameters of a beam or column to the modeling parameters needed for input in the lumped plasticity model.

The database adopted for the calibration includes RC columns with both ductile and non-ductile detailing, and varying levels of axial load and geometries and, for each, reports force-displacement history and other relevant data. Approximately 35 of the 255 column tests have non-ductile detailing and failed in flexure-shear, as expected for the older RC columns of interest in this study. However, the model cannot capture explicitly the onset of shear failure with the subsequent axial collapse of column, because the column model does not incorporate axial-shear interaction. Post-processing for identifying this non-simulated failure mode is discussed in detail in Section 6.2.3.

6.2.2. Joints modeling

To capture nonlinear behavior and deterioration associated with degradation of shear strength and stiffness in the beam-column joint regions, the shear panel is modeled with an inelastic rotational spring and rigid offsets spreading into the joint panel, namely by means of the so-called scissors model (Alath and Kunnath, 1996).

A review of the modeling approaches for beam-column joints existing in literature was carried out in Chapter 2, with a particular focus on exterior unreinforced joints.

It was pointed out that models with multiple nodes and multiple springs (e.g. Lowes and Altoontash, 2003; Shin and LaFave, 2004b; Sharma et al., 2011) allow to capture more realistically the joint panel kinematic behavior and simulate the horizontal translation that can occur between the centerlines of the columns above and below the joint. Vice-versa, the scissors model by Alath and Kunnath (1996) does not capture this possible kinematic response, but it is the simplest and computationally less demanding joint model and it seems to be sufficiently accurate in predicting the experimental beam-column joint panel response for simulating the seismic response of non-conforming RC frames for purposes of fragility assessment and performance-based earthquake engineering (Celik and Ellingwood, 2008).

Therefore, both for exterior and interior joints, the scissors model has been adopted. No springs at the interface between the joint panel and the adjacent beam representing the bond-slip contribution are introduced in these analyses because the deformability contribution due to bond slip is already accounted for in beam/column rotational springs.

The joint panel model adopted herein for exterior joints is implemented by defining duplicate nodes, node A (master) and node B (slave), with the same coordinates at the center of the joint panel. Node A is connected to the column rigid link and node B is connected to the beam rigid link. A zero length rotational spring connects the two nodes and allows only relative rotation between them through a constitutive model which describes the shear deformation of the joint panel zone, and that is different for exterior and interior joints. In both cases, such a rotational spring is defined as a quadrilinear moment (M_j) – rotation (γ_j) spring characterized by four points for J- and BJ-mode of failure, separately: cracking, pre-peak, peak and residual points.

In particular, in this study, the model proposed and presented in Chapter 5 is adopted for exterior joints. The proposed model provides the backbone of the joint moment-rotation relationship. The calibration of the cyclic behavior, that is essential to perform dynamic nonlinear analyses, is carried out (see Section 6.2.2.1) including cyclic degradation in unloading and reloading stiffness and pinching effects.

Moreover, the calibration of the joint moment-rotation relationship proposed by Celik and Ellingwood (2008), within the modeling approach of the scissors model, is adopted for interior joints, as explained in Section 6.2.2.2.

6.2.2.1 Exterior joints

As shown in Chapter 5, the joint panel zone model for exterior unreinforced joints was calibrated through tests well documented in the literature, different for the failure mode they exhibited, namely J-failure (by Pantelides et al., 2002 – here referred to as Pant2, Pant3, Pant5, Pant6) and BJ-failure (by Clyde et al., 2000 – here referred to as Cly2, Cly4, Cly5, Cly6), for which experimental stress-strain relationships for joint panel were available. Key parameters defining the quadri-linear backbone of the joint rotational spring have been described in details in Chapter 5.

The same test adopted for the calibration of the backbone are considered to calibrate the cyclic behavior of the joint shear stress-strain response of these typology of joints.

The calibration is performed in OpenSees (McKenna et al. 2010) on the basis of the hysteresis rules characterizing the Pinching4 material, so that the obtained parameters can be practically employed in modeling of RC frames.

Pinching4 material (see Figure 6.3) is a four-points uniaxial material developed by Lowes et al. (2003) and belonging to the library of OpenSees, that allows to model the cyclic degradation of unloading and reloading stiffness (through the parameters g_k and g_D , respectively), degradation in strength (through the parameters g_F) and pinching effects (through the parameters $rDisp$, $rForce$ and $uForce$).

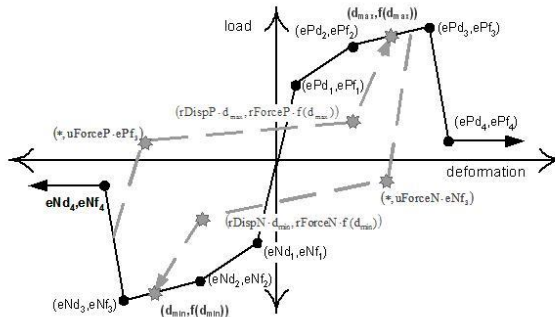


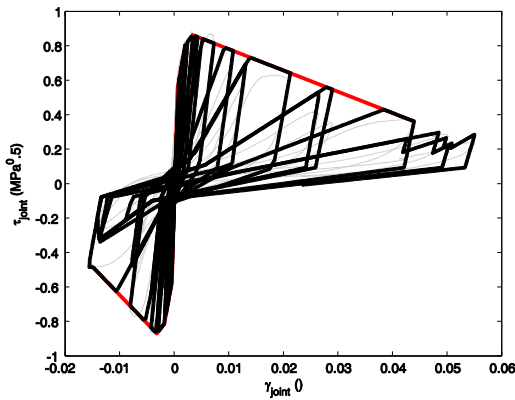
Figure 6.3. Pinching4 uniaxial material (Lowes et al. 2003)

Calibration of these key parameters was performed starting from the experimental shear stress-strain backbones (the same adopted in Chapter 5 to

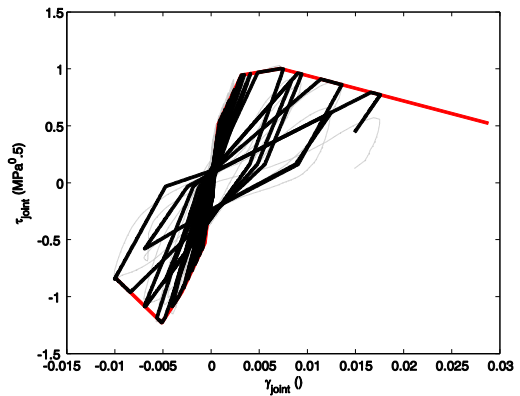
calibrate the numerical backbone) and minimizing the error in terms of energy dissipated between the numerical and the experimental response. No degradation in strength was introduced since it is already included in the backbone of the joint response obtained from experimental data.

In Figure 6.4 numerical and experimental cyclic responses are compared: experimental backbone and cyclic response are reported in red and grey, respectively; numerical cyclic response is reported in black.

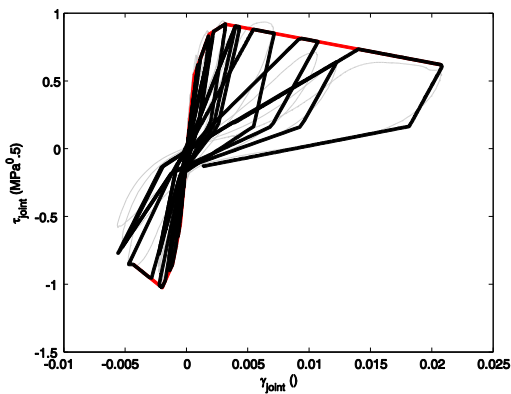
From these figures, it can be seen that the analytical results are well-correlated with experimental results with regard to un-loading stiffness, and pinching effects.



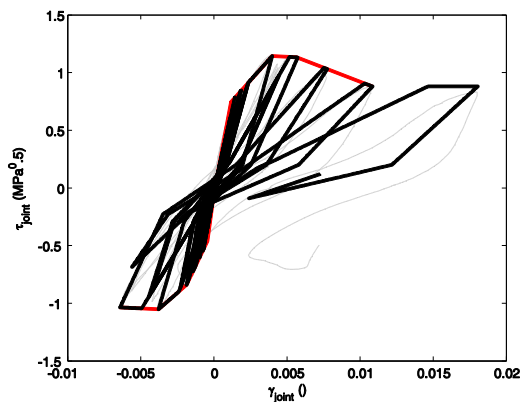
(a)



(b)



(c)



(d)

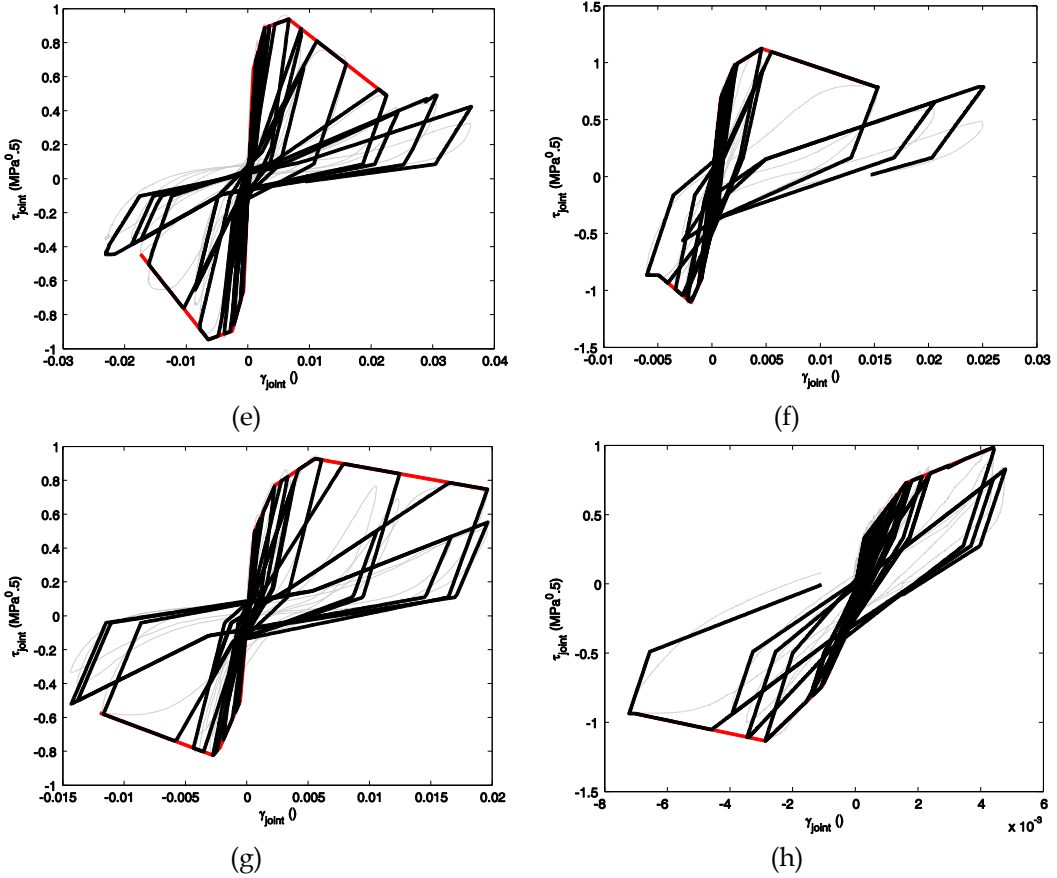


Figure 6.4. Cyclic behavior calibration for tests by Pantelides (a, c, e, g); Clyde et al. (2000) (b, d, f, h). Experimental backbone and cyclic response are reported in red and grey, respectively; numerical cyclic response is reported in black.

Table 6.1 presents the modeling parameters of the Pinching4 material (in positive “P” and negative “N” loading directions) adopted to obtain a good fit of the experimental response of the analyzed non-ductile exterior beam-column joints. The mean value of these parameters will be utilized in structural analyses for a probabilistic performance assessment.

	Pant2	Pant3	Pant6	Pant5	Cly2	Cly4	Cly5	Cly6	Mean	Adopted
rDisp P	0.2	0.2	0.2	0.2	0.1	0.2	0.2	0.2	0.19	0.16
rDisp N	0.2	0.2	0.2	0.2	-0.1	0.2	-0.1	0.3	0.14	
rForce P	0.2	0.2	0.2	0.2	0.2	0.2	0.2	0.2	0.20	0.23
rForce N	0.2	0.2	0.2	0.2	0.2	0.2	0.4	0.4	0.25	
uForce P	-0.2	-0.2	-0.2	-0.05	-0.05	-0.25	-0.2	-0.5	-0.21	-0.22
uForce N	-0.2	-0.2	-0.2	-0.2	-0.2	-0.2	-0.2	-0.4	-0.23	
gK1	0.9	0.9	0.9	0.8	0.9	0.95	0.95	0.5	0.85	0.85
gK3	0.1	0.1	0.1	0.1	0.1	0.2	0.15	0.1	0.12	0.12
gKlim	0.95	0.95	0.95	0.95	0.95	0.99	0.95	0.95	0.96	0.96
gD1	0.35	0.35	0.35	0.35	0.25	0.35	0.6	0.4	0.38	0.38
gD3	0.15	0.15	0.15	0.15	0.15	0.15	0.9	0.9	0.34	0.34
gDlim	0.95	0.95	0.95	0.95	0.95	0.95	0.99	0.99	0.96	0.96

$gF1 = gF2 = gF3 = gF4 = gFlim = 0; gK2 = gK4 = 0; gD2 = gD4 = 0.$

Table 6.1. Parameters adopted to reproduce the hysteretic behavior of exterior unreinforced joints in Pinching4 material

6.2.2.2 Interior joints

The joint moment-rotation constitutive relationship proposed by Celik and Ellingwood (2008) is adopted in this study for interior joints.

This relationship was based on a statistical analysis carried out on the basis of experimental tests.

As shown in Chapter 2, Celik and Ellingwood also suggested that the shear stress-strain backbone curve for the panel zone in typical non-conforming RC beam-column joints can be defined through four key points, which correspond to joint shear cracking, reinforcement yielding, joint shear strength or contemporary achievement of adjoining beam or column capacity, and residual joint strength, respectively. The ordinates of the backbone points were reduced if the shear failure of the joint occurs before beams or columns reach their capacities. Shear failure of the joint is assumed to depend on the kind of joint (interior/exterior) and the anchorage conditions.

In particular, the abscissas of the four key points $\gamma_{j,cr}$, $\gamma_{j,y}$, $\gamma_{j,max}$, $\gamma_{j,res}$, typically fall within the following ranges: 0.0001-0.0013, 0.002-0.010, 0.01-0.03, and 0.03-0.10 radians, respectively. Joint shear strength $\tau_{j,max}$ is proposed in analogy with ASCE-SEI/41 prescription (as explained in Chapter 2) and it falls within

the range $0.75-1.00(\text{MPa})^{0.5}$ for interior beam-column joints. Residual strength is assumed equal to shear stress corresponding to joint cracking (evaluated by means of Uzumeri 1977 formulation).

Mean values of the proposed ranges are adopted in this study, since modeling uncertainties are not considered in structural analyses herein.

The relationship between joint strength and joint moment were reported in Appendix 5, for interior joints also.

The proposal by Celik and Ellingwood also included joint moment-rotation constitutive relationship for exterior joints. However, from the analysis of the experimental dataset they adopted, it was observed that the proposed joint shear strain values for the four key points are related to interior joints tests only; such values are very high if compared with shear strain values obtained from experimental tests on exterior beam-column joints. Therefore, the proposal by Celik and Ellingwood is adopted for interior joints only.

In the proposal by Celik and Ellingwood (2008), anchorage failure was also taken into account through a reduced envelope for the joint shear stress-strain relationship. However, in this study, no reduction of joint shear stress is considered, since the hypothesis that a sufficient anchorage length or efficient anchorage devices are guaranteed, thus excluding this failure mode.

The advantage of this model is that, by proposing that joint strength should be assumed as the minimum between empirical shear strength and the maximum joint shear stress related to beam/column flexural capacity, it is the only one able to reproduce the softening response of the joint panel also when a BJ-failure occurs. This is in accordance with the modeling adopted for exterior joints (since the nature of the strength model by Park and Mosalam 2012 adopted for exterior joints) and with observed experimental results (Park and Mosalam 2013), which showed that beam-column intersections always exhibited a degradation response if joint cracking was occurred.

Moreover, the backbone is calibrated on the basis of experimental tests and a range of values of shear strength and strain capacity for each characteristic point is also proposed with a uniform probability distribution (Celik and Ellingwood, 2010), so that the model can be easily adopted in future structural analysis devoted to a seismic performance evaluation that takes into account also modeling uncertainties.

Furthermore, since the proposal by Celik and Ellingwood suggests only pinching parameters to model joints hysteretic response, the parameters

calibrated by Jeon et al. (2015) for the Pinching4 material in OpenSees for the hysteretic response of interior joints are adopted herein. However, these parameters are modified so that no strength degradation was taken into account (since strength degradation is already included in the backbone of the joint response obtained from experimental data).

It is worth noting that, in order reproduce the softening response of the joint when a BJ-failure occurs - as observed experimentally (e.g. Park and Mosalam 2013) - also for interior joints, the adjacent beams have to be modeled with no post-peak strength degradation. In fact, in the case of BJ failure, the peak strength of interior joints is defined as the maximum shear stress corresponding to the contemporary achievement of flexural capacity in both the adjacent beams. If beam response degrades after its peak is reached, it is highly unlikely that this condition can be achieved during the analysis thus leading the interior joint to go through its softening branch. Since the adjacent beams are in series with the joint panel spring, it was necessary to model the beams response as perfectly-plastic after the peak strength is reached. In this way, the contemporary achievement of peak strength in the adjacent beams can be obtained and thus the joint can reach its peak strength, then starting to degrade. For the same reasons, no degradation in strength should be modeled in beams.

6.2.3. *Post-processed failure modes*

The simulation model is not able to capture all possible collapse modes, in particular degrading behavior after shear failures in columns and axial load failure in beam-column joints. To avoid non-conservative under-prediction of seismic fragility, these non-simulated failure modes are detected in this study by post-processing dynamic analyses results.

6.2.3.1 *Shear failure in columns*

Shear failure of beams and columns is characterized by shear cracking in concrete and yielding, pull-out or fracture of transverse reinforcement. This mode of deterioration is particularly dangerous for columns with significant axial load, as shear failure can lead to subsequent vertical collapse of the column (Elwood and Moehle 2005). Modeling the cyclic response of a RC element experiencing shear deterioration is complex due to the interactions of

shear, moment, and axial forces, as well as the overall brittle nature of the deterioration mode.

The review of previous researches on the shear behavior of existing columns carried out in Chapter 2 indicated that it is quite difficult that column shear models satisfy all the needed requirements of accuracy, computationally efficiency and compatibility with existing software programs. Although the problem is still an open and important issue, in the present work the attention will be not directly focused on this topic, but shear failures are detected by post-processing the dynamic analyses.

In fact, even if the calibration of beam/column behavior (explained in Section 6.2.1) took into account also few experimental tests on “non-ductile” columns, the model is not suitable to detect directly shear failure and the subsequent axial collapse of column. Therefore, where this failure mode is not prevented through capacity design provisions, as in the analyzed frames, post-processing of dynamic analysis data is necessary to account for possible column collapse associated with shear failure.

To this end, in this study, two different approaches are adopted:

- a force-based approach, that detects the onset of shear failure when shear demand on the column overcomes shear strength;
- a displacement-based approach, that detects the onset of shear failure when column drift ratio overcomes a certain capacity limit.

Anyway, the degradation in column response after shear failure up to the subsequent axial collapse cannot be properly detected in both these approaches.

For the first approach, the shear strength model by Sezen and Moehle (2004) (see Eq. 6.1) has been adopted in the hypothesis that no strength degradation occurs after yielding (namely, the coefficient k in Eq. (6.1) is equal to 1) (as in Jeon et al. 2015).

$$V_n = k \cdot (V_c + V_s) = k \left(\frac{\sqrt{f_c}}{a/d} \sqrt{1 + \frac{P}{0.5\sqrt{f_c} A_g}} 0.8A_g + \frac{A_{st} f_{yt} d}{s} \right) \quad (6.1)$$

In Eq. (6.1), V_c and V_s are the contributions of concrete and transverse reinforcement, respectively, to the overall shear strength; P , A_g and f_c represent axial load, gross area and concrete strength (in MPa), respectively; a/d is the

shear span-to-effective depth ratio; A_{st} and f_y , represent transverse reinforcement area and steel yielding strength, respectively. The coefficient k represents shear strength degradation due to cyclic loading and varies from 1 (no degradation condition) to 0.7 (maximum shear strength degradation).

This approach can be considered exact only if column fails in shear before the beginning of shear strength degradation, namely when total ductility demand is lower than the ductility demand at which shear strength degradation begins (i.e. 2 in model by Sezen and Moehle, 2004).

In the second approach, fragility functions developed by Aslani (2005) on the basis of 92 cyclic tests of RC columns are adopted. Aslani (2005) defines four damage states for flexure-shear critical RC columns: light cracking, severe cracking, shear failure and loss of axial carrying capacity. Lognormal fragility functions predict the probability of being in each damage state as a function of the column drift ratio, column axial load ratio and amount of transverse reinforcement.

Column drift ratio is analogous to the more commonly used interstory drift ratio, except that it excludes the drift that occurs due to rotation of the beams and deformations in joints, because the fragility functions are largely based on data from column component tests. Column drift ratio in this study are obtained directly from dynamic analysis and approximated to the interstory drift. The third damage state (DS3) is used to identify the onset of column shear failure, manifested by the characteristic X-cracking and yielding of transverse reinforcement. The related equation that provides IDR capacity at DS3 is reported in Eq. (6.2):

$$IDR_{DS3} = \frac{1}{0.26 \frac{P}{A_g f_c \rho''} + 25.4} \geq \frac{1}{100} \quad (6.2)$$

In Eq. (6.2), P , A_g , f_c , ρ'' represent axial load, gross area, concrete strength and transversal reinforcement ratio in column, respectively.

It is worth noting that, in a displacement-based approach, such as the approach described above, as well as other approaches existing in literature (e.g. Elwood, 2004), shear failure will be detected anyway (when IDR demand overcomes a certain minimum demand - generally 1%), even if nonlinear

behavior of the element should be classified as ductile, based on the comparison between degrading shear strength model and plastic shear or according to other classification criteria. Thus, a classification of the element behavior (ductile/ brittle) and the consequent choice of the related more suitable modeling approach should be always carried out.

6.2.3.2 Axial failure in beam-column joints

Likewise, axial failure in beam-column joint regions will be detected in post-processing because of the lack of experimental data and reliable models that allow to capture this failure mode explicitly in numerical modeling. Unfortunately very few unconfined joint tests are available with confirmed axial failure, since, generally, during laboratory joint tests, a common practice has been to terminate the test after dropping to 80% of lateral load resistance without testing the axial capacity of the joint.

In this study, the empirical shear-friction capacity model proposed by Hassan and Moehle (2013) calibrated on the basis of available experimental data is adopted. The expression of the IDR threshold ($IDR_{Ax,J}$) that identifies the onset of joint axial failure is reported in Eq. (6.3):

$$IDR_{Ax,J} = 0.057 \cdot \left(\frac{P \cdot \text{tg} \theta}{A_{sb} \cdot f_{yb}} \right)^{-0.5} \quad (6.3)$$

where P is the axial load acting on the joint, A_{sb} and f_{yb} are longitudinal reinforcement area and strength, respectively, of the bottom beam bars, and θ represents the shear critical angle, as reported in Hassan and Moehle (2013).

Such a proposal leads to a test-to-model drift capacity ratio equal to 1.07 and COV of 0.26.

Thus, axial failure in joints is assumed to occur when IDR during the analysis achieves the limit value $IDR_{Ax,J}$.

6.2.4. Modeling limitations

The nonlinear simulation model developed for non-ductile RC frame structures is an idealization of the structural geometry, loading and dynamic behavior, but it has some deficiencies that may limit the generalization of the results.

First of all, the simulation model for RC frames is a two-dimensional planar analysis of the lateral resisting system, thus drastically reducing the computational efforts required by a three-dimensional structure. Nevertheless, a two-dimensional model cannot capture the effects of bidirectional loading, torsion, or floor diaphragm flexibility in the analysis. Columns are likely to be much more highly stressed under biaxial loading. The lack of three-dimensional loading on the columns is partially compensated for by designing the columns only for loading in one direction, so that, both the capacity of the column and the demand on the column are underestimated from the real, three-dimensional situation.

In addition to the limitation in detecting post-shear failure behavior, further limitations are present in modeling of element deterioration and collapse modes of RC frame structures. Behavior related to flexural hinging, which is modeled using a lumped plasticity material model calibrated to experimental data for RC columns, lacks flexural-axial interaction, and thus cannot simulate changes in axial load due to overturning. Moreover, there is a need for columns tested at large deformations so as to permit more accurate calculation of post-peak response and there is a need for pairs of an higher number of identical columns tested under monotonic and various types of cyclic loading protocols (Haselton et al. 2007).

Additionally, the model does not incorporate masonry infills and non-structural components. The effects of infills on structural response was shown in Chapter 3 within a N2 framework, and they are not reproduced herein in order to clearly highlight the influence primarily of joints on seismic response. It is clear that a future effort to take into account joints and infills and above all their possible interaction is decidedly necessary and it is still an open issue.

6.3 Case study frames

Two symmetric four-story three-bay frames are designed, modeled as explained in Section 6.2, and assessed. These case-study frames are the internal frames of a structure with 5 m- transverse bay (L_y). Figure 6.5 represents a schematic frontal and in-plane view of the frames. Table 6.2 summarizes longitudinal and transverse bay-lengths (L_1, L_2, L_3 and L_y) and the interstorey height (H).

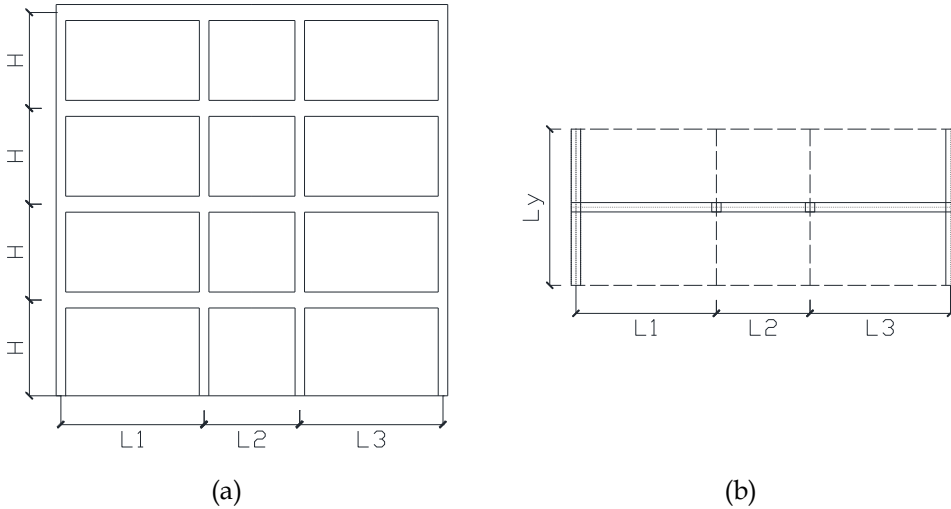


Figure 6.5. Case-study frames: frontal (a) and in plane (b) view

L_y	H	L_1	L_2	L_3
(m)	(m)	(m)	(m)	(m)
5.0	3.0	4.5	3.0	4.5

Table 6.2. Geometric dimensions of the case-study frames

Expected levels of gravity loading are applied to the model, including the computed dead load and live load for dwellings, as reported in Table 6.3. These expected gravity loads are also used in defining seismic masses, which are assigned at each floor of the building. Since, the analyzed frames are representative of internal frames, the tributary width used in determining the seismic mass is equal to the bay width L_y .

Story	$G_{k1}+G_{k2}$ kN/m ²	Q_k kN/m ²
1,2,3	7	2
4	5	1

Table 6.3. Dead and live loads applied for design and assessment

The first case-study frame (hereinafter referred to as OLD SLD) is intended to be realized in 1980s after the Irpinia earthquake (1980) and it is designed by means of a simulated procedure according to an obsolete technical code (Decreto Ministeriale 1975) in force in Italy until 1990s, by means of the allowable tensile stress method. The structure is located in a first-category site, corresponding to a design horizontal acceleration equal to 0.1g. Element dimensions are calculated according to the allowable stresses method; the design value for maximum concrete compressive stress is assumed equal to 6.0 and 8.0 MPa for axial load (σ_c) and axial load combined with bending ($\sigma_{c,t}$), respectively. Reinforcing bars (FeB38K) are deformed and their allowable design stress (σ_s) is equal to 220 MPa. Section dimensions are (30x50) cm² for beams and columns of the third and fourth levels, and (30x60) cm² for beams and columns of the first and the second levels. Stirrups spacing in columns was defined as the minimum amount of transverse reinforcement required by the adopted code. The complete characterization of this frame is reported in Figure 6.6.

The second one (hereinafter referred to as GLD) is designed by means of a simulated design procedure according to code prescriptions and design practices in force in Italy in 1970s for gravity loads only (Decreto Ministeriale 1972). The structural configuration follows the parallel plane frames system. Beams in transverse direction are present only in the external frames. Element dimensions are calculated according to the allowable stresses method; the same design values for maximum concrete compressive stress and steel stress adopted in the OLD SLD frame are used also for GLD frame. Column dimensions are calculated according only to the axial load based on the tributary area of each column, beam dimensions and reinforcement are determined from bending due to loads from slabs. Section dimensions are (30x50) cm² for beams, and (30x30) cm² for all columns, except than for the internal columns at the first story, where columns section is (30x40) cm². Stirrups spacing in columns was defined as the minimum amount of transverse reinforcement required by the adopted code. The complete characterization of this frame is reported in Figure 6.7.

Expected values of material properties adopted in the simulated design procedure and in the assessment phase for both frames are summarized in

Table 6.4, where f_c , f_y and f_{yw} represent concrete compressive strength, steel yielding strength for longitudinal and transverse reinforcement, respectively.

Simulated design			Assessment		
σ_s	$\sigma_{c,c}$	$\sigma_{c,f}$	f_c	f_y	f_{yw}
(MPa)	(MPa)	(MPa)	(MPa)	(MPa)	(MPa)
220	6.0	8.5	20	450	450

Table 6.4. Material properties

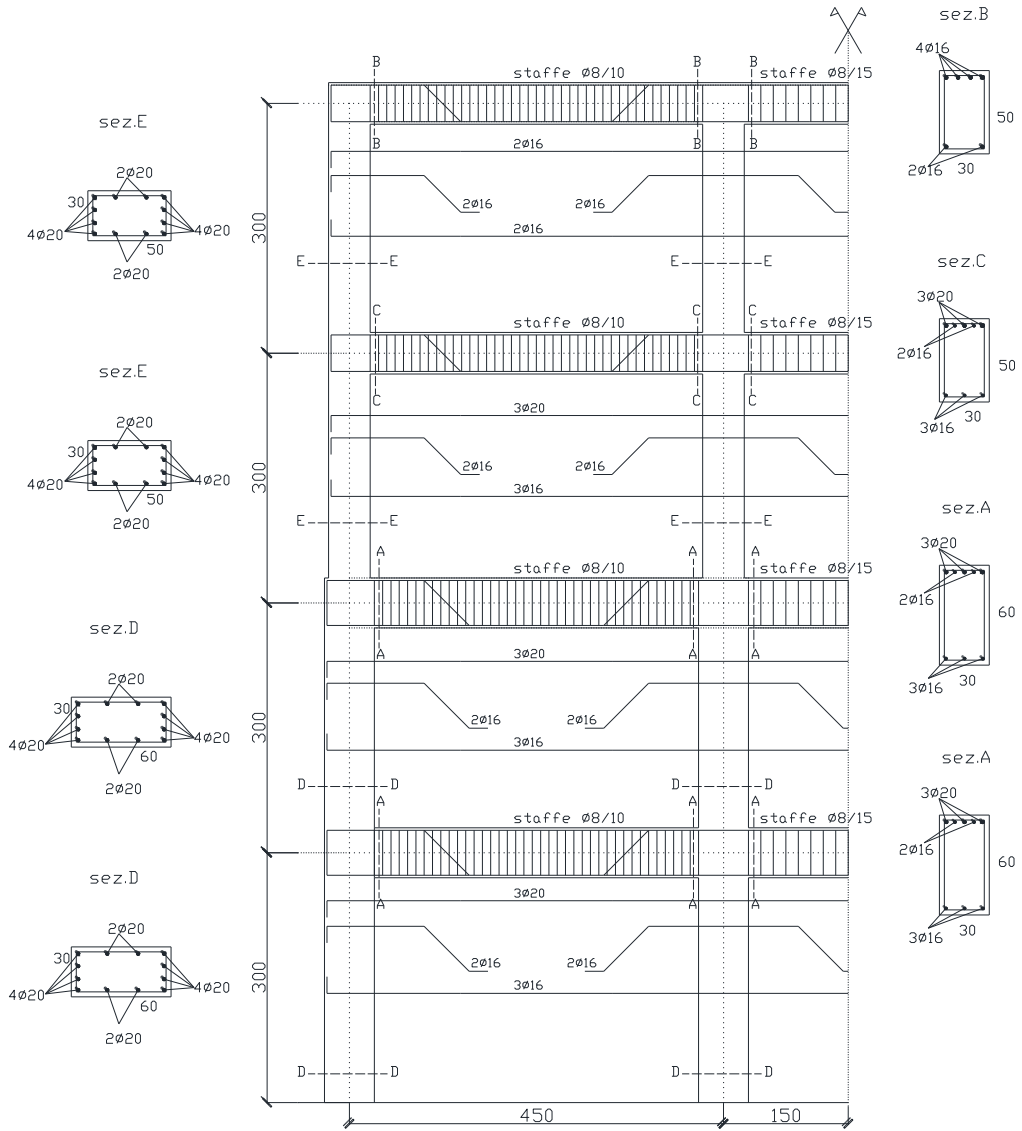


Figure 6.6. OLD SLD frame

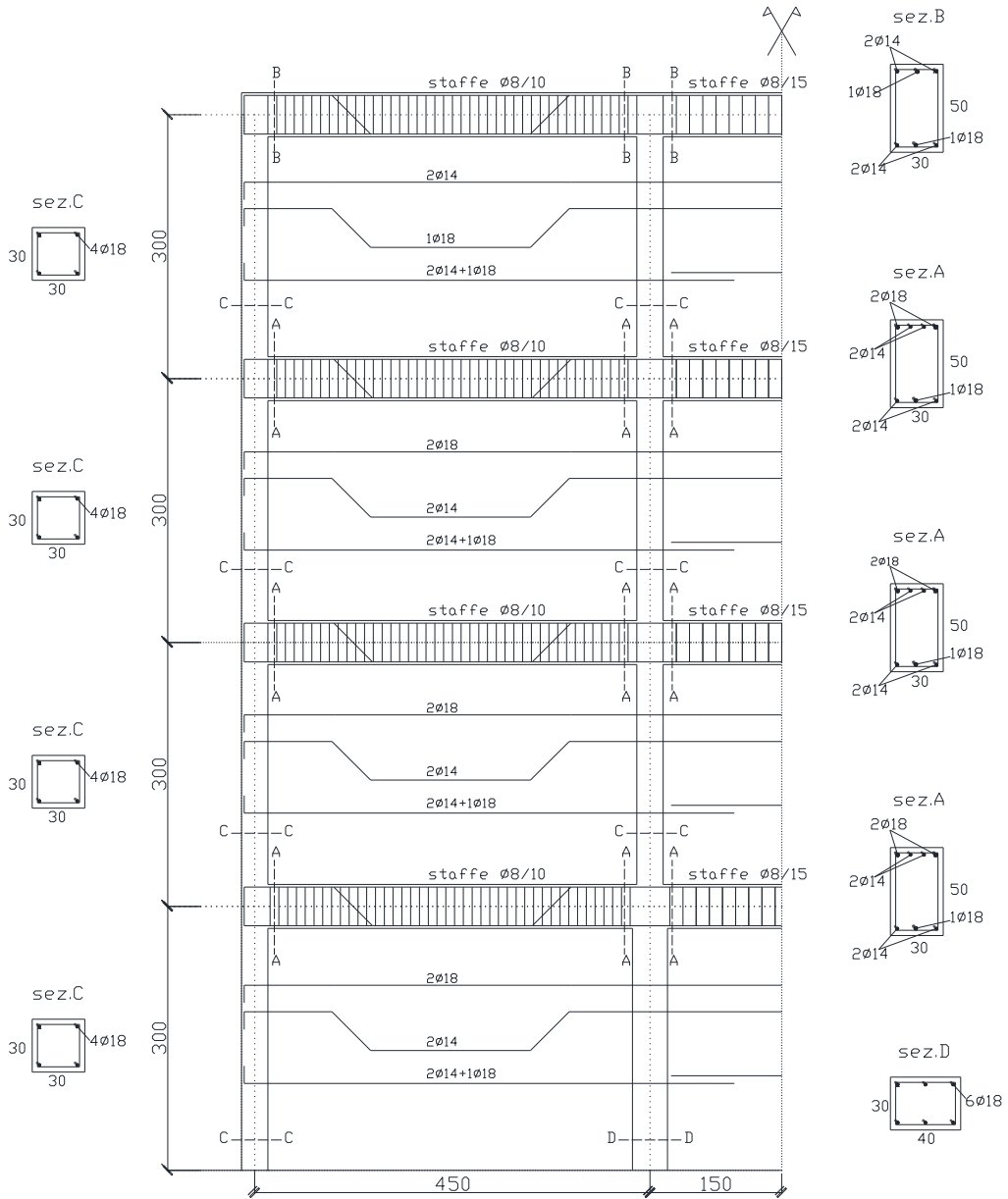


Figure 6.7. GLD frame

In Table 6.5 and Table 6.6 main properties of exterior and interior columns in OLD SLD frame, respectively, are reported. In particular, depth (b), width (h), concrete cover (c), top, bottom and web longitudinal reinforcement (A_s ,

A_s' , and A_{sh}), axial load (N), yielding and maximum moment (M_y and M_{cap} , respectively), plastic shear (V_{pl}), stirrup spacing (s), transverse reinforcement area (A_{sw}), and maximum shear strength evaluated according to the model by Sezen and Moehle (2004) without degradation (V_u) are shown.

Exterior columns	b	h	c	A_s	A'_s	A_{sh}	N	M_y	M_{cap}	V_{pl}
story	mm	mm	mm	mm ²	mm ²	mm ²	kN	kNm	kNm	kN
1	300	600	40	1256	1256	1256	316	432	524.23	388.32
2	300	600	40	1256	1256	1256	231	414	504.23	420.19
3	300	500	40	1256	1256	1256	145	322	392.22	313.77
4	300	500	40	1256	1256	1256	60	307	375.61	300.49

Exterior columns	b	h	c	A_{sw}	s	V_u
story	mm	mm	mm	mm ²	mm	kN
1	300	600	40	100.00	240	285.72
2	300	600	40	100.00	240	296.42
3	300	500	40	100.00	240	206.09
4	300	500	40	100.00	240	194.11

Table 6.5. Flexural and shear characterization of exterior columns - OLD SLD

Interior columns	b	h	c	A_s	A'_s	A_{sh}	N	M_y	M_{cap}	V_{pl}
story	mm	mm	mm	mm ²	mm ²	mm ²	kN	kNm	kNm	kN
1	300	600	40	1256	1256	1256	527	475	572.55	381.70
2	300	600	40	1256	1256	1256	384	446	540.01	360.00
3	300	500	40	1256	1256	1256	242	338	410.81	273.87
4	300	500	40	1256	1256	1256	99	314	383.27	255.51

Interior columns	b	h	c	A_{sw}	s	V_u
story	mm	mm	mm	mm ²	mm	kN
1	300	600	40	100.00	240	311.96
2	300	600	40	100.00	240	319.61
3	300	500	40	100.00	240	221.31
4	300	500	40	100.00	240	199.83

Table 6.6. Flexural and shear characterization of interior columns - OLD SLD

In Table 6.7 the main properties of beams in OLD SLD frame are reported. In particular A_s^- and A_s^+ are the top and bottom reinforcement, respectively, and M_{cap}^- and M_{cap}^+ the corresponding flexural capacities.

story	beam	b	h	c	A_s^-	A_s^+	M_{cap}^-	M_{cap}^+
		mm	mm	mm	mm ²	mm ²	kNm	kNm
1	ext	300	600	40	1344	603	376.52	205.94
	int	300	600	40	1344	603	376.52	205.94
2	ext	300	600	40	1344	603	376.52	205.94
	int	300	600	40	1344	603	376.52	205.94
3	ext	300	500	40	1344	603	306.29	167.53
	int	300	500	40	1344	603	306.29	167.53
4	ext	300	500	40	804	402	186.16	95.21
	int	300	500	40	804	402	186.16	95.21

Table 6.7. Main properties related to beams – OLD SLD

Finally, in Table 6.8, it is shown that column-to-beam flexural capacity (M_c/M_b) is significantly higher than the unity; therefore, strong column-weak beam hierarchy characterizes this frame. By reporting beam flexural capacity to the joint centerline ($M_{j,b}$) and by comparing $M_{j,b}$ and joint moment strength ($M_{j,R}$), it can be observed that prevalently J-failures characterize this frame. $M_{j,R}/M_{j,b}$ is equal to the unity when joint strength is limited to the flexural capacity of the adjacent beams, according to the modeling approach described in Section 6.2.2.

story	joint	M_b	M_c	M_c/M_b	$M_{j,R}$	$M_{j,b}$	$M_{j,R}/M_{j,b}$	failure mode
		kNm	kNm	()	kNm	kNm	()	
1	ext	376.52	1028.46	2.73	384.12	434.45	0.88	J
	int	582.46	1112.56	1.91	528.27	693.41	0.76	J
2	ext	376.52	896.44	2.38	358.46	434.45	0.83	J
	int	582.46	950.81	1.63	423.42	693.41	0.61	J
3	ext	306.29	767.83	2.51	294.69	344.57	0.86	J
	int	473.82	794.07	1.68	333.49	546.71	0.61	J
4	ext	186.16	375.61	2.02	209.43	209.43	1.00	BJ
	int	281.37	383.27	1.36	324.66	324.66	1.00	BJ

Table 6.8. Beam/column hierarchy and joints classification – OLD SLD

The same information are reported for GLD frame in Table 6.9, Table 6.10, Table 6.11 and Table 6.12. In this case, column plastic shear is lower than the maximum non-degraded shear strength, both for exterior and interior columns. Thus, if no degradation in shear strength is considered, no shear failures is detected, as it will be shown in Section 6.6.

Exterior columns	b	h	c	A_s	A'_s	A_{sh}	N	M_y	M_{cap}	V_{pl}
story	mm	mm	mm	mm ²	mm ²	mm ²	kN	kNm	kNm	kN
1	300	300	40	508	508	0	316	88	105.86	76.99
2	300	300	40	508	508	0	231	79	95.59	76.47
3	300	300	40	508	508	0	145	70	84.81	67.85
4	300	300	40	508	508	0	60	60	73.74	58.99

Exterior columns	b	h	c	A_{sw}	s	V_u
story	mm	mm	mm	mm ²	mm	kN
1	300	300	40	100.00	240	100.20
2	300	300	40	100.00	240	100.48
3	300	300	40	100.00	240	94.57
4	300	300	40	100.00	240	87.87

Table 6.9. Flexural and shear characterization of exterior columns - GLD

Interior columns	b	h	c	A_s	A'_s	A_{sh}	N	M_y	M_{cap}	V_{pl}
story	mm	mm	mm	mm ²	mm ²	mm ²	kN	kNm	kNm	kN
1	300	400	40	508	508	508	527	170.22	203.52	148.01
2	300	300	40	508	508	0	384	95.14	113.84	91.07
3	300	300	40	508	508	0	242	80.28	96.94	77.55
4	300	300	40	508	508	0	99	64.72	78.88	63.10

Interior columns	b	h	c	A_{sw}	s	V_u
story	mm	mm	mm	mm ²	mm	kN
1	300	400	40	100.00	240	168.25
2	300	300	40	100.00	240	109.79
3	300	300	40	100.00	240	101.21
4	300	300	40	100.00	240	91.10

Table 6.10. Flexural and shear characterization of interior columns - GLD

story	beam	b	h	c	A_s⁻	A_s⁺	M_{cap}⁻	M_{cap}⁺
		mm	mm	mm	mm ²	mm ²	kNm	kNm
1	ext	300	500	40	816	562	189.30	132.06
	int	300	500	40	816	562	189.30	132.06
2	ext	300	500	40	816	562	189.30	132.06
	int	300	500	40	816	562	189.30	132.06
3	ext	300	500	40	816	562	189.30	132.06
	int	300	500	40	816	562	189.30	132.06
4	ext	300	500	40	562	562	131.91	131.91
	int	300	500	40	562	562	131.91	131.91

Table 6.11. Main properties related to beams – GLD

story	joint	M_b	M_c	M_c/M_b	M_{j,R}	M_{j,b}	M_{j,R}/M_{j,b}	failure mode
		kNm	kNm	()	kNm	kNm	()	
1	ext	189.30	201.45	1.06	152.44	219.77	0.69	J
	int	321.36	317.36	0.99	186.45	346.21	0.54	J
2	ext	189.30	180.40	0.95	152.44	216.48	0.70	J
	int	321.36	210.78	0.66	186.45	252.93	0.74	J
3	ext	189.30	158.56	0.84	152.44	190.27	0.80	J
	int	321.36	175.82	0.55	186.45	210.98	0.88	J
4	ext	131.91	73.74	0.56	88.49	88.49	1.00	CJ
	int	263.81	78.88	0.30	94.65	94.65	1.00	CJ

Table 6.12. Beam/column hierarchy and joints classification – GLD

Column-to-beam flexural capacity (M_c/M_b) is generally lower than the unity; therefore, as typically expected for this kind of design approach, strong beam-weak column hierarchy characterizes this frame. By reporting column flexural capacity to the joint centerline ($M_{j,c}$) and by comparing $M_{j,c}$ and joint moment strength ($M_{j,R}$), it can be observed that prevalently J-failures characterize also this frame. $M_{j,R}/M_{j,c}$ is equal to the unity when joint strength is limited to the flexural capacity of the adjacent columns.

Joint moment-rotation backbones for interior and exterior joints obtained as explained in Section 6.2.2 are shown in Figure 6.8 for OLD SLD (a) and GLD (b) frames.

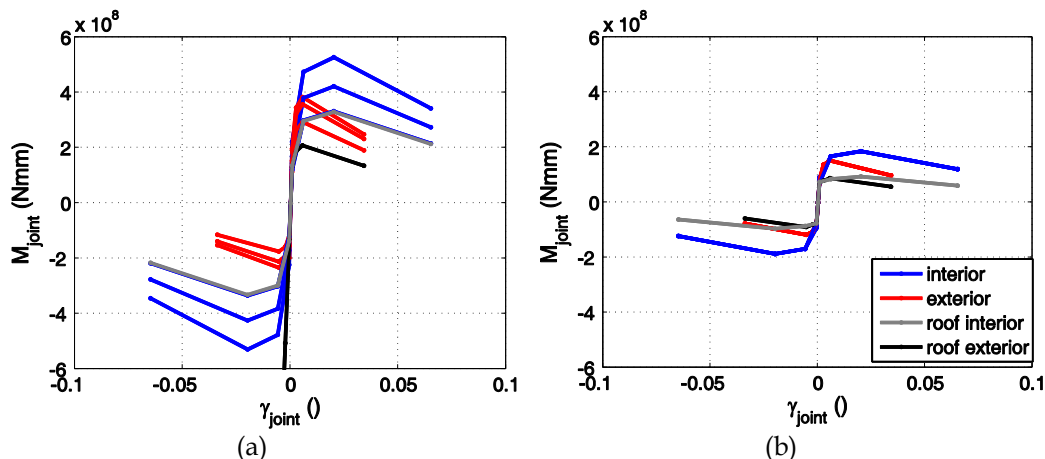


Figure 6.8. Joint moment-rotation backbones for OLD SLD (a) and GLD (b) frames

6.4 Selected ground motion records and performance levels

In order to perform dynamic analyses, input ground motion records have to be selected and performance levels of interest should be identified.

In this study, natural records representing Italian seismicity are selected and scaled to different levels of seismicity in order to obtain IDA curves. The records selection has been performed by using REXEL software (Iervolino et al. 2010), from ITACA strong-motion database. Earthquakes characterized by a low-medium magnitude levels (between 4.4 and 5.7), with a source-to-site distance ranging between 10 and 40 km, and recorded on soil class B are selected. On the whole 50 ground motion records are selected. A summary of the main properties of the these records is reported in Appendix 6. The related spectra in terms of pseudo-acceleration are reported in Figure 6.9.

As far as performance levels of interest are concerned, the structural capacities are primarily defined by the maximum interstorey drifts (IDR) that correspond to three widely used performance levels (or limit states) in the earthquake community (e.g. Celik and Ellingwood, 2010): immediate occupancy (IO), life safety or significant damage (SD), and collapse prevention (CP).

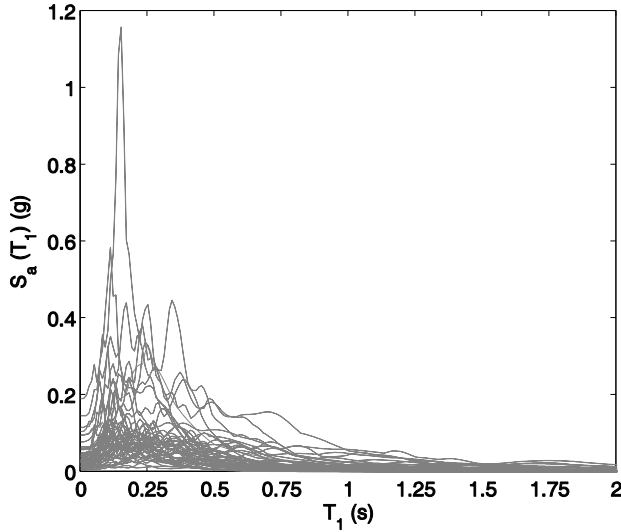


Figure 6.9. Pseudo-acceleration spectra of the selected ground motion records

These performance levels are adopted so that the results can be compared to works published previously by other researchers. As shown in Chapter 2 (Section 2.2), the IO level is described by the limit below which the structure can be occupied safely without significant repair, and is defined by the value of maximum IDR at which the frame enters the inelastic range. The “life safety” level occurs at a deformation at which “significant” damage occurred, but at which a substantial margin remains against incipient collapse. This limit is quite hard to quantify in terms of IDR or other structural response parameters, and it is commonly identified as the maximum IDR at which significant structural damage has occurred. Finally, the CP level is defined by the point of incipient collapse of the frame due to either severe degradation in strength of members and connections or significant P- Δ effects resulting from excessive lateral deformations.

Table 6.13 reports the values of the IDR thresholds (IDR_{LS}) for the selected performance levels, chosen on the basis of previous literature researches (Celik 2007, Celik and Ellingwood 2010).

	IO LS	SD LS	CP LS
IDR_{LS}	0.2%	2%	5%

Table 6.13. IDR thresholds for the selected performance levels

Additional LSs, defined on the basis of the achievement of characteristic points in the nonlinear response of the primary structural elements, are adopted. In particular the first achievement of a particular condition or a “conventional failure” is detected, in analogy with the approach of typical European code prescriptions (e.g. CEN 2005, DM 2008), as shown in Figure 6.10.

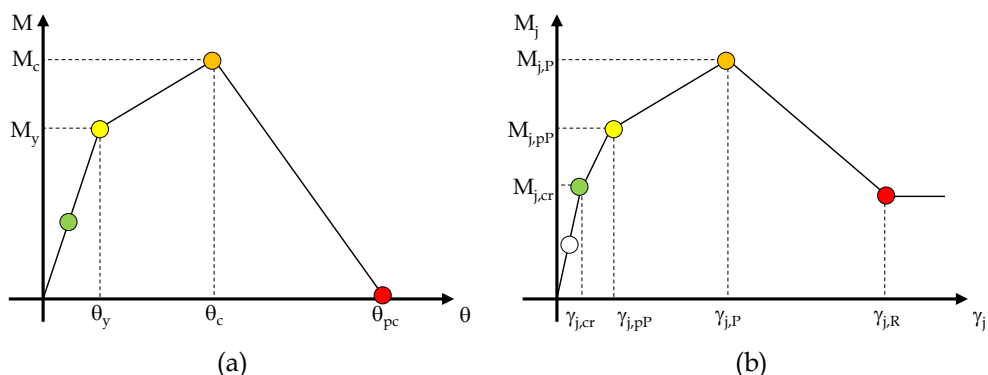


Figure 6.10. Characteristic points of columns (a) and joints (b) response

For columns, green circles represent a pre-yielding condition; yellow, orange and red circles indicate the achievement of yielding, capping and post-peak rotations, respectively.

For beam-column joints, white circle identifies a pre-cracking condition of joint; while green, yellow, orange and red circles represent the achievements of joint cracking, pre-peak point, peak joint strength, and residual strength, respectively.

Such a convention will be adopted hereinafter when damage states in RC elements are presented. The corresponding LSs will be referred to as summarized in Table 6.14.

FY	first element at yielding (yellow circle)
FC	first element at capping (orange circle)
FPC	first element at post-capping (red circle)
FcrJ	first joint cracking (green circle)
FpPJ	first joint at pre-peak point (yellow circle)
FPJ	first joint at peak strength (orange circle)
FRJ	first joint at residual strength (red circle)

Table 6.14. Additional LSs acronyms

6.5 Preliminary nonlinear static analyses

Preliminary, nonlinear static analyses with first-mode-shape--proportional lateral load pattern are performed in OpenSees (McKenna et al, 2010) on the structural models (obtained as described in Section 6.2) for OLD SLD and GLD frames and in a double condition: (i) with “rigid joints”, assuming a very high stiffness and shear strength for beam-column connections and (ii) “with joints”, explicitly modeling the nonlinear behavior of joints, as explained in Section 6.2.2. Results of this kind of analysis are reported in this Section.

6.5.1. OLD SLD frame

First of all, elastic periods from modal analysis are reported in Table 6.15 for both conditions (“rigid joints” and “with joints”). An increment of about 8% in elastic period is observed when joint elastic deformability is taken into account.

	Rigid joints	With joints
T_1 (s)	0.694	0.747

Table 6.15. Elastic periods – OLD SLD frame

6.5.1.1 Rigid joints

Rigid joints condition exhibited a global collapse mechanism for OLD SLD frames, as expected due to the strong-column-weak-beam hierarchy observed in Section 6.3. Static pushover (SPO) curve is reported in Figure 6.11 together with the collapse mechanism and the damage level in each beam/column hinge at the last step.

In this case no red circle (namely, no joints that reach post-peak rotation) is present, since SPO was interrupted before the first element reached its post-peak rotation capacity because of convergence issue.

IDR distributions and qualitative deformed configurations at peak load (a) and at last step (b) are reported in Figure 6.12.

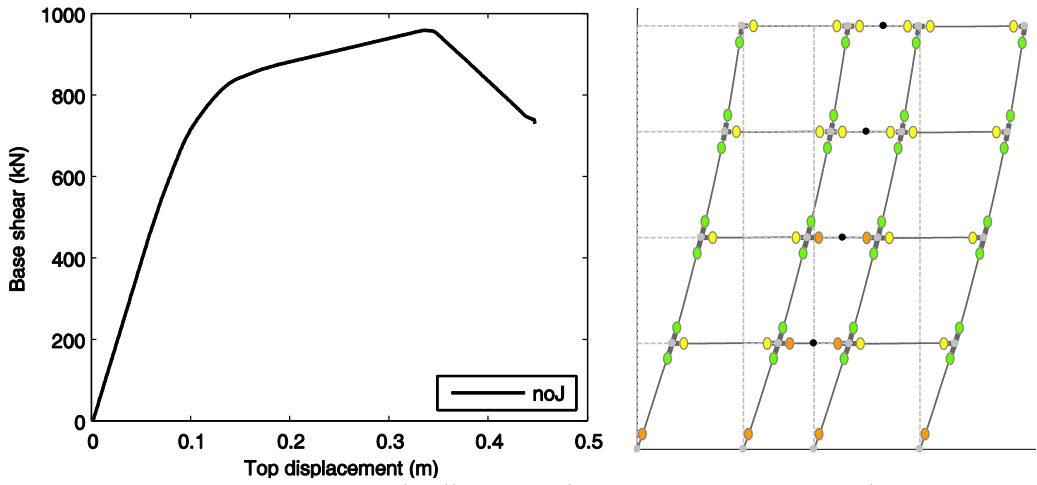


Figure 6.11. SPO curve and collapse mechanism – OLD SLD - rigid joints

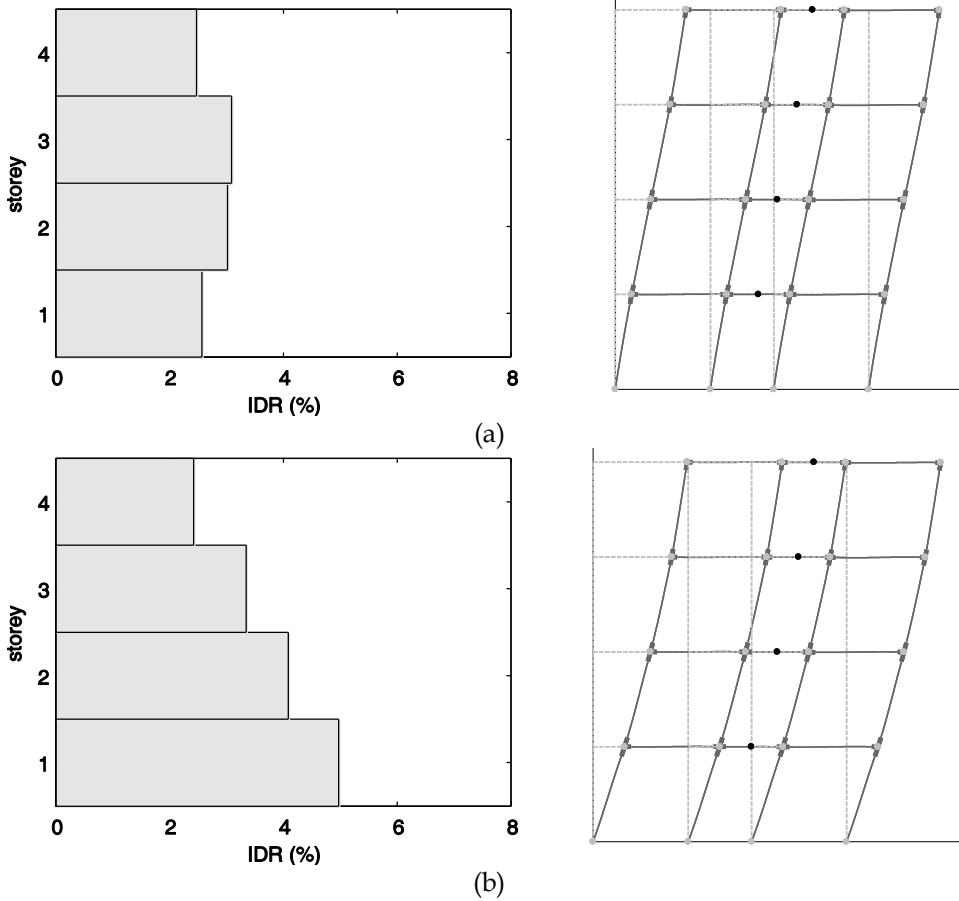


Figure 6.12. IDR distributions and deformed configuration at peak load (a) and at last step (b) – OLD SLD - rigid joints

6.5.1.2 With joints

When nonlinear response of beam-column joints is modeled, OLD SLD frame still exhibited a global collapse mechanism.

Static pushover (SPO) curve is reported in Figure 6.13 together with the collapse mechanism and the damage level in each beam/column hinge at the last step.

In this case it can be observed that a quite distributed damage level in beam-column joints is exhibited, especially from the first to the third story.

IDR distributions and qualitative deformed configurations at peak load (a) and at last step (b) are reported in Figure 6.14.

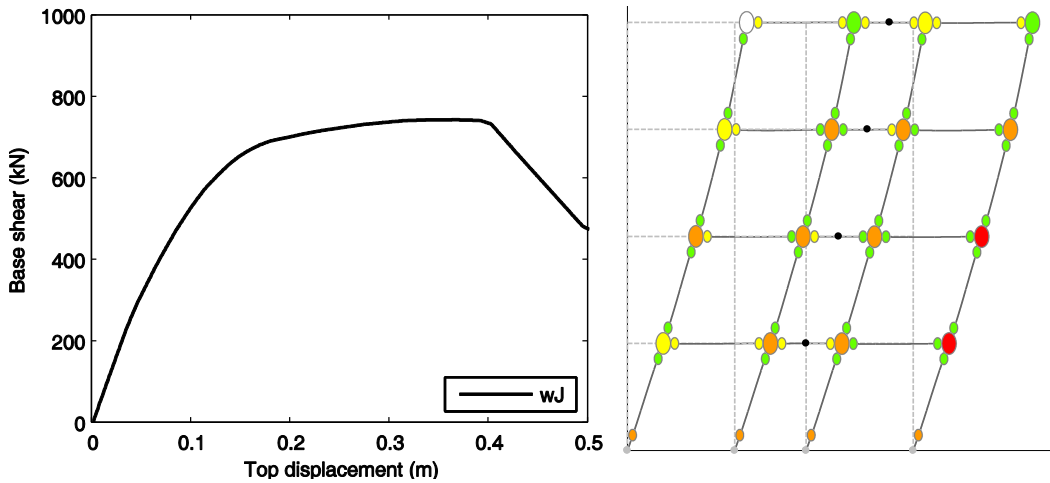
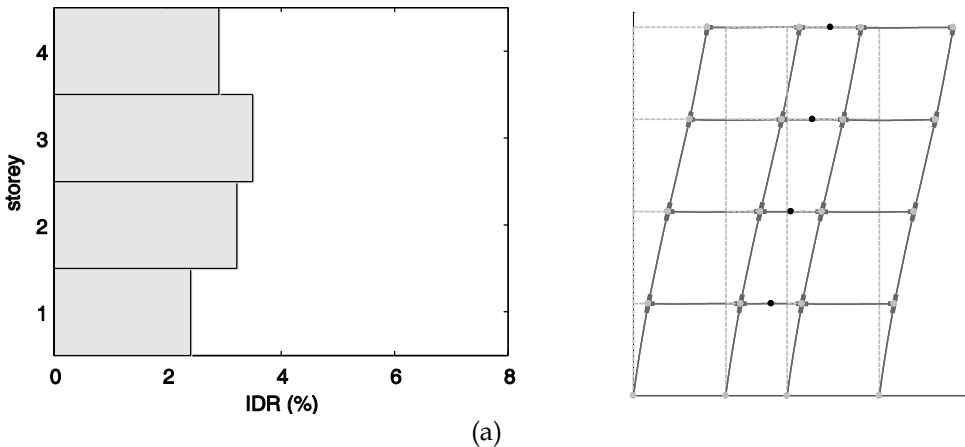


Figure 6.13. SPO curve and collapse mechanism - OLD SLD - with joints



(a)

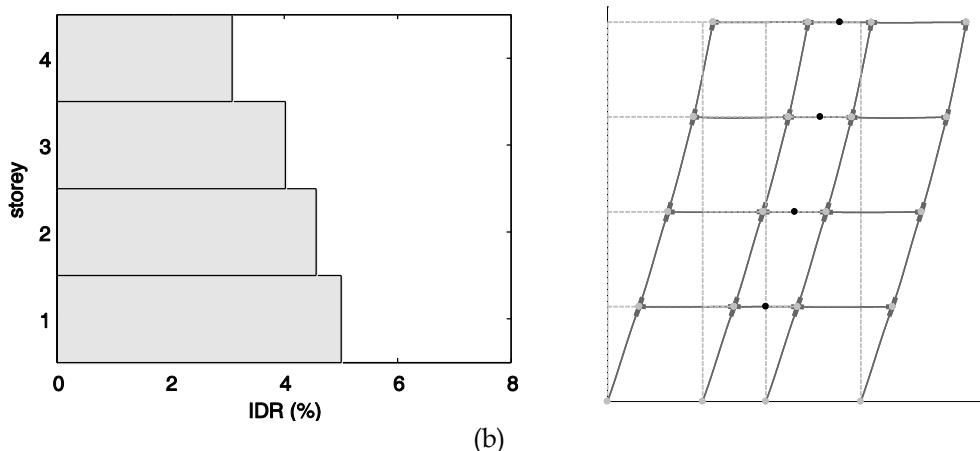


Figure 6.14. IDR distributions and deformed configuration at peak load (a) and at last step (b) – OLD SLD - with joints

6.5.1.3 Comparison

In Table 6.16 a comparison in terms of peak base shear ($V_{b,max}$) and the corresponding displacement (D_{max}) in SPO analyses with joint (wJ) and with rigid joints (noJ) is carried out. A graphical comparison also in terms of SPO curves is shown in Figure 6.15.

	$V_{b,max}$ (kN)	D_{max} (m)	$V_{b,max\ wJ} / V_{b,max\ noJ}$ (-)	D_{wJ} / D_{noJ} (-)
noJ	959.5	0.343	0.79	1.06
wJ	745.2	0.362		

Table 6.16. Comparison in terms of peak base shear and peak displacement in SPO - with joint (wJ) and rigid joints (noJ) – OLD SLD

It can be observed that the explicit modeling of beam-column joints in the structural analysis implies a reduction of the maximum base shear (equal to 21%) and a higher peak deformability (that increases of about 6%).

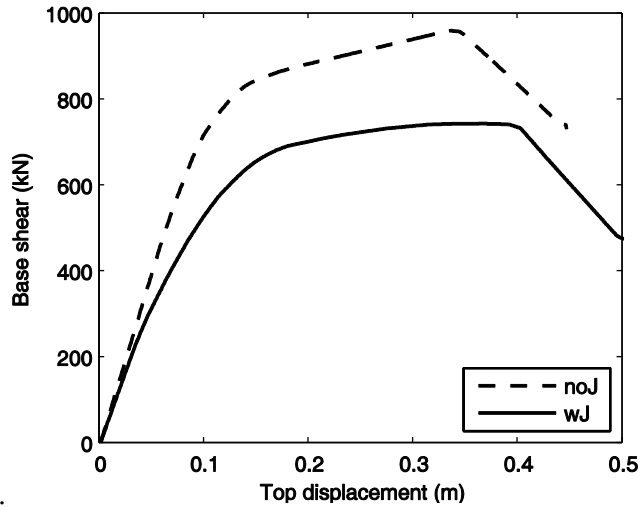


Figure 6.15. Comparison in terms of SPO curves - OLD SLD

6.5.2. GLD frame

Elastic periods from modal analysis are reported in Table 6.17 for both conditions “rigid joints” and “with joints”. An increment of 6% in elastic period is observed when joint elastic deformability is taken into account.

	Rigid joints	With joints
T_1 (s)	1.154	1.227

Table 6.17. Elastic periods - GLD frame

6.5.2.1 Rigid joints

Rigid joints condition exhibited a local collapse mechanism for GLD frames located at the second story, as expected due to the weak-column-strong-beam hierarchy observed in Section 6.3. Static pushover (SPO) curve is reported in Figure 6.16 together with the collapse mechanism and the damage level in each beam/column hinge at the last step. Inelasticity demand is clearly concentrated in the second story.

IDR distributions and qualitative deformed configurations at peak load (a) and at last step (b) are reported in Figure 6.17.

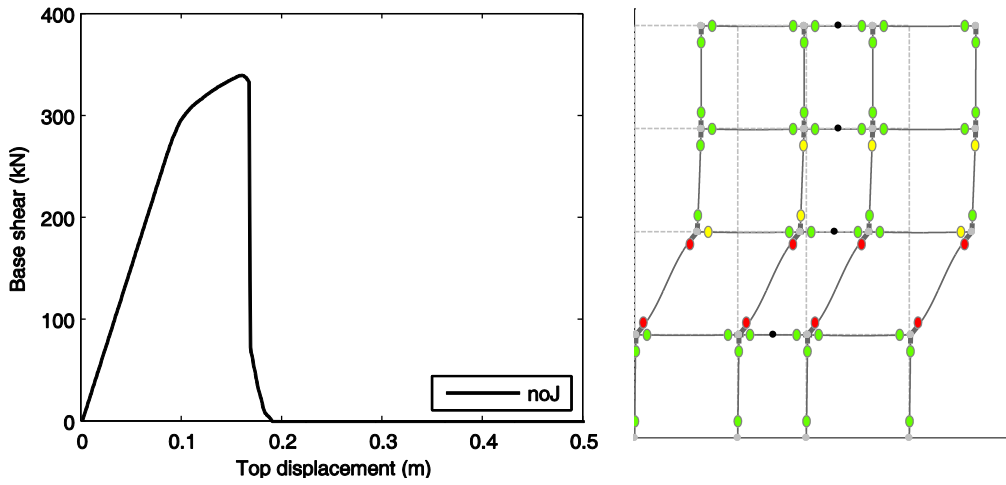


Figure 6.16. SPO curve and collapse mechanism - GLD - rigid joints

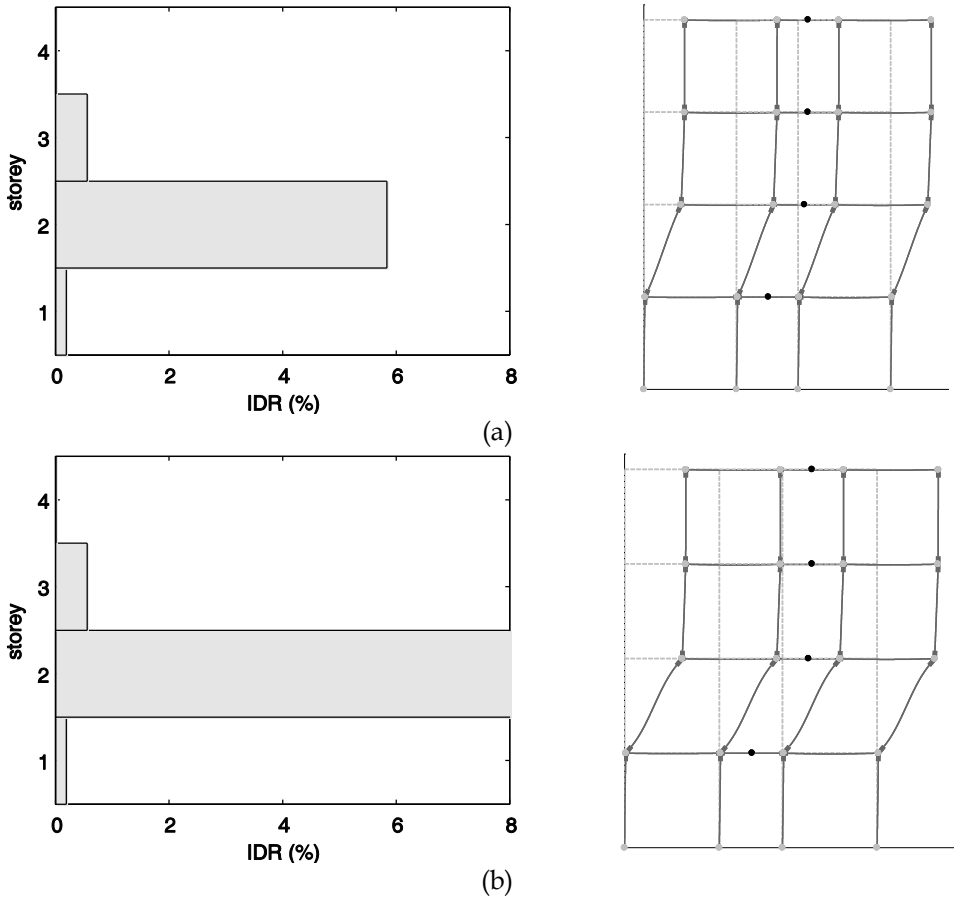


Figure 6.17. IDR distributions and deformed configuration at peak load (a) and at last step (b) - GLD - rigid joints

6.5.2.2 With joints

When nonlinear response of beam-column joints is modeled, GLD frame exhibited a collapse mechanism that involves the first and the second stories.

Static pushover (SPO) curve is reported in Figure 6.18 together with the collapse mechanism and the damage level in each beam/column hinge at the last step.

In this case it can be observed that joints at the second story are particularly invested by inelastic demand reaching their residual strength.

IDR distributions and qualitative deformed configurations at peak load (a) and at last step (b) are reported in Figure 6.19.

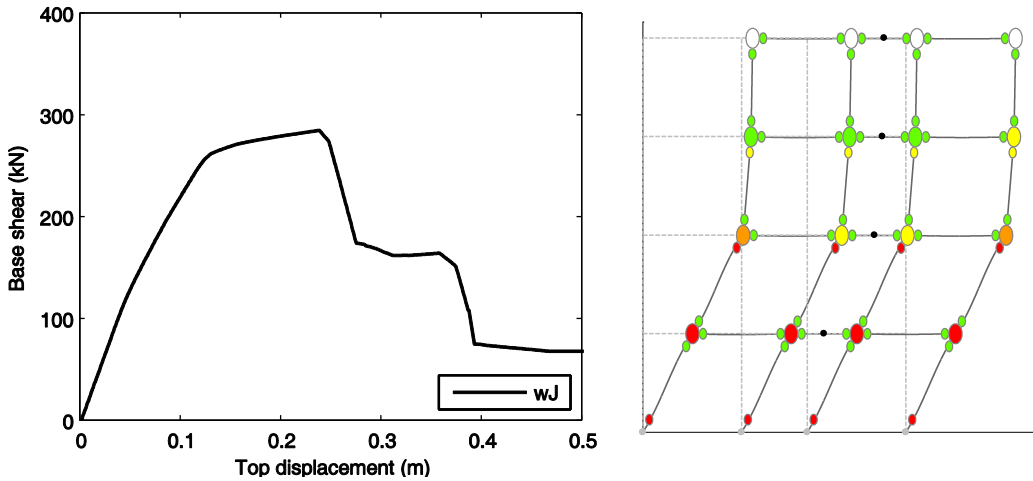
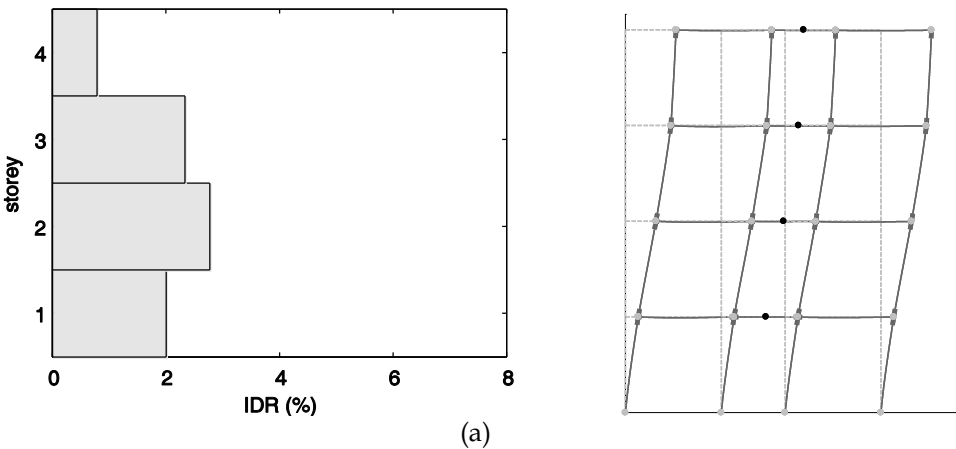


Figure 6.18. SPO curve and collapse mechanism – GLD - with joints



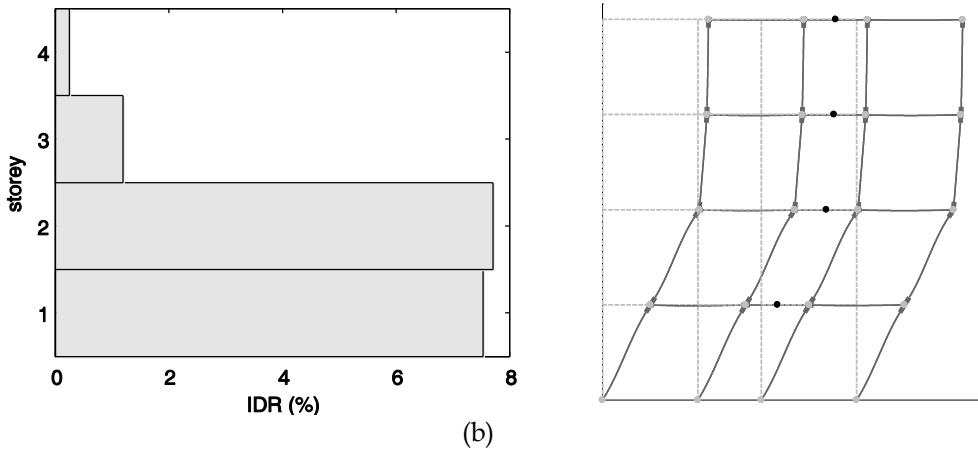


Figure 6.19. IDR distributions and deformed configuration at peak load (a) and at last step (b) – GLD – with joints

In this case, it can be observed a more uniform distribution along the height of the IDR demand, that is one of the main effects of joint damage on the structural response, as already highlighted in other literature studies, e.g. Calvi et al. (2002) or Celik and Ellingwood (2008).

6.5.2.3 Comparison

In Table 6.18, a comparison in terms of peak base shear ($V_{b,max}$) and the corresponding displacement (D_{max}) in SPO analyses with joint (wJ) and with rigid joints (noJ) is carried out for GLD frame. A graphical comparison also in terms of SPO curves is shown in Figure 6.20.

	$V_{b,max}$ (kN)	D_{max} (m)	$V_{b,max\ wJ} / V_{b,max\ noJ}$ (-)	D_{wJ} / D_{noJ} (-)
noJ	340.414	0.161	0.839	1.472
wJ	285.73	0.237		

Table 6.18. Comparison in terms of peak base shear and peak displacement in SPO – with joint (wJ) and rigid joints (noJ) – GLD

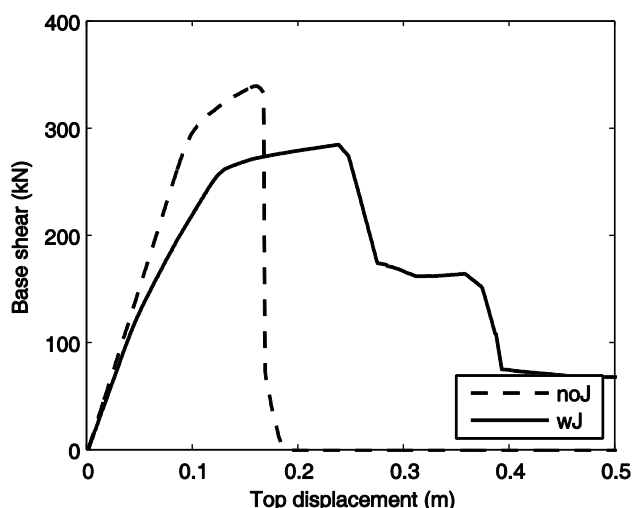


Figure 6.20. Comparison in terms of SPO curves -GLD

It can be observed that, in the case of weak column-strong beam design, the joint damage reduces the maximum interstorey drift demand implying a prevention of the soft-story mechanism and a reduction of the maximum base shear (equal to about 16%).

Actually, the effects of joint damage has been experimentally observed to protect or delay soft-story mechanisms (in a predominant weak-column/strong-beam system), by reducing the rotation demand in the adjacent column elements (Calvi et al. 2002). Shake table tests on reduced-scale frame models conducted at Cornell University (El-Attar et al., 1997) showed that GLD RC frames, typically with weak column-strong beam designs, are susceptible to soft-story collapses under earthquake effects: in the case of the three-story 1/8-scale frame, the collapse occurred when plastic hinges developed at both ends of the first story columns and formed a soft-story failure mechanism, without significant damage in the beams, joint panels, or column splice regions, indicating that weak column-strong beam behavior leads to premature soft-story mechanisms before the other problematic reinforcing details are subjected to significant demands.

As well as in OLD SLD frame (with weak-beam/strong-column hierarchy), the effect of joint damage results in a higher deformability and thus higher displacement demand. The increment in peak displacement is equal to about 50%.

6.6 Nonlinear dynamic analyses

The incremental nonlinear dynamic analyses (IDAs) (Vamvatsikos and Cornell, 2002) are conducted in OpenSees (McKenna et al, 2010) with the selected ground motion records for both case-study frames. Robust convergence algorithms for solving simultaneous equations when strength and stiffness are degrading are implemented.

Five percent mass- and tangent stiffness-proportional Rayleigh damping is applied to the first and third mode of elastic response.

In this Section the results of these analyses will be presented and discussed for both OLD SLD and GLD frames in a double condition: (i) with “rigid joints”, assuming a very high stiffness and shear strength for beam-column connections and (ii) “with joints”, explicitly modeling the nonlinear behavior of joints, as explained in Section 6.2.2.

First, IDA curves have been obtained and, then, fragility curves have been calculated.

A seismic fragility is defined as the probability of reaching stipulated performance levels as a function of a specified intensity measure of ground motion. The fragility is described by the conditional probability that the structural capacity, C , fails to resist the structural demand, D , given the seismic intensity measure, IM , and it is commonly modeled by a lognormal cumulative distribution function.

Therefore, if IM capacity is “observed” in a building under a population of ground motion records, according to a frequentist approach, the cumulative frequency distribution of these observations provides the fragility curve (based on that IM measure) for that building and for that Limit State, based on the definitions themselves of fragility curve and IM capacity. In this way, the fragility functions have been obtained, at different LSs (defined as explained in Section 6.4) taking into account only aleatoric uncertainty, namely record-to-record variability.

In this study, the structural demand measure is selected to be the maximum interstory drift in the frame, IDR_{max} , that occurs during its dynamic response to earthquake shaking. At lower levels of excitation, the IDR typically provides insight regarding the potential for damage to non-structural components, while at higher levels it is closely related to structural or local collapse. The seismic intensity measure is the spectral acceleration at the fundamental period

of the frame, $Sa(T_1)$, for 5% damping, a measure that is consistent with that used in previous studies and that is generally considered as a more efficient parameter to characterize earthquake intensity than peak ground acceleration (Shome et al. 1998).

6.6.1. OLD SLD frame

In this Section, IDAs and fragility curves at different LSs for the OLD SLD frame are reported and commented. It is worth noting that IDA curves have been scaled to $Sa(T_1)$, where T_1 is the elastic period of the “with joints” configuration, namely 0.747 s.

6.6.1.1 Rigid joints

In Figure 6.21 IDAs curves related to the “rigid joints” model obtained from all the ground motion records (50) are shown in terms of first-period spectral acceleration $Sa(T_1)$ versus maximum IDR, together with the related median IDA curve, $\eta_{Sa(T_1)|IDR_{max}}$.

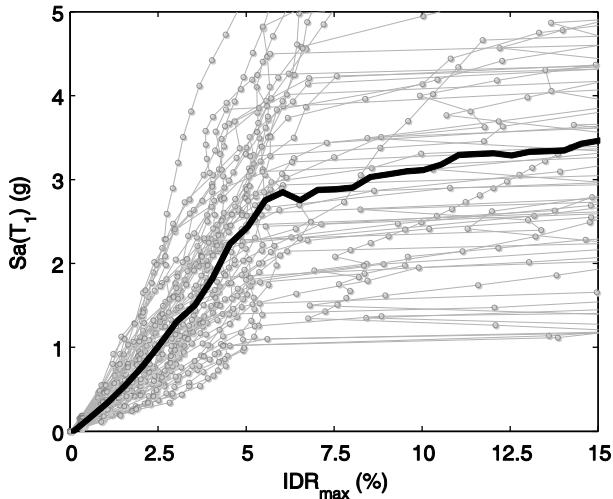


Figure 6.21. IDA curves and median IDA – OLD SLD – rigid joints

Starting from such IDAs, fragility curves at LSs defined as the achievement of a given maximum IDR can be easily obtained, by means of a lognormal fit of $Sa(T_1)$ given the value of IDR threshold. In this way, fragility curves shown in Figure 6.22 have been calculated.

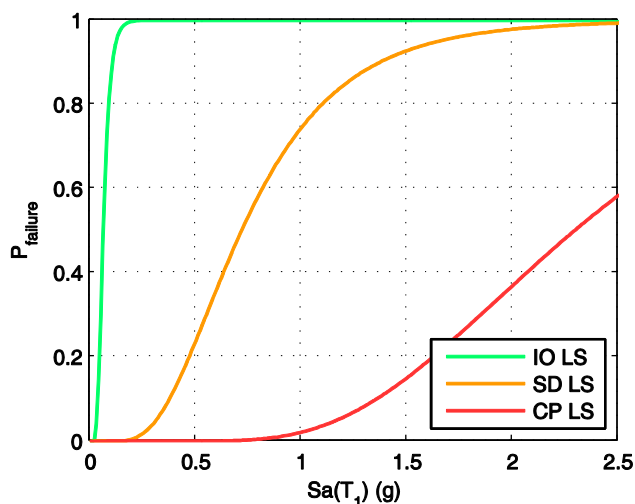


Figure 6.22. Fragility curves at IO, SD, and CP LSs - OLD SLD - rigid joints

Related parameters are reported in Table 6.19, with μ and β representing the estimated median (expressed in (g)) and logarithmic standard deviation of $Sa(T_1)$ capacity, respectively, at IO, SD, and CP LSs. β coefficient provides an useful indication about the overall sensitivity of seismic capacity to the variability of the ground motion record, confirming that record-to-record variability is a very important source of uncertainty.

Table 6.19 also reports the maximum IDR threshold (IDR_{max}) corresponding to IO, SD, and CP LSs and the median values of $Sa(T_1)$, given the maximum IDR.

LS	$Sa(T_1)_{median}$ (g)	IDR_{max} (%)	μ (g)	β
IO	0.067	0.20	0.062	0.417
SD	0.783	2.00	0.717	0.506
CP	2.455	5.00	2.293	0.411

Table 6.19. Fragility parameters at IO, SD, and CP LSs - OLD SLD - rigid joints

By means of the same approach based on a lognormal fit of the intensity measure capacities, fragility curves related to the achievement of a certain condition in the elements response (see Figure 6.14) for the first time (i.e. in the first element) can be calculated. These fragility curves are reported in Figure

6.23 and the related parameters in Table 6.20, where $Sa(T_1)_{\text{median}}$ is the median value of $Sa(T_1)$ capacity and median value of IDR_{max} .

It can be observed the yielding condition in the first element (FY LS) occurs for a value of median value of $Sa(T_1)$ equal to 0.158g, while the achievement of the peak strength for the first time (FC LS) occurs for a quite high value of $Sa(T_1)$ median (1.648g) thanks to the uniform distribution of inelastic demand in the frame. Also in this case it can be observed that the record-to-record variability provides a logarithmic standard deviation of $Sa(T_1)$ capacity (β) of about 45% for these LSs.

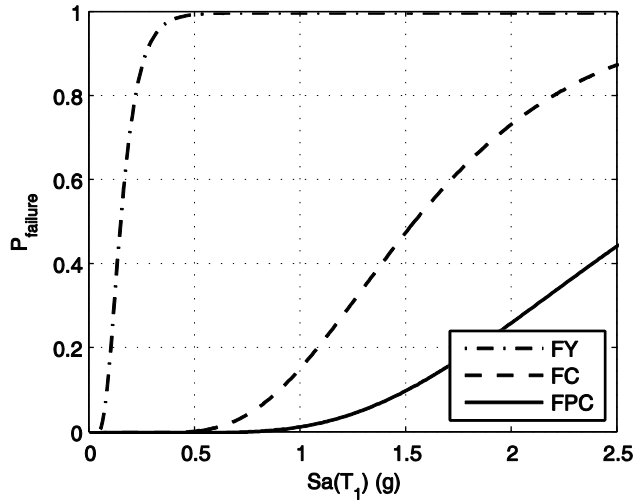


Figure 6.23. Fragility curves at FY, FC, FPC LSs - OLD SLD - rigid joints

LS	$Sa(T_1)_{\text{median}}$ (g)	IDR_{max} (%)	μ (g)	β
FY	0.158	0.47	0.145	0.464
FC	1.648	3.71	1.532	0.422
FPC	2.722	5.43	2.656	0.449

Table 6.20. Fragility parameters at FY, FC, FPC LSs - OLD SLD - rigid joints

6.6.1.2 With joints

The same results are reported also for the structural model that explicitly takes into account joints nonlinear behavior. Figure 6.24 shows IDAs curves related to the model “with joints” obtained from all the ground motion records, together with the related median IDA curve, $\eta_{Sa(T_1)|IDR_{max}}$.

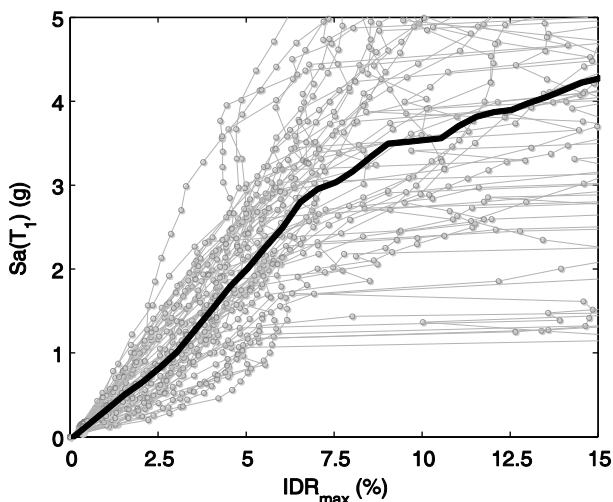


Figure 6.24. IDA curves and median IDA – OLD SLD – with joints

Figure 6.25 reports the fragility curves at IO, SD, and CP LSs, obtained by means of a lognormal fit of $Sa(T_1)$ given the value of IDR threshold for each LS, and Table 6.21 shows the related parameters.

Figure 6.26 and Figure 6.27 report fragility curves obtained in this case at FY, FC, and FPC LSs, but also, at LSs defined as the achievement of particular “limit conditions” in joints response, namely F_{crJ} , F_{pPJ} , FPJ , and FRJ (defined in Table 6.14). The related parameters are reported in Table 6.22, where $Sa(T_1)_{median}$ is the median value of $Sa(T_1)$ capacity and IDR_{max} the corresponding median value of maximum IDR.

It can be observed that the first achievement of peak strength in beam-column joints anticipates the first achievement of capping strength in beams or columns; the achievement of the peak strength in beams or columns occurs for a value of $Sa(T_1)$ quite close to that corresponding to the achievement of the first residual strength in joints, thus confirming that joint damage can be very critical in such a frame.

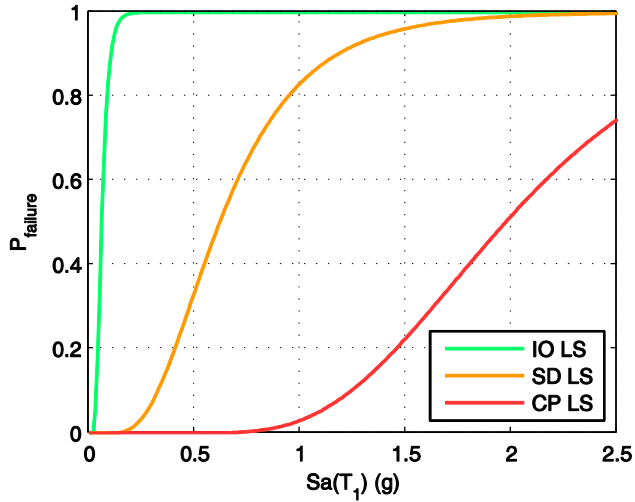


Figure 6.25. Fragility curves at IO, SD, and CP LSs - OLD SLD - with joints

LS	$Sa(T_1)_{\text{median}}$ (g)	IDR_{max} (%)	μ (g)	β
IO	0.070	0.20	0.059	0.432
SD	0.665	2.00	0.617	0.502
CP	2.034	5.00	1.969	0.362

Table 6.21. Fragility parameters at IO, SD, and CP LSs - OLD SLD - with joints

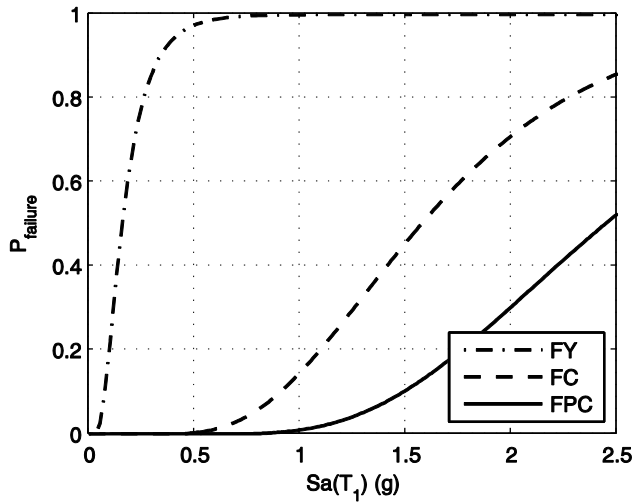


Figure 6.26. Fragility curves at FY, FC, FPC LSs - OLD SLD - with joints

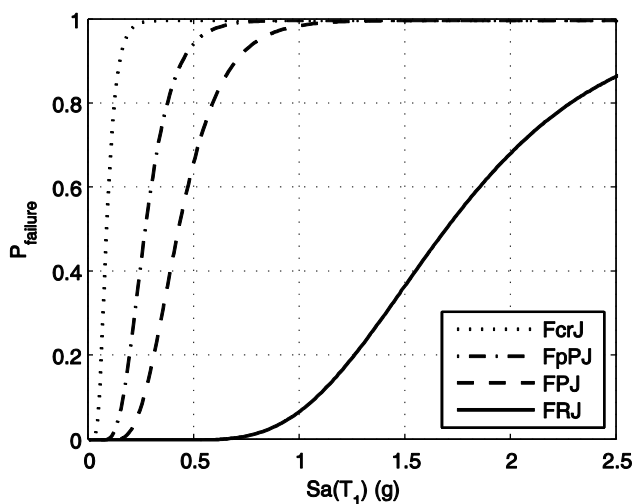


Figure 6.27. Fragility curves at FcrJ, FpPJ, FPJ, and FRJ LSs - OLD SLD - with joints

DS	$Sa(T_1)_{\text{median}}$ (g)	IDR_{max} (%)	μ (g)	β
FY	0.166	0.49	0.157	0.594
FC	1.614	4.14	1.572	0.433
FPC	2.349	5.66	2.441	0.389
FcrJ	0.081	0.24	0.082	0.435
FpPJ	0.296	0.87	0.265	0.394
FPJ	0.470	1.37	0.421	0.385
FRJ	1.706	4.31	1.685	0.354

Table 6.22. Fragility parameters at FY, FC, FPC, FcrJ, FpPJ, FPJ, and FRJ LSs - OLD SLD - with joints

Also when joints are explicitly modeled into the numerical model, the possible axial failure of joints cannot be captured directly due to the features of the adopted model (see Section 6.2.2). As anticipated in Section 6.2, a post-processing of the nonlinear analyses can lead to the detection of such kind of failure when the maximum IDR in a story overcomes the minimum IDR capacity (IDR_{AxJ}) between joints at that story. In this way, the achievement of the first axial failure (FAXJ LS) has been detected for each ground motion record and the related fragility curve (Figure 6.28 and Table 6.23) has been obtained by means of a lognormal fit. It can be observed that a maximum IDR equal to 7.54% leads to the first joint axial failure.

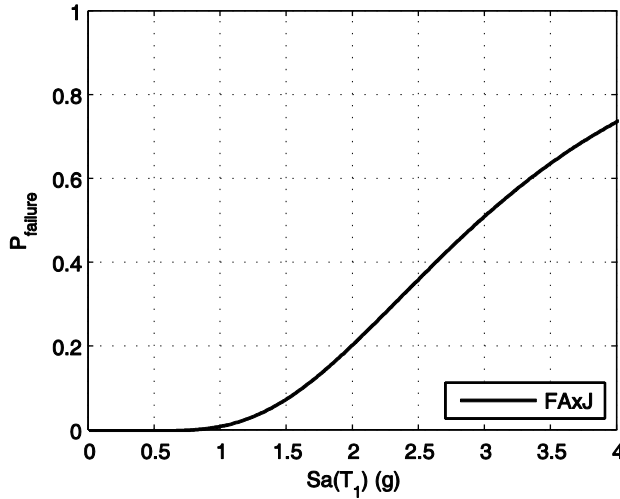


Figure 6.28. Fragility curve at FAXJ - OLD SLD - with joints

LS	$Sa(T_1)_{\text{median}}$ (g)	IDR_{max} (%)	μ (g)	β
FAXJ	3.059	7.54	2.947	0.476

Table 6.23..Fragility parameters at FAXJ LSs - OLD SLD - with joints

6.6.1.3 Comparison

By comparing median IDA curves between the two analyzed frame models (“rigid joints” and “with joints”), as in Figure 6.29, it can be observed that joint damage leads to lower $Sa(T_1)$ capacity for a given maximum IDR, until about 6% maximum IDR is achieved; successively, when joints involved in the mechanism reach their residual strength thus starting to go through a constant-strength branch, IDA curves “with joints” (wJ) keeps increasing, while IDA related to “noJ” frame goes toward a “flatline”.

The difference in $Sa(T_1)$ capacity given IDR that can be observed from the comparison between IDA, produces the “distance” between fragility curves that can be observed in Figure 6.30.

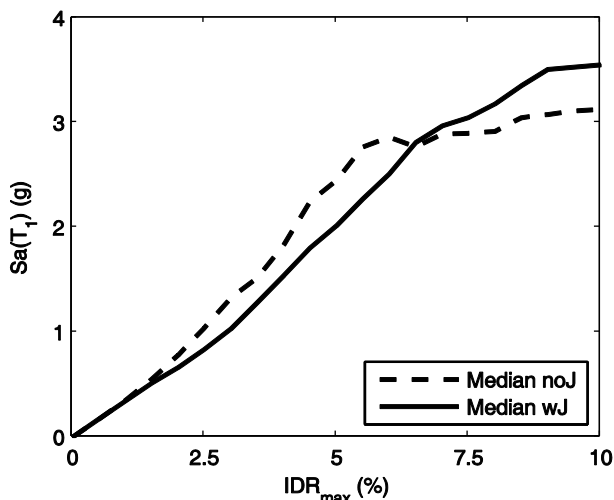


Figure 6.29. Comparison between median IDA curves – OLD SLD

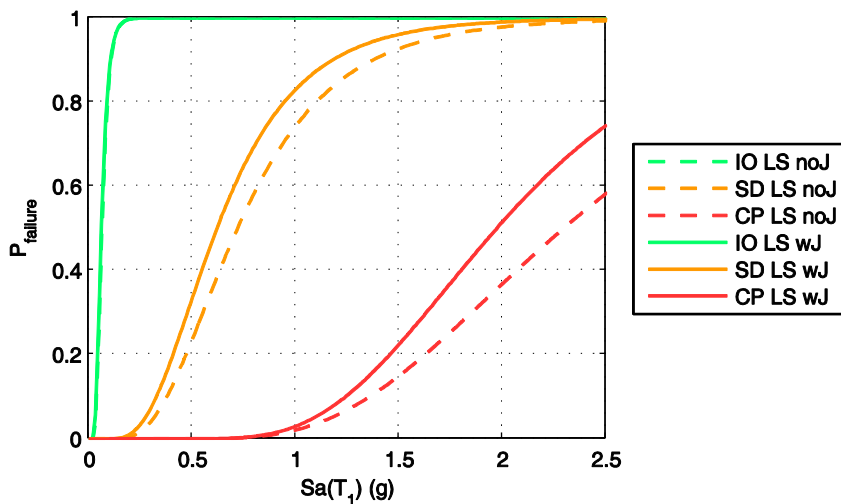


Figure 6.30. Comparison between fragility curves at IO, SD, and CP LSs – OLD SLD

The comparison between median $Sa(T_1)$ capacity (from lognormal fitting) with rigid joints (noJ) and with joints (wJ) for the OLD SLD frame is summarized in Table 6.24 for IO, SD, CP LSs, but also at FY, FC, FPC LSs. The minimum ratio between $Sa(T_1)$ capacity with and without nonlinear joint modeling (Sa_{wJ}/Sa_{noJ}) is related to higher seismic intensity, namely at SD and CP LSs, thus highlighting that the influence of joints in seismic assessment becomes more relevant at higher performance levels.

LS	Sa_{noJ} (g)	Sa_{wJ} (g)	Sa_{wJ}/Sa_{noJ} (-)
IO	0.062	0.059	0.96
SD	0.717	0.617	0.86
CP	2.293	1.969	0.86
FY	0.145	0.157	1.08
FC	1.532	1.572	1.03
FPC	2.656	2.441	0.92

Table 6.24. Comparison between median $Sa(T_1)$ capacity with rigid joints (noJ) and with joints (wJ) – OLD SLD

It was anticipated in Section 6.2 that column shear failures are detected by post-processing analyses results in two different approaches: in a force-based approach (according to the shear strength model by Sezen and Moehle, 2004) and in a displacement-based approach (adopting the IDR threshold value proposed by Aslani, 2005).

The first approach leads to the calculation of the fragility curves related to the first shear failure “FSF_V” LS shown in Figure 6.31; in the second approach, fragility curves (at the so called “FSF_IDR” LS) in Figure 6.32 are obtained. The parameters related to these fragility curves are reported in Table 6.25.

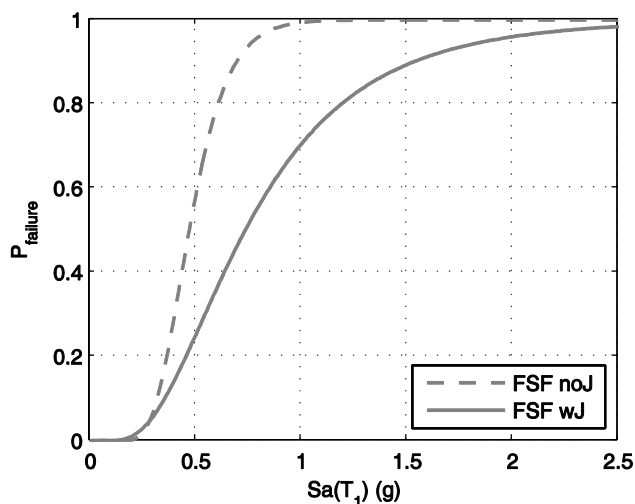


Figure 6.31. Fragility curves at FSF with rigid joints (noJ) and with joints (wJ) in force-based approach (FSF_V) – OLD SLD

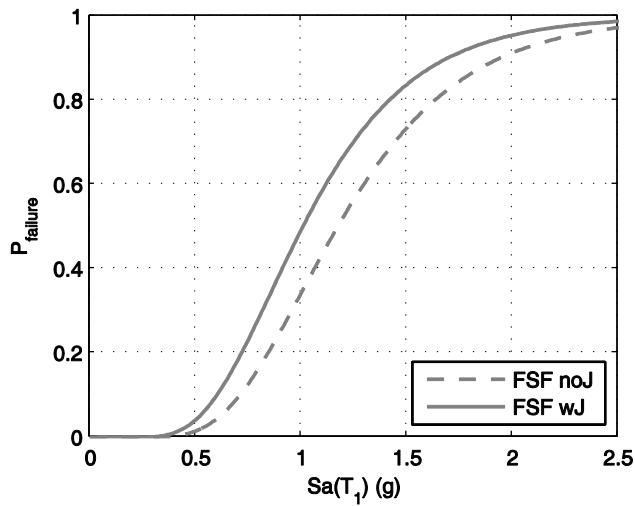


Figure 6.32. Fragility curves at FSF with rigid joints (noJ) and with joints (wJ) in displacement-based approach (FSF_IDR) - OLD SLD

LS		$Sa(T_1)_{\text{median}}$ (g)	μ (g)	β
FSF_V (force-based)	noJ	0.473	0.469	0.305
	wJ	0.799	0.734	0.573
FSF_IDR (displ-based)	noJ	1.218	1.172	0.393
	wJ	1.052	1.007	0.404

Table 6.25. Fragility parameters at FSF LS - OLD SLD

When a force-based approach is adopted, joints leads to a limitation of shear demand in columns, thus delaying their shear failures and increasing median $Sa(T_1)$ capacity at this LS from 0.473 to 0.799 g.

In a displacement-based approach, vice-versa, median $Sa(T_1)$ capacity is lower if joints nonlinear behavior is explicitly modeled since shear failure detected in this way generally occurs for maximum IDR demands that are lower than 6%, namely the IDR value beyond which the hierarchy between IDA curves changes (as shown in Figure 6.29).

6.6.2. GLD frame

In this Section, IDAs and fragility curves at the considered LSs for the GLD frame are reported and commented. IDA curves have been scaled to $Sa(T_1)$, where T_1 is the elastic period of the “with joints” configuration, namely 1.227 s.

6.6.2.1 Rigid joints

In Figure 6.33, IDAs curves related to the “rigid joints” model obtained from all the ground motion records (50) are shown in terms of first-period spectral acceleration $Sa(T_1)$ versus maximum IDR, together with the related median IDA curve, $\eta_{Sa(T_1) | IDR_{max}}$.

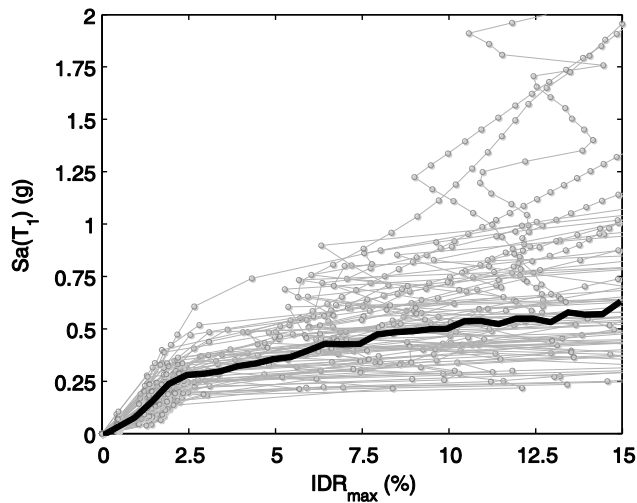


Figure 6.33. IDA curves and median IDA – GLD – rigid joints

Starting from such IDAs, fragility curves at LSs defined as the achievement of a given maximum IDR have been obtained, by means of a lognormal fit of $Sa(T_1)$ given the value of IDR threshold. In this way, fragility curves shown in Figure 6.34 have been calculated.

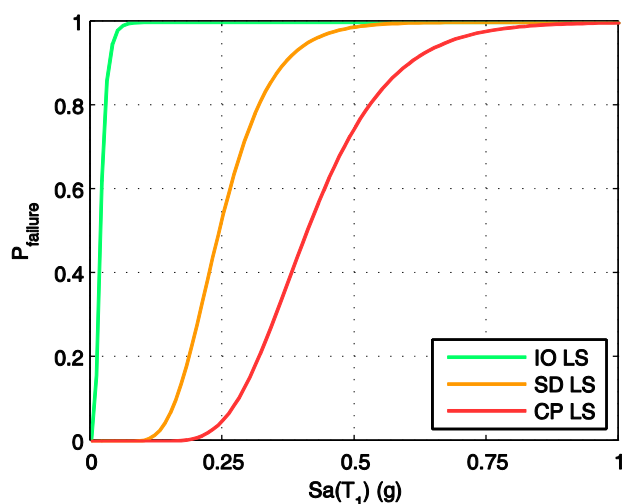


Figure 6.34. Fragility curves at IO, SD, and CP LSs - GLD - rigid joints

Related parameters are reported in Table 6.26, with μ and β representing the estimated median (expressed in (g)) and logarithmic standard deviation of $Sa(T_1)$ capacity, respectively, at IO, SD, and CP LSs. Table 6.26 also reports the maximum IDR threshold (IDR_{max}) corresponding to IO, SD, and CP LSs and the median values of $Sa(T_1)$, given the maximum IDR.

LS	$Sa(T_1)_{median}$ (g)	IDR_{max} (%)	μ (g)	β
IO	0.017	0.20	0.017	0.528
SD	0.256	2.00	0.242	0.321
CP	0.405	5.00	0.408	0.301

Table 6.26. Fragility parameters at IO, SD, and CP LSs - GLD - rigid joints

By means of the same approach based on a lognormal fit of the intensity measure capacities, fragility curves related to the achievement of a certain condition in the elements response (see Table 6.14) for the first time (i.e. in the first element) can be calculated. These fragility curves are reported in Figure 6.35 and the related parameters in Table 6.27, where $Sa(T_1)_{median}$ is the median value of $Sa(T_1)$ capacity and IDR_{max} the corresponding median value of maximum IDR.

It can be observed that the yielding condition in the first element (FY LS) occurs for a median value of $Sa(T_1)$ equal to 0.066g, while the achievement of the peak strength for the first time (FC LS) occurs for a median value of $Sa(T_1)$ equal to 0.251g, quite close to the $Sa(T_1)$ related to the FY, due to the concentrated inelastic demand generally in only one story (as revealed also by nonlinear static analysis). In this case it can be observed that the record-to-record variability provides a logarithmic standard deviation of $Sa(T_1)$ capacity (β) generally lower than the OLD SLD frame, especially for higher performance levels.

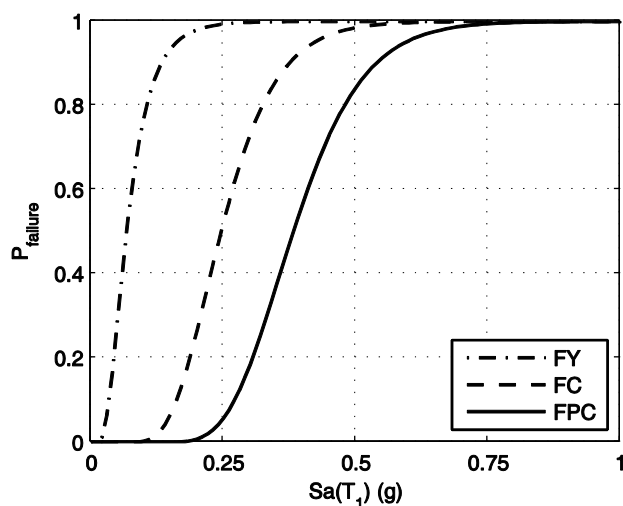


Figure 6.35. Fragility curves at FY, FC, FPC LSs - GLD - rigid joints

LS	$Sa(T_1)_{\text{median}}$ (g)	IDR_{max} (%)	μ (g)	β
FY	0.066	0.73	0.067	0.534
FC	0.251	1.99	0.245	0.329
FPC	0.381	5.56	0.382	0.269

Table 6.27. Fragility parameters at FY, FC, FPC LSs - GLD - rigid joints

6.6.2.2 With joints

The same results are reported also for the structural model that explicitly takes into account joints nonlinear behavior. Figure 6.36 shows IDAs curves

related to the model “with joints” obtained from all the ground motion records, together with the related median IDA curve, $\eta_{Sa(T_1)|IDR_{max}}$.

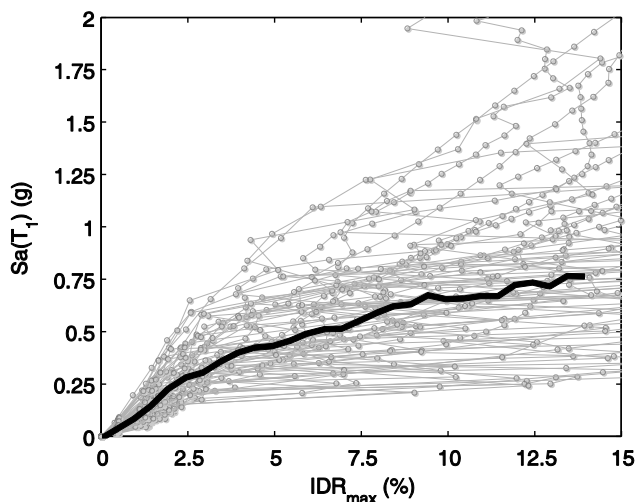


Figure 6.36. IDA curves and median IDA - GLD - with joints

Figure 6.37 reports the fragility curves at IO, SD, and CP LSs, obtained by means of a lognormal fit of $Sa(T_1)$ given the value of IDR threshold for each LS, and Table 6.28 shows the related parameters.

Figure 6.38 and Figure 6.39 report fragility curves obtained in this case at FY, FC, and FPC LSs, but also, at LSs defined as the achievement of particular “limit conditions” in joints response, namely FcrJ, FpPJ, FPJ, and FRJ (defined in Table 6.14). The related parameters are reported in Table 6.29, where $Sa(T_1)_{median}$ is the median value of $Sa(T_1)$ capacity and IDR_{max} the corresponding median value of maximum IDR.

It can be observed that the first achievement of peak strength in beam-column joints is very close to the first achievement of capping strength in beams or columns; however the first column reaching its post-peak rotation (FPC) anticipates the first joint residual strength (FRJ), due to the predominance of soft-story mechanism nevertheless the presence of joints.

As already shown for nonlinear static analyses, in the case of weak column-strong beam design, the joint damage reduces maximum interstorey drift demand and rotation demand in the adjacent column elements (as asserted by Calvi et al. 2002), but not always obtaining a prevention of the soft-story mechanism in the fifty dynamic analyses.

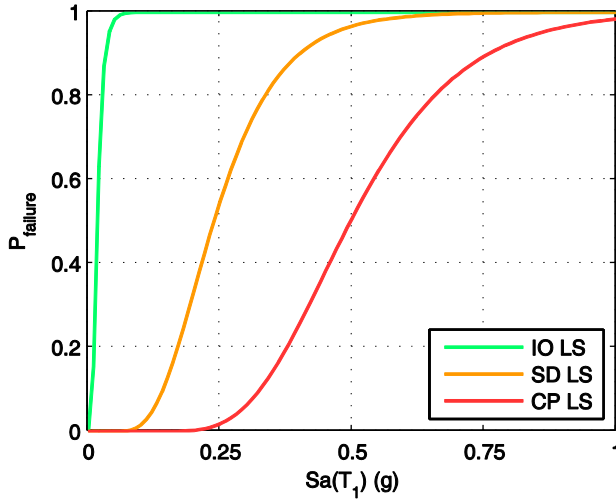


Figure 6.37. Fragility curves at IO, SD, and CP LSs - GLD - with joints

LS	$Sa(T_1)_{\text{median}}$ (g)	IDR_{max} (%)	μ (g)	β
IO	0.017	0.20	0.017	0.513
SD	0.240	2.00	0.237	0.405
CP	0.490	5.00	0.496	0.330

Table 6.28. Fragility parameters at IO, SD, and CP LSs - GLD - with joints

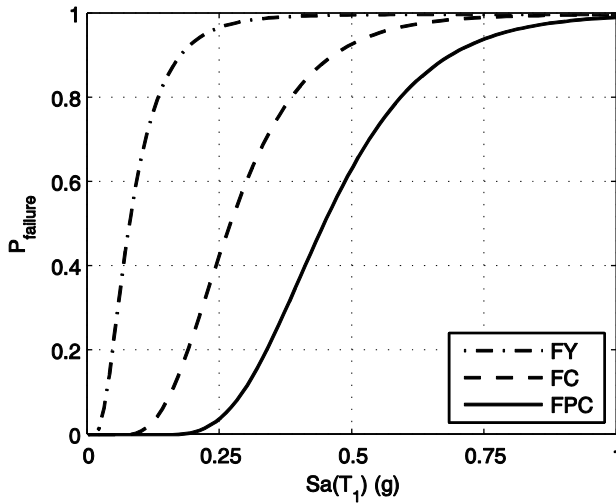


Figure 6.38. Fragility curves at FY, FC, FPC LSs - GLD - with joints

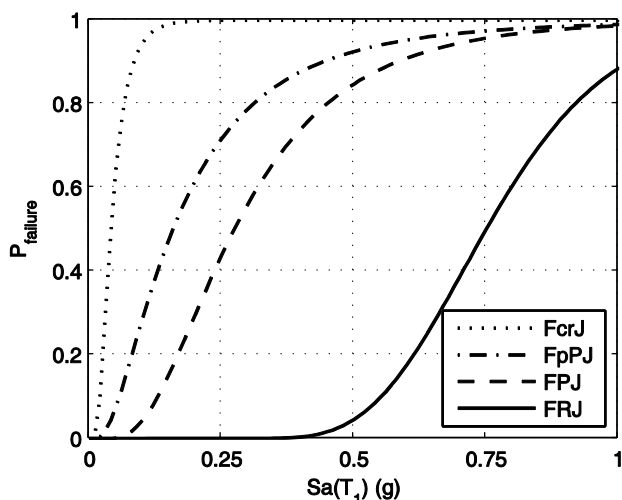


Figure 6.39. Fragility curves at FcrJ, FpPJ, FPJ, and FRJ LSs - GLD - with joints

DS	$Sa(T_1)_{median}$ (g)	IDR_{max} (%)	μ (g)	β
FY	0.086	0.879	0.077	0.627
FC	0.247	2.035	0.268	0.423
FPC	0.452	5.198	0.444	0.333
FcrJ	0.037	0.375	0.041	0.561
FpPJ	0.133	1.258	0.158	0.802
FPJ	0.236	1.933	0.274	0.587
FRJ	0.737	12.232	0.750	0.240

Table 6.29. Fragility parameters at FY, FC, FPC, FcrJ, FpPJ, FPJ, and FRJ LSs - GLD - with joints

A post-processing of the nonlinear analyses has led to the detection of joint axial failure when the maximum IDR in a story overcomes the minimum IDR capacity (IDR_{AxJ}) between joints at that story. In this way, the achievement of the first axial failure (FAXJ LS) is detected for each ground motion record and the related fragility curve (Figure 6.40 and Table 6.30) can be obtained by means of a lognormal fit. It can be observed that a maximum IDR equal to 8.22% leads to the first joint axial failure. Moreover, it should be noted that, since the independence of IDR threshold suggested by Aslani (2005) and the joint model adopted in this study, maximum IDR corresponding to the first

joint axial failure could be lower than the maximum IDR related to the first residual joint strength, as in this case.

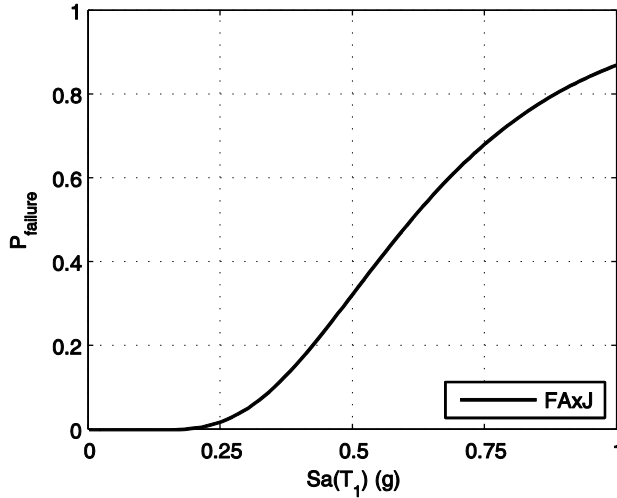


Figure 6.40. Fragility curve at FxJ - GLD - with joints

LS	$Sa(T_1)_{\text{median}}$ (g)	IDR_{max} (%)	μ (g)	β
FxJ	0.649	8.22	0.607	0.437

Table 6.30 Fragility parameters at FxJ LSs - GLD - with joints

6.6.2.3 Comparison

By comparing median IDA curves between the two analyzed frame models (“rigid joints” and “with joints”), as in Figure 6.41, a substantial overlapping of the two curves can be observed up to a maximum IDR equal to 2.5%. For higher values of maximum IDR, joint damage leads to a more uniform distribution of IDR, namely to a lower value of maximum IDR demand for a given intensity measure ($Sa(T_1)$). Actually, the GLD frame considered is a weak column-strong beam design, and its expected failure mode is a soft-story collapse. The soft-story behavior produces very high interstory drifts in the first or in the second story of the frame with rigid joints. The first and the second story of the frame “with joints” also sustains large deformations, but the upper stories experience drifts that are larger than those in the rigid-joint

frame. Thus, the roof drifts in the frame with the proposed joint model are higher due to the increased flexibility of the frame, but the maximum interstorey drifts are less than those in the rigid-joint frame.

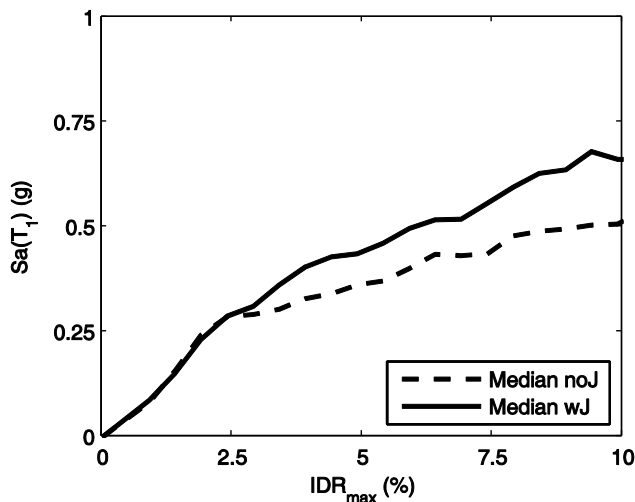


Figure 6.41. Comparison between median IDA curves – GLD

Since the rigid joint assumption precludes any damage at the joint, it is not realistic in the presence of weak column-strong beam behavior and exaggerates the soft-story effect. On the other hand, the rigid joint assumption can be considered plausible for frames designed for seismic effects according to modern seismic code provisions.

The difference in $Sa(T_1)$ capacity given IDR that can be observed from the comparison between IDA curves, produce the “distance” between fragility curves that can be observed in Figure 6.42.

The comparison between median $Sa(T_1)$ capacity with rigid joints (noJ) and with joints (wJ) for the GLD frame is summarized in Table 6.31 for IO, SD, CP LSs, and also at FY, FC, FPC LSs. Joints delay the achievement of the first yielding, capping and post-capping point in beam/column elements; at higher intensity levels (CP LS), the ratio between $Sa(T_1)$ capacity (from lognormal fitting) with and without nonlinear joint modeling (Sa_{wJ}/Sa_{noJ}) is higher than the unity, as expected since the evidences commented before.

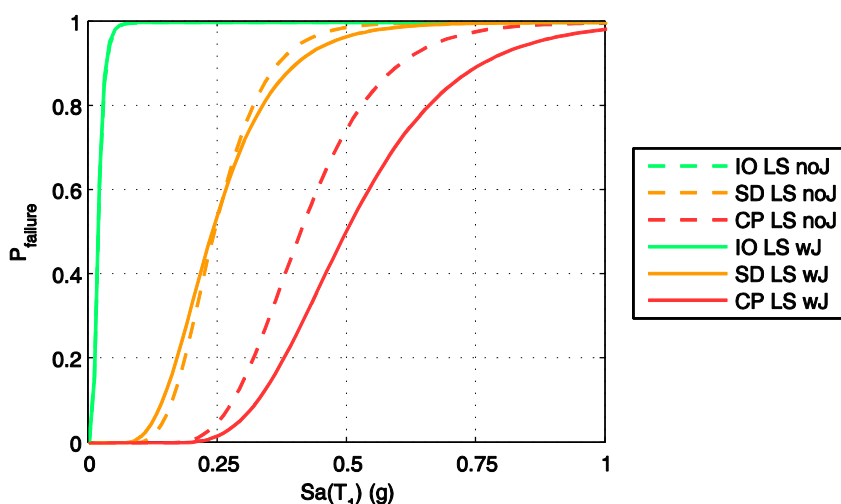


Figure 6.42. Comparison between fragility curves at IO, SD, and CP LSs - GLD

DS	Sa noJ (g)	Sa wJ (g)	Sa wJ/Sa noJ (-)
IO	0.017	0.017	0.99
SD	0.242	0.237	0.98
CP	0.408	0.496	1.22
FY	0.067	0.077	1.16
FC	0.245	0.268	1.09
FPC	0.382	0.444	1.16

Table 6.31 Comparison between median $Sa(T_1)$ capacity with rigid joints (noJ) and with joints (wJ) - GLD

Also in this case column shear failures have been detected by post-processing analyses results in two different approaches: in a force-based approach (according to the shear strength model by Sezen and Moehle, 2004) and in a displacement-based approach (adopting the IDR threshold value proposed by Aslani, 2005).

However, in this case, when the first approach is adopted, no shear failures in column are detected since the plastic shear in columns is lower than the maximum shear strength (calculated without degradation due to ductility demand), as already shown in Section 6.3.

In the second approach, fragility curves (at the so called "FSF_IDR" LS) in Figure 6.43 are obtained. The parameters related to these fragility curves are

reported in Table 6.32. In a displacement-based approach, median $Sa(T_1)$ capacity is quite similar in the two cases (“rigid joints” and “with joints”). In both cases, the achievement of FSF_IDR LS anticipates SD and FC LSs, thus confirming that more attention should be addressed to such kind of failures, especially for GLD frames.

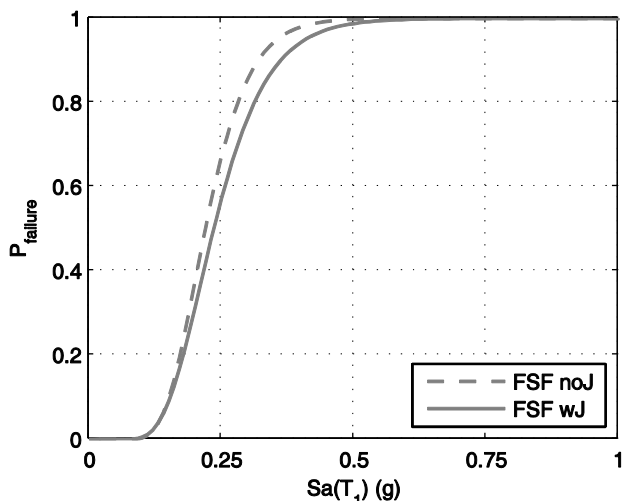


Figure 6.43. Fragility curves at FSF with rigid joints (noJ) and with joints (wJ) in displacement-based approach (FSF_IDR) - GLD

		$Sa(T_1)_{\text{median}}$ (g)	μ (g)	β
FSF_IDR	noJ	0.226	0.219	0.293
	wJ	0.240	0.235	0.336

Table 6.32. Fragility parameters at FSF LS - GLD

6.7 Summary

In this Chapter, a numerical investigation on the influence of joint failures on the seismic performance at different performance levels of two RC case study frames - designed for gravity loads only (GLD) and for seismic loads according to an obsolete technical code (OLD SLD) - was presented. A preliminary classification of joint failure typology within the frames and the definition of the corresponding nonlinear behavior were carried out. Structural models that explicitly include beam-column joints were built. In particular, the joint model proposed and presented in Chapter 5 was applied for exterior joints, in conjunction with modeling proposals from literature for interior joints and beam/column behavior. A probabilistic assessment based on nonlinear dynamic simulations of the structural response was performed taking into account record-to-record variability.

The structural capacities were primarily defined by the maximum interstorey drifts (IDR) that correspond to three widely used performance levels (or limit states) in the earthquake community: immediate occupancy, life safety or significant damage, and collapse prevention. Additionally LSs, defined on the basis of the achievement of characteristic points in the nonlinear response of the primary structural elements, have been adopted. In particular, the first achievement of a particular condition or a “conventional failure” has been detected, in analogy with the approach of typical European code prescriptions (e.g. Eurocode 8, DM 2008).

Preliminary nonlinear static analyses and incremental nonlinear dynamic analyses under selected ground motion records have been performed in OpenSees (McKenna et al, 2010) in a double condition:

- (i) with “rigid joints”, assuming a very high stiffness and shear strength for beam-column connections;
- (ii) “with joints”, explicitly modeling the nonlinear behavior of joints.

In the case of the OLD SLD frame (characterized by strong column-weak beam design), it was observed that

- the minimum ratio between $S_a(T_1)$ capacity with and without nonlinear joint modeling is related to higher seismic intensity

levels, thus highlighting that the influence of joints in seismic assessment becomes more relevant at higher performance levels;

- as far as column shear failures are concerned, when a force-based approach is adopted to detect column shear failures, joints lead to a limitation of shear demand in columns, thus delaying their shear failures and increasing median seismic capacity.
- in a displacement-based approach, vice-versa, median $S_a(T_1)$ capacity related to the first column shear failure is lower if joints nonlinear behavior is explicitly modeled.

In the case of the GLD frame, characterized by weak column-strong beam design, it can be concluded that:

- the joint damage reduces the maximum interstorey drift demand implying a prevention or a delay of the soft-story mechanism, by reducing the rotation demand in the adjacent column;
- since the rigid joint assumption precludes any damage at the joint, it is not realistic in the presence of weak column-strong beam behavior and exaggerates the soft-story effect. On the other hand, the rigid joint assumption can be considered plausible for frames designed for seismic effects according to modern seismic code provisions;
- when column shear failures are detected in a force-based approach, no shear failures in columns are captured since their plastic shear is lower than the maximum shear strength (calculated without degradation due to ductility demand);
- vice-versa, in a displacement-based approach, the achievement of the first column shear failure anticipates the achievement of Severe Damage and “first capping” limit state, thus confirming that more attention should be addressed to such kind of failures, especially for GLD frames.

Incremental dynamic analysis alone does not account for how well the nonlinear simulation model represents the real building, since no modeling uncertainties have been considered. These modeling uncertainties are especially important in predicting collapse, because of the high degree of empiricism and uncertainty in predicting deformation capacity and other

critical parameters for modeling collapse. Thus, also modeling uncertainties should be accounted for in future works to a more reliable evaluation of seismic performance.

Another important improvement of the study presented in this Chapter will be an explicitly modeling shear failures with degrading behavior after detection and consequent axial failure by means of a reliable, realistic and computational sustainable model.

Additionally, the analyzed models do not incorporate masonry infills and non-structural components. The effects of infills on structural response was shown in Chapter 3 within a N2 framework, and they are not reproduced herein in order to clearly highlight the influence primarily of joints on seismic response. It is clear that a future effort to take into account joints and infills and above all their possible interaction is necessary and it is still an open issue.

Appendix 6: selected ground motion records

Working Group ITACA (2008) - Data Base of the Italian strong motion data (http://itaca.mi.ingv.it)									
Waveform ID	EQ ID	Station ID	Earthquake Name	M_w	Fault Mechanism	Epicentral Distance (km)	PG_{Ax} (m/s^2)	PG_{Vx} (m/s)	Site class
5	3	TLM1	FRIULI	4.8	Thrust	23.5349	0.957	0.044	B
16	5	TLM1	FRIULI	4.9	Thrust	27.2795	1.147	0.037	B
17	6	TLM1	FRIULI	4.4	Thrust	26.0094	0.421	0.015	B
18	7	FRC	FRIULI	5.1	Thrust	24.9471	0.409	0.013	B
19	7	TLM1	FRIULI	5.1	Thrust	31.7127	0.354	0.011	B
20	8	FRC	FRIULI	4.7	Thrust	10.4485	0.303	0.010	B
22	9	TLM1	FRIULI	5	Thrust	10.3021	0.245	0.010	B
32	14	FRC	FRIULI	4.6	Normal	20.0131	0.451	0.020	B
47	17	FRC	FRIULI	4.7	Normal	16.0989	0.446	0.017	B
48	17	GMN	FRIULI	4.7	Normal	28.1469	0.414	0.007	B
73	22	FRC	FRIULI	5.1	Thrust	16.0768	0.946	0.042	B
85	24	FRC	FRIULI	4.6	Normal	17.122	0.267	0.007	B
96	26	FRC	FRIULI	4.9	Normal	14.092	0.574	0.020	B
113	29	FRC	FRIULI	4.6	Predominately thrust	12.2554	0.273	0.008	B
115	30	FRC	FRIULI	4.4	Normal	22.2481	0.143	0.005	B
116	30	GMN	FRIULI	4.4	Normal	10.1623	0.408	0.009	B
125	32	TLM1	FRIULI	5.3	Thrust	11.3944	0.642	0.049	B
149	40	NRC	VAL NERINA	5	n/a	10.6285	1.881	0.047	B
185	48	STR	IRPINIA	4.4	n/a	16.3766	0.243	0.013	B
186	49	BGI	IRPINIA	5	Normal	17.011	0.307	0.027	B
187	49	CLT	IRPINIA	5	Normal	17.3497	0.102	0.010	B
188	49	MRT	IRPINIA	5	Normal	42.7021	0.140	0.009	B
189	49	STR	IRPINIA	5	Normal	26.6295	0.284	0.011	B
193	52	CLT	IRPINIA	5	Normal	32.1909	0.136	0.011	B
197	54	BRN	IRPINIA	4.5	n/a	41.9101	0.282	0.010	B
198	54	CLP	IRPINIA	4.5	n/a	20.1463	0.241	0.019	B
199	54	CNB	IRPINIA	4.5	n/a	12.7241	0.276	0.019	B
200	54	CNP	IRPINIA	4.5	n/a	12.2489	0.463	0.036	B

Chapter 6

Influence of joint response on seismic assessment of non-conforming RC frames

201	54	CR1	IRPINIA	4.5	n/a	14.3901	0.493	0.020	B
203	54	CR3	IRPINIA	4.5	n/a	14.0392	0.329	0.017	B
253	68	FRN	FRIGNANO	5	Predominately thrust	20.922	0.330	0.016	B
1025	69	CTC	GUBBIO	5.6	Normal	38.1316	0.489	0.036	B
283	71	STG	VAL COMINO	5.5	Normal	37.0984	0.263	0.017	B
334	88	RNR	POTENTINO	4.8	Strike-slip	34.101	0.317	0.011	B
343	90	RNV	POTENTINO	5.1	Strike-slip	28.9119	0.329	0.011	B
344	90	TRR	POTENTINO	5.1	Strike-slip	31.6771	0.179	0.013	B
443	111	NRC	APP. UMBRO- MARCHIGIA NO	5.4	Normal	33.2226	0.308	0.011	B
467	114	NRC	APP. UMBRO- MARCHIGIA NO	5.2	Normal	19.2315	0.371	0.027	B
539	126	NRC	APP. UMBRO- MARCHIGIA NO	4.5	Normal	10.7404	0.607	0.021	B
556	129	NRC	APP. UMBRO- MARCHIGIA NO	5	Normal	22.9349	0.166	0.008	B
570	130	SELE	APP. UMBRO- MARCHIGIA NO	5.3	n/a	30.1095	0.127	0.007	B
571	130	SELW	APP. UMBRO- MARCHIGIA NO	5.3	n/a	30.2693	0.220	0.010	B
583	131	SELE	APP. UMBRO- MARCHIGIA NO	5.1	Normal	35.7286	0.135	0.006	B
584	131	SELW	APP. UMBRO- MARCHIGIA NO	5.1	Normal	35.8448	0.200	0.010	B
599	133	SELE	APP. UMBRO- MARCHIGIA NO	4.8	Normal	35.8577	0.059	0.002	B
600	133	SELW	APP. UMBRO- MARCHIGIA NO	4.8	Normal	35.99	0.064	0.003	B
847	181	AQK	Gran Sasso	5.1	Normal	12.1648	0.403	0.024	B
869	183	AQF	L'Aquila	5.6	Normal	14.783	0.772	0.031	B
870	183	AQG	L'Aquila	5.6	Normal	15.1391	1.040	0.063	B
874	183	AQV	L'Aquila	5.6	Normal	15.0648	1.441	0.054	B

Reference

- ACI (2002). Building Code Requirements for Structural Concrete (ACI 318).
- Altoontash, A. (2004). Simulation and Damage Models for Performance Assessment of reinforced concrete beam-column joints.
- Aslani, H. (2005). Probabilistic Earthquake Loss Estimation and Loss Disaggregation in Buildings, Doctoral Dissertation, Stanford University.
- Aycardi, L. E., J. Mander and A. Reinhorn (1994). "Seismic Resistance of Reinforced Concrete Frame Structures Designed Only for Gravity Loads: Experimental Performance of Subassemblages." *ACI Structural Journal* 91(5): 552-563.
- Calvi, Gian Michele, Guido Magenes, and Stefano Pampanin. "Relevance of beam-column joint damage and collapse in RC frame assessment." *Journal of Earthquake Engineering* 6.spec01 (2002): 75-100.
- Celik OC and Ellingwood BR (2008) "Modeling Beam-Column Joints in Fragility Assessment of Gravity Load Designed Reinforced Concrete Frames", *Journal of Earthquake Engineering*. 12:357-381.
- Celik OC. Probabilistic assessment of non-ductile reinforced concrete frames susceptible to Mid-America ground motions. PhD dissertation, School of Civil and Environmental Engineering, Georgia Institute of Technology, Atlanta, GA; 2007.
- Celik, OC, and Ellingwood, BR (2010) "Seismic fragilities for non-ductile reinforced concrete frames—Role of aleatoric and epistemic uncertainties", *Structural Safety*, 32(1): 1-12.
- CEN (2005) European standard EN1998-3. Eurocode 8: design provisions for earthquake resistance of structures – Part 3: assessment and retrofitting of buildings. European Committee for Standardisation, Brussels
- Decreto Ministeriale del 30/5/1972. Norme tecniche alle quali devono uniformarsi le costruzioni in conglomerato cementizio, normale e precompresso, ed a struttura metallica. G.U. n. 190 del 22/7/1972. (in Italian)
- Decreto Ministeriale n. 40 del 3/3/1975. Approvazione delle norme tecniche per le costruzioni in zone sismiche. G.U. n. 93 dell'8/4/1975. (in Italian)
- DM 2008, Decreto Ministeriale del 14/1/2008. Approvazione delle nuove norme tecniche per le costruzioni. G.U. n. 29 del 4/2/2008. (in Italian)
- El-Attar AG, White RN, Gergery P (1997) "Behavior of gravity load designed reinforced concrete buildings subjected to earthquakes," *ACI Structural Journal* 94(2): 133– 145.
- Elwood, Kenneth J. "Modelling failures in existing reinforced concrete columns." *Canadian Journal of Civil Engineering* 31.5 (2004): 846-859.
- Filiatrault, A., E. Lachapelle and P. La montagne (1998). "Seismic performance of ductile and nominally ductile reinforced concrete moment resisting frames I. Experimental Study ." *Canadian Journal of Civil Engineering* 25(2): 331-341.
- Haselton, C. B. (2006). Assessing Seismic Collapse Safety of Modern Reinforced Concrete Frame Buildings, Doctoral Dissertation, Stanford University.
- Haselton, C., A. Liel, S. Taylor Lange and G. G. Deierlein (2007). Beam-Column Element Model Calibrated for Predicting Flexural Response Leading to Global Collapse of RC Fra me

- Buildings, Pacific Earthquake Engineering Research Center 2007/03, University of California at Berkeley.
- Hassan and Moehle (2013) "Quantification of residual axial capacity of beam-column joints in existing concrete buildings under seismic load reversals", Compdyn – Kos Island, Greece, 12–14 June 2013.
- Iervolino I., Galasso C., Cosenza E., REXEL: computer aided record selection for code-based seismic structural analysis, *Bulletin of Earthquake Engineering*, 8(2), 339-362, 2010.
- Ibarra, L. (2003). *Global Collapse of Frame Structures under Seismic Excitations*, Doctoral Dissertation (Blume Center TR 152), Stanford University.
- Ibarra, L. F. , R. A. Medina and H. Krawinkler (2005). "Hysteretic Models that Incorporate Strength and Stiffness Deterioration." *Earthquake Engineering and Structural Dynamics* 34: 1489- 1511.
- Jeon, J. S., Lowes, L. N., DesRoches, R., & Brilakis, I. (2015). "Fragility curves for non-ductile reinforced concrete frames that exhibit different component response mechanisms." *Engineering Structures* 85: 127-143.
- Kunnath, S. K., G. Hoffmann, A. M. Reinhorn and J. B. Mander (1995). "Gravity-Load-Designed Reinforced Concrete Buildings -Part I: Seismic Evaluation of Existing Constr. uction." *ACI Structural Journal* 92(3): 343-354.
- Kurama, Y. C., S. P. Pes siki, R. Sause and S. Wu (1994). "Seismic Behavior of Non-Ductile Concrete Frame Structures." *ASCE Structures Congress*.
- Liel, Abbie B. *Assessing the collapse risk of California's existing reinforced concrete frame structures: Metrics for seismic safety decisions*. Diss. Stanford University, 2008.
- Lowes, L. N., N. Mitra and A. Altoontash (2004). *A Beam-Column Joint Model for Simulating the Earthquake Response of Reinforced Concrete Frames*, PEER.
- McKenna, F., Fenves, G.L., Scott, M.H. (2010). *OpenSees: Open System for Earthquake Engineering Simulation*. Pacific Earthquake Engineering Research Center. University of California, Berkeley, CA, USA. <http://opensees.berkeley.edu>
- Reinforced Concrete Beam-Column Joints*, Doctoral Dissertation, Stanford University.
- Sezen, H. and J. Moehle (2004). "Shear Strength Model for Lightly Reinforced Concrete Columns." *Journal of Structural Engineering* 130(11): 1692-1703.
- Shome N, Cornell CA, Bazzurro P, Carballo JE. Earthquakes, records, and nonlinear responses. *Earthquake Spectra (EERI)* 1998;14(3):469–500.
- Vamvatsikos D., Cornell C.A., Incremental dynamic analysis. *Earthquake Engineering and Structural Dynamics*, 31(3), 491-514, 2002.

Chapter 7

EXPERIMENTAL INVESTIGATION ON EXTERIOR NON-CONFORMING BEAM- COLUMN JOINTS

In the previous Chapters it was highlighted that in the assessment of the performance of typical existing buildings, seismic collapse safety might be significantly affected by the non-linear behavior of the joints that are involved in the failure mechanisms especially if they are characterized by poor structural detailing, such as the lack of an adequate transverse reinforcement in the joint panel. Commonly accepted tools to assess existing joint capacity – which is the starting point for a rational retrofit strategy – are not available in literature. Few reliable approaches for modeling all sources of nonlinearity are proposed in literature for poorly designed beam-column joints mainly because of relatively poor information from experimental tests.

Thus, this Chapter aimed to improve the understanding of exterior joints seismic performance without transverse reinforcement in existing RC buildings through experimental tests.

Two full-scale exterior unreinforced beam-column joint sub-assemblages are tested under cyclic loading. The specimens are different for beam longitudinal reinforcement ratio and they are both reinforced with deformed bars. Two different kinds of joint failure are expected, with or without the yielding of the adjacent beam. Strain gauges located on beam bars and displacement transducers on the joint panel allow the complete definition of both the deformability contributions of fixed-end-rotation and shear strain of the panel. Design criteria, adopted setup and main experimental results are described herein.

Finally experimental results are compared with numerical results carried out through the adoption of the model proposed and presented in Chapter 5.

7.1 Introduction

Reinforced Concrete (RC) buildings designed for gravity loads only or according to obsolete seismic codes are widespread in Italian and Mediterranean building stock. For these buildings, beam-column joints represent a critical issue; the lack of capacity design principles leads to a low shear strength of the joint, potentially leading to a shear failure that limits the deformation capacity of adjoining beams and/or columns (Park and Mosalam, 2013; Celik and Ellingwood, 2008).

Past earthquakes showed that shear failure in beam-column joints can lead to building collapse (Moehle and Mahin 1991) which often can be attributed to inadequate joint confinement. In recent earthquakes all around the world (Izmit earthquake (Sezen et al. 2000), Tehuacan earthquake (EERI 1999a), Chi-Chi earthquake (EERI 1999c)), the inadequacy of building joints designed according to earlier rather than more current standards was one of the main causes of severe damages or collapses. In particular, the observations of damage after L'Aquila earthquake (2006) indicated that some RC buildings designed in Italy before the mid-1990s may have serious structural deficiencies especially in joint regions, mainly due to a lack of capacity design approach and/or poor detailing of reinforcement (Ricci et al. 2011).

A significant amount of research on the seismic performance of RC beam-column joints has been carried out in the last forty years (see Chapter 2 and Chapter 5). The majority of the research literature has emphasized the improvement of the performance of RC beam-column joints through new design concepts and improved details such as joint hoops or improved anchorage.

Several researchers have focused on an array of different variables, in particular including the effect of column axial load, concrete strength, joint aspect ratio, beam longitudinal reinforcement ratio. However, most of the authors did not fully investigate experimentally the effect of all the above parameters, likely because of the different interests associated with single national design standards and above all due to the difficulty in carrying out extensive experimental tests programs. Still nowadays, the influence of some parameters such as the axial load in the column was not always fully recognized.

In most of the tests the focus was given to the ultimate shear strength of the joint; thus only few authors have measured joint shear strain (e.g., Clyde, 2000; Pantelides, 2002 for plain exterior joints or Hassan 2011 and Park and Mosalam 2013 for corner joints). However a complete characterization of the nonlinear local response of the joint panel and fixed-end-rotation contribution is necessary to clearly understand beam-column joint behavior also within the context of a RC frame.

Thus, this Chapter aimed to improve the understanding of exterior joints seismic performance without transverse reinforcement in existing RC buildings through two experimental tests, different for failure typology, analyzing also local shear stress-strain response of the joint panel and longitudinal bars slippage contribution to the overall deformability.

7.2 Experimental program

7.2.1. Specimens: design and construction

Two full-scale exterior unreinforced beam-column joint sub-assemblages have been tested under cyclic loading.

The two specimens are different for beam longitudinal reinforcement ratio and they are both reinforced with deformed bars. Specimens are designed to obtain two different kinds of joint failure, with or without the yielding of the adjacent beam.

Columns were designed according to capacity design principles in order to obtain a weak beam-strong column hierarchy. Beam longitudinal reinforcement was designed to observe beam yielding after (Test #1) or before (Test #2) joint shear failure occurrence. Stirrup spacing in beam and column is designed to avoid shear failure, while no transverse reinforcement is located in the joint panel zone.

The two tests are identical for geometry: the beam is 50 cm wide and 30 cm deep and the column section is 30x30 cm².

As shown in Figure 7.1, in Test #1, the beam is symmetrically reinforced with 4 ϕ 20 bars for both the positive and negative reinforcement (corresponding to a compression and tension reinforcement ratio equal to $\rho'=\rho=0.84\%$); also column is symmetrically reinforced with 4 ϕ 20 bars for top and bottom sides, corresponding to a total reinforcement ratio ($\rho'+\rho$) equal to

2.79%.

As shown in Figure 7.2, in Test #2, the beam is symmetrically reinforced with 4 ϕ 12 bars for both the positive and negative (corresponding to a compression and tension reinforcement ratio equal to $\rho'=\rho=0.30\%$); also column is symmetrically reinforced with 4 ϕ 12 bars for top and bottom sides, corresponding to a total reinforcement ratio ($\rho'+\rho$) equal to 1.01%.

In both cases, top and bottom beam longitudinal bars are hooked bent at 90° into the joint core.

The transverse reinforcement consists of a 8 mm diameter closed stirrup with 90° bend and 10 cm extension on both ends. The stirrups are spaced at 10 cm along the beam and the column except within 62 cm of beam and column end, where the spacing is reduced to 5 cm to give adequate strength at the location where forces are applied during the test.

The longitudinal reinforcement in the column extends continuously up through the joint from the bottom to the top of the column.

Column length was designed to be representative of typical interstory height (3.4 m) and beam length (1.8 m) is intended to be representative of a portion up to a zero point of bending moment diagram in frames designed for gravity loads.

The test unit reinforcement cages were constructed according to Figure 7.1 and Figure 7.2 and cast in place in pairs horizontally (see Figure 7.3). A high-frequency vibrator was used to consolidate the concrete. Each test unit was allowed to cure for at least 72 hours before they were removed from the forms.

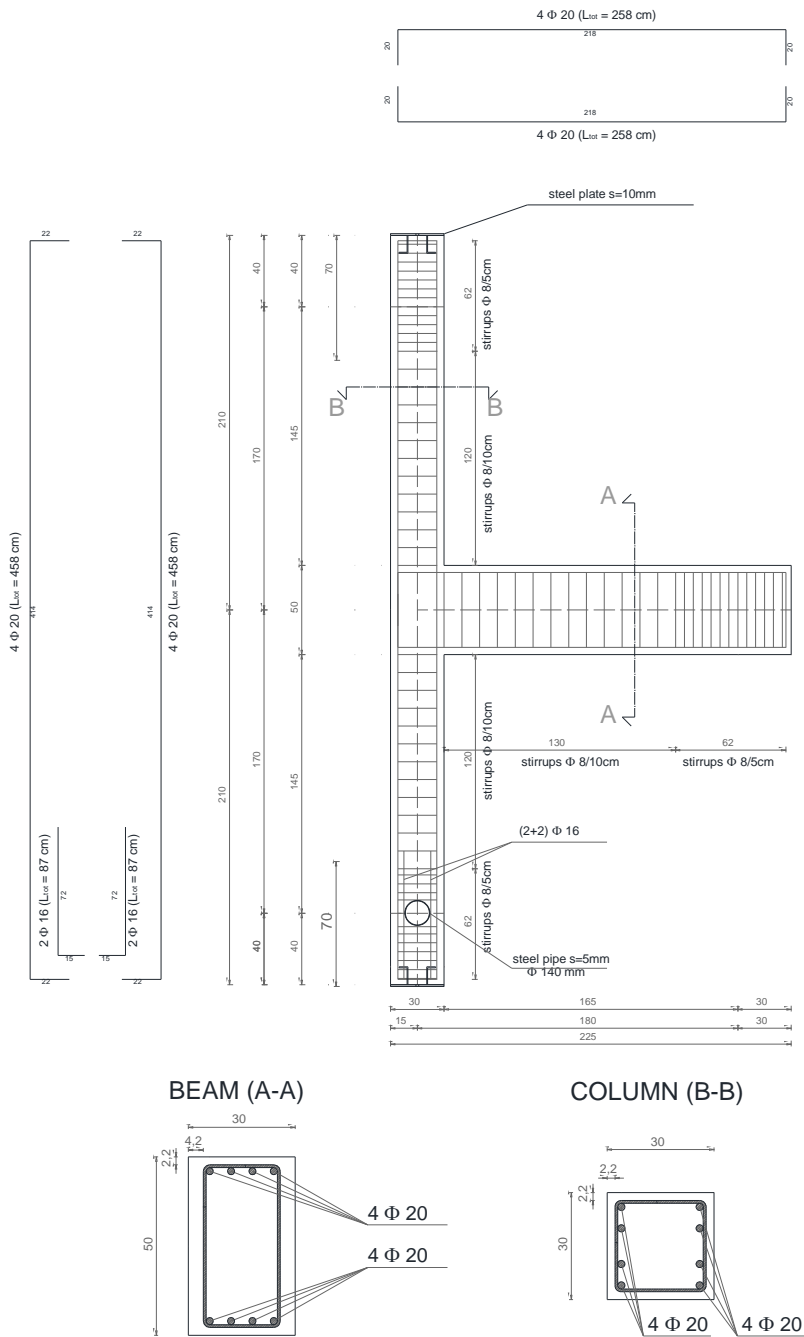


Figure 7.1. Geometry and reinforcement details - Test #1

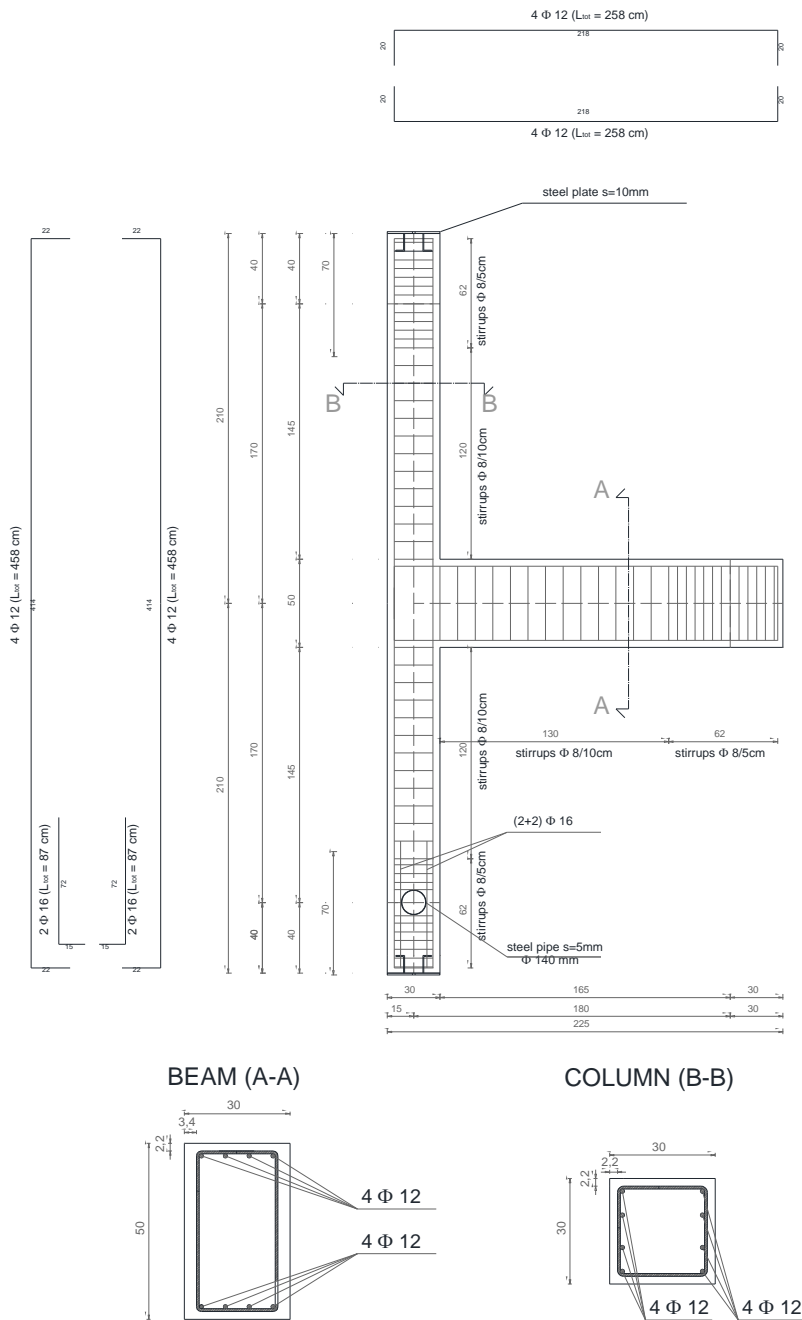


Figure 7.2 . Geometry and reinforcement details - Test #2



Figure 7.3. Specimens construction

7.2.2. Materials

Concrete compressive strength for all specimens was evaluated on four 15×15×15 cm³ cubic samples (CSs) of the casted concrete. Values of 28-day cylindrical strength for each CS and their mean value is reported in Table 7.1.

Cubic sample	Cylindrical compressive strength (f_c) (MPa)
CS1	27.2
CS2	29.2
CS3	31.2
CS4	27.4
mean	28.8

Table 7.1. Properties of concrete

Commercial typology of reinforcing steel adopted is B450C (NTC 2008), i.e., class C reinforcement with $f_{yk}=450$ MPa according to Annex C provisions of Eurocode 2 (EN 1992-1-1:2004 Annex C). Tensile tests were carried out on three samples for each bar diameter. Table 7.2 reports mean values of their mechanical properties, namely yield strength (f_y), ultimate strength (f_t) and hardening ratio (f_t/f_y). In Appendix 7A steel stress-strain behavior are reported for each sample.

Diameter (mm)	Yield strength (f_y) (MPa)	Ultimate strength (f_t) (MPa)	Hardening ratio (f_t/f_y) (-)
20	486.5	595.5	1.22
12	459.1	559.7	1.22
8	492.0	606.8	1.23

Table 7.2. Properties of steel

7.2.3. Test setup

A schematic of the loading apparatus is shown in Figure 7.4. The column was mounted horizontally with pinned supports at both ends and the specimen was constrained to the strong floor by means of two rigid steel frames. Steel spherical hinges were placed between the beam end and floor to limit friction and to allow tip beam free movement.

The axial load was applied using a small hydraulic jack in load control and transferred to the column through a system constituted by four pre-stressed rods connected to strong steel plates located on the top and bottom of the column. Four strain gauges (sgs B1, B2, B3 and B4 in Figure 7.5), one on each pre-stressed rod, were used to check axial stress acting on bars. In particular, a constant value of axial load equal to 260 kN (corresponding to an axial load ratio equal to 0.1) was adopted.

An hydraulic actuator applies the lateral load in displacement control at the end of the beam by means of a loading collar. A load cell situated between the hydraulic actuator and the loading collar measured the quasi-static cyclic load applied to the beam. The actuator was pinned at the end to allow rotation during the test.

Five Linear Variable Displacement Transducers (LVDTs) were employed as shown in Figure 7.5 to measure rotation of the joint (E, D, F), hinge rotation (A, B) and eventual rigid body movement of the specimen.

Twelve linear potentiometer sensors (LPs) adopted to measure joint shear strain and fixed-end-rotations were located in the joint panel along longitudinal reinforcement layers of beam and column and along the diagonals of the joint panels, as shown in Figure 7.6(a).

A wire potentiometer was placed at the end of the beam to measure beam deflection.

Strains in beam longitudinal reinforcement were measured, too, by means of six strain gauges (sgs) located as shown in Figure 7.6(b) (three on a bar in the top layer and three on a bar in the bottom layer).

Additional two LVDTs located along beam deep were used in Test #2 in order to have a more reliable measure of beam fixed-end-rotation contribution.

Figure 7.7 shows a photo of test setup (a) and joint panel zone

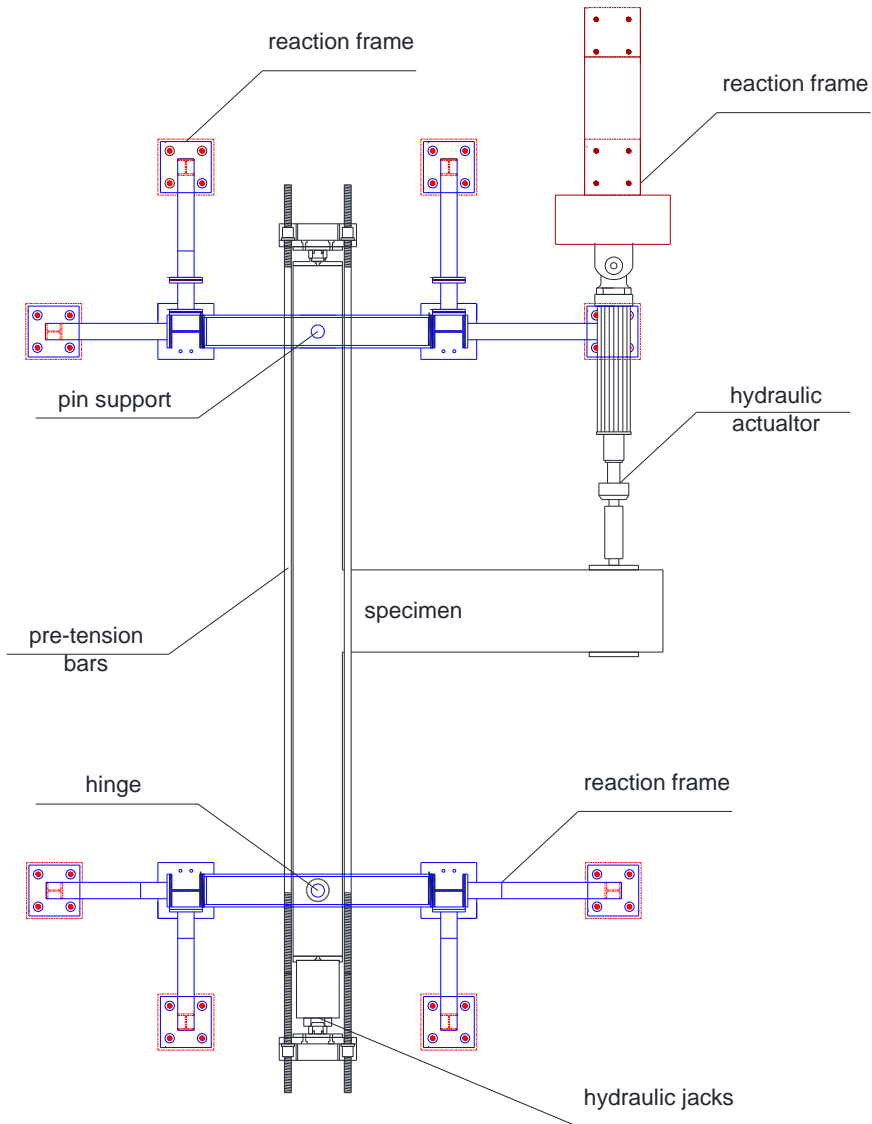


Figure 7.4. Test setup

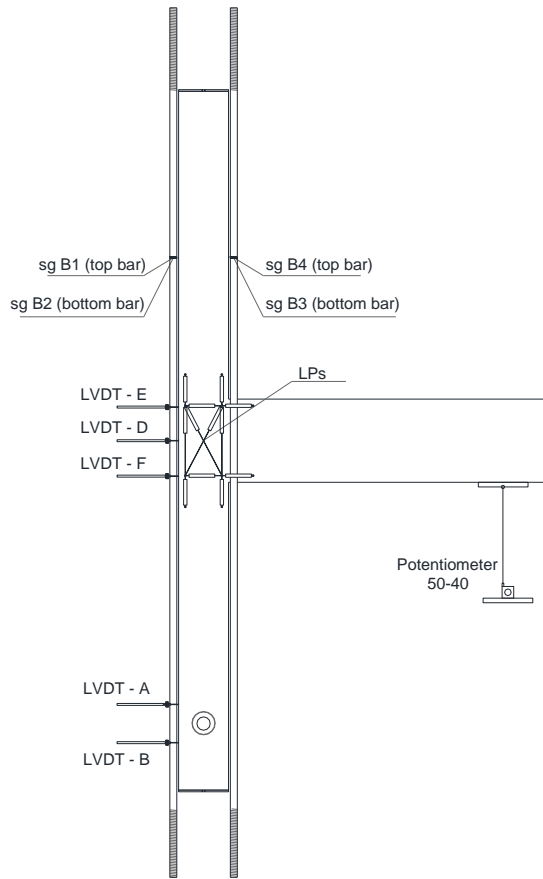


Figure 7.5. Instrumentation layout

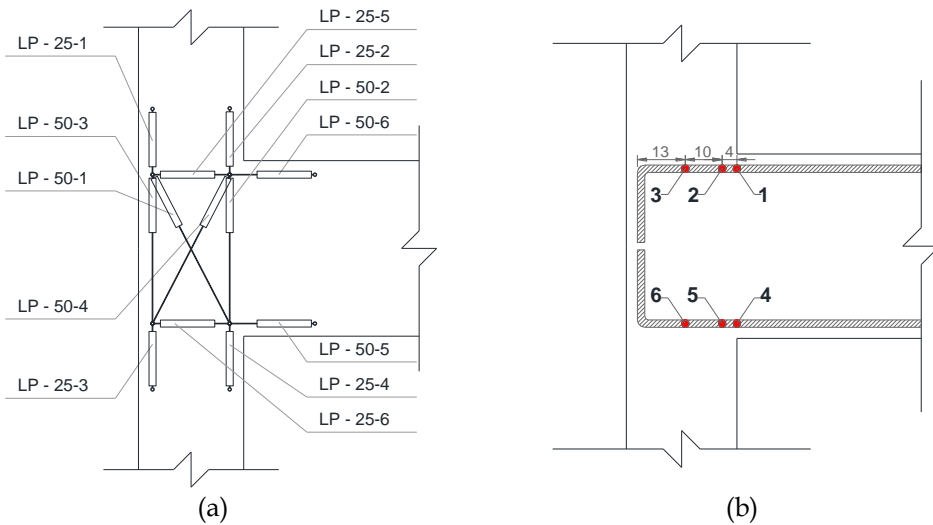


Figure 7.6. Linear potentiometers (LPs) on joint panel (a) and strain gauges location (b)

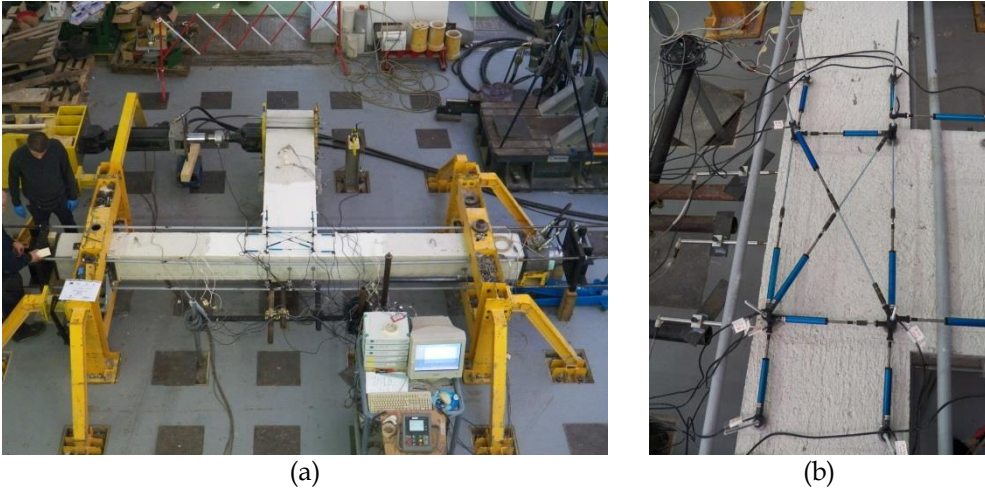


Figure 7.7. Test setup (a) and joint panel instrumentation (b)

7.2.4. Load Pattern

Before beginning each test, the axial load was slowly applied to the column until the appropriate level was achieved. Then, the lateral load was applied cyclically, in a quasi-static way, at the end of the beam. The loading procedure consisted of displacement-controlled steps beginning at a 0.25% drift followed by steps of 0.50%, 0.75%, 1.0%, 1.5%, 2.0%, 3.0%, 4.0% and 6.0% drift. Each drift step consisted of 3 cycles of push and pull.

The loading procedure can be stopped before it is fully completed if the hydraulic jack cannot sustain in safe the column axial load.

Table 7.3 and Figure 7.8 show in details the patter load program.

Pattern load program					
Cycle #	Drift [%]	Displacement [mm]	N° of cycles [-]	Velocity [mm/sec]	Time [sec]
1	0.25	4.50	3	0.5	108
2	0.5	9.00	3	0.5	216
3	0.75	13.50	3	0.5	324
4	1	18.00	3	0.5	432
5	1.5	27.00	3	0.5	648
6	2	36.00	3	0.5	864
7	3	54.00	3	1	648
8	4	72.00	3	1	864
9	6	108.00	3	1	1296

Table 7.3. Pattern load program

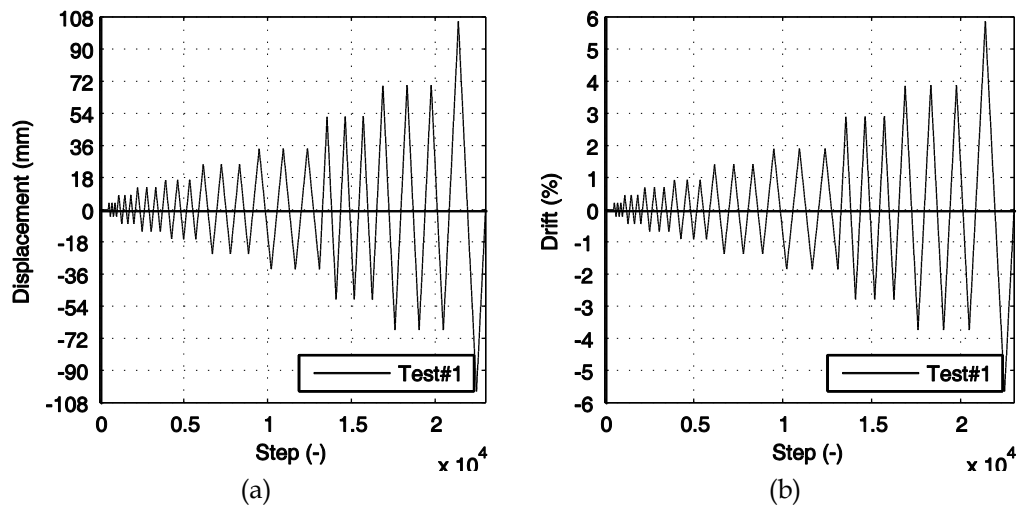


Figure 7.8. Imposed displacement (a) and drift (b) history

7.3 Analysis of results

In this Section, lateral load-displacement response of the specimens is analyzed (mainly referring to response envelope), and the evolution of observed damage with increasing imposed displacement is described (Section 7.3.1). Then local response is investigated (Section 7.3.2) in terms of joint shear strain γ_j and fixed-end rotation θ_s . The convention on signs adopted herein for beam load, beam drift and related local response (joint shear strain γ_j and fixed-end rotation θ_s) is reported in Figure 7.9.

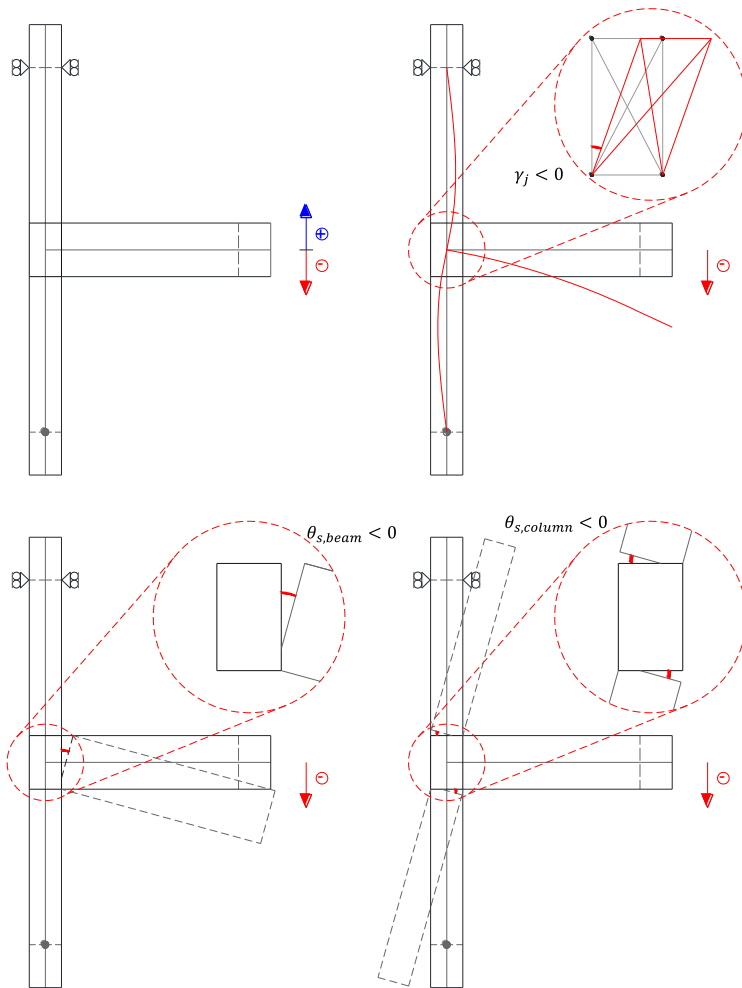


Figure 7.9. Convention on sign of beam load, beam drift, joint shear strain and fixed-end-rotation

7.3.1. Global response and observed damage

7.3.1.1 Beam lateral load versus drift

Test #1

Test #1 exhibited an initial uncracked stiffness, calculated as the secant to the experimental backbone in its first point, equal to 14970 N/mm. Such a stiffness slightly decreased up to 12654 N/mm in the first millimeter of displacement applied to the beam end, and showed a more significant reduction when the applied drift ranges between 0.5% and 0.75%, when first joint panel cracking occurred, as better shown in Section 7.3.1.2.

Experimental response was quite symmetric during the push-pull cycles. Peak load was reached for a drift equal to 1.40% for positive loading direction and -1.38% for negative loading direction. Peak values of beam lateral load were 74.02 kN and -72.35 kN, respectively for positive and negative loading direction.

Since beam yielding is expected to occur for a beam lateral load value of 155.6 kN, such a test can be classified as J-failure, namely joint shear failure happens before yielding of beam. Such a classification will be confirmed by the measures of bar strains provided by the adopted strain gauges.

When the test was interrupted (at the first cycle of 6% drift) the strength reduction (evaluated from first steps for each cycle) was equal to 47% and 53%, respectively in positive and negative direction.

Beam lateral load (measured by means of the load cell) versus drift (measured by means of the wire potentiometer 50-40) response related to Test #1 is reported in Figure 7.10.

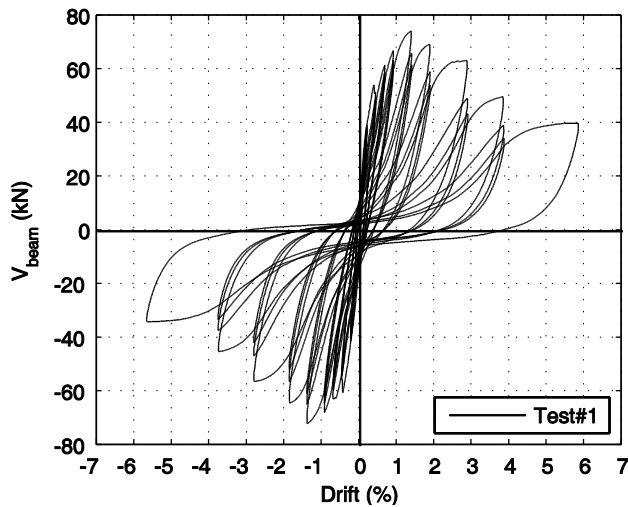


Figure 7.10. Beam lateral load-drift response – Test #1

Test #2

Test #2 exhibited an initial uncracked stiffness, calculated as the secant to the experimental backbone in its first point, equal to 15122 N/mm. Such a stiffness rapidly decreased up to 14482 N/mm in the first millimeter of displacement applied to the beam end, and showed a more significant reduction when the applied drift ranges between 0.25% and 0.50%, when first cracks along beam-joint interface started to occur, as better shown in Section 7.3.1.2.

Experimental response is quite symmetric during the push-pull cycles. Peak load was reached for a drift equal to 0.88% for positive loading direction and -0.69% for negative loading direction. Peak values of beam lateral load were 58.33 kN and -53.27 kN, respectively for positive and negative loading direction.

Since beam yielding is expected to occur for a beam lateral load value of 52.9 kN, such a test can be classified as BJ-failure, namely joint shear failure happens after yielding of beam. Such a classification will be confirmed by the measures of bar strains provided by the adopted strain gauges.

Test #2 was interrupted when the three cycles at 2% drift were fully completed because the hydraulic jack cannot more sustain in safe the column axial load, as explained in details in Section 7.3.2.4. When the test was interrupted the strength reduction (evaluated from first steps for each cycle) was equal to 27% and 31%, respectively in positive and negative direction.

Beam lateral load (measured by means of the load cell) versus drift (measured by means of the wire potentiometer 50-40) response related to Test #2 is reported in Figure 7.11.

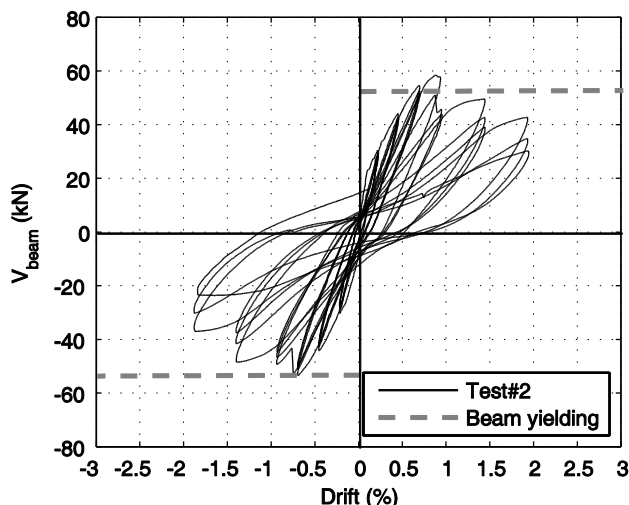


Figure 7.11. Beam lateral load-drift response – Test #2

Peak values of beam lateral load for positive ($V_{b,max,POS}$) and negative ($V_{b,max,NEG}$) loading directions and corresponding drifts ($Peak_{DriftPOS}$ and $Peak_{DriftNEG}$, respectively) are summarized in Table 7.4, together with beam load value corresponding to beam yielding.

	$V_{b,max,POS}$ (kN)	$Peak_{Drift,POS}$ (%)	$V_{b,max,NEG}$ (kN)	$Peak_{Drift,NEG}$ (%)	$V_{b,beam_yiel}$ (kN)
Test #1	74.02	1.40	-72.35	-1.38	155.6
Test #2	58.33	0.88	-53.27	-0.69	52.9

Table 7.4. “Peak points” and yielding beam load

Complete experimental data related to the backbones of beam lateral load-drift are reported in Appendix 7B.

7.3.1.2 Observed damage

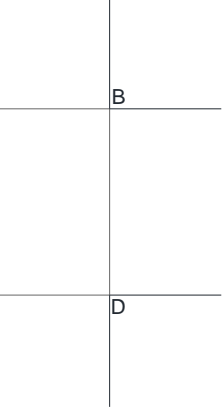
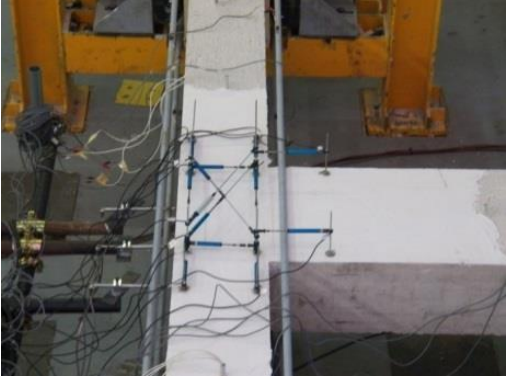
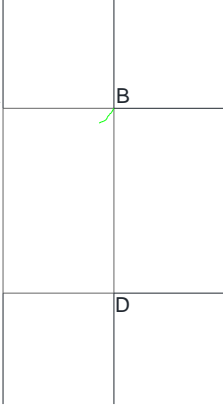
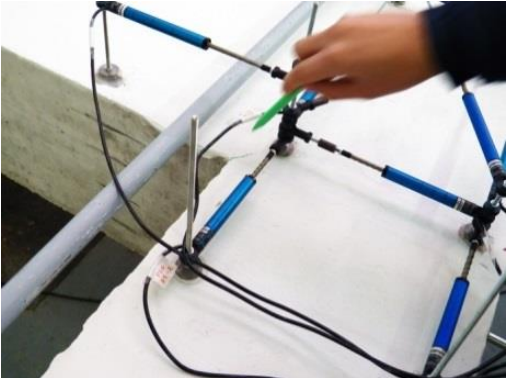
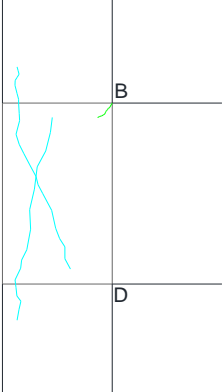
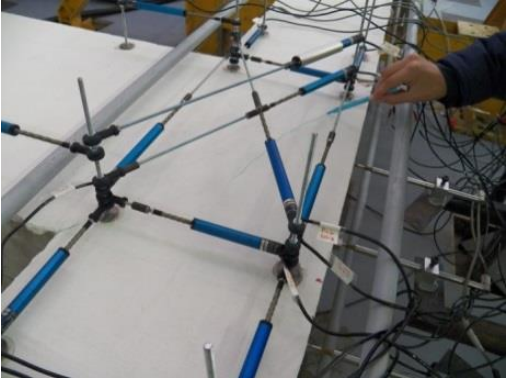
Test #1

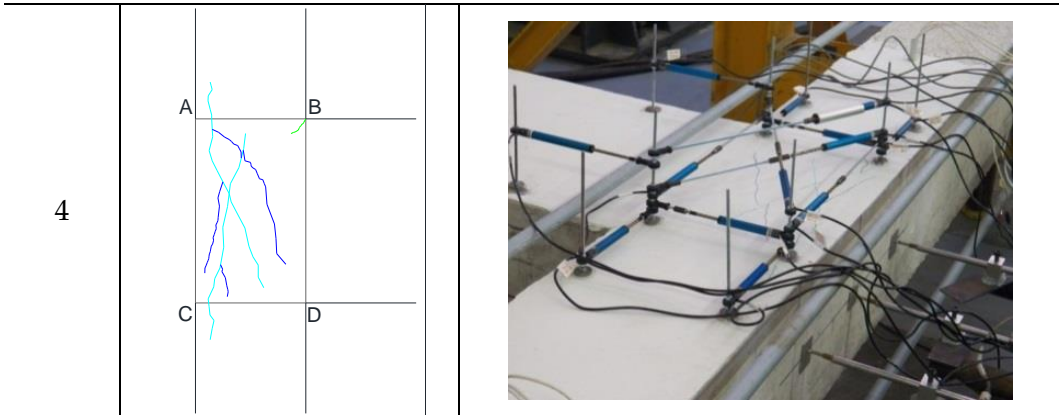
First cracks in the joint panel started to appear when a drift ratio equal to 0.5% was imposed, starting from corner B, as shown in Figure 7.12. Between a drift value that ranges between 0.5% and 0.75%, diagonal cracks in the joint panel occurred and spread along column longitudinal bars. When a drift value equal to 2% was reached, cracks at beam-joint interface started to appear and increase progressively their width, mainly due to fixed-end-rotation of the beam. At 3% drift, existing cracks in the joint panel increased their width and concrete cover spalling started to occur from corner C (see Figure 7.12). Concrete cover spalling was complete when a drift value of 6% was reached.

In Figure 7.12 the evolution of joint panel damage state is visually reported and Figure 7.13 shows the final damage state of the specimen. In Figure 7.14 the global response is associated to the corresponding damage states of the joint panel.

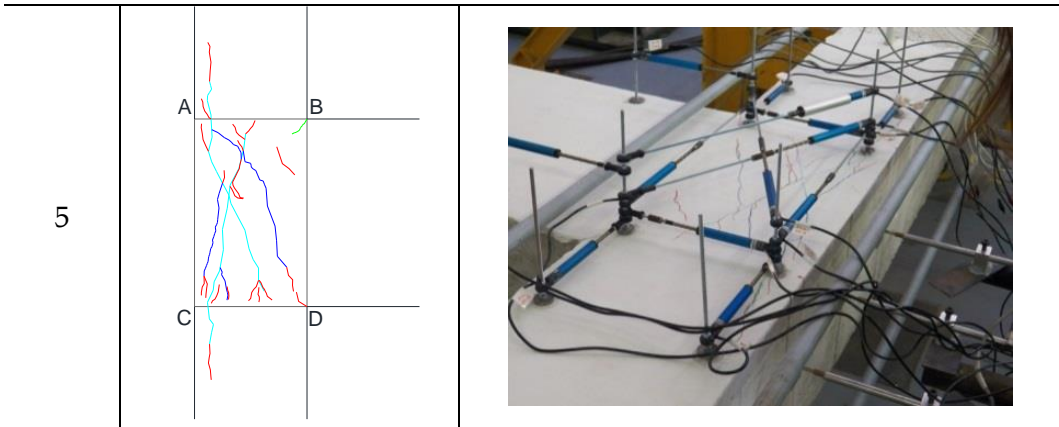
Table 7.5 summarizes the evolution of the observed damage for Test #1 described above.

Furthermore, Figure 7.15 represents displacement (δ) measured by means of the linear potentiometer (LPs) located along the diagonals of the joint panel. The data are cut at the step 12600, corresponding to 2% drift, when cracks significantly involved the supported points of LPs, causing unreliable lectures. It can be observed that LP 50-4 provides the higher values of cracks width (up to about 7 mm), proving that joint panel damage was more important along the diagonal A-D (perpendicular to LP 50-4 direction).

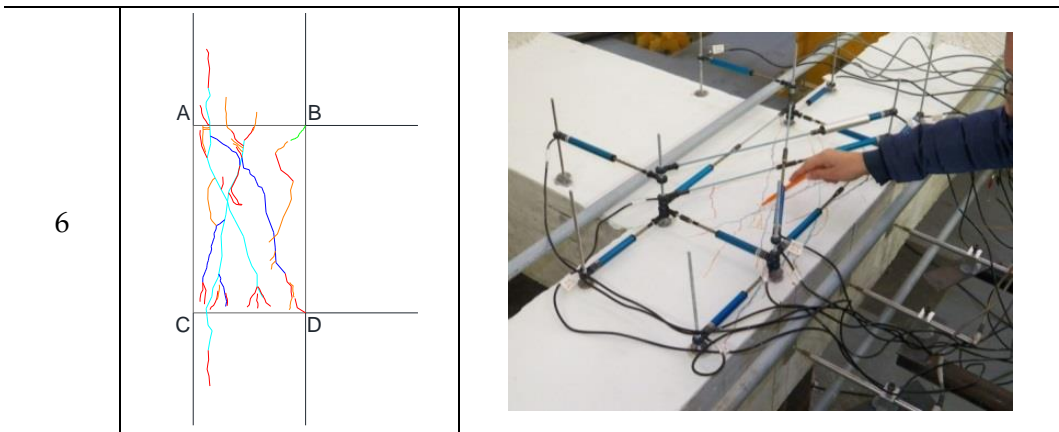
Cycle	Joint panel damage state - Test #1		
1			
Initial state - Drift 0.25%			
2			
Drift 0.5%			
3			
Drift 0.75%			



Drift 1%



Drift 1.5%



Drift 2%

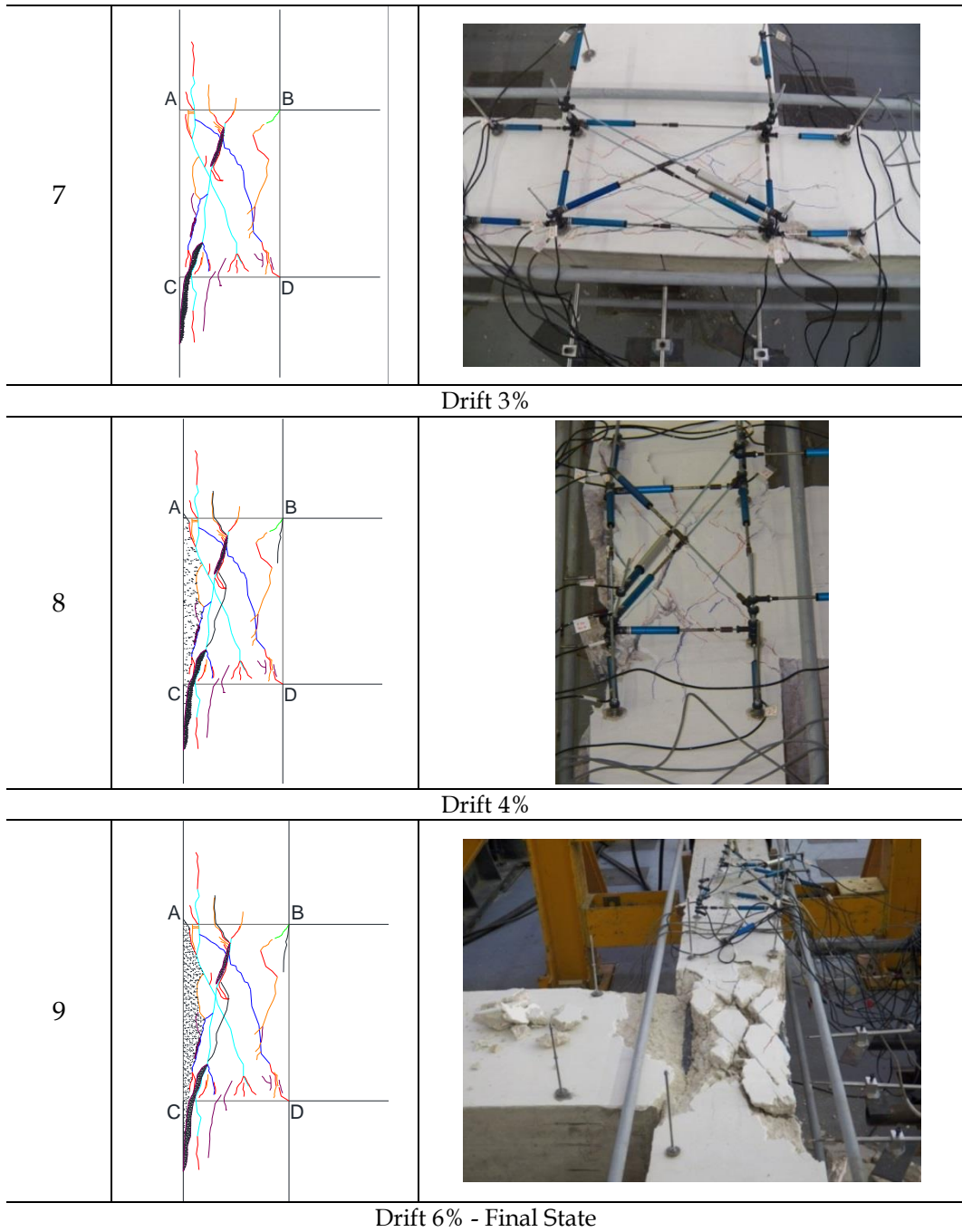


Figure 7.12. Evolution of damage - Test #1



Figure 7.13. Final damage state: joint panel and beam-joint interface – Test #1

Cycle	Drift (%)	Damage description		
		Joint	Beam	Column
1	0.25	-	-	-
2	0.5	First light cracks at corner B	-	-
3	0.75	Diagonal cracks in the joint panel spreading along column longitudinal bars	-	-
4	1	New diagonal cracks and spreading of existing cracks	-	-
5	1.5	New diagonal cracks	-	-
6	2	New diagonal cracks	Crack opening at beam-joint interface along beam width	Spreading of cracks along longitudinal bars
7	3	Spreading of existing cracks and beginning of concrete cover spalling starting from corner C	Lengthen of existing cracks at beam-joint interface	-
8	4	New diagonal cracks, significant cracks lengthen, concrete cover spalling alongside A-C	-	-
9	6	Complete concrete cover spalling	-	-

Table 7.5. Description of the evolution of damage during Test #1

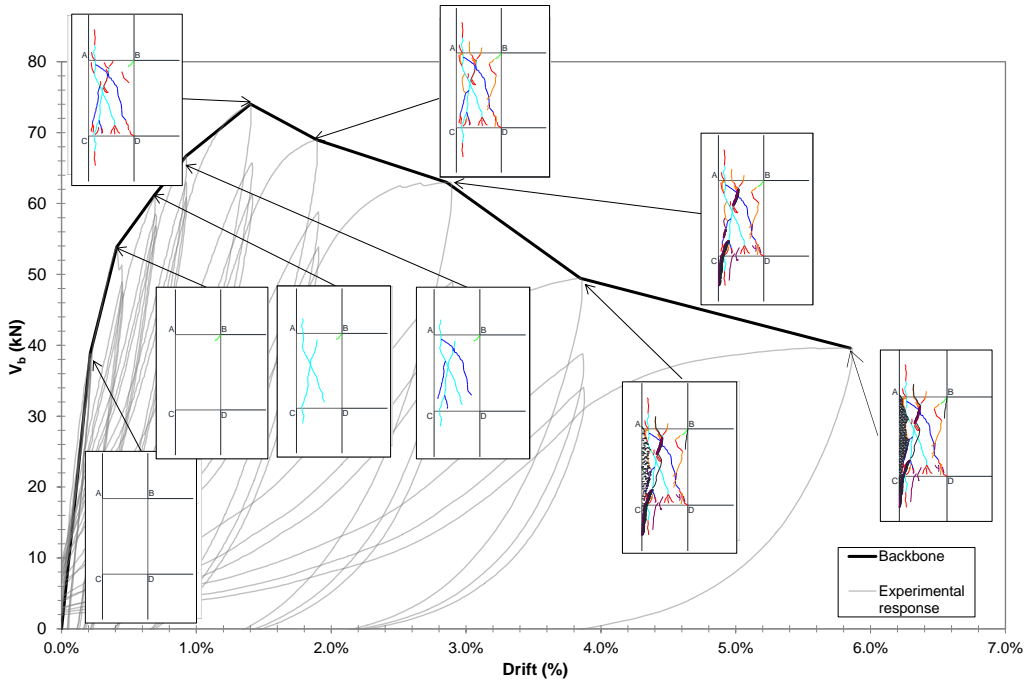


Figure 7.14. Global response and corresponding damage states of the joint panel - Test#1

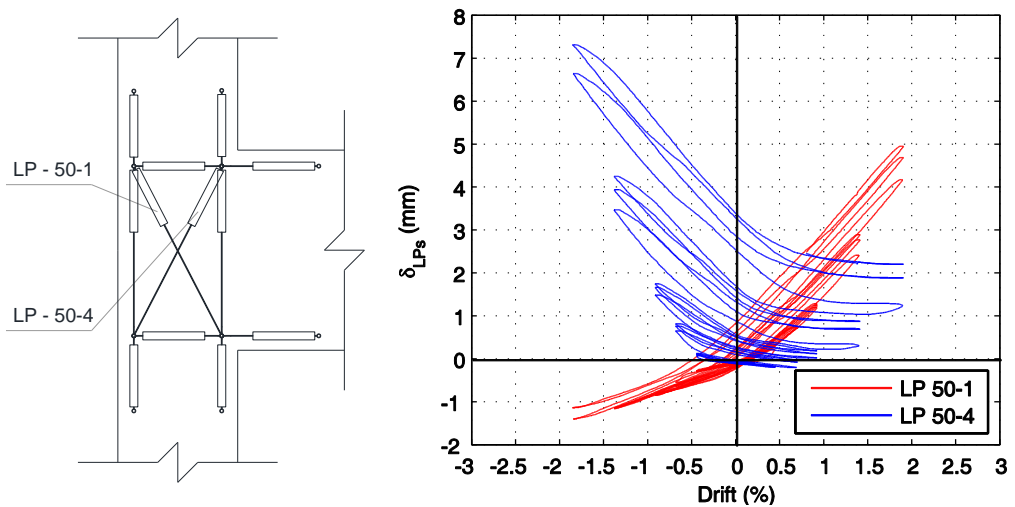


Figure 7.15. LPs displacements along the diagonals of the joint panel - Test #1

Figure 7.16 shows the experimental envelope for Test #1 and beam load corresponding to joint cracking strength prediction according to two of the

most adopted models in literature: Uzumeri (1977) and Priestley (1997). Starting from the observed damage described above and from the observation of changes in the slope of the experimental backbone, it can be concluded that model by Uzumeri predicts very well joint cracking strength.

Table 7.6 summarizes beam load values ($V_{b,cr}$) corresponding to joint cracking strength predictions by Uzumeri and Priestley and the related beam end displacements (D_{cr}) drift and cracking stiffness (k_{cr}) for Test #1.

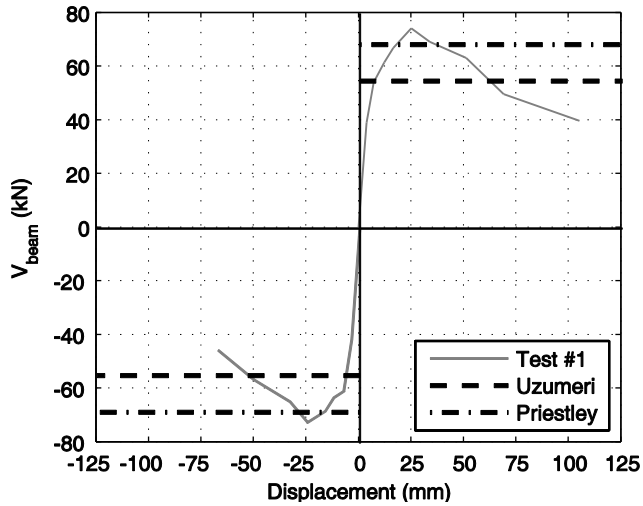


Figure 7.16. Joint cracking strength - Test #1

	$V_{b,cr}$ (kN)	D_{cr} (mm)	$Drift_{cr}$ (%)	k_{cr} (MPa)
Priestley	68.5	18.68	1.04	3664
Uzumeri	54.9	8.08	0.45	6795

Table 7.6. Beam lateral load, displacement, drift and secant stiffness corresponding to joint cracking - Test #1

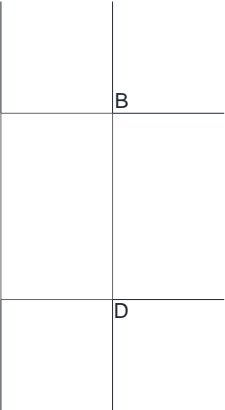
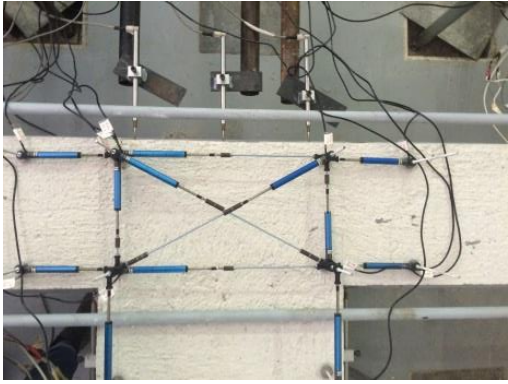
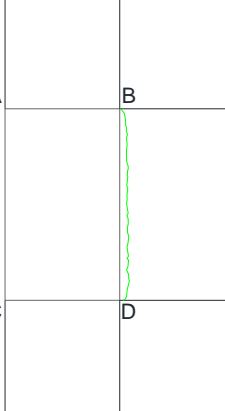
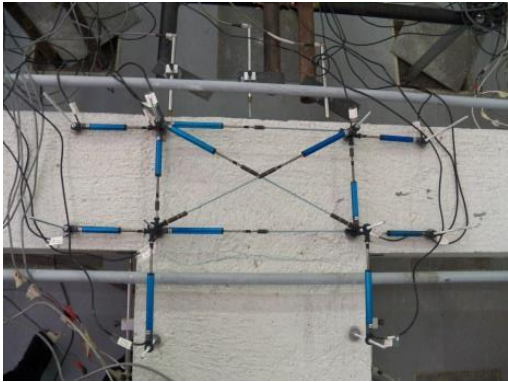
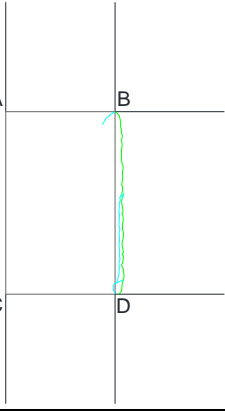
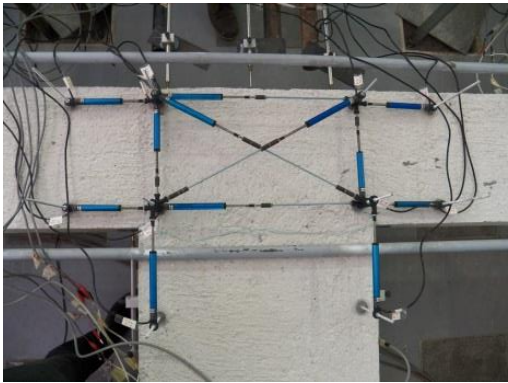
Test #2

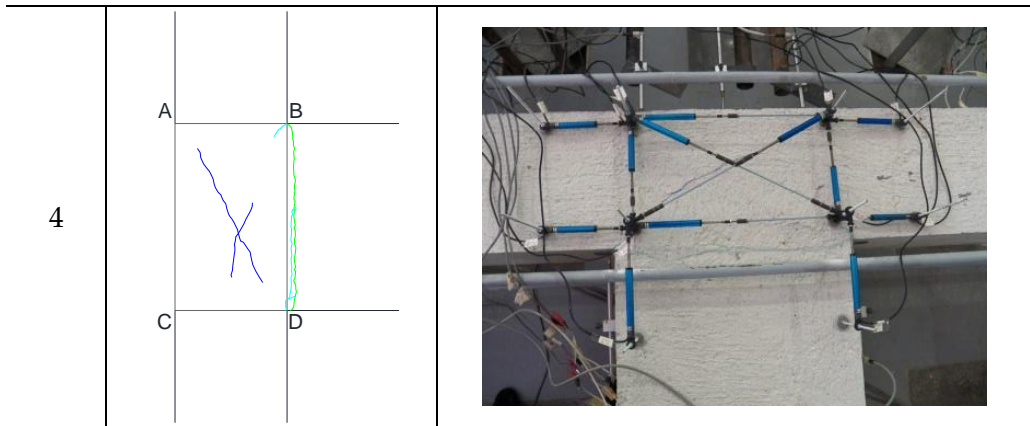
First cracks started to appear at beam-joint interface when a drift ratio equal to 0.5% was imposed, as shown in Figure 7.17. When the drift value was equal to 1%, diagonal cracks in the joint panel occurred and spread along column longitudinal bars. At 1.5% drift, cracks at beam-joint interface increased progressively their width, mainly due to fixed-end-rotation of the beam, and new diagonal cracks appeared in the joint core. At 2% drift, existing cracks significantly increased their width and buckling of longitudinal bars of column and sudden complete cover spalling occurred at the third step of the sixth cycle. Hydraulic jack was not able more to sustain in safe column axial load.

In Figure 7.17 the evolution of joint panel damage state is visually reported and Figure 7.18 shows the final damage state of the specimen. In Figure 7.19 the global response is associated to the corresponding damage states of the joint panel.

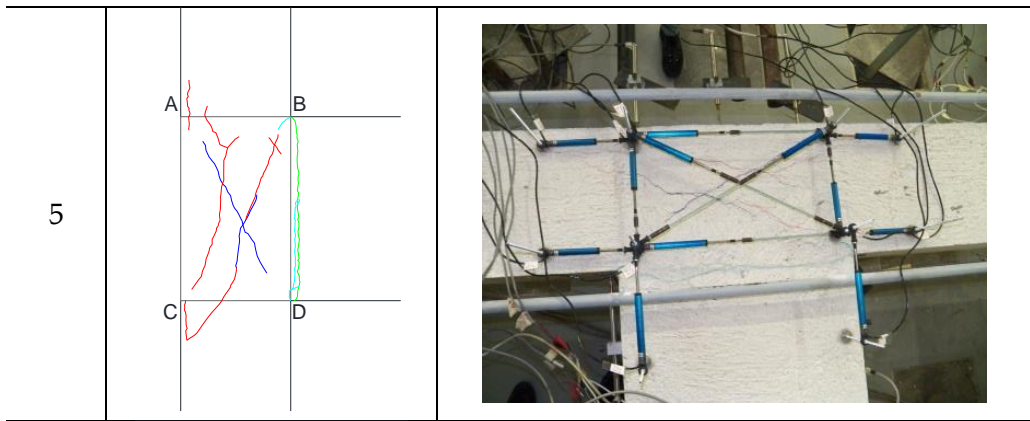
Table 7.7 summarizes the evolution of the observed damage for Test #2 described above.

Moreover, Figure 7.20 represents displacement δ measured by means of the linear potentiometer (LPs) located along the diagonals of the joint panel. Data are cut at the end of the second cycle at 2% drift, when cracks significantly involved the supported points of LPs, causing unreliable lectures. It can be observed that LP 50-1 provides the higher values of cracks width (up to about 7 mm), proving that joint panel damage is more important along the diagonal B-C (perpendicular to LP 50-1 direction).

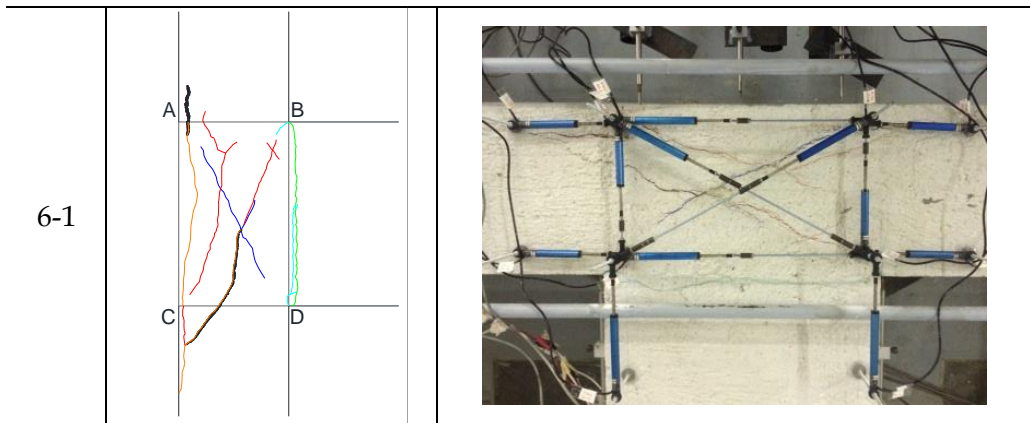
Cycle	Joint panel damage state - Test #2	
1		
Initial state - Drift 0.25%		
2		
Drift 0.5%		
3		
Drift 0.75%		



Drift 1%



Drift 1.5%



Drift 2% - Cycle 1

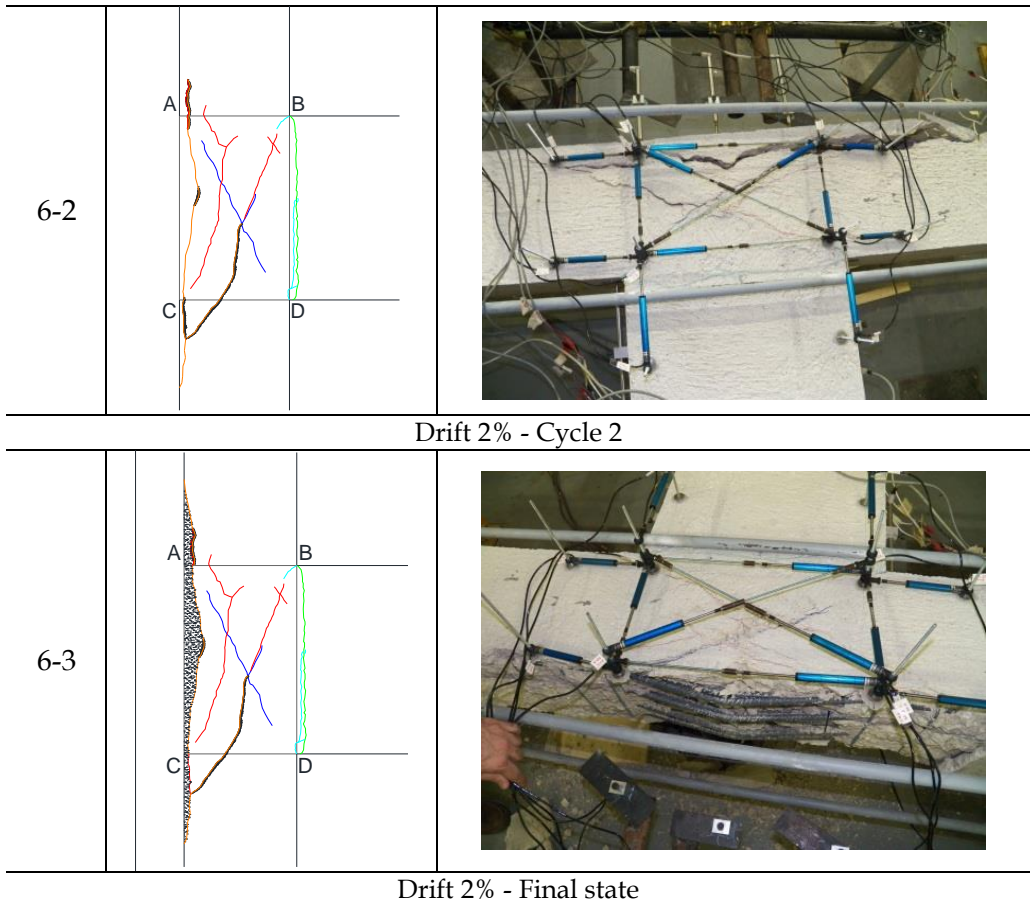


Figure 7.17. Evolution of damage - Test #2



Figure 7.18. Final damage state: joint panel and beam-joint interface - Test#2

Cycle	Drift (%)	Damage description		
		Joint	Beam	Column
1	0.25	-	-	-
2	0.5	-	Light cracks at beam-joint interface	-
3	0.75	-	New cracks at beam-joint interface	-
4	1	Light diagonal cracks in the joint panel	-	-
5	1.5	New diagonal cracks in the joint panel and light cracks along column longitudinal bars	Lengthen of existing cracks at beam-joint interface	Cracks along longitudinal bars
6-1	2	New diagonal cracks in the joint panel	-	-
6-2	2	Significant lengthen of existing cracks	-	-
6-3	2	Concrete cover spalling alongside A-C	-	Bars buckling

Table 7.7. Description of the evolution of damage during Test #2

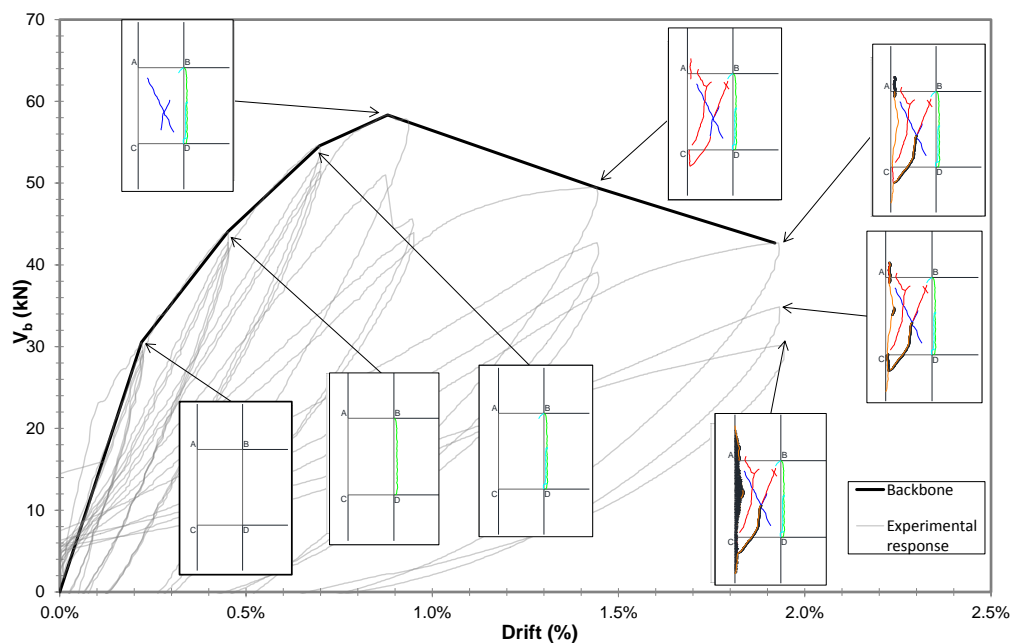


Figure 7.19. Global response and corresponding damage states of the joint panel - Test#2

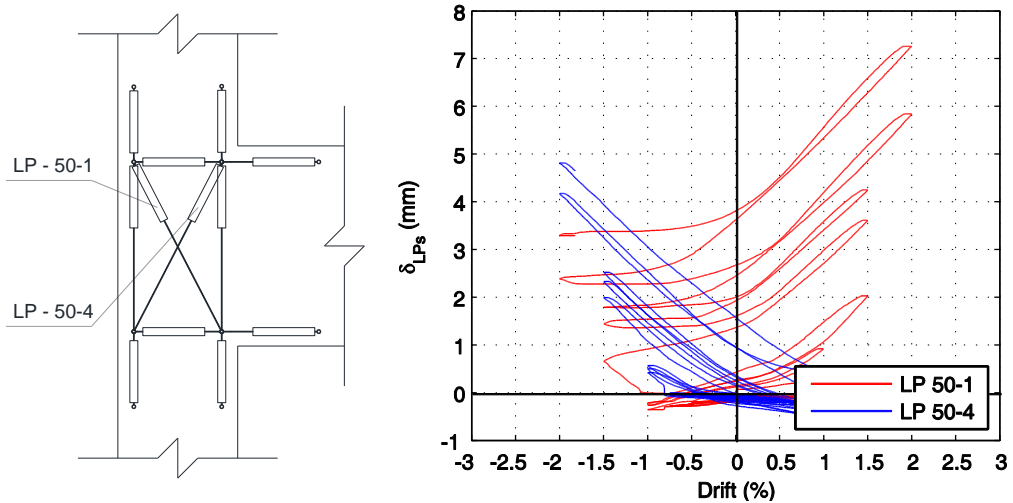


Figure 7.20. LPs displacements along the diagonals of the joint panel - Test #2

Figure 7.21 shows the experimental envelope for Test #2 and beam load corresponding to joint cracking strength prediction according to the models by Uzumeri (1977) and Priestley (1997). Starting from the observed damage described above and from the changes in the slope of the experimental backbone, it can be concluded that model by Uzumeri predicts joint cracking strength better than model by Priestley also for this test. The latter provides a joint cracking strength that is higher than the experimental strength. However, a significant change in the slope of the experimental backbone is observed before joint cracking because of the previous onset of cracks along beam-joint interface.

Table 7.8 summarizes beam load values ($V_{b,cr}$) corresponding to joint cracking strength predictions by Uzumeri and Priestley and the related beam end displacements (D_{cr}), drift and cracking stiffness (k_{cr}) for Test #2.

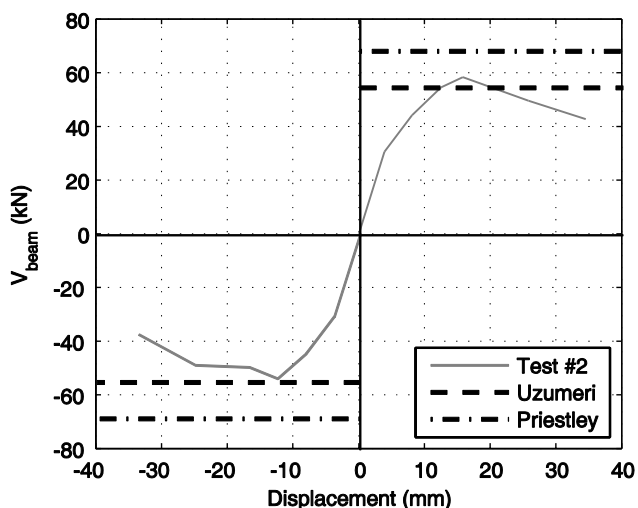


Figure 7.21 - Joint cracking strength - Test #2

	$V_{b,cr}$ (kN)	D_{cr} (mm)	$Drift_{cr}$ (%)	k_{cr} (MPa)
Priestley	68.5	-	-	-
Uzumeri	54.9	12.84	0.71	4273

Table 7.8. Beam lateral load, displacement, drift and secant stiffness corresponding to joint cracking - Test #2

7.3.1.3 Dissipated energy

In this Section, dissipated energy of Test #1 and #2 is reported, respectively in Figure 7.22 and Figure 7.23, and compared.

Dissipated energy obviously increases with imposed drift and it is higher for Test #1 than for Test #2, on equal drift (Figure 7.24), mainly due to the higher beam load values of Test #1. Thus, in order to better compare the dissipated energy of the two tests, it appears more convenient to normalize the energy to the experimental peak beam load of each test. Such a comparison is shown in Figure 7.25 and proves that normalized dissipated energy and, consequently, the “shape” of hysteretic loops, are quite similar in the two cases.

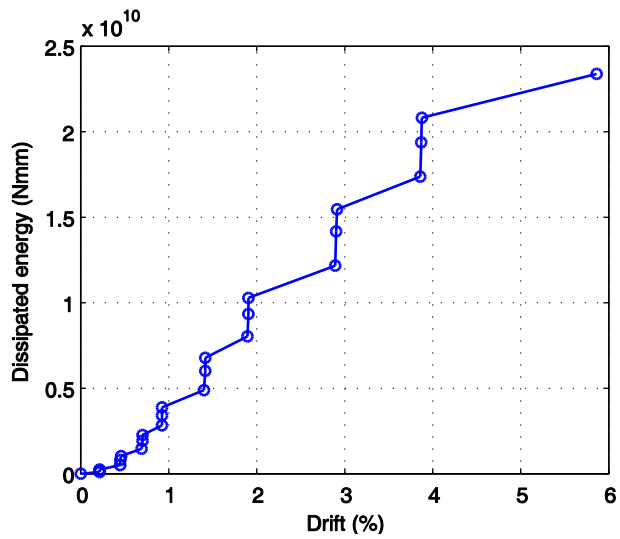


Figure 7.22. Dissipated energy – Test #1

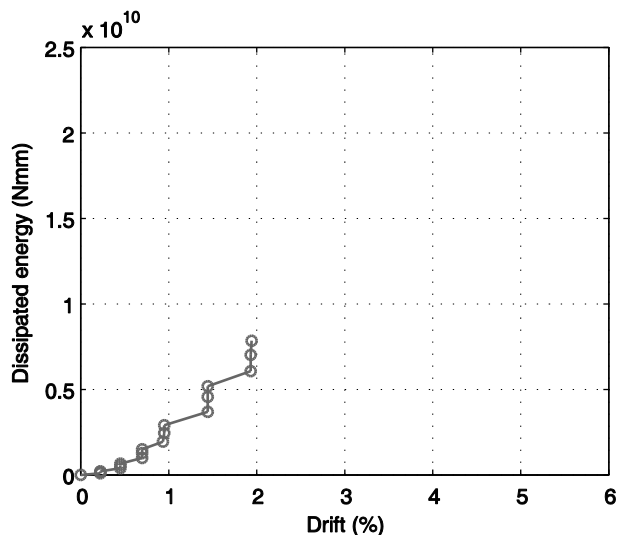


Figure 7.23. Dissipated energy – Test #2

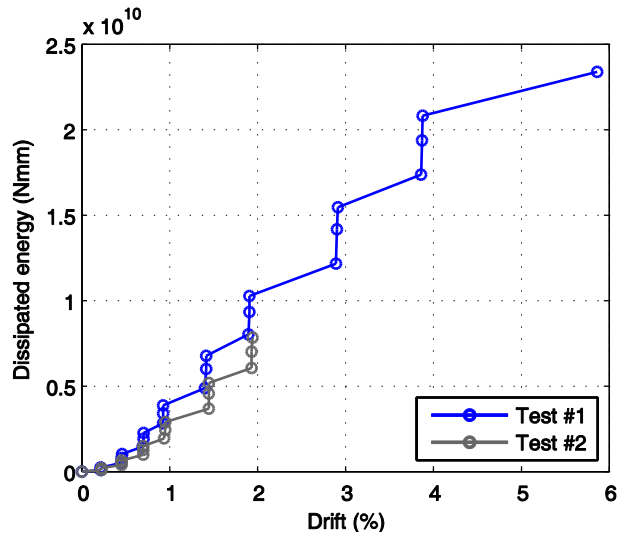


Figure 7.24. Dissipated energy - comparison

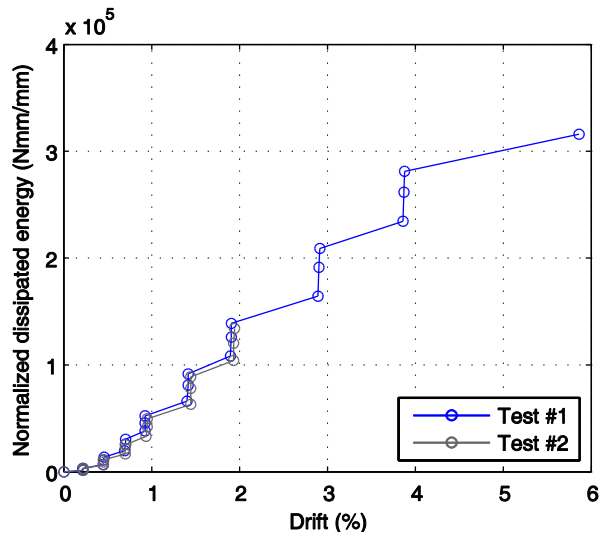


Figure 7.25. Normalized dissipated energy - comparison

7.3.2. Local behavior

In this Section, most significant local measurement data, related to main damage and deformation mechanisms observed in specimens, are discussed.

7.3.2.1 Joint panel response

Linear potentiometers located on the joint panel are employed to calculate joint shear strain, as suggested by previous experimental studies (e.g. Engindeniz, 2008 and Hassan, 2011). Joint shear strain can be expressed as shown in Eq. (7.1)

$$\gamma_{s,i} = \frac{\varepsilon_{\theta} - \varepsilon_x \cos^2 \theta - \varepsilon_y \sin^2 \theta}{\sin \theta \cos \theta} \quad (7.1)$$

where, $\gamma_{s,i}$ is the joint shear strain obtained using a certain set of strain measures, ε_x and ε_z are strains in the horizontal and vertical directions, respectively, and ε_{θ} is the strain in the diagonal direction with an angle of θ measured from the horizontal axis. Four estimates of the joint shear strain were obtained by four triangles of LPs located in the joint panel (Figure 7.26) by using Eq. (7.1), as follows

$$\gamma_{s,1} = \frac{\varepsilon_6 - \varepsilon_1 \cos^2 \theta - \varepsilon_4 \sin^2 \theta}{-\sin \theta \cos \theta} \quad (7.2)$$

$$\gamma_{s,2} = \frac{\varepsilon_5 - \varepsilon_1 \cos^2 \theta - \varepsilon_2 \sin^2 \theta}{\sin \theta \cos \theta} \quad (7.3)$$

$$\gamma_{s,3} = \frac{\varepsilon_5 - \varepsilon_3 \cos^2 \theta - \varepsilon_4 \sin^2 \theta}{\sin \theta \cos \theta} \quad (7.4)$$

$$\gamma_{s,4} = \frac{\varepsilon_6 - \varepsilon_3 \cos^2 \theta - \varepsilon_2 \sin^2 \theta}{-\sin \theta \cos \theta} \quad (7.5)$$

Joint strain (γ_{joint}) is finally calculated as the mean of these four estimates.

Sign convention for shear strain is related to beam displacement sign convention (see Figure 7.9), i.e. negative joint shear strain (see Figure 7.26) corresponds to downward beam displacement (hydraulic actuator pulls the

beam, beam load is negative - measured by the load cell - and drift is negative - measured by the wire potentiometer 50-40).

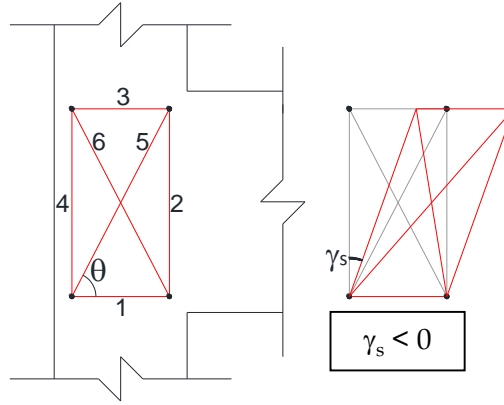


Figure 7.26. Joint shear strain calculation

Joint shear stress is calculated on the base of equilibrium equations, in conjunction with strain gauges measures (see Section 7.3.2.3). In particular, joint shear V_{jh} is calculated as shown in Eq. (7.6)

$$V_{jh} = T - V_c \quad (7.6)$$

where T is the tensile force acting in beam longitudinal bars and V_c represents column shear force. Tensile force T is obtained as shown in Eq. (7.7)

$$T = \varepsilon_s E_s A_s \leq \varepsilon_{s,y} E_s A_s \quad (7.7)$$

where ε_s is the strain measures obtained from strain gauges located at beam-joint interface (sgs #1 and #4), A_s is the area of longitudinal tensile bars of beam and E_s represents the Young modulus of steel. Column shear force V_c is calculated from the equilibrium, as shown in Eq. (7.8).

$$2L_c \cdot V_c = V_b \cdot L_b \Rightarrow V_c = \frac{V_b \cdot L_b}{2L_c} \quad (7.8)$$

where L_b is the total length of the beam and $2L_c$ represents the total length of bottom and top column.

Joint shear stress (τ_{joint}) can be calculated as the ratio between joint shear

force (V_{jh}) and joint horizontal area (A_{jh}).

Hereinafter, τ_{joint} will represent joint shear stress divided by the square root of concrete strength f_c .

In Figure 7.27 and Figure 7.28, τ_{joint} versus joint strain (γ_{joint}) experimental responses are reported for Test #1 and #2, respectively. Data are represented until LPs measures are considered reliable, i.e. until cracks significantly involved the supported points of LPs.

Test #1

In Test #1, the peak values of τ_{joint} are 0.63 and -0.616 (MPa)^{0.5} for positive and negative direction, respectively. The corresponding γ_{joint} are equal to 0.532% and -1.182%. It is worth noting that maximum joint shear strain is achieved in negative direction, thus proving that higher cracks width should occur along the joint diagonal A-D. LPs 50-1 and 50-4 shown before in Figure 7.15 confirms this assertion.

Joint stress corresponding to joint cracking according to the prediction by Uzumeri (1977) – that better predicts experimental behavior – is 0.39 (MPa)^{0.5} for both tests.

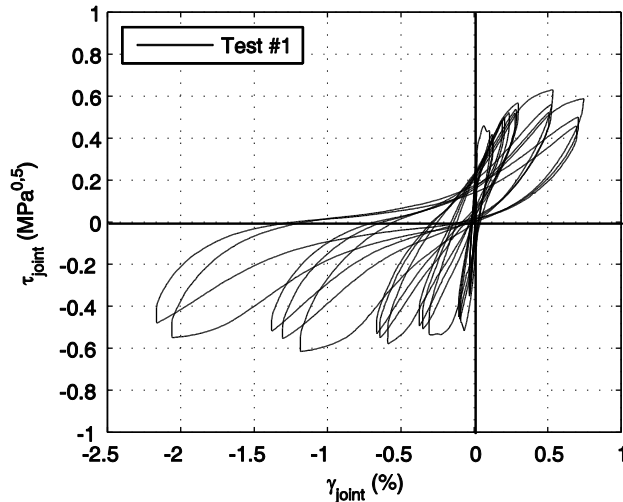


Figure 7.27. Joint shear stress – strain experimental response – Test #1

Test #2

In Test #2, the peak values of τ_{joint} are 0.423 and -0.388 (MPa)^{0.5} for

positive and negative direction, respectively. The corresponding γ_{joint} are equal to 0.04% and -0.067%. These peak points were reached at the end of the elastic phase of behavior of the joint that exhibited a high (pre-cracking) stiffness. When positive peak point was reached, joint cracking occurred, causing a significant reduction in stiffness and a reduction in strength, following by a strength recovery up to $0.359 \text{ (MPa)}^{0.5}$ for positive direction at 0.642% of γ_{joint} . Then a softening phase with a very low (negative) stiffness occurred. In this case, cracking strength (evaluated according to the prediction by Uzumeri, 1977) and joint stress corresponding to beam yielding (namely $0.38 \text{ MPa}^{0.5}$) are very close to each other.

For Test #2 maximum joint shear strain is achieved in positive direction, thus proving that higher cracks width should occurs along the joint diagonal BC. LPs 50-1 and 50-4 shown before in Figure 7.20 confirms this assertion.

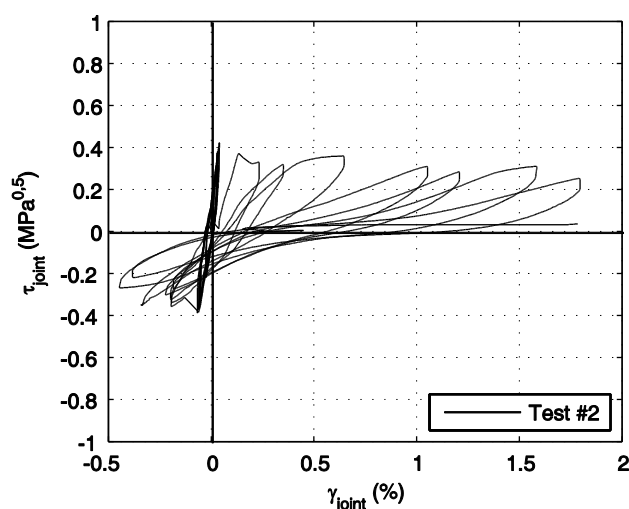


Figure 7.28. Joint shear stress – strain experimental response – Test #2

Complete experimental data related to joint stress-strain backbones for both tests is reported in Appendix 7B.

7.3.2.2 Fixed-end-rotation

Fixed-end-rotation (θ_s) contribution to the overall deformability can be estimated through LPs located along longitudinal bars of beam and column

(see Figure 7.29). In particular, since for Test #2 a more significant deformability contribution due to beam was expected, two LVDTs more (037 and G) were employed (only) for this test (located as shown in Figure 7.29a), in order to have a more accurately measure of θ_s .

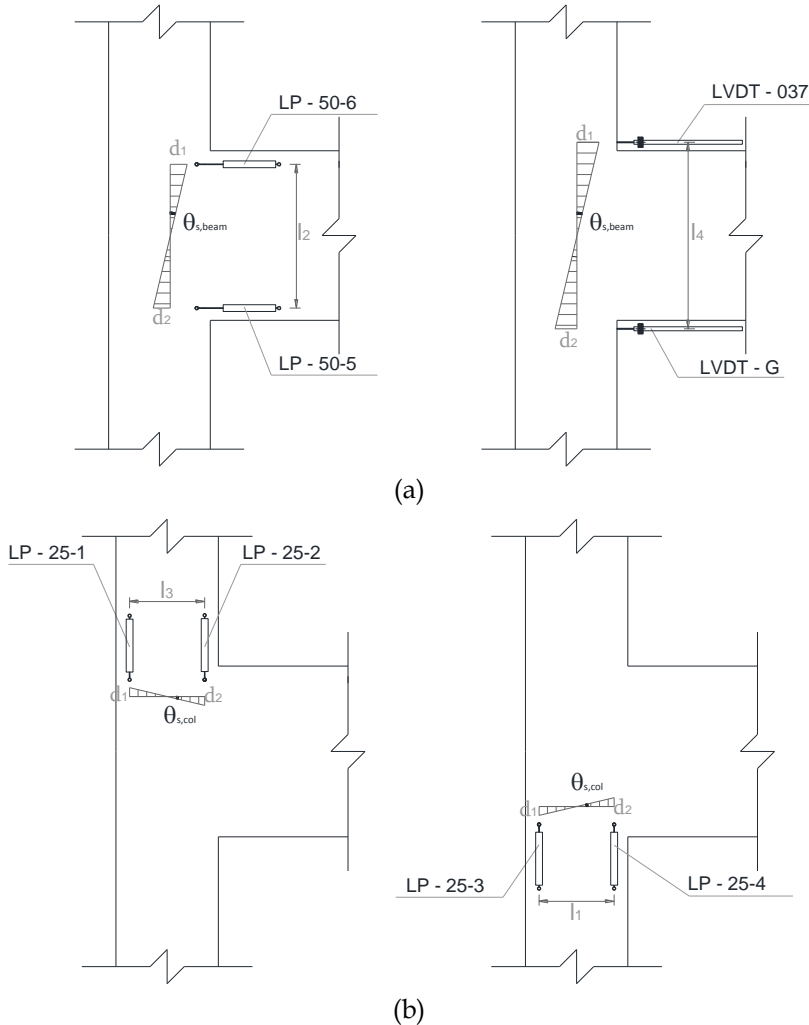


Figure 7.29. Fixed-end-rotation measures for beam (a) and top and bottom columns (b)

Starting from each pair of LPs or LVDTs (providing displacement lectures d_1 and d_2) located at a distance l , fixed-end-rotation is calculated according to Eq. (7.9):

$$\theta_s = \frac{d_1 - d_2}{l} \tag{7.9}$$

Fixed-end-rotation is assumed negative when it is clockwise, as previously shown in Figure 7.9.

Test #1

Figure 7.30, Figure 7.31 and Figure 7.32 show the fixed-end-rotation contribution for Test #1 evaluated for beam, top column and bottom column, respectively. Experimental data are plotted until supported points of LPs were involved in significant cracks (i.e. a drift value equal to 3% for the beam and 2% for the column was reached). It can be observed that fixed-end-rotation contribution to the overall deformability related to the column is lower than fixed-end-rotation related to the beam and, however, the maximum of deformability contribution related to the beam reaches a peak value of 0.8‰, i.e. less than one third of the total imposed drift.

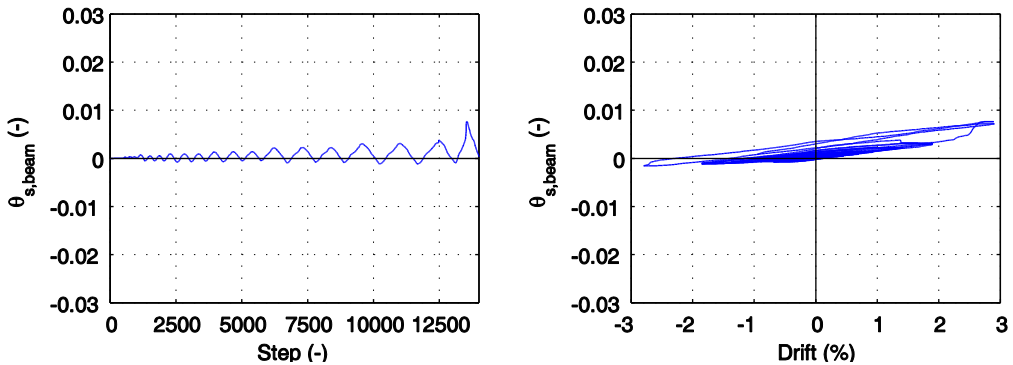


Figure 7.30. Fixed-end-rotation related to the beam – Test #1

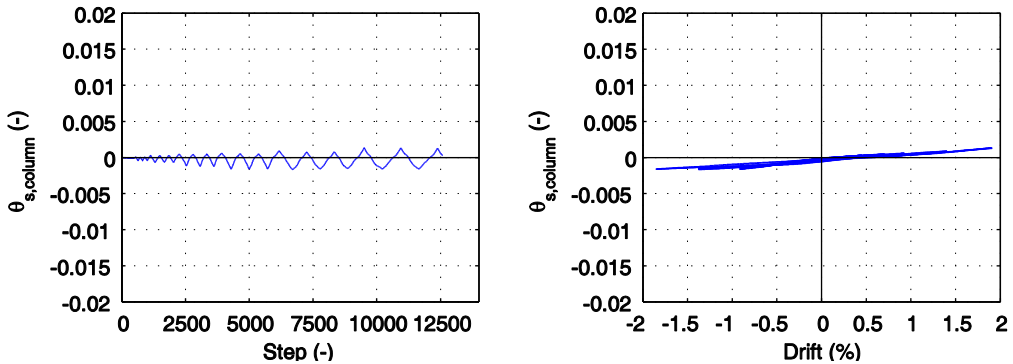


Figure 7.31. Fixed-end-rotation related to the top column

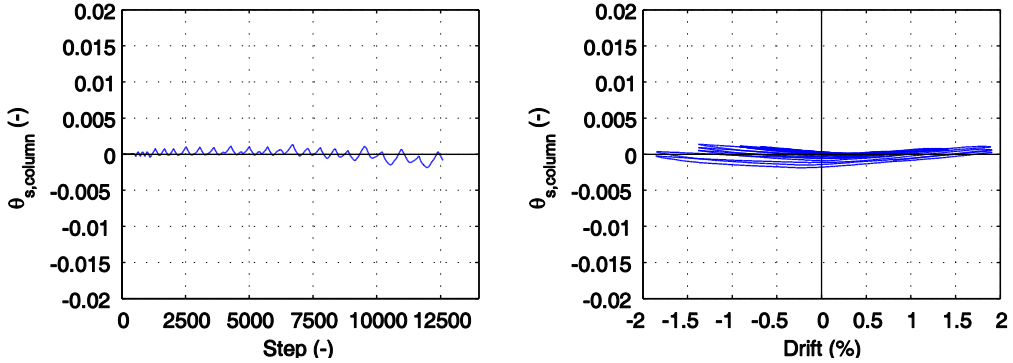
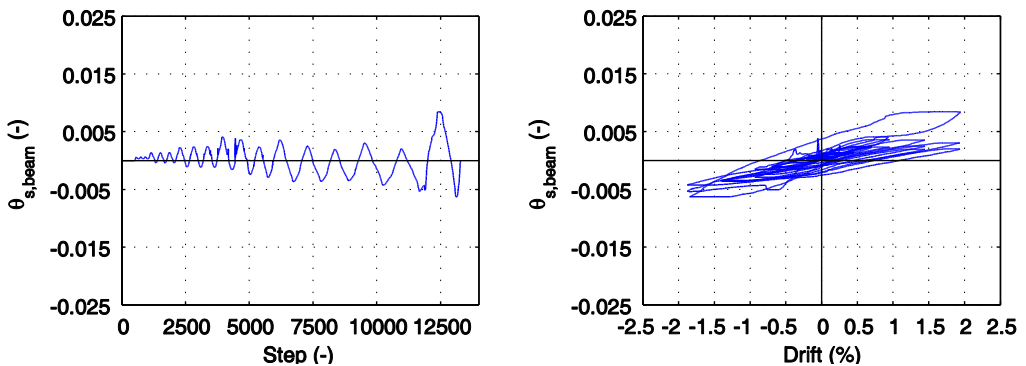


Figure 7.32. Fixed-end-rotation related to the bottom column – Test #1

Test #2

Figure 7.33, Figure 7.34 and Figure 7.35 show the fixed-end-rotation contribution for Test #2 evaluated for beam, top column and bottom column, respectively. In particular, in Figure 7.33a fixed-end-rotation related to the beam is evaluated through LPs 50-5 and 50-6, while in Figure 7.33b through LVDTs 037 and G: in first measurement, peak values can be also 50% higher, but such measures appear less confusing and more reliable than the second. It can be observed that fixed-end-rotation related to the column is significantly lower than fixed-end-rotation related to the beam. The latter is more than 50% ($\theta_{s,beam,max}=1.2\%$) of the total imposed drift at the end of the test (2%).



(a)

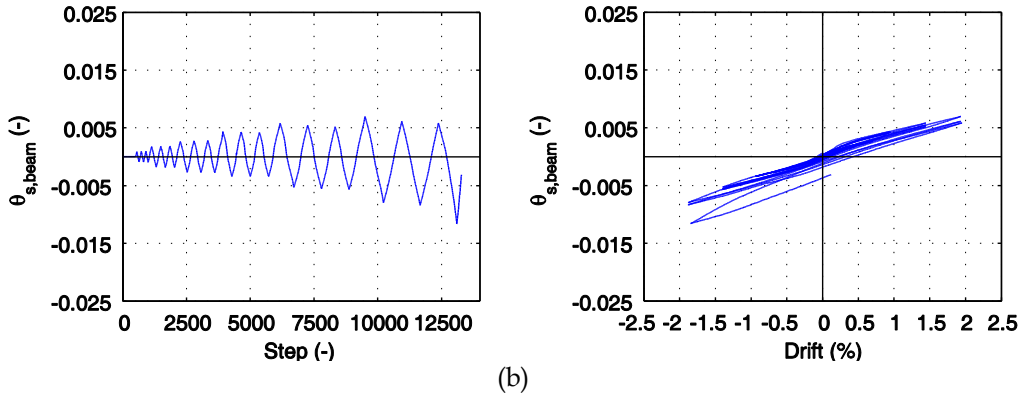


Figure 7.33. Fixed-end-rotation related to the beam evaluated through LPs 50-5 and 50-6 (a) or evaluated through LVDTs 037 and G (b) – Test #2

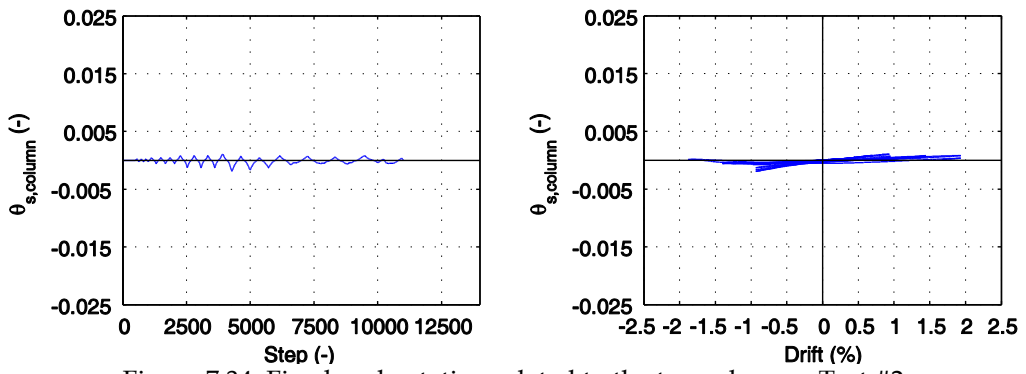


Figure 7.34. Fixed-end-rotation related to the top column – Test #2

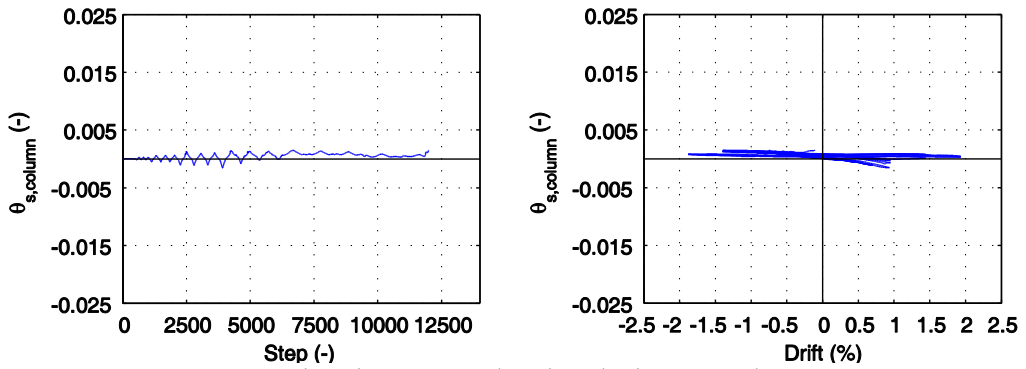


Figure 7.35. Fixed-end-rotation related to the bottom column – Test #2

By summing up deformability contributions due to fixed-end-rotation related to the beam and joint shear strain the quantity $\theta_{s,tot}$ is obtained (see Figure 7.36 and Figure 7.37). It can be observed that these two contributions

represent the quasi-totality of the imposed drift for both tests, especially in the direction where joint shear strain is predominant.

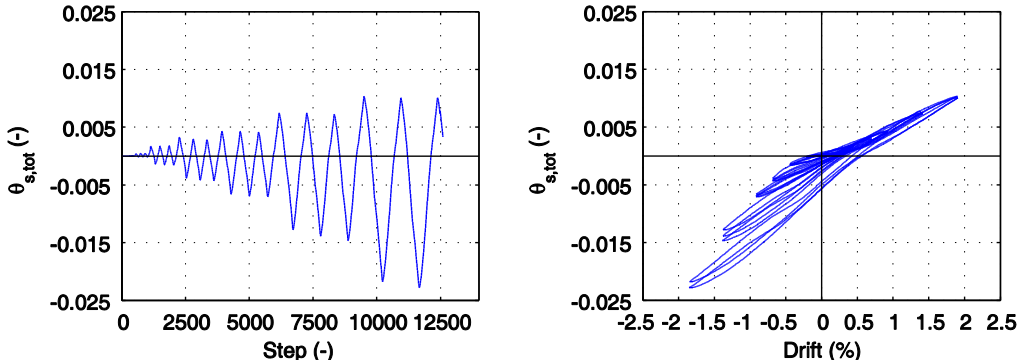


Figure 7.36. Sum of joint shear panel and beam fixed-end-rotation ($\theta_{s,tot}$) – Test #1

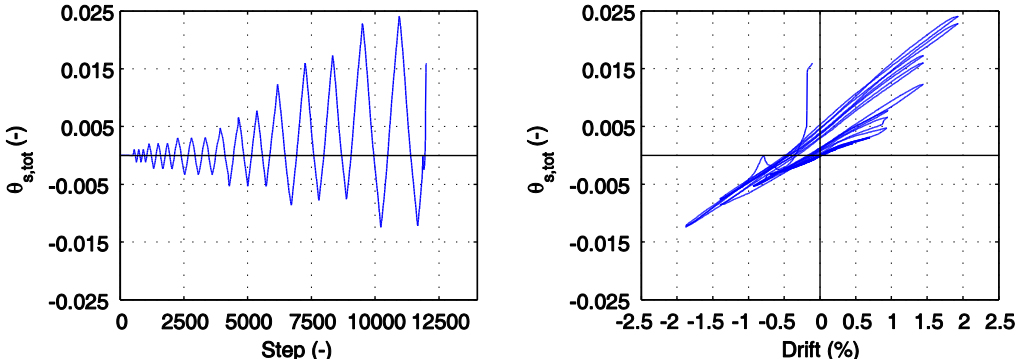


Figure 7.37. Sum of joint shear panel and beam fixed-end-rotation ($\theta_{s,tot}$) – Test #2

7.3.2.3 Beam bars strains

In this Section axial strain measures related to the beam longitudinal reinforcement bars are plotted for strain gauges located at beam-joint interface, namely sg #1 and sg #4. Complete data related to all the employed strain gauges are reported in Appendix 7C.

Steel strain of longitudinal beam bars in Test #1 reaches a maximum value of 1‰ and thus it is always much lower than the strain corresponding to yielding ($\epsilon_{yielding}=2.43\text{‰}$), thus confirming the failure mode classification for this test as J-failure.

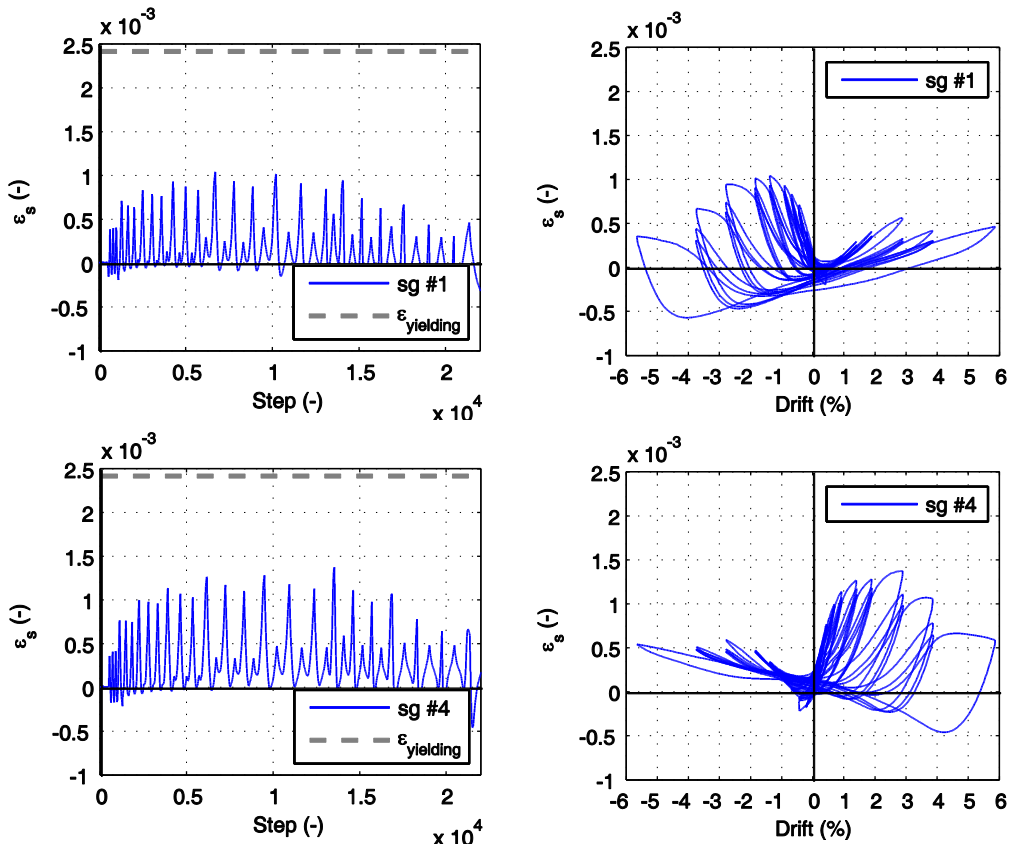


Figure 7.38. Beam bars strain – Test #1

Steel strain of longitudinal beam bars in Test #2 reaches a maximum value of 2.8‰ (when 1% imposed drift was reached) and thus overcomes the yielding strain ($\epsilon_{yielding}=2.30\%$), thus confirming that Test #2 can be classified as BJ-failure.

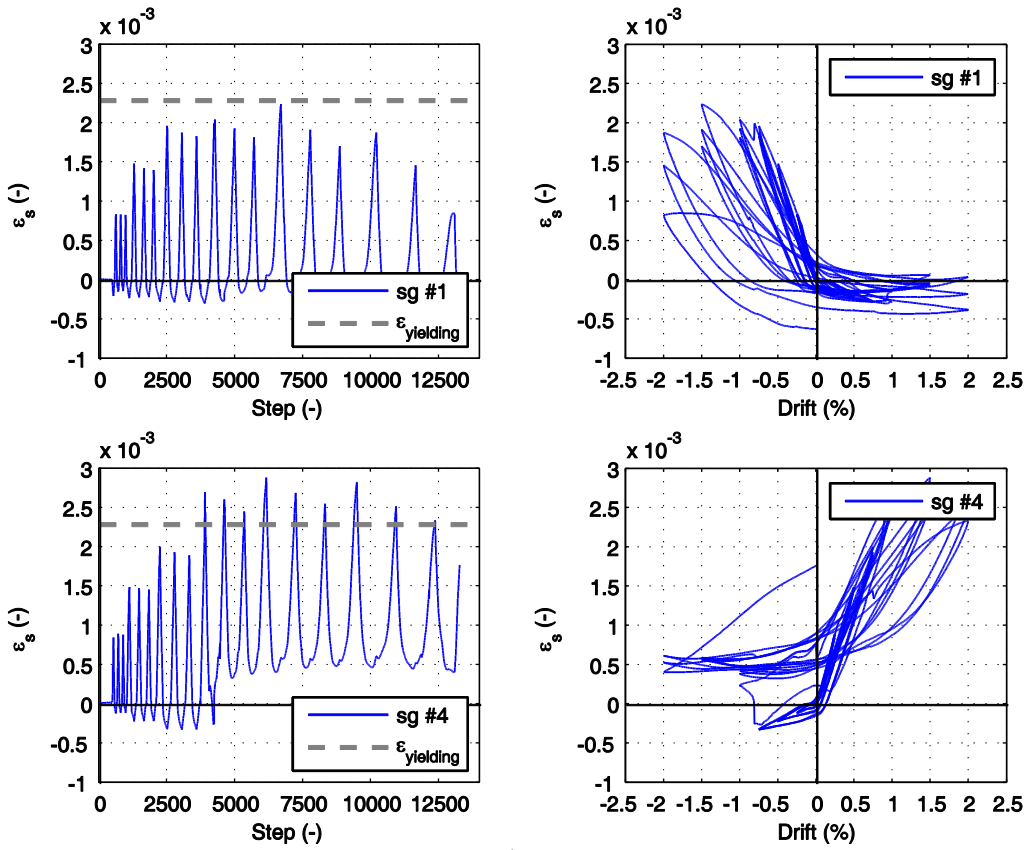


Figure 7.39. Beam bars strain – Test #2

7.3.2.4 Bar buckling - Test #2

As explained in previous Sections, Test #2 was interrupted when 2% drift was reached. In fact, at this step, concrete cover spalling and sudden buckling of column longitudinal bars cause a fast development of damage to the specimen, thus forcing a sudden elongation of the hydraulic jack that was no more able to support in safe column axial load. Final state of damage in the joint area due to bars buckling is shown in Figure 7.40.



Figure 7.40. Bar buckling - Test #2

The initial step of the phenomenon can be identified from lectures related to the hydraulic jack M2 acting on column and LVDTs located against the vertical face of the joint. In particular it can be identified a certain step characterized by a sudden increase in the elongation of the hydraulic jack (Figure 7.41) and, contemporary, a sudden increase in displacement measured by means of the LVDT F (Figure 7.42). This step is identified with a red circle in Figure 7.41 and Figure 7.42 and it corresponds to a global imposed drift equal to 2% and a beam lateral load that is very close to zero.

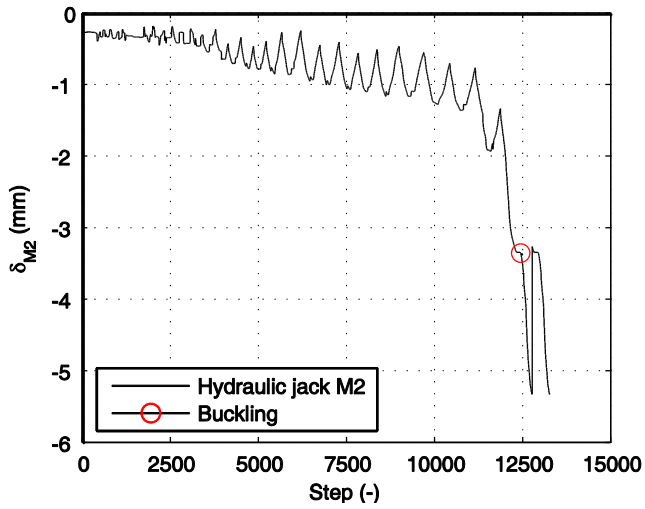
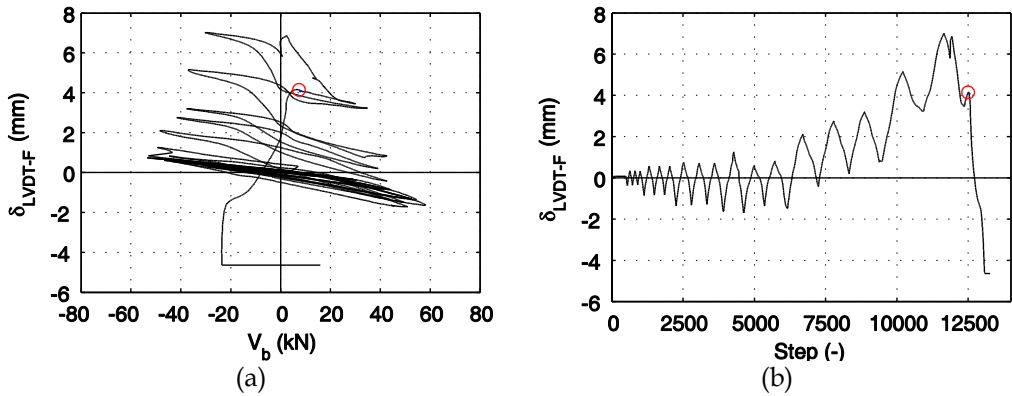


Figure 7.41. Hydraulic jack M2 acting on column

Figure 7.42. LVDT-F displacement versus beam lateral load V_b (a); LVDT-F displacement versus step (b)

7.4 Comments and comparisons

In this Section, local joint panel responses of Tests #1 and #2 are compared

- with strength models existing in literature (Section 7.4.1), and
- with joint shear stress-strain nonlinear behavior (Section 7.4.2) presented and proposed in Chapter 5.

7.4.1. Strength models from literature

Figure 7.43 shows the envelope of the experimental shear stress-strain joint response related to Test #1. Experimental peak strength ($\tau_{\text{joint,max}}$) can be compared with joint strength predicted by some of the more diffused formulations from codes and literature (discussed in Chapter 5), namely:

- ASCE-SEI/41, providing $\tau_{\text{joint,max}}$ depending on the joint typology and the transverse reinforcement ratio (equal to $0.5\text{MPa}^{0.5}$ for unreinforced exterior joints without transverse beams);
- Priestley (1997), which suggests to limit the maximum value of principal tensile stress to $0.42f_c^{0.5}$;
- Park and Mosalam (2012), a mechanical approach accounting for joint shear strength degradation after beam yielding and directly providing a definition of the failure mode.

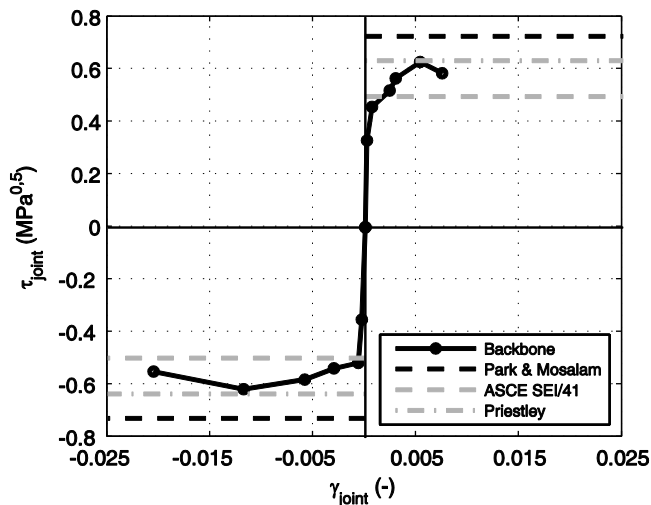


Figure 7.43. Joint shear stress-strain: envelope and comparison between experimental response and strength models from literature - Test #1

In particular, in Figure 7.43 it can be observed that code proposal adopted here as a reference (namely, ASCE-SEI/41) underestimates the experimental strength, as expected. The model that better predicts experimental strength is model by Priestley (1997). Finally, model by Park and Mosalam (2012) overestimates the maximum strength: the ratio $\tau_{jn,P\&M}/\tau_{joint,max}$ is equal to 1.14.

Since Test #1 exhibited J-failure mode, joint stress corresponding to beam yielding is about two times the peak experimental value.

A summary of joint shear strength from different models for Test #1 is reported in Table 7.9.

$\tau_{joint,max}$	$\tau_{jn,P\&M}$	$\tau_{jn,ASCE\ SEI/41}$	$\tau_{jn,Priestley}$	$\tau_{y,beam}$
0.64	0.73	0.50	0.64	1.30

Table 7.9. Experimental strength and models from literature - Test #1

Figure 7.44 shows the envelope of the experimental shear stress-strain joint response related to Test #2 and joint strength values predicted by some of the more diffused formulations from codes and literature. In this case, the model by Park and Mosalam (2012) shows the better agreement with experimental response: the ratio $\tau_{jn,P\&M}/\tau_{joint,max}$ is equal to 0.97.

Joint shear stress corresponding to beam yielding is lower than the peak experimental value, thus confirming the classification of Test #2 as a BJ-failure mode. Moreover, in this case, joint cracking point and beam yielding were very close to each other.

A summary of joint shear strength from different models for Test #2 is reported in Table 7.10.

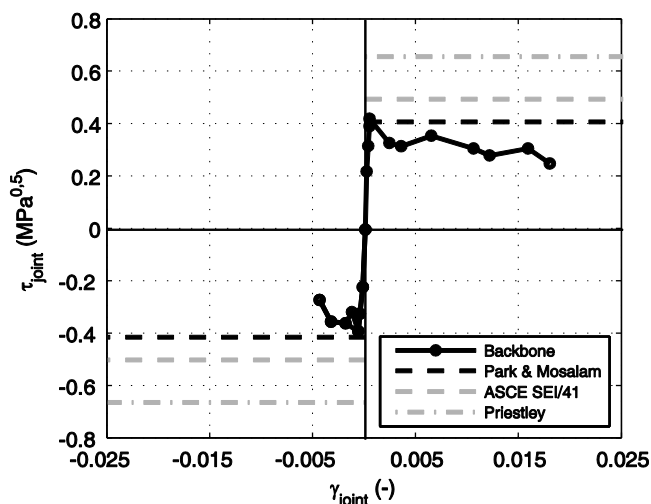


Figure 7.44. Joint shear stress-strain: envelope and comparison between experimental response and strength models from literature - Test #2

$\tau_{\text{joint,max}}$	$\tau_{\text{Jn,P\&M}}$	$\tau_{\text{Jn,ASCE SEI/41}}$	$\tau_{\text{Jn,Priestley}}$	$\tau_{\text{y,beam}}$
0.42	0.41	0.50	0.66	0.38

Table 7.10. Experimental strength and models from literature - Test #2

7.4.2. Comparison between experimental results and the proposed model

In this Section, local joint panel responses of Tests #1 and #2 are compared with joint shear stress-strain nonlinear behavior presented and proposed in Chapter 5 (hereinafter referred to as “predicted”). Comparison between experimental and predicted backbones for Test #1 and #2 is reported in Figure 7.45 and Figure 7.46, respectively. Characteristic points of the predicted backbone are summarized in Table 7.11 and Table 7.12 for Test #1 and #2, respectively.

In Test #1 joint shear strength is overestimate (as for model by Park and Mosalam 2012, that was adopted in the proposed model). Joint shear strain corresponding to peak strength is quite well predicted for the positive direction, but underestimated in negative direction; predicted softening slope is quite close to the experimental behavior.

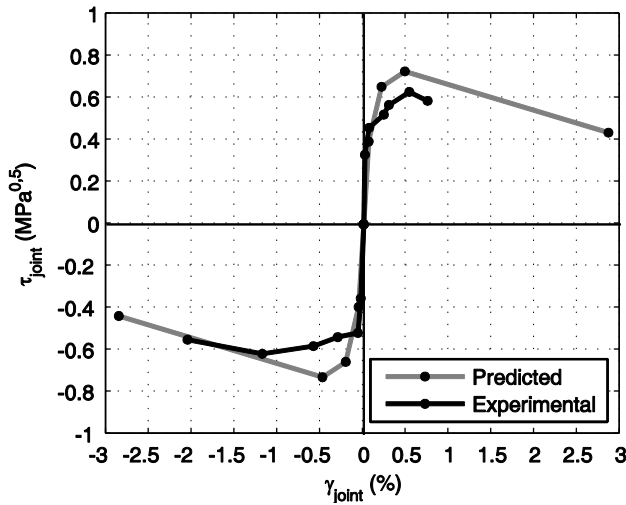


Figure 7.45. Comparison between experimental and predicted joint response – Test #1

Test #1		
	γ_{joint} (%)	τ_{joint} (MPa) ^{0.5}
Cracking	0.06	0.39
Pre-peak	0.21	0.66
Peak	0.48	0.73
Residual	2.86	0.44

Table 7.11. Characteristic points of joint stress-strain “predicted” response – Test #1

Test #2 shows a “singularity” in the predicted backbone since stress corresponding to beam yielding (that represents the pre-peak point of the proposed joint backbone) is lower than cracking strength predicted by Uzumeri (1977) (that was assumed as cracking strength in the proposed backbone) but is it associated to a joint shear strain that is higher than strain corresponding to joint cracking.

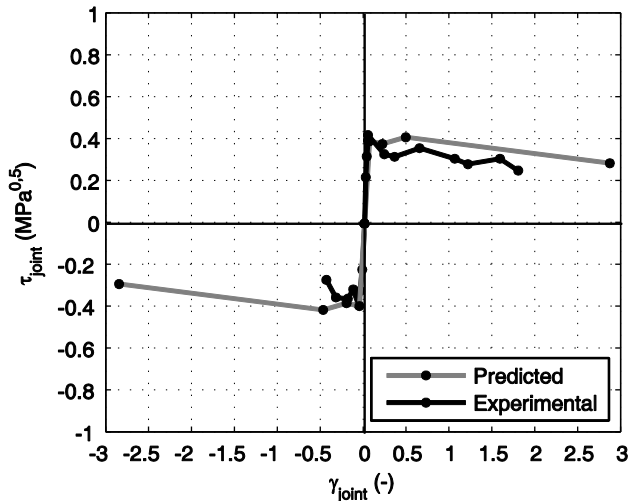


Figure 7.46. Comparison between experimental and predicted joint response - Test #2

Test #2		
	γ_{joint} (%)	τ_{joint} (MPa) ^{0.5}
Cracking	0.06	0.39
Pre-peak	0.26	0.38
Peak	0.63	0.41
Residual	3.03	0.29

Table 7.12. Characteristic points of joint stress-strain “predicted” response - Test #2

The comparison between predicted model and experimental response has been conducted also regarding the hysteretic behavior, starting from the experimental backbones (as shown in Figure 7.47 and Figure 7.48).

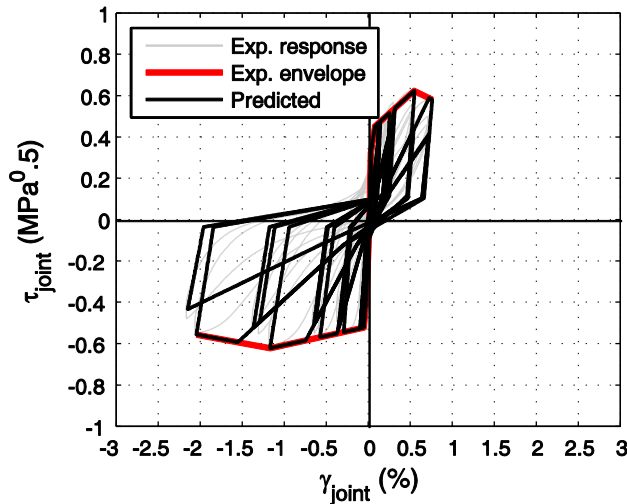


Figure 7.47. Numerical simulation through proposed joint model in terms of joint panel cyclic response (experimental envelope) - Test #1

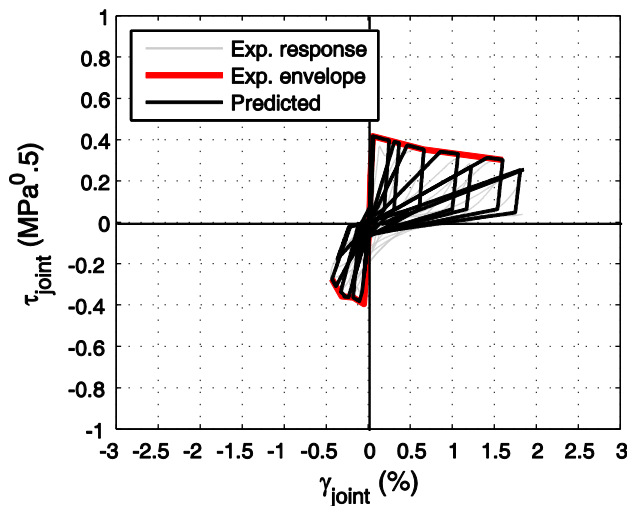


Figure 7.48. Numerical simulation through proposed joint model in terms of joint panel cyclic response (experimental envelope) - Test #2

Mean values of the parameters defining pinching and cyclic degradation in reloading and unloading stiffness are adopted as far as the predicted response is concerned (as shown in Chapter 5). It can be noted that pinching experimental response is less pronounced than the predicted one, both for Test #1 and #2. Vice-versa, experimental unloading stiffness cyclically degrades more than in the predicted response.

Finally predicted joint shear stress-strain responses were introduced into a numerical model of the sub-assembly, identical to that adopted for the validation phase in Chapter 5 (see Figure 5.11).

The finite element analyses of such a model were performed using OpenSees (McKenna and Fenves, 2010).

In particular, flexural response of beam and column was modeled in a fiber approach. Kent-Scott-Park model was adopted for concrete (Kent and Park, 1971; Scott et al., 1982) and an elastic-plastic-hardening stress-strain relationship was adopted for steel (Concrete01 and ReinforcingSteel uniaxial materials in OpenSees software, respectively). Rigid offset were located in the joint core area and additional springs representing fixed-end-rotation contribution are located at elements-joint interfaces.

The results of these simulations - under monotonic load - are reported in Figure 7.49 and Figure 7.50 for Test #1 and #2, respectively.

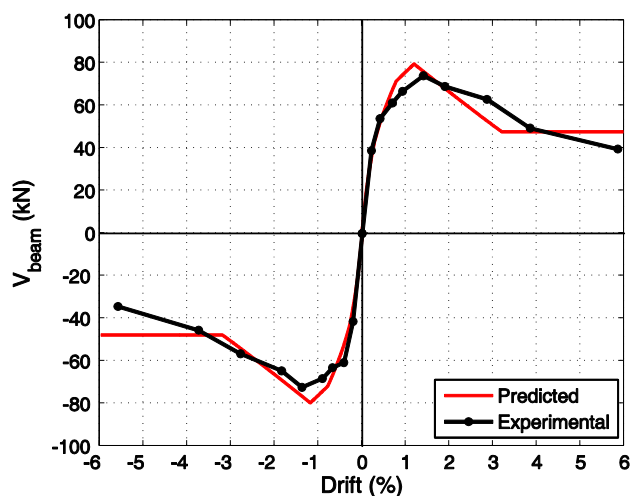


Figure 7.49. Numerical simulation through proposed joint model in terms of load-drift envelope - Test #1

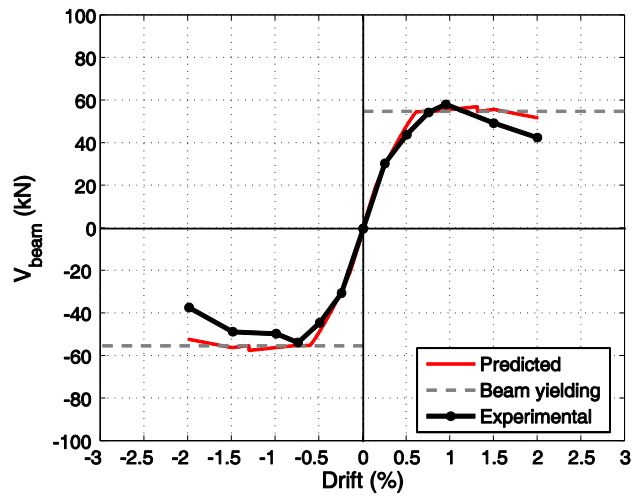


Figure 7.50. Numerical simulation through proposed joint model in terms of load-drift envelope - Test #2

7.5 Summary

In this Chapter, the experimental results of two tests on unreinforced exterior RC beam-column joints have been presented and commented.

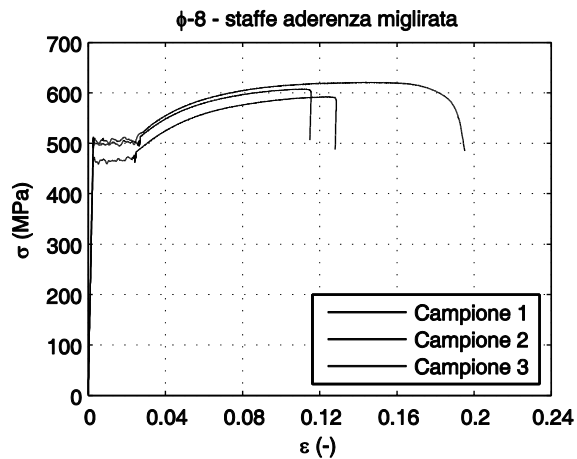
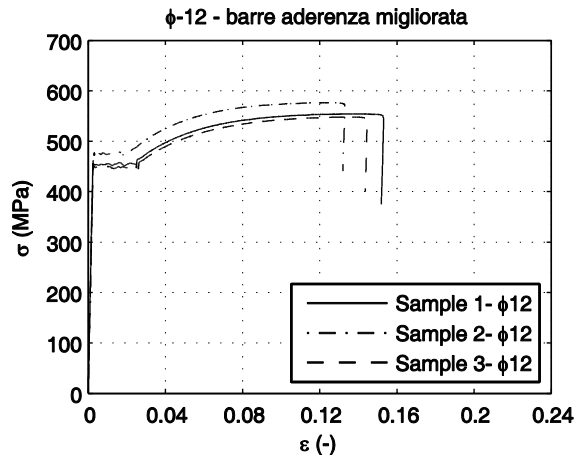
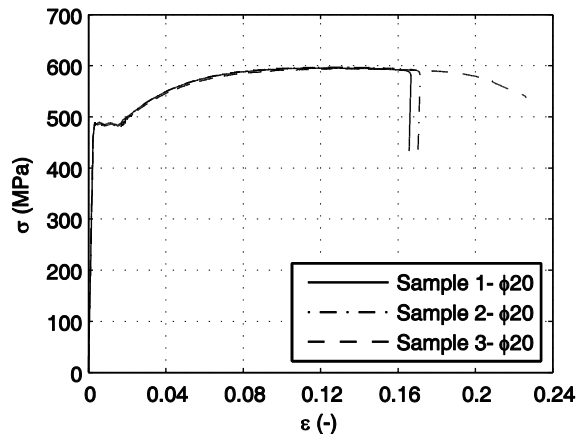
Tests were designed in order to show failure of joint panel without (Test #1) or with (Test #2) yielding of longitudinal bars.

Experimental results show, in the former case, that the attainment of maximum strength and the post-peak degrading behaviour are controlled by joint failure, prior to flexural yielding of the beam, as expected.

In the latter case, yielding of beam longitudinal bars is observed very close to cracking of joint panel, after which a first strength decrease is shown. Complete failure is attained corresponding to buckling of longitudinal bars of column and sudden complete cover spalling, together with observed failure of anchorage of beam longitudinal bars.

The experimental tests described herein can provide a very useful contribution to the characterization of the seismic behavior of unreinforced RC beam-column joints, in order to validate/propose capacity models for the assessment of existing, non-ductile RC buildings. In particular, experimental responses have been compared with predicted proposed joint shear stress-strain responses presented in Chapter 5; a very good agreement between experimental and numerical response was found.

Appendix 7A: stress-strain behavior of steel samples



Appendix 7B: experimental data

TEST #1 - positive direction:

Positive direction						
Cycle	Step	Imposed Drift	Beam lateral load	Drift (Potentiometer 50-40)	Joint shear strength coefficient	Joint shear strain
		Δ (%)	$V_{b,max}$	(%)	$\tau_{j,max}$ (MPa ^{0.5})	γ_j (%)
1	1	0.25	38.87	0.21	0.331	0.017
	2		38.18	0.21	0.325	0.013
	3		37.59	0.21	0.320	0.015
2	1	0.50	53.87	0.41	0.458	0.065
	2		48.96	0.45	0.417	0.122
	3		47.53	0.45	0.404	0.125
3	1	0.75	61.29	0.69	0.522	0.236
	2		58.55	0.70	0.498	0.204
	3		56.86	0.70	0.484	0.189
4	1	1.00	66.72	0.93	0.568	0.297
	2		63.05	0.93	0.537	0.283
	3		60.86	0.93	0.518	0.276
5	1	1.50	74.02	1.40	0.630	0.532
	2		65.73	1.41	0.559	0.525
	3		61.29	1.42	0.522	0.508
6	1	2.00	68.98	1.89	0.587	0.746
	2		58.80	1.90	0.500	0.708
	3		53.86	1.91	0.458	0.695
7	1	3.00	62.98	2.86	0.536	-
	2		48.94	2.90	0.416	-
	3		43.14	2.90	0.367	-
8	1	4.00	49.46	3.85	0.421	-
	2		38.81	3.87	0.330	-
	3		34.04	3.87	0.290	-
9	1	6.00	39.60	5.85	0.337	-
	2		-	-	-	-
	3		-	-	-	-

TEST #1 - negative direction:

Negative direction						
Cycle	Step	Imposed Drift	Beam lateral load	Drift (Potentiometer 50-40)	Joint shear strength coefficient	Joint shear strain
		$\Delta(\%)$	$V_{b,max}$	(%)	$\tau_{j,max} (MPa^{0.5})$	$\gamma_j (\%)$
1	1	0.25	-41.37	-0.21	-0.352	-0.033
	2		-40.41	-0.21	-0.344	-0.032
	3		-39.75	-0.20	-0.338	-0.032
2	1	0.50	-60.70	-0.42	-0.517	-0.069
	2		-54.39	-0.44	-0.463	-0.098
	3		-53.10	-0.44	-0.452	-0.105
3	1	0.75	-63.10	-0.68	-0.537	-0.304
	2		-59.89	-0.68	-0.510	-0.349
	3		-58.09	-0.68	-0.494	-0.373
4	1	1.00	-68.16	-0.91	-0.580	-0.587
	2		-64.39	-0.91	-0.548	-0.638
	3		-62.31	-0.91	-0.530	-0.663
5	1	1.50	-72.35	-1.38	-0.616	-1.182
	2		-65.08	-1.38	-0.554	-1.305
	3		-61.04	-1.38	-0.519	-1.380
6	1	2.00	-64.60	-1.84	-0.550	-2.058
	2		-56.49	-1.85	-0.481	-2.163
	3		-52.16	-1.85	-0.444	-2.232
7	1	3.00	-56.57	-0.21	-0.481	-
	2		-47.02	-0.21	-0.400	-
	3		-42.19	-0.20	-0.359	-
8	1	4.00	-45.48	-0.42	-0.387	-
	2		-37.60	-0.44	-0.320	-
	3		-33.45	-0.44	-0.285	-
9	1	6.00	-34.34	-0.68	-0.292	-
	2		-	-	-	-
	3		-	-	-	-

TEST #2 – positive direction:

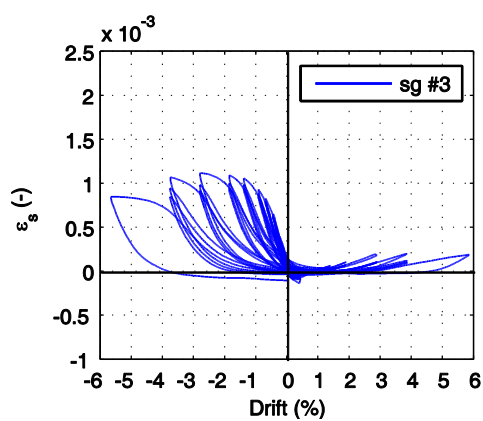
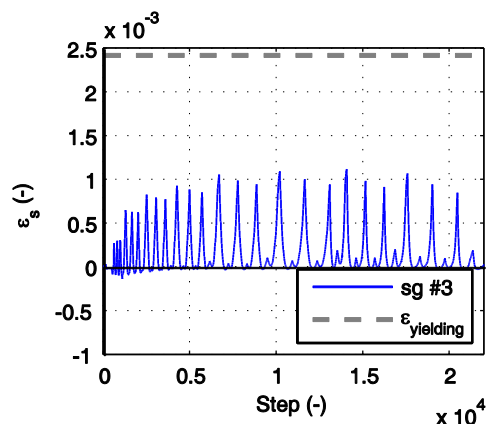
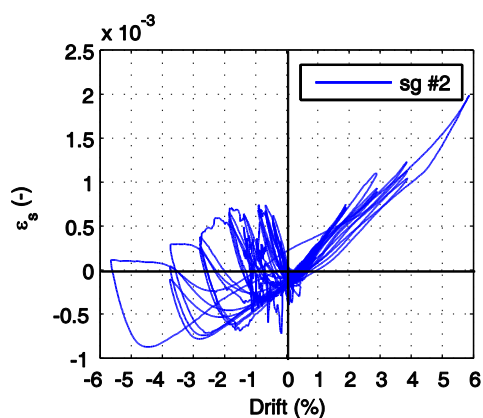
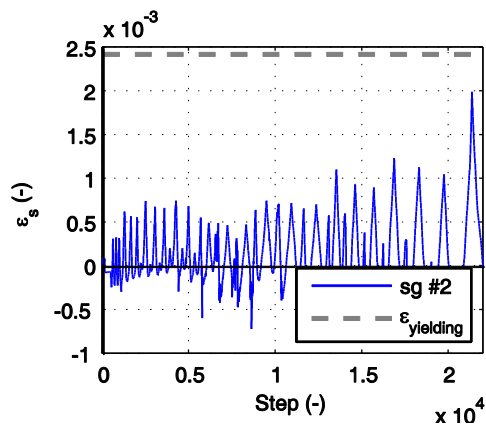
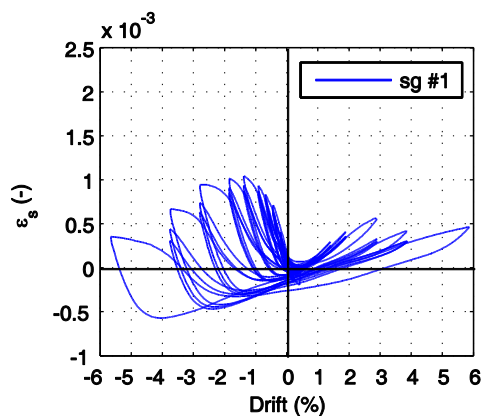
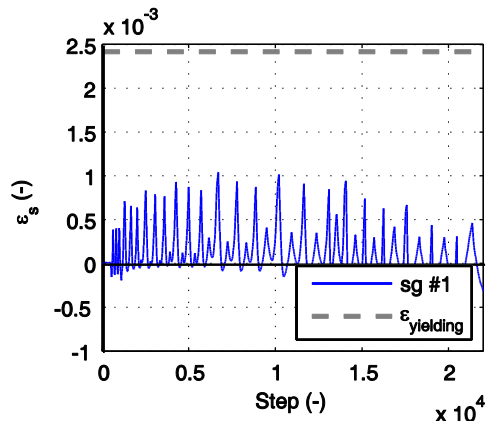
Positive direction						
Cycle	Step	Imposed Drift	Beam lateral load	Drift (Potentiometer 50-40)	Joint shear strength coefficient	Joint shear strain
		Δ (%)	$V_{b,max}$	(%)	$\tau_{j,max}$ (MPa ^{0.5})	γ_j (%)
1	1	0.25	30.53	0.22	0.222	0.013
	2		29.53	0.22	0.214	0.010
	3		29.02	0.22	0.211	0.009
2	1	0.50	44.07	0.45	0.320	0.027
	2		42.76	0.45	0.310	0.026
	3		42.08	0.45	0.305	0.026
3	1	0.75	54.55	0.70	0.396	0.040
	2		52.61	0.70	0.382	0.031
	3		51.45	0.70	0.373	0.030
4	1	1.00	58.33	0.88	0.423	0.040
	2		45.61	0.95	0.331	0.233
	3		43.95	0.95	0.319	0.350
5	1	1.50	49.51	1.44	0.359	0.642
	2		42.72	1.44	0.310	1.052
	3		39.10	1.44	0.284	1.207
6	1	2.00	42.67	1.92	0.310	1.581
	2		34.85	1.93	0.253	1.793
	3		30.13	1.93	0.219	-

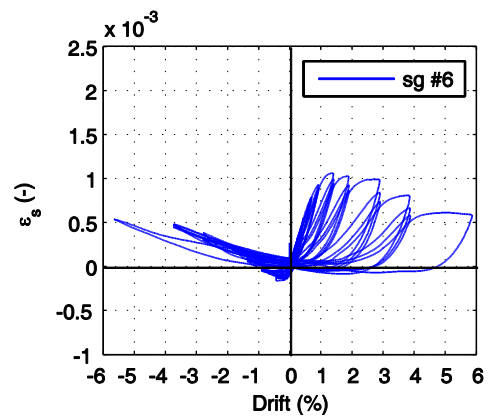
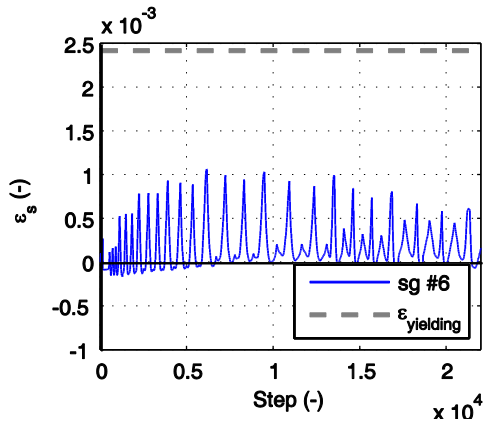
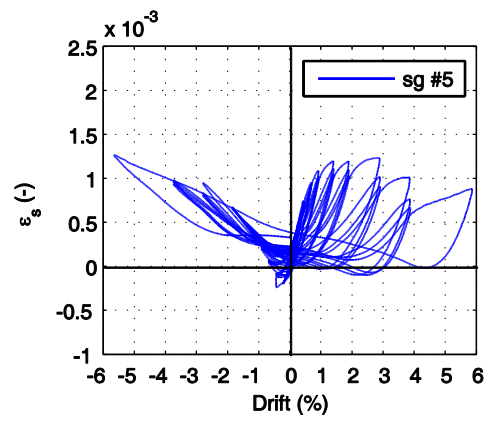
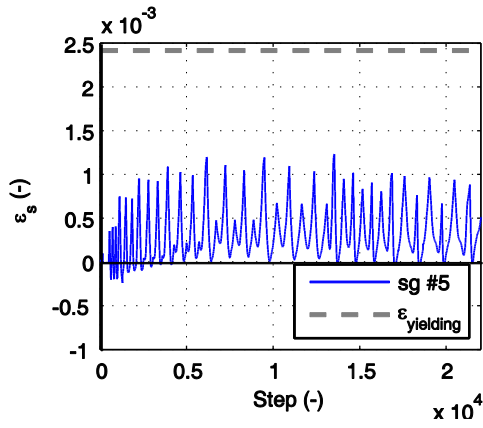
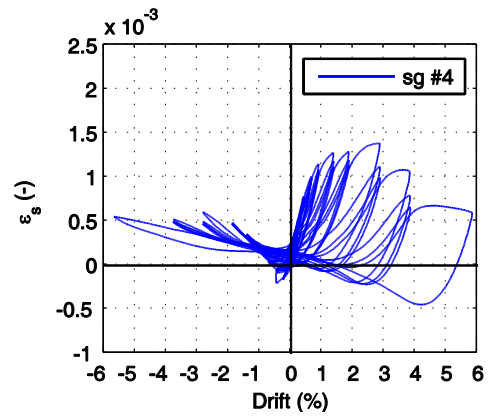
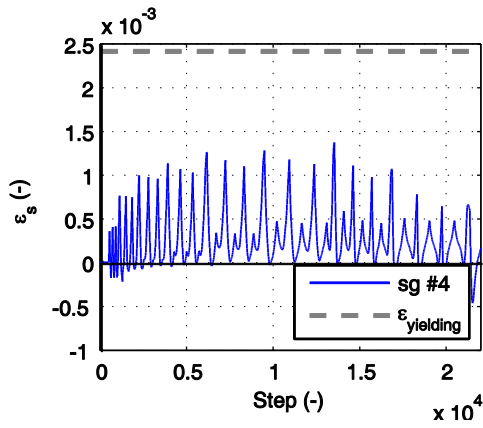
TEST #2 - negative direction:

Negative direction						
Cycle	Step	Imposed Drift	Beam lateral load	Drift (Potentiometer 50-40)	Joint shear strength coefficient	Joint shear strain
		$\Delta(\%)$	$V_{b,max}$	(%)	$\tau_{j,max} (MPa^{0.5})$	$\gamma_j (\%)$
1	1	0.25	-30.33	-0.21	-0.220	-0.025
	2		-29.13	-0.21	-0.211	-0.024
	3		-28.53	-0.21	-0.207	-0.024
2	1	0.50	-44.29	-0.45	-0.321	-0.052
	2		-42.69	-0.45	-0.310	-0.051
	3		-41.87	-0.45	-0.304	-0.050
3	1	0.75	-53.53	-0.69	-0.388	-0.067
	2		-51.28	-0.70	-0.372	-0.060
	3		-50.16	-0.69	-0.364	-0.057
4	1	1.00	-49.35	-0.93	-0.358	-0.193
	2		-46.74	-0.93	-0.339	-0.191
	3		-44.72	-0.93	-0.325	-0.196
5	1	1.50	-48.50	-1.39	-0.352	-0.334
	2		-41.63	-1.40	-0.302	-0.222
	3		-37.66	-1.40	-0.273	-0.184
6	1	2.00	-37.07	-1.87	-0.269	-0.445
	2		-30.33	-1.88	-0.220	-0.381
	3		-23.45	-1.84	-0.170	-

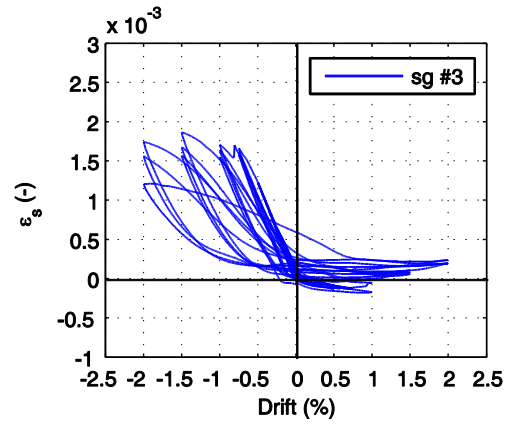
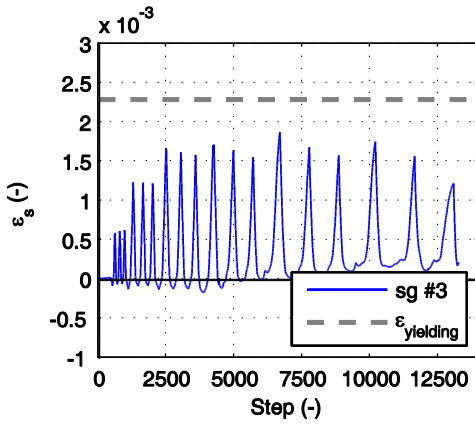
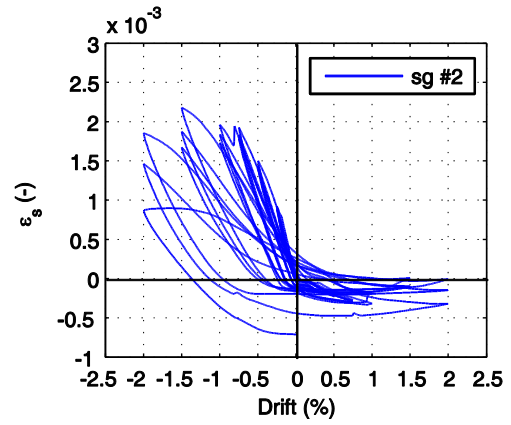
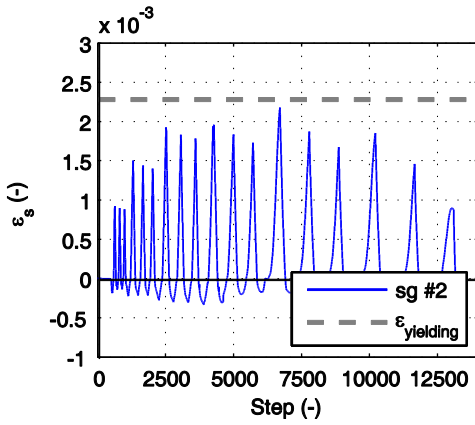
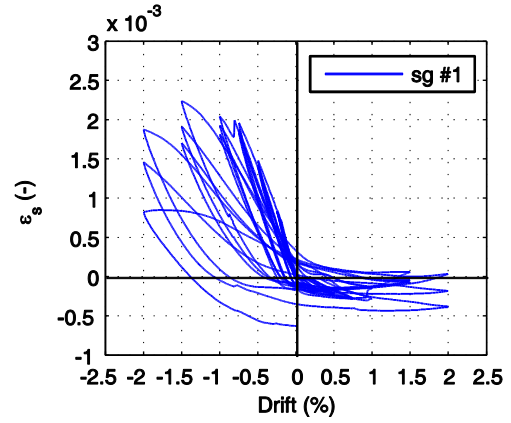
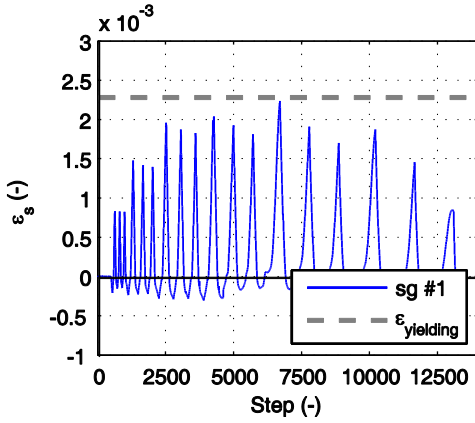
Appendix 7C: data from strain gauges on beam longitudinal bars

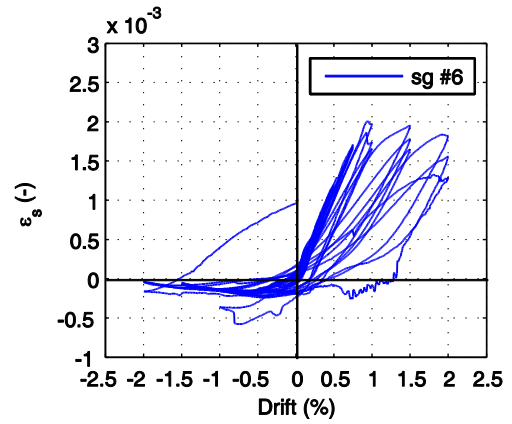
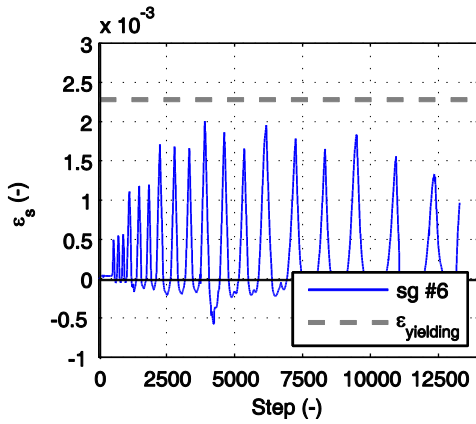
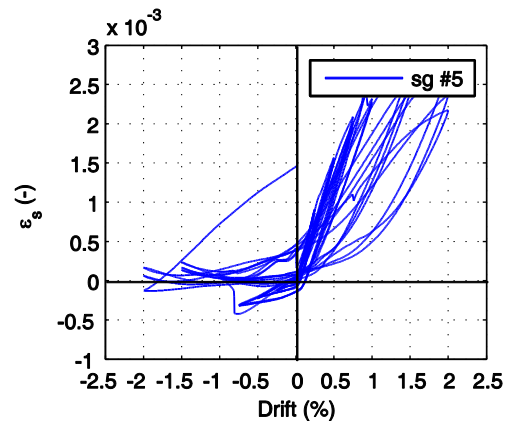
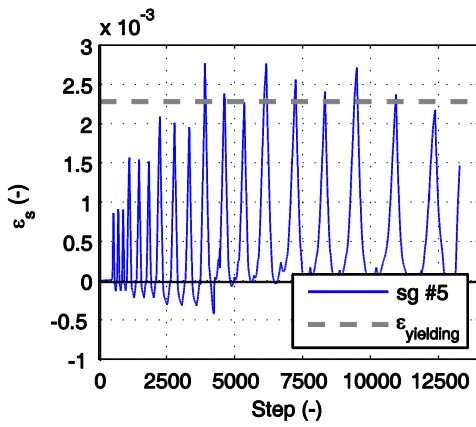
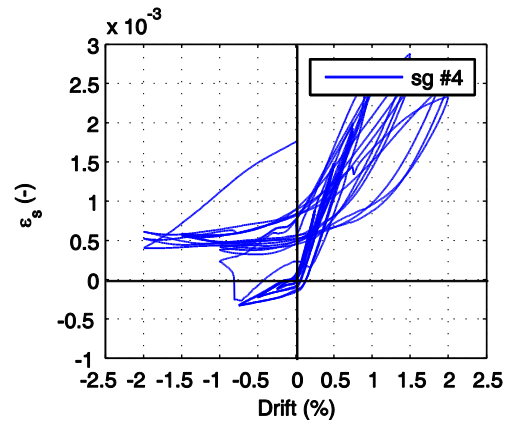
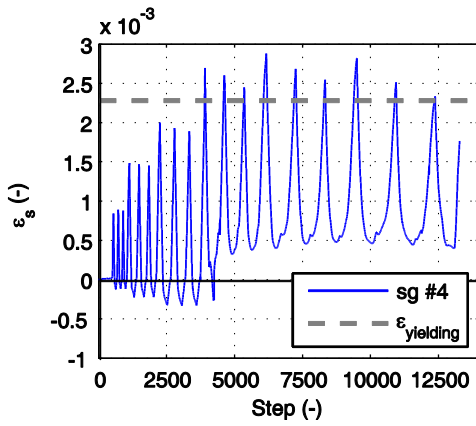
Test#1:





Test#2:





References

- ASCE/SEI 41, Seismic rehabilitation of existing buildings. American Society of Civil Engineers, Reston, VA, USA, 2007.
- Celik OC and Ellingwood BR (2008) “Modeling Beam-Column Joints in Fragility Assessment of Gravity Load Designed Reinforced Concrete Frames”, *Journal of Earthquake Engineering*. 12:357-381.
- CEN, 2004. European standard EN1992-1-1. Eurocode 2: Design of concrete structures - Part 1-1: General rules and rules for buildings. Comité Européen de Normalisation, Brussels.
- Clyde C, Pantelides CP, Reaveley LD (2000) “Performance-Based Evaluation of Exterior Reinforced Concrete Buildings Joints for Seismic Excitation”, PEER Report, No. 2000/05, Pacific Earthquake Engineering Research Center, University of California, Berkeley, USA.
- Decreto Ministeriale del 14/1/2008. Approvazione delle nuove norme tecniche per le costruzioni. G.U. n. 29 del 4/2/2008, 2008. (in Italian)
- Earthquake Engineering Research Institute. (1999a). EERI Special Earthquake Report – September 1999. The Tehuacan, Mexico, Earthquake of June 15, 1999. <http://www.eeri.org/>
- Earthquake Engineering Research Institute. 1999b. EERI Special Earthquake Report – December 1999. The Chi-Chi, Taiwan Earthquake of September 21, 1999. <http://www.eeri.org/earthquakes/earthquakes.html>
- Engindeniz, M. (2008), “Repair and Strengthening of Pre-1970 Reinforced Concrete Corner Beam-Column Joints Using CFRP Composites”, PhD Thesis, Civil and Environmental Engineering Department, Georgia Institute of Technology, August 2008.
- Hassan WM (2011) Analytical and Experimental Assessment of Seismic Vulnerability of Beam-Column Joints without Transverse Reinforcement in Concrete Buildings, PhD Dissertation, University of California, Berkeley, California, USA. <http://www.eeri.org/earthquakes/earthquakes.html>
- McKenna, F., Fenves, G.L., Scott, M.H. (2010). OpenSees: Open System for Earthquake Engineering Simulation. Pacific Earthquake Engineering Research Center. University of California, Berkeley, CA, USA. <http://opensees.berkeley.edu>
- Mochle, J.P. and Mahin, S.A. (1991). Observations on the behavior of reinforced concrete buildings during earthquakes. *Earthquake-Resistant Concrete Structures Inelastic Response and Design SP-127*, American Concrete Institute, ed. S.K. Ghosh, Detroit.
- Ricci P., De Luca F., Verderame G.M. (2011). 6th April 2009 L’Aquila earthquake, Italy: reinforced concrete building performance. *Bulletin of Earthquake Engineering*. Vol. 9, Issue 1, pp. 285-305.
- Pantelides CP, Hansen J, Nadauld J, Reaveley LD (2002) “Assessment of Reinforced Concrete Building Exterior Joints with Substandard Details”, PEER Report, No. 2002/18, Pacific Earthquake Engineering Research Center, University of California, Berkeley, USA.
- Park S and Mosalam KM (2013) “Simulation of Reinforced Concrete Frames with Nonductile Beam-Column Joints”, *Earthquake Spectra*, 29(1), 233-257.
- Park S and Mosalam KM (2012) “Analytical model for predicting the shear strength of unreinforced exterior beam-column joints”, *ACI Structural Journal* 109, 149–159.

- Priestley, M. J. N. 1 (1997) “Displacement-based seismic assessment of reinforced concrete buildings”. *Journal of earthquake Engineering* 1: 157-192.
- Sezen, H., Elwood, K.J., Whittaker, A.S., Mosalam, K. M., Wallace, J.W., and Stanton, J.F. 2000. Structural engineering reconnaissance of the August 17, 1999 earthquake: Kocaeli (Izmit), Turkey, PEER-2000/09, Berkeley: Pacific Earthquake Engineering Research Center, University of California, Dec.
- Uzumeri SM (1977) “Strength and ductility of cast-in-place beam-column joints”. From the American Concrete Institute Annual Convention, Symposium on Reinforced Concrete Structures in Seismic Zones, San Francisco, 1974. No. SP-53.

Chapter 8

CONCLUSIONS AND FUTURE DEVELOPMENTS

Among the natural hazards, earthquakes are paramount due to their impact on civil structures worldwide. The considerable direct economic losses (property losses) due to earthquakes in conjunction with social impact and indirect economic losses have prompted a great interest in performance assessment of the civil structures to future seismic events. Therefore, performance evaluations, beyond the traditional goal of life safety, are required to rightly estimate expected losses. A key ingredient of this evaluation process is the fragility, which describes the probability of failure to meet a performance objective depending on demand on the system, providing the link between seismic hazard and building loss estimation.

It is well known that a correct fragility evaluation necessitates the development of reliable nonlinear analysis models that are able to simulate the behavior of structures from the onset of damage through collapse. Therefore, proper prediction of the nonlinear behavior and formulation of analytical models are essential prerequisites for a reliable evaluation of structural fragility and, then, of seismic performance and risk assessment of RC structures. Moreover, within the performance-based approach, it is also essential to understand which mechanisms/elements have a higher influence on seismic performance depending on the analyzed performance level.

A lot of work should still be done towards this direction, especially for existing *under-designed* or *non-ductile* structures, namely designed for gravity loads only or according to obsolete seismic and technical codes.

A contribution towards this direction has been carried out. Starting from the analysis of typical deficiencies of non-ductile RC frames and the definition of performance levels of interest, this work aimed to contribute to PBEE framework with (i) a critical overview on analysis methodologies and analytical modeling of the salient components of RC frames, namely flexural or

shear-dominated beams and columns, and more in detail, beam-column joints and masonry infills, the core of this work, and (ii) with new proposals in terms of nonlinear modeling and analysis procedures to provide a more reliable evaluation of seismic performance and risk assessment of infilled RC structures, accounting for structural and nonstructural (in particular masonry infills) elements, at different performance levels.

For these purposes, existing analytical modeling techniques for frames' critical components were first reviewed and discussed. Then, a deep investigation on the influence of infills on seismic performance at different limit states, also for new constructions, has been carried out, in order to highlight the critical points that can interest also this kind of structures regarding infill presence.

The effect of infills on the global seismic behavior of RC frames was investigated, by analyzing their influence on global stiffness and strength, on the kind of collapse mechanism, on the displacement capacity and, consequently, on seismic capacity and seismic fragility at different performance levels, depending on the main characteristics of the RC frame, such as the design typology and the number of stories.

The effect of main parameters influencing the seismic capacity of infilled RC buildings has been investigated through a sensitivity analysis. Such analysis has shown that the rotational capacity of columns, directly influencing the displacement capacity, has the highest influence on the PGA capacity at higher seismic intensity for all of the investigated structures. Concrete compressive strength significantly influences the capacity at collapse, too, through its influence on the rotational capacity of columns. As far as PGA capacity at Damage Limitation Limit State is concerned, mechanical characteristics of infills have the highest influence on the response of the uniformly infilled frame, which is assumed to attain the Damage Limitation Limit State when the first infill in a story reaches its maximum resistance, whereas for pilotis and above all for bare frames also steel yield strength has a relatively high influence on PGA capacity at Damage Limitation, since this Limit State can be due to the first yielding in RC members. Presence of infills significantly influences the collapse mechanism even if the bare structure is designed according to Capacity Design principles.

Fragility curves were also obtained for the analyzed infilled RC structures, through the application of a Response Surface Method, considering materials, modeling and seismic input variability.

It was pointed out that, at higher seismic intensity, a beneficial effect on PGA capacity generally exists when a regular distribution of infill panels is considered, whereas a detrimental effect is shown by structures with an irregular infill distribution.

Moreover, in seismic designed structures, the presence of infills can significantly change the (global) collapse mechanism expected for structures designed according to Capacity Design, thus influencing displacement, ductility and PGA capacities.

Seismic performances of gravity loads (only) designed structures are more affected in terms of PGA capacity by infill panels, especially for low-rise structures. Same trends were found for low- and mid-rise structures, even if eight-story structures have a greater variability in collapse mechanisms depending on infill configuration, input parameters and design typology, and are less affected by infill presence in terms of PGA capacity at lower seismic intensity.

Moreover, it should be pointed out that a special attention should be addressed in future works to the potential brittle failure mechanisms due to the local interaction between masonry infills and structural RC elements and potential out of plane failures - which have not been accounted for herein - especially for existing RC buildings that have not been designed adopting general principles and detailing rules prescribed by modern seismic codes according to Capacity Design philosophy.

Recognized the importance of infills especially at lower seismic intensity and the widespread of linear analysis methodology among practitioner, new procedures have been proposed as tools to better taking into account damage to infills also in linear analyses with or without the explicit modeling of infills in the numerical model. The attention has been focused both on the design of new constructions and the assessment of existing structures, providing a contribution towards desirable more comprehensive future code prescriptions - that depend on mechanical properties of infills and proper displacement capacity thresholds - at lower seismic intensity within the context of linear analyses.

In particular, when infills take explicitly part of the numerical model, the attention was focused on the evaluation of an effective stiffness to assign to infill panels to perform linear analyses. Vice-versa, if infills are not included into the numerical model, limitation of damage to infills should be pursued through a proper limitation of displacement demand on the structure. Therefore, starting from the analysis of performance criteria and associated drift capacity limits for infill panels, two procedures were proposed and applied in order to provide modeling tools to be used in seismic assessment via linear analyses.

Nonlinear IDAs were carried out on structural models explicitly including infills in order to evaluate the intensity measure level corresponding to the achievement of Damage Limitation Limit State. Then, the results of such analyses were used as a reference. First, the “equivalent” displacement limit capacity – in terms of IDR – to be used in “bare” numerical models (without infills) was obtained. Then, the effective stiffness of infill panels to be used in infilled models was provided, thus allowing explicitly including these elements also within this kind of analysis approach.

The methodologies aimed at the estimation of such parameters were proposed and applied to 4- and 8-story infilled frames, designed for seismic loads (according to the current Italian technical code) or for gravity loads only (according to an obsolete technical code).

Equivalent IDR values highlighted a general conservatism of code provisions, increasing with the contribution of infill panels to stiffness/strength of the infilled RC frame. Effective stiffness values, based on the adopted model for infill panels, highlighted the need for a reduction of initial elastic stiffness of infills, in order to take into account first cracking prior to the attainment of Damage Limitation Limit State, but also the conservatism of the widespread Mainstone’s approach, which is also proposed by technical codes (e.g. ASCE-SEI/41).

Foreseen developments of this study should include the analysis of the sensitivity of equivalent IDR or effective stiffness of infills to additional characteristics of the infilled RC frames and of their response under seismic action up to DL LS, namely displacement capacity and hysteresis rules for infills or post-cracking stiffness of RC members, infill-to-RC stiffness and strength ratio. More generally, a comprehensive study could be carried out in order to attempt to provide predictive formulations both for equivalent IDR

and effective stiffness of infills, depending on geometrical and mechanical characteristics of infills and RC elements. Finally, proposed approaches to linear modeling and analysis of infilled RC frames at DL LS could be evaluated within the Response Spectrum Analysis approach, since the latter is the most widespread method of analysis, especially for seismic design of new structures.

From the point of view of the bare structure and in particular referring to higher intensity levels, proceeding from Damage Limitation towards Near Collapse Limit State, the analysis of RC frames different for design typology has confirmed the vulnerability points of such frames, already pointed out by experimental tests and past seismic events. In particular the influence of beam-column joints has been deeper investigated, with particular attention to exterior unreinforced joints.

In literature there is not yet a commonly accepted approach for the determination of the shear strength and for nonlinear modeling of RC beam-column joints in moment resisting RC frames. In many studies, beam-column connections are modeled as rigid. However, many nonlinear joint models are available, but most of them may be unsuitable for modeling all sources of nonlinearity for the assessment of older concrete buildings, or calibrated independently on the failure typology. Some of them were developed and calibrated for confined beam-column joints or they are too complicated to implement.

On the basis of an extensive and critical review of previous experimental tests and existing joint modeling approaches, a new shear constitutive relationship is proposed for exterior unreinforced joints, different for failure typology, in order to describe nonlinear behavior of joint panels, to be used in conjunction with an explicit bond-slip spring, thus taking into account all sources of nonlinearity and different possible kinds of deficiencies.

The proposed model depends on the joint failure typology and it has been defined in a “semi-empirical” approach. First, an experimental database consisting of 39 tests on exterior unreinforced beam-column joints that exhibited J-, BJ- or Anchorage failure mode has been collected and illustrated. Then, the joint panel constitutive parameters have been defined in order to reproduce the experimental joint shear stress-strain behavior, when they were available from tests. The proposed model for joint panel is a scissors model

characterized by a quadri-linear Moment–Rotation spring with four points for J- and BJ-mode of failure, namely: cracking, pre-peak, peak, and residual point.

The peak strength has been evaluated according to the model by Park and Mosalam (2012a), which directly provides joint shear strength depending on the failure typology and shows a very good agreement with analyzed experimental tests. Bond-slip has been taken into account by introducing an explicit slip spring (at the beam-joint interface) whose properties are analytically calculated using a finite difference model of the bar anchored into the joint panel.

Cases of anchorage failure due to an insufficient embedment length of the straight longitudinal bar into the joint core (which represents typical anchorage conditions of bottom reinforcement layer at beam’s ends in non-conforming frames designed for gravity loads only) have been taken into account limiting the peak strength of the slip spring consistent with the maximum stress allowed in the bar.

The proposed joint model has been finally validated using some of the experimental tests included in the database, and a comparison between the proposed model and other models from literature and code provisions has been carried out. It was highlighted that the proposed model conducts to the lower errors in terms of peak strength, peak drift and residual strength, if compared with the other models.

Future investigations shall be conducted to calibrate a similar shear stress-strain relationship for interior unconfined joints, starting from the available cyclic experimental response of the joint panel. Joint axial failure should be better investigated and introduced directly into the model.

The proposed joint model - completed with the calibration of cyclic parameters to be used in the adopted software (OpenSees) - has been also adopted for nonlinear dynamic analyses of gravity-loads-designed only and old-seismic-designed RC frames, in order to investigate on the influence of joint behavior on seismic performance at different performance levels, both in terms of strength and deformability contribution, also taking into account the record-to-record variability.

In order to assess the influence of joints on structural seismic performance, the capacities were primarily defined by the maximum interstorey drifts (IDR) that correspond to three widely used performance levels (or limit states) in the

earthquake community: immediate occupancy, life safety or significant damage, and collapse prevention. Additional limit states, defined on the basis of the achievement of characteristic points in the nonlinear response of the primary structural elements, have been adopted, detecting a “conventional failure” in analogy with the approach of typical European code prescriptions (e.g. Eurocode 8, DM 2008).

Preliminary nonlinear static analyses and incremental nonlinear dynamic analyses under selected ground motion records have been performed in a double condition: (i) with “rigid joints”, assuming a very high stiffness and shear strength for beam-column connections and (ii) “with joints”, explicitly modeling the nonlinear behavior of joints.

Joint axial failures and column shear failures have been detected by a post-processing of the analyses results. A review of previous researches on the shear behavior of existing columns indicates that a reliable column shear failure model that satisfies the requirements of accuracy, computationally efficiency and compatibility with existing software programs, in order to practically conduct numerous nonlinear dynamic analyses, is quite difficult to calibrate and to find in literature. Although the problem is still an open and important issue, in the present work the attention will be not directly focused on this topic.

For the strong-column-weak-beam designed frame, it was observed that the minimum ratio between seismic capacity with and without nonlinear joint modeling is related to higher seismic intensity levels, thus highlighting that the influence of joints in seismic assessment becomes more relevant at higher performance levels. Moreover, as far as column shear failures are concerned, when a force-based approach is adopted to detect column shear failures, joints leads to a limitation of shear demand in columns, thus delaying their shear failures and increasing median seismic capacity. In a displacement-based approach, vice-versa, median seismic capacity is lower if joints nonlinear behavior is explicitly modeled.

In the case of weak-column-strong-beam designed frame, the joint damage reduces the maximum interstorey drift demand implying prevention or delay of the expected soft-story mechanism, by reducing the rotation demand in the adjacent column. The roof drifts in the frame with the proposed joint model are higher due to the increased flexibility of the frame, but the maximum interstorey drifts are less than those in the rigid-joint frame. Since the rigid

joint assumption precludes any damage at the joint, it is not realistic in the presence of weak column-strong beam behavior and exaggerates the soft-story effect. On the other hand, the rigid joint assumption can be considered plausible for frames designed for seismic effects according to modern seismic code provisions. Moreover, when column shear failures are detected in a force-based approach, no shear failures in columns are captured since their plastic shear is lower than the maximum shear strength (calculated without degradation due to ductility demand). Vice-versa, in a displacement-based approach, the achievement of the first column shear failure anticipates severe damage limit state limit state, thus confirming that more attention should be addressed to such kind of failures, especially for frames designed for gravity loads only.

Actually, incremental dynamic analysis alone does not account for how well the nonlinear simulation model represents the real building, since no modeling uncertainties have been considered in these analyses. These modeling uncertainties are especially important in predicting collapse, because of the high degree of empiricism and uncertainty in predicting deformation capacity and other critical parameters for modeling collapse. Thus, also modeling uncertainties should be accounted for in future works to a more reliable evaluation of seismic performance.

Another important improvement of this study will be the explicitly modeling shear failures with degrading behavior after detection and consequent axial failure by means of a reliable, realistic and computational sustainable model.

Additionally, the analyzed models do not incorporate masonry infills and non-structural components. The effects of infills on structural response was shown in Chapter 3 within a N2 framework, highlighted the most important influence at low seismic demand levels of infill panels. Infills are not modeled in these dynamic analyses in order to clearly highlight the influence primarily of joints on seismic response, but it is clear that a future effort to take into account both joints and infills and above all their possible interaction in the numerical model is necessary and it is still an open issue.

Finally, investigated the sensitivity of joint response to the main mechanical and geometrical properties of beam-column sub-assemblages, in order to improve the understanding of exterior joints seismic performance without

transverse reinforcement in existing RC buildings, two experimental tests with deformed bars and different failure typology were designed and conducted under cyclic loading. Experimental results have been analyzed and compared with numerical results carried out through the adoption of the proposed numerical model. It was observed that the proposed model shows a good agreement with experimental results and that the main contributions of the overall deformability of the sub-assemblages are provided by shear deformation of the joint panel and fixed-end-rotation related to the adjoins beam (since the strong-column-weak-beam designed).

In the future, a more comprehensive experimental investigation on exterior and also interior unreinforced joints should be carried out in order to improve reliability of the provided numerical models, and also to better analyze the sensitivity of these kind of tests to axial load ratio, anchorage detailing, slab contribution, joint aspect ratio and bar typology (plain or deformed). In particular, very few tests are presented in literature in the case of longitudinal plain bars or taking into account the slab contribution.